Porosity, Mineralization, Tissue Type and Morphology Interactions at the Human Tibial Cortex

A Thesis

Submitted to the Faculty

of

Drexel University

by

Naomi A. Hampson

in partial fulfillment of the

requirements for the degree

of

Doctor of Philosophy

November 2013

Acknowledgements

My research and this dissertation would not have been possible without the help and support of many people. First, I would like to thank my advisors Dr. Haviva Goldman and Dr. Surya Kalidindi. This project is a meld of materials science and physical anthropology, and it came together with the influence and knowledge of both Dr. Goldman and Dr. Kalidindi. I would like to thank Dr. Goldman specifically for nurturing my interest in bone and helping me understand the biological complexities of a field in which I had little prior experience. I would like to thank Dr. Kalidindi for helping me find a project that fit my interests and my expertise.

I would also like to thank Dr. Karl Jepsen and all of my collaborators at Mt. Sinai School of Medicine in New York City. Dr. Jepsen and his students did all of the sample procurement and initial preparation, as well as the pQCT and ash content tests. I would like to acknowledge Felipe Guillermo, who did all of the ash content experiments. I was extremely fortunate to be able to contribute to a larger project and apply the materials science framework to answer existing biological questions. This study builds directly on the work of Dr. Steven Tommasini, and without his initial investigations, this project would not have happened.

A big thank you to my other two committee members, Dr. Richard Knight, who helped me focus and improve my research and thesis, and Dr. Zavaliangos who agreed to join the committee and lend his knowledge of μCT imaging. Thank you very much to Dr. Michele Marcolongo and her lab for allowing me to use their facilities during sample preparation for the μCT study. I would also like to acknowledge everyone at Microphotonics who helped with noise reduction and scanning protocols for the μCT. Thanks are also due, as well, to everyone in the MMG research group.

I would not have been able to get through all of the data processing without the help of everyone in Dr. Goldman's lab. Thank you to Matt Chin for µCT reconstructions, Eric Gallagher for image processing, Alka Basnet for ROI extraction, Ashley Campbell for histological sample processing and light microscopy imaging, and David Lin for imaging, ROI extraction, and histology tracings. This project included a great deal of data and processing, and without the help of everyone, I would never have made it through it all. I also need to thank Dr. Robert Gallop, from West Chester University, who helped me with the statistical analysis of the data.

Finally, I need to thank my family and friends for all of their unwavering support through the years. To my husband, Andrew, I could not have done this without you by my side. You listened to me go over my presentations time and again, and helped me with anything I needed. To my parents, Marcy and Roger Barth thank you for always believing in me and always pushing me to succeed, and to my brother David for his support and late-night proofreading. Thank you to all of my friends who stood by me over the years, who listened to me worry about my results without understanding them, and taking the time to let me run through my thought processes until I came to a better understanding.

Table of Contents

List of Tables ..... **viii**

List of Figures ..... **ix**

Abstract ..... **xv**

Chapter 1: Introduction **1**

1.1: Introduction **1**

1.2: Study Design **4**

1.3: Broader Significance of the Project **6**

1.4: Thesis Organization **8**

Chapter 2: Background **8**

2.1: Introduction **8**

2.2: General Background **10**

2.2.1: Bone Composition *10*

2.2.2: Bone Organization *11*

2.2.3: Bone Cells *13*

2.2.4: Bone Formation and Bone Modeling *13*

2.2.5: Bone Tissue Types *15*

2.2.6: Bone Remodeling (Intracortical Remodeling) *17*

2.2.7: Bone Properties Relative to Structure *19*

2.2.8: Bone Quality *20*

2.2.9: Bone Mechanics *23*

2.2.10: Geometry - Microstructure Tradeoffs *26*

2.2.11: Age and Sex Variation *28*

Chapter 3: Methods **31**

3.1: Introduction **31**

3.2: Sample Population **31**

3.3: Specimen Preparation Methods **32**

3.3.1: Specimen Collection, Initial Sectioning & Storage *32*

3.3.2: Preparation of Histological Sections *35*
3.4: Data Acquisition Methods **36**
3.4.1: Peripheral Quantitative Computed Tomography *36*
3.4.1.1: Background of the technique 36
3.4.1.2: Imaging methods for the current project 37
3.4.1.3: Calculation of robustness 38
3.4.2: Micro Computed Tomography *39*
3.4.2.1: Background of technique 39
3.4.2.2: Imaging methods for the current project 41
3.4.2.3: μCT reconstruction 43
3.4.2.4: μCT region of interest selection and noise reduction 45
3.4.2.5: ROIs within the rings 47
3.4.3: Ash content *49*
3.4.3.1: Background of technique 49
3.4.3.2: Other techniques that provide information about mineralization density 50
3.4.3.3: Methods for the current project 51
3.4.4: Histology *52*
3.4.4.1: Background of technique 52
3.4.4.2: Methods for the current project 53
Chapter 4: Inter-individual Relationships **57**
4.1: Introduction **57**
4.2: Methods **59**
4.2.1: Sample Population *59*
4.2.2: Sectioning and Imaging *59*
4.2.3: Statistical Analysis *62*
4.3: Results **63**
4.3.1: Validation Study *63*
4.3.2: Correlations with Robustness *64*
4.3.3: Relationships between the 38% and 66% sites *67*
4.3.4: Correlations between remodeling variables *71*
4.4: **Discussion** **76**

4.4.1: Porosity, Ash Content, and Tissue Type as Reflections of Intracortical Remodeling *76*

4.4.2: Robustness Correlations with Porosity, Tissue Type, and Ash Content *78*

4.4.3: Patterns of Variation Between the 38% and 66% Sites *80*

4.4.4: Relationships Between Remodeling Variables *83*

4.4.5: Unexplored Sources of Variability *86*

4.5: Conclusions **87**

Chapter 5: Site-specific Variations of Porosity, Tissue Mineralization, and Tissue Type around the Cortex and Their Relationships to Robustness **90**

5.1: Introduction **90**

5.2: Methods **92**

5.2.1: The Sample *92*

5.2.2: Sectioning and Imaging *92*

5.2.3: Statistical Analysis *95*

5.3: Results **95**

5.3.1: Porosity *95*

5.3.1.1: Multivariate analysis 95

5.3.1.2: Variation in porosity by wedge 96

5.3.1.3: Variation in porosity between rings 99

5.3.1.4: Variation in porosity within rings by wedge 102

5.3.1.5: Relationship Between Porosity and Robustness by Wedge and Ring 108

5.3.2: Ash Content *114*

5.3.2.1: Multivariate analysis 115

5.3.2.2: Variation in Ash Content by Wedge 115

5.3.3: Tissue Type *119*

5.3.3.1: Multivariate analysis 120

5.3.3.2: Variation in tissue type between rings 120

5.3.3.3: Variations in tissue type within rings by wedge 123

5.3.4: Correlations Between the Two Sites, 38% and 66% *129*

5.3.5: Co-variation Between Variables *133*

5.3.6: Comparison Between μCT Porosity and LM Secondary Tissue *137*

5.4: Discussion **141**

5.4.1: Variation in Porosity, Ash Content, and Tissue Mineralization as a Reflection of Robustness and Age *141*

5.4.2: Regional Variability *142*

5.4.2.1: Regional variability in porosity 142

5.4.2.2: Regional variability in ash content 144

5.4.2.3: Regional variability in tissue type 147

5.4.3: Relationships with Robustness *153*

5.4.3.1: Porosity and robustness 153

5.4.3.2: Ash content and robustness 154

5.4.4: Relationships Between the 38% and 66% Sites *154*

5.4.5: Co-variation Between Variables *156*

5.4.5.1: Co-variation between ash content and porosity 156

5.4.5.2: Co-variation of μCT and LM derived porosity and amount of secondary tissue 157

5.4.6: Reflections of the Bone Remodeling Process *158*

5.4.7: Limitations and Future Work *160*

5.5: Conclusions 161

Chapter 6: Concluding Statement 163

List of References 165

Appendix A: Abbreviations 185

Appendix B: Nomenclature 186

Appendix C: Terms of Location in the Skeleton 187

Appendix D: Tissue Type Images 188

Vita 190

List of Tables

Table 3.1: Data acquisition parameters for μCT imaging.....43

Table 3.2: Noise reduction steps for μCT images.....46

Table 5.1: ANOVA table for 38% mid-cortex porosity by wedge 104

Table 5.2: ANOVA table for 66% mid-cortex porosity by wedge 105

Table 5.3: ANOVA table for 38% periosteal porosity by wedge 106

Table 5.4: ANOVA table for 66% periosteal porosity by wedge 107

Table 5.5: ANOVA table for 38% mid-cortex amount of secondary bone by wedge. 125

Table 5.6: ANOVA table for 66% mid-cortex amount of secondary bone by wedge. 126

Table 5.7: ANOVA table for 38% periosteal amount of secondary bone by wedge 127

Table 5.8: ANOVA table for 66% periosteal amount of secondary bone by wedge 128

Table 5.9: Wedges with high and low porosity at the 38% site. 143

Table 5.10: Wedges with high and low porosity at the 66% site. 143

Table 5.11: Wedges with high and low amounts of secondary tissue at the 38% site. 149

Table 5.12: Wedges with high and low amounts of secondary tissue at the 66% site. 149

Table 5.13: Summary of regional porosity and tissue types results at the 38% site. 151

Table 5.14: Summary of regional porosity and tissue types results at the 66% site. 151

List of Figures

Figure 1.1: (a) Two cross-sectional sites (b) Six radial wedges around the cortex (b) Three rings, in which regions of interest were investigated. 6

Figure 2.1: Complex hierarchical structure of bone with features in the nm scale on up through the macroscopic scale. Figure by Dr. Haviva Goldman, cross-section and tissue level images by Dr. Alan Boyde, used with permission. 10

Figure 2.2: Two macroscopic organizations of bone: (a) cortical bone, which is very dense, and (b) cancellous bone, which is very porous. 11

Figure 2.3: Long bones schematic of (a) external structure and (b) cross-sectional structure. 12

Figure 2.4: Schematic of cortical drift. 15

Figure 2.5: Different types of bone tissue identifiable under a microscope. In this piece, circumferential lamellar bone (a type of primary bone) and osteonal bone (a type of secondary bone) are visible. Field width = 5mm 17

Figure 2.6: Relationship between radius and I of a cylinder with an (a) round cross-section and (b) elliptical cross-section. 25

Figure 3.1: Overall schematic of sample locations in the tibia, showing the 3 sample locations at both the 38% and 66% sites. Location A is a 2.5 mm thick cross section used for pqCT and ashing. Location B is a 2.5 mm thick cross section later cut into 6 radial wedges used for µCT and ashing. Location C is a 5 mm thick cross section embedded in PMMA and later made into ~100 µm thick sections histology sections. 33

Figure 3.2: The terminology for the locations of the samples. (a) Two cross-sectional sites, (b) six wedges at each site, and (c) three rings at each site. 34

Figure 3.3: Embedded 5 mm cross section before sectioning and preparation for histological imaging. 36

Figure 3.4: Schematic of computed tomography setup. X-rays from the source pass through the sample to the detector to form a projection image. 40

Figure 3.5: Screen capture from DataViewer (Skyscan, Kontich, Belgium) used for aligning the dataset. The three projections allow for proper alignment. 44

Figure 3.6: Post processing for separating the cortical bone from the cancellous bone. (a) The coarse ROI around the cortical bone in the unprocessed image and (b) the final binary image. .. 45

Figure 3.7: Three dimensional pore structure of a wedge from a (a) slender individual and (b) robust individual 47

Figure 3.8: Regions of interest for each ring around the cortex: endosteal, mid-cortex, and periosteal. 48

Figure 3.9: Histological thin sections imaged by (a) transmitted light (b) circularly polarized transmitted light, (c) a combination of the transmitted and circularly polarized light images. (Field Width = 1mm) 54

Figure 3.10: The different tissues types after determination and hand tracing. (Field Width = 1mm) 55

Figure 4.1: (a) Overall shape of the tibia, imaged using pQCT. (b) pQCT images of cross-sections from both the 38% and 66% location of a slender and a robust individual. (c) Photograph of a cross-section with the 6 radial wedges marked. 60

Figure 4.2: (a) Single reconstructed slice from μCT showing the coarse ROI used to remove the trabecular bone before image processing. (b) The same slice after removal of trabecular bone and binarization. 61

Figure 4.3: (a) ROI from the transmitted light image. (b) ROI from the circularly polarized transmitted light image. (c) A schematic of locations of ROIs. (d) Combined light microscopy image. (e) Hand traced tissue types from the combined light microscopy image. 62

Figure 4.4: Comparison between porosity of the entire wedge and porosity of the mid-cortex only. 64

Figure 4.5: Relationship of porosity with robustness. 65

Figure 4.6: Relationship of ash content with robustness. 65

Figure 4.7: Relationship of tissue type with robustness. 66

Figure 4.8: Relationship of TMD with robustness. 66

Figure 4.9: Comparison between the robustness of individuals at the 38% and 66% sites shows there is a linear relationship, and for each individual the robustness is lower at the 38% site than it is at the 66% site. 68

Figure 4.10: Comparison between the porosity of individuals at the 38% and 66% sites shows there is a linear relationship, and for each individual the porosity is lower at the 38% site than it is at the 66% site. 69

Figure 4.11: Comparison between the ash content of individuals at the 38% and 66% sites shows there is a linear relationship, and for most individuals the ash content is higher at the 38% site than it is at the 66% site. 70

Figure 4.12: Comparison between the amount of secondary bone (mid-cortex ROIs only) of individuals at the 38% and 66% sites shows there is a linear relationship, and for most individuals there is more secondary tissue at the 38% site than there is at the 66% site. 70

Figure 4.13: Comparison between the TMD of individuals at the 38% and 66% sites shows there is a linear relationship, and for most individuals the TMD is higher at the 38% site than it is at the 66% site. 71

Figure 4.14: Relationship between porosity and TMD is linear through data points from both the 38% and 66% sites. 72

Figure 4.15: Relationship between ash content and TMD is significantly linear only at the 66% site. 73

Figure 4.16: Relationship between ash content and porosity at the 38% site. 74

Figure 4.17: Relationship between ash content and porosity at the 66% site. 75

Figure 5.1: (a)The proximal (66%) and distal (38%) sites investigated in this work (b) pQCT images of robust and slender cross section at each site. (c) Photograph of the cross-section before sectioning into radial wedges. 93

Figure 5.2: (a) coarse ROI and (b) binarized slices µCT image. 94

Figure 5.3: LM CPL combined and traced labeled (a) transmitted light microscopy image (b) circularly polarized transmitted light microscopy image c) schematic of locations of ROIs (c) combined image (d) traced tissue types 94

Figure 5.4: Porosity at each wedge around the cortex at the 38% site. 96

Figure 5.5: Porosity at each wedge around the cortex at the 66% site. 97

Figure 5.6: Relationships between porosity and robustness at the 38% site at (a) anterior wedge (b) anterior-lateral wedge (c) posterior-lateral wedge (d) posterior wedge (e) posterior-medial wedge (f) anterior-medial wedge. 98

Figure 5.7: Relationships between porosity and robustness at the 66% site at the (a) anterior wedge (b) anterior-lateral wedge (c) posterior-lateral wedge (d) posterior wedge (e) posterior-medial wedge (f) anterior-medial wedge. 99

Figure 5.8: Porosity comparison by ring for each location. 100

Figure 5.9: Porosity between rings for each wedge at the 38% site. 101

Figure 5.10: Porosity between rings for each wedge at the 66% site. 102

Figure 5.11: Porosity in the mid-cortex ring for each wedge at the 38% site. 103

Figure 5.12: Porosity in the mid-cortex ring for each wedge at the 66% site. 105

Figure 5.13: Porosity in the periosteal ring for each wedge at the 38% site. 106

Figure 5.14: Porosity in the periosteal ring for each wedge at the 66% site. 107

Figure 5.15: Relationships between porosity and robustness in the endosteal ring at the 38% site at the (a) anterior wedge (b) anterior-lateral wedge (c) posterior-lateral wedge (d) posterior wedge (e) posterior-medial wedge (f) anterior-medial wedge. 109

Figure 5.16: Relationships between porosity and robustness in the endosteal ring at the 66% site at the (a) anterior wedge (b) anterior-lateral wedge (c) posterior-lateral wedge (d) posterior wedge (e) posterior-medial wedge (f) anterior-medial wedge. 110

Figure 5.17: Relationships between porosity and robustness in the mid-cortex ring at the 38% site at the (a) anterior wedge (b) anterior-lateral wedge (c) posterior-lateral wedge (d) posterior wedge (e) posterior-medial wedge (f) anterior-medial wedge. 111

Figure 5.18: Relationships between porosity and robustness in the mid-cortex ring at the 66% site at the (a) anterior wedge (b) anterior-lateral wedge (c) posterior-lateral wedge (d) posterior wedge (e) posterior-medial wedge (f) anterior-medial wedge. 112

Figure 5.19: Relationships between porosity and robustness in the periosteal ring at the 38% site at the (a) anterior wedge (b) anterior-lateral wedge (c) posterior-lateral wedge (d) posterior wedge (e) posterior-medial wedge (f) anterior-medial wedge. 113

Figure 5.20: Relationships between porosity and robustness in the periosteal ring at the 66% site at the (a) anterior wedge (b) anterior-lateral wedge (c) posterior-lateral wedge (d) posterior wedge (e) posterior-medial wedge (f) anterior-medial wedge. 114

Figure 5.21: Variation of ash content at the 38% site around the cortex. 116

Figure 5.22: Variation of ash content at the 66% site around the cortex. 117

Figure 5.23: Relationship between ash content and robustness at the 38% at the (a) anterior wedge (b) anterior-lateral wedge (c) posterior-lateral wedge (d) posterior wedge (e) posterior-medial wedge (f) anterior-medial wedge. 118

Figure 5.24: Relationship between ash content and robustness at the 66% at the (a) anterior wedge (b) anterior-lateral wedge (c) posterior-lateral wedge (d) posterior wedge (e) posterior-medial wedge (f) anterior-medial wedge. 119

Figure 5.25: Comparison of amount of secondary tissue between mid-cortex and periosteum at each site 121

Figure 5.26: Amount of secondary tissue at each wedge by ring at the 38% site. 122

Figure 5.27: Amount of secondary tissue at each wedge by ring at the 66% site. 123

Figure 5.28: Amount of secondary tissue at each wedge in the mid-cortex ring at the 38% site. 124

Figure 5.29: Amount of secondary tissue at each wedge in the mid-cortex ring at the 66% site. 125

Figure 5.30: Amount of secondary tissue at each wedge in the periosteal ring at the 38% site. . 127

Figure 5.31: Amount of secondary tissue at each wedge in the periosteal ring at the 66% site. .128

Figure 5.32: Comparison between the porosity of the 38% and the 66% sites at the (a) anterior wedge (b) anterior-lateral wedge (c) posterior-lateral wedge (d) posterior wedge (e) posterior-medial wedge (f) anterior-medial wedge. 129

Figure 5.33: Comparison between the µCT derived porosity of the endosteal ring of the 38% and the 66% sites at the (a) anterior wedge (b) anterior-lateral wedge (c) posterior-lateral wedge (d) posterior wedge (e) posterior-medial wedge (f) anterior-medial wedge. 130

Figure 5.34: Comparison between the µCT derived porosity of the mid-cortex ring of the 38% and the 66% sites at the (a) anterior wedge (b) anterior-lateral wedge (c) posterior-lateral wedge (d) posterior wedge (e) posterior-medial wedge (f) anterior-medial wedge. 131

Figure 5.35: Comparison between the µCT derived porosity of the periosteal ring of the 38% and the 66% sites at the (a) anterior wedge (b) anterior-lateral wedge (c) posterior-lateral wedge (d) posterior wedge (e) posterior-medial wedge (f) anterior-medial wedge. 132

Figure 5.36: Comparison between the ash content of the 38% and the 66% sites at the (a) anterior wedge (b) anterior-lateral wedge (c) posterior-lateral wedge (d) posterior wedge (e) posterior-medial wedge (f) anterior-medial wedge. 133

Figure 5.37: Relationships for all individuals, slender individuals, and robust individuals, between ash content and porosity at the 38% location at the (a) anterior wedge (b) anterior-lateral wedge (c) posterior-lateral wedge (d) posterior wedge (e) posterior-medial wedge (f) anterior-medial wedge. 135

Figure 5.38: Relationships for all individuals, slender individuals, and robust individuals, between ash content and porosity at the 66% location at the (a) anterior wedge (b) anterior-lateral wedge (c) posterior-lateral wedge (d) posterior wedge (e) posterior-medial wedge (f) anterior-medial wedge. 136

Figure 5.39: Linear comparison of µCT derived porosity and LM derived porosity from the (a) periosteal ring at the 38% site (b) periosteal ring at the 66% site (c) mid-cortex ring at the 38% site (d) mid-cortex ring at the 66% site.....138

Figure 5.40: Comparison at each wedge around the cortex between LM derived and µCT derived data at the 38% site. (a) µCT derived porosity - periosteal ring (b) LM derived porosity - periosteal ring (c) LM derived amount of secondary tissue - periosteal ring (d) µCT derived porosity - mid-cortex ring (e) LM derived porosity - mid-cortex ring (f) LM derived amount of secondary tissue - mid-cortex ring. 139

Figure 5.41: Comparison at each wedge around the cortex between LM derived and µCT derived data at the 66% site. (a) µCT derived porosity - periosteal ring (b) LM derived porosity - periosteal ring (c) LM derived amount of secondary tissue - periosteal ring (d) µCT derived porosity - mid-cortex ring (e) LM derived porosity - mid-cortex ring (f) LM derived amount of secondary tissue - mid-cortex ring. 140

Figure Appendix C: The location of the tibia in the skeleton (red) and the terminology for locations within the skeleton.....187

Figure Appendix D.1: Tissue type images from the 38% site arranged age.....188

Figure Appendix D.2: Tissue type images from the 66% site arranged age.....189

Abstract

Porosity, Mineralization, Tissue Type and Morphology Interactions at the Human Tibial Cortex

Naomi A. Hampson

Haviva Goldman, Ph.D. and Surya Kalidindi, Ph.D.

Prior research has shown a relationship between tibia robustness (ratio of cross-sectional area to bone length) and stress fracture risk, with less robust bones having a higher risk, which may indicate a compensatory increase in elastic modulus to increase bending strength. Previous studies of human tibiae have shown higher ash content in slender bones. In this study, the relationships between variations in volumetric porosity, ash content, tissue mineral density, secondary bone tissue, and cross sectional geometry, were investigated in order to better understand the tissue level adaptations that may occur in the establishment of cross-sectional properties.

In this research, significant differences were found between porosity, ash content, and tissue type around the cortex between robust and slender bones, suggesting that there was a level of co-adaption occurring. Variation in porosity correlated with robustness, and explained large parts of the variation in tissue mineral density. The nonlinear relationship between porosity and ash content may support that slender bones compensate for poor geometry by increasing ash content through reduced remodeling, while robust individuals increase porosity to decrease mass, but only to a point. These results suggest that tissue level organization plays a compensatory role in the establishment of adult bone mass, and may contribute to differences in bone aging between different bone phenotypes. The results suggest that slender individuals have significantly less

remodeled bone, however the proportion of remodeled bone was not uniform around the tibia. In the complex results of the study of 38% vs. 66% sites the distal site was subject to higher strains than the 66% site, indicating both local and global regulators may be affecting overall remodeling rates and need to be teased apart in future studies.

This research has broad clinical implications on the diagnosis and treatment of fragility fractures. The relationships that were found between local variables and global geometry indicate that there was a fundamental difference between robust and slender bones, which affect the overall properties of the bone. This could allow for simple testing of bone geometry to predict an individual's fracture risk.

Chapter 1: Introduction

1.1: Introduction

Bone is a complex material with an anisotropic structure, and small changes in composition, microstructure, and geometry can lead to changes in fracture risk. Understanding these connections can perhaps help lead to an understanding of why some people get fractures and others don't. The interactions between bone geometry and tissue level structure are not well understood, and this project addresses questions left unanswered by previous studies about these interactions.

The geometric properties of long bones, such as the tibia, are determined both by loading conditions during growth as well as heredity factors (Enlow 1963; Frost 1973; Pandey *et al.*, 2009; Susanne *et al.* 1983). The vital role of genetics in the determination of both the length of the bones and their cross-sectional geometry can be appreciated by looking at traits such as robustness, an inherited morphological trait that is established by about 2 years of age (Susanne *et al.*, 1983). The robustness of long bones, defined in this work as the total cross-sectional area normalized to bone length (Jepsen *et al.*, 2011), directly relates to the bone's resistance to bending along the long axis of the bone, with slender bones being less resistant to bending than robust ones.

Previous research (Giladi *et al.*, 1987; Milgrom *et al.*, 1989) has shown that individuals with slender bones, meaning their bone shafts have a narrow cross section when compared to total bone length and thus a smaller robustness value, are more at risk of fracture than those people with robust bones (larger robustness value). This was

specifically demonstrated in the tibia, the shin bone, which is particularly prone to stress fractures along its shaft.

Based on geometry alone, one would expect a more slender bone to have a higher risk of fracture, due to the relatively lower resistance to bending of a bone with a small area moment of inertia, but there may be an influence due to local bone composition as well. In a study of the femurs of two different strains of adult inbred mice, A/J and C57BL/6J (B6), Jepsen and colleagues found that the mouse strain with a more slender bone phenotype, A/J, had a higher bone mineral content, measured by ash content (68.6 ± 0.8), than the mouse strain with the more robust bone phenotype, B6 (66.0 ± 1.2) (Jepsen *et al.*, 2001). This relationship was investigated in humans by Tommasini *et al.*, who found a negative relationship between robustness and mineral content (Tommasini *et al.*, 2005; 2007; 2008). Tommasini and colleagues also found that ash content was significantly negatively correlated to post yield strain and toughness and significantly positively correlated to elastic modulus (Tommasini *et al.*, 2008). Additionally, Tommasini *et al.* performed 4-point bending on the bone samples to determine monotonic failure properties as well as damage accumulation. Significant negative correlations were found between tibia morphology and modulus, and significant positive correlations between morphology and total energy, post yield strain, and damageability (Tommasini *et al.*, 2005; 2007). The results of the Tommasini *et al.* studies indicated that there is some level of co-adaptation between overall geometry and local properties, but these relationships need to be further investigated in order to try and explain this phenomenon.

A possible explanation for the co-adaption as discussed by Tommasini and colleagues is as follows. If the tibia needs to exhibit a minimum overall stiffness in order to withstand normal loading and the geometry is insufficient, then the elastic modulus of the bone tissue would need to be increased. One way that this could be accomplished would be by adjusting the remodeling rate of the bone, which is the process by which bone at a single site is removed and replaced with new tissue. This is a process that occurs throughout life as part of the normal renewal process of bone, and it can have huge effects on the material properties of a bone. The longer a piece of bone tissue stays in the body, the more mineralized it becomes, and therefore, the stiffer it becomes. Bone with a greater degree of mineralization is also more brittle than bone with lesser degree of mineralization.

Despite what is known from previous studies, there are still questions remaining, and the goal of this research is to try to provide answers to some of those questions. The research presented in this dissertation supports the theory that the differences in fracture risk between individuals with different whole bone geometries relate to compensatory mechanisms that influence remodeling rates and can cause changes in the local structure and composition of bone (Tommasini *et al.*, 2005; 2007; 2008). Specifically, the hypothesis governing this work is that individuals with slender tibiae will have a decreased remodeling rate in their tibiae. This decreased remodeling rate is a compensatory mechanism that would lead to an increase in the elastic modulus. In order to test this hypothesis, surrogate measures that are reflective of remodeling, namely porosity, mineralization density, and tissue type, were used to determine the

compensatory relationships. Additionally, these relationships were investigated at different locations along the length of the tibia and around the cortex to try to tease out these relationships from other location based relationships.

1.2: Study Design

In order to investigate the hypothesized relationships described above, two studies were designed, both utilizing a small, but well characterized, sample of cadaveric tibiae. Each study addressed a specific aim and several hypotheses, as follows:

1. In the first study, whole cross sections taken from two sites along the tibial diaphysis were examined in order to investigate *inter*-individual relationships in porosity, ash content, tissue mineral density, tissue type, and geometry (see Figure 1.1a). The aim of this investigation was to study the relationships between aspects of tissue quality at the cross-sectional level in order to better understand the tissue level adaptations that may occur in the establishment of whole bone function. It was hypothesized that individuals with cross sectional geometry that is disadvantageous for whole bone stiffness (lower robustness) compensate at the local level by a decreased remodeling rate which leads to an increase in the mineralization of the tissue, and therefore, the elastic modulus.

It is important to investigate these relationships at the cross-sectional level, as similar information can be ascertained from current clinical diagnostic techniques, however, this is not a complete picture. Bone is not homogeneous, and the microstructure and composition vary greatly around the cortex, so it is also important to investigate the site-specific relationships.

2. In the second study, the cross sections were sectioned into six radial wedges each, and the *intra*-individual variation of porosity and ash content were examined around the cortex (see Figure 1.1b). Additionally, regions of interest (ROIs) within each wedge in each of the three rings (periosteal, mid-cortex, and endosteal) and were investigated for variations in porosity and regions of interest within each wedge at each of two rings (periosteal and mid-cortex) were investigated for tissue type variations (see Figure 1.1c). It was hypothesized that there is regional variation around the tibia in the amount of porosity, ash content, and tissue type and the variation can be explained in part by robustness and in part by regional variation in mechanical loading as reflected in geometric axes (e.g. tensile vs. compressive cortices relative to the axis of greatest bending rigidity). It was also hypothesized that the relationship between the variables is site-specific, the relationship modulated by both local (strain) and global (robustness) phenomena. Bone is not loaded evenly from weight bearing and locomotion or muscle pulls, and since bone responds to mechanical stimuli, there is no reason to believe that all of the relationships between microstructure and composition would be the same around the cortex.

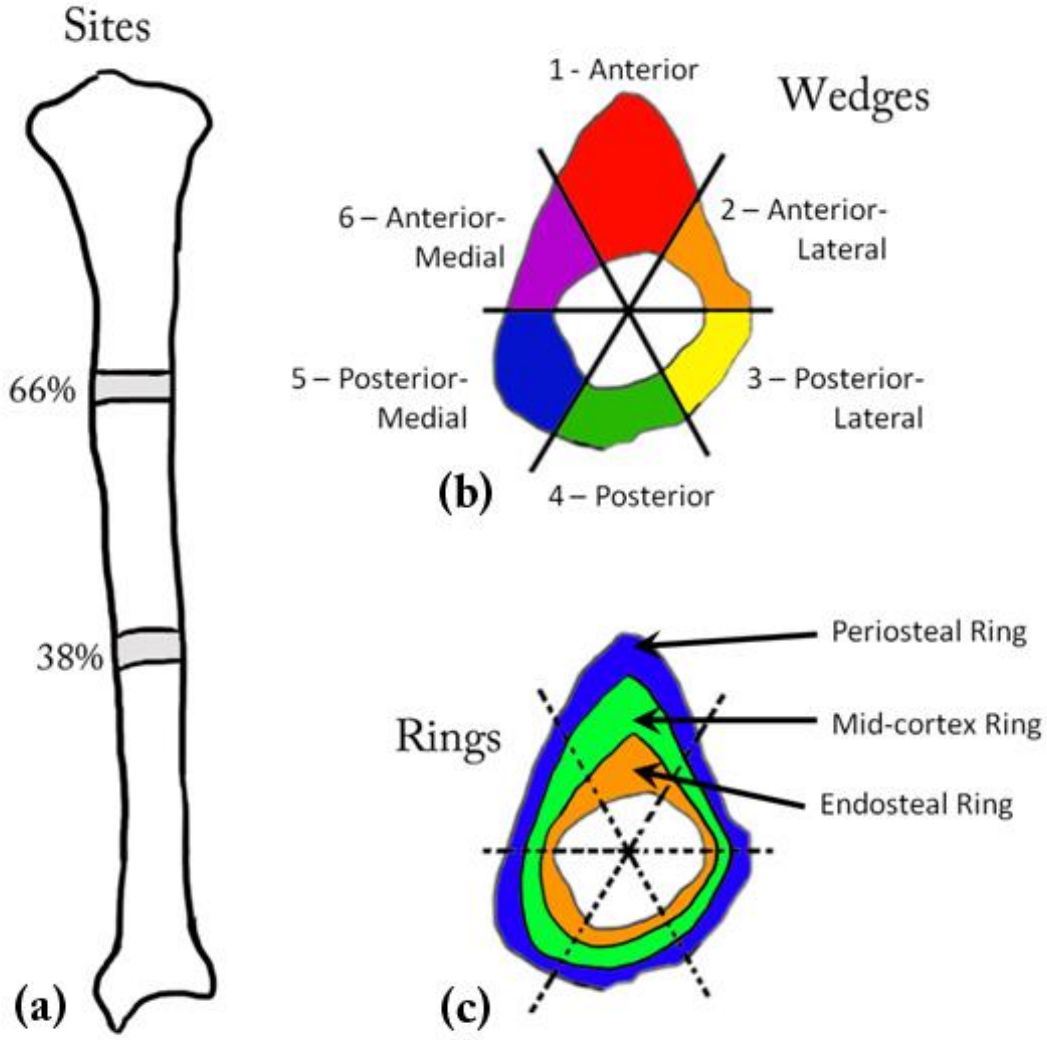

Figure 1.1: (a) Two cross-sectional sites (b) Six radial wedges around the cortex (b) Three rings, in which regions of interest were investigated.

1.3: Broader Significance of the Project

With the increase in the average age of the population, understanding skeletal fragility and how to diagnose it becomes a greater concern. This research will give a

better understanding of human cortical bone at the tissue level and insight into co-adaptations that can affect the bone quality. Even as imaging tools continue to improve for *in-vivo* investigations, these tools cannot be used to their full potential if there is not a basis for understanding the results. A better understanding of the relationships between the structure, composition, and properties of bone will allow for better evaluations of fracture risk in individuals in the future as well as how best to treat those fractures.

The methods and techniques utilized in this study allow comparisons to be made of the bone structure, composition, and mechanical properties at different locations around the bone. In this study, composition and microstructure data were collected across entire bone cortices, taking into account different tissue types that could not be accounted for in known previous studies. This allowed for better understanding of the properties of the bone around the cortex, and allows for targeted analysis of different areas of the cortex. With higher resolution *in-vivo* clinical imaging tools becoming available, it is necessary to pinpoint where in the cortex the imaging would be most beneficial, and in order to do this, good understanding of the structure and organization of the bone tissue around the cortex is vital.

This research is a pilot study of a relatively small sample. The techniques developed and utilized for this thesis can be used on other bones and in other areas of the body without major changes to the tools or techniques. This allows for this technique to be easily scaled for a larger sample in the future.

1.4: Thesis Organization

This thesis is organized to reflect this study design. Following a general background and methods chapter, the two studies are presented, each as a separate chapter that can stand alone with its specific hypothesis, methods, results and conclusions. Each study builds on the next, introducing specific questions that are then answered by the next study.

This project was done in collaboration with Dr. Karl Jepsen (Mount Sinai School of Medicine and now U. Michigan) and his students at MSSM. The samples were the contralateral legs of ten of the individuals investigated by Tommasini *et al.* (2005; 2007; 2008) while at MSSM. Much of the sample preparation, sectioning, cleaning, and embedding was performed at MSSM. Peripheral quantitative computed tomography (pQCT) analysis was performed at MSSM to determine cross-sectional geometry and tissue mineral density. Cleaned, sectioned samples were sent to Drexel University to be imaged by micro computed tomography (μCT) by the author, and these sections were subsequently ashed for compositional data at MSSM. All porosity measurements and analysis were performed at Drexel University by the author, who also oversaw the histological processes, which included sample sectioning to prepare thin sections for light microscopy and the tracings and analysis of the images. Medical students (Jerrald Chen, Matt Chin and Eric Gallagher) and Master's level graduate students (Ashley Campbell, David Lin, Alka Basnet) assisted with various steps of the data collection. All of the data analysis and statistical correlations in this dissertation were performed by the author.

Chapter 2: Background

2.1: Introduction

Skeletal fragility can be generalized as the skeleton's increased susceptibility to fracture which may be caused by poor bone quality and/or quantity. Increased skeletal fragility can lead to stress fractures, a problem frequently seen in the tibiae of young athletes and military recruits (Gilbert and Johnson, 1966; Belkin, 1980, Giladi *et al.*, 1987; Shaffer *et al.*, 2006). Stress fractures are of particular interest because they occur in young, otherwise healthy, individuals (Beck *et al.*, 2000; Chatzipapas *et al.*, 2008). Skeletal fragility may also lead to low impact fractures, which often affect the elderly and those with known bone and/or underlying metabolic diseases.

In order to determine who is at risk for fracture, and how best to direct treatment, better ways to identify skeletal fragility are needed. Currently, the most commonly used method of diagnosing bone diseases, such as osteoporosis, are measures of bone mineral density (BMD) which do not necessarily accurately identify fracture risk (Frasca *et al.*, 1977; Marshall *et al.*, 1996), as the techniques are unable to take into account aspects of bone quality. Given that bone has a complicated hierarchical structure, understanding relationships between the properties and composition at multiple length scales (from the tissue level to the whole bone level) will allow for better assessments of the changes in bone quality that occur during aging and disease, and may allow for determination of which people will be at risk for problems later in life.

As bone is a dynamic tissue that is constantly changing to adapt to everyday loads both in whole bone geometry and microstructural organization, one would expect

compensatory relationships between bone properties and composition at different length scales. There is increasing evidence in humans that bone morphology and tissue level bone structures co-adapt in order to arrive at the best possible properties within the constraints influenced by genetics and environment (Goldman *et al.*, 2005; Tommasini *et al.*, 2005; 2007; 2008; Ural and Vashishth, 2006). For this work, it is hypothesized that global factors related to geometry may be a factor in local structure and composition. Specifically, it is believed that the cross sectional geometry, described for this work as a measure of bone width relative to length of the human tibia is an important factor in determining remodeling rate at the local level. It is hypothesized that individuals with cross sectional geometry that is disadvantageous for whole bone stiffness (smaller cross sectional area relative to bone length) compensate at the local level by a decreased remodeling rate which leads to an increase in the mineralization of the tissue, and therefore the elastic modulus.

The two studies that make up this dissertation focus on testing these hypotheses using a small, young-adult sample of human tibial cortical bone samples. Variables that are reflective of remodeling history in the bone are examined relative to geometric parameters that reflect bone width relative to body size. This study represents a first step towards increasing an understanding of how global factors can affect local remodeling. This in turn, may help for better determinations from simple clinical procedures, who is at risk for fractures. By understanding the linkages between geometry, density, mineralization, and remodeling, it may be possible to accomplish targeted analysis and fracture risk evaluation in the future utilizing clinically available technologies that are in use today.

2.2: General Background

2.2.1: Bone Composition

Bone is a complex composite material consisting of an inorganic phase made of a crystal similar to hydroxyapatite - a mineral form of calcium apatite with the formula $Ca_{10}(PO_4)_6(OH)_2$ (Kay and Young, 1964), and an organic phase made of collagen fibrils (see Figure 2.1).

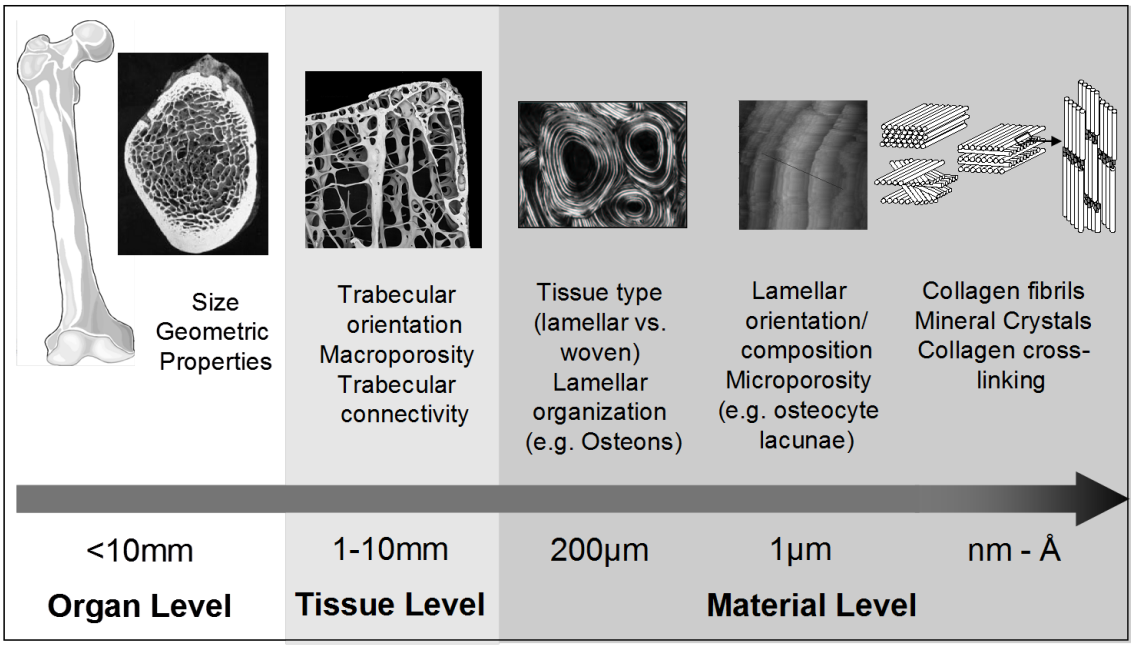

Figure 2.1: Complex hierarchical structure of bone with features in the nm scale on up through the macroscopic scale. Figure by Dr. Haviva Goldman, cross-section and tissue level images by Dr. Alan Boyde, used with permission.

In mature adult bone, the mineral/organic material form layered structures called lamellae, which are generally 2-7 μm thick (Boyde, 1972; Marotti, 1993; Weiner and Wagner, 1998). This lamellar bone may be organized into either sheets (circumferential lamellar bone) or as Haversian Systems (Secondary Osteons) in which the lamellae are organized concentrically around a central Haversian Canal.

2.2.2: Bone Organization

At the macro scale, bone is comprised of two basic structures, cortical (compact) bone and trabecular (cancellous) bone, see Figure 2.2.

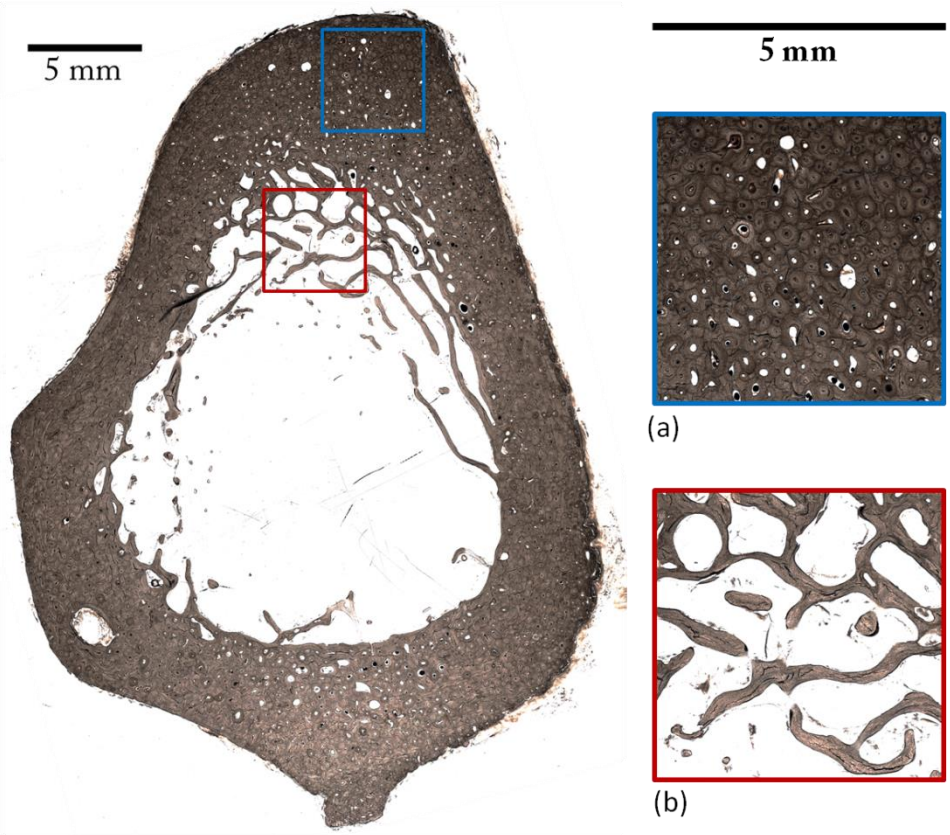

Figure 2.2: Two macroscopic organizations of bone: (a) cortical bone, which is very dense, and (b) cancellous bone, which is very porous.

Cortical bone is densely packed with around 5-10% porosity (Martin et al., 1998), and forms the outer shell of all bones. The shafts of long bones are made primarily of cortical bone with the mid-shaft being almost entirely cortical. Trabecular bone is made of thin plates and rods of bone that are arranged into highly interconnected struts and is mostly found in the ends of the long bones, the flat bones of the skull and the vertebrae. 75-90% of the volume of trabecular bone is made of marrow-filled pores which are between the bone struts (Martin et al., 1998). 80% of the skeleton is made of cortical bone and it plays a vital role in the majority of the skeleton's supportive and protective function (Jee, 1988; 2001), see Figure 2.3.

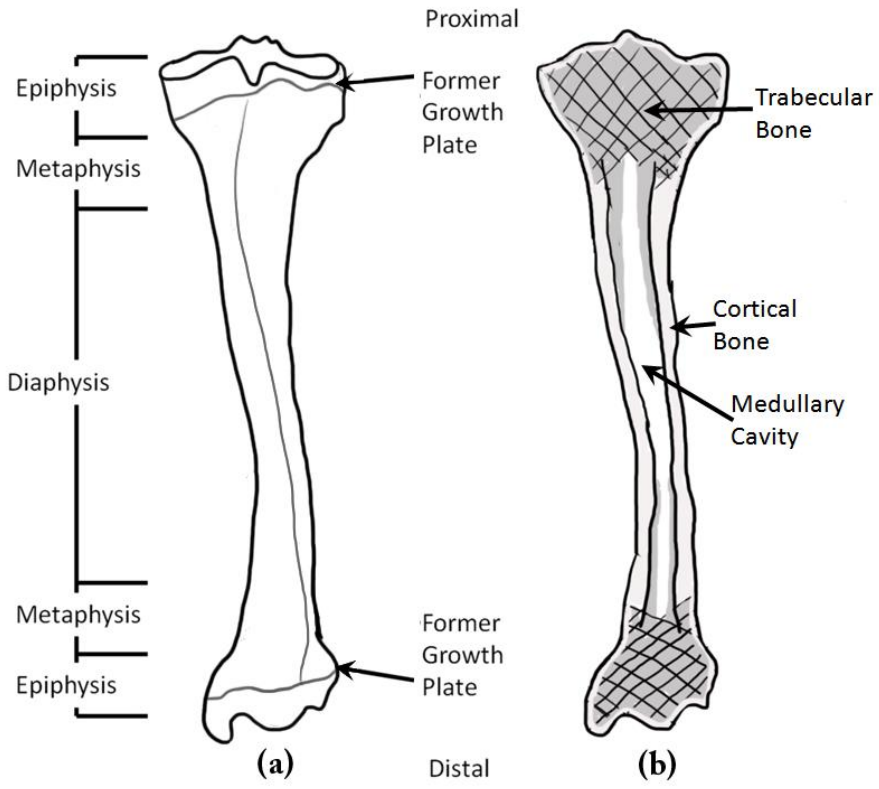

Figure 2.3: Long bones schematic of (a) external structure and (b) cross-sectional structure.

2.2.3: Bone Cells

Several types of cells are responsible for the formation, removal, and maintenance of bone tissue, including osteoclasts, osteoblasts, and osteocytes. Osteoclasts are large (~ 100 μm) multinucleated cells that are responsible for bone removal, or resorption. Osteoclasts are generally found on the bone surface in depressions called Howship's lacunae, which are made by the osteoclasts themselves (Baron, 1999). The osteoclasts resorb bone by both changing the local pH to create a microenvironment conducive to the breakdown of the bone minerals and secreting enzymes which digest the organic components of the matrix (Boyle *et al.*, 2003; Jee, 2001). Osteoclasts are cells that are responsible for bone formation, or deposition. They are cuboidal in shape and can be generally found on the bone surface. Osteoblasts lay down the unmineralized bone matrix called osteoid, which is later mineralized over time (Jee, 2001; Lian and Stein, 1999). When an osteoblast becomes trapped in the bone, it becomes an osteocyte, and resides in an enclosed space called a lacuna (plural = lacunae). Osteocytes are thought to be involved in signaling and sensing and responding to strain (Burger and Klein-Nulend, 1999; Cowin, 2002; Cowin *et al.*, 1991; Doty, 1981; Jee, 2001; Majeska, 2001; Nijweide et al., 1996). Research suggests that there are bone cells, likely osteocytes, which can sense mechanical loads and cause a physiological response to loads that are too low or high (Corwin, et al. 1991, Lanyon, 1993, Mullender and Huiskes, 1995; 1997).

2.2.4: Bone Formation and Bone Modeling

Bone formed during growth and development is very different in organization and properties from the bone of an adult, however, in order to understand the distribution of adult tissue in a cortex, one must understand how it was initially formed. Much of the

long bones were initially formed of cartilage. Increases in bone length are accomplished through the proliferation of chondrocytes (cells that make cartilage) at the growth plates, whose matrix later calcifies and provides a scaffold for bone to form, as part of endochondral ossification. Increases in bone width, on the other hand, are accomplished through the addition of bone tissue at the periosteal surface, essentially via intramembranous ossification, meaning bone is laid down by osteoblasts directly at the surface without a cartilaginous precursor (see Martin *et al.*, 1998 for more detail). As an individual grows the bone does not simply increase in length, the shape also has to change. During this process bone must be removed through osteoclastic activity in some areas while in other areas bone must be laid down via osteoblastic activity. This process is called "growth remodeling" (Enlow, 1962; 1963; Enlow, 1982) or modeling (Frost, 1973). During this process, bone is deposited on one cortex and resorbed on the opposite cortex, leading to a shift in the position of bone laid down at an earlier time compared to newer bone. This shift is known as cortical drift and affects the heterogeneity of the bone tissue organization and tissue age across the cortex (Enlow, 1963) see Figure 2.4. Bone that is laid down during the modeling process along existing bone surfaces as the bone grows is called primary bone.

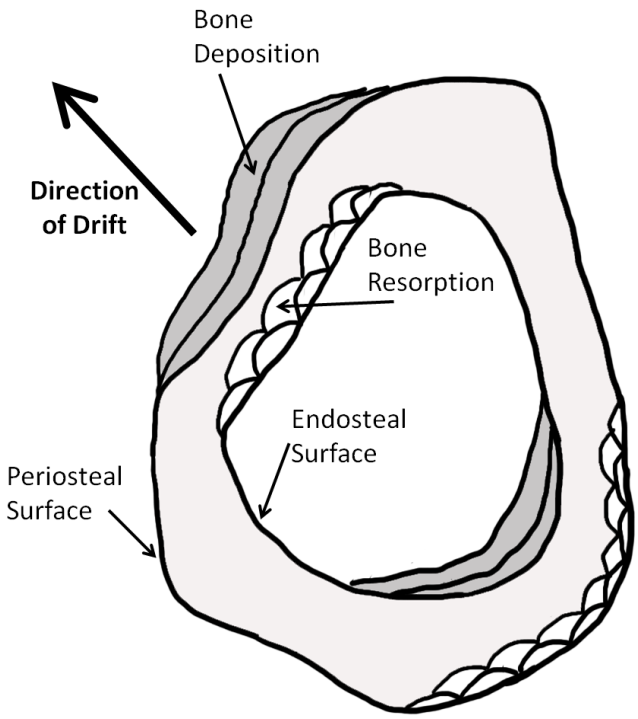

Figure 2.4: Schematic of cortical drift.

2.2.5: Bone Tissue Types

Primary bone tissues may vary in histological appearance depending on the speed at which they were deposited. Bone formed during the initial ossification process is called woven bone. Woven bone is characterized by its random arrangement of collagen fibers; its irregularly shaped and randomly organized osteocytes; and its amorphous mineral component. This type of bone can be formed rapidly and is found in areas of the fetal skeleton and in rapidly growing regions of the post-natal skeleton. It is also found in areas of callus formation in adults (Castanet *et al.*, 1993; Francillon-Vieillot, 1989; de Ricqlés *et al.*, 1991; Martin *et al.*, 1998). Fibrolamellar bone is lamellar bone interspersed with woven bone, and is often laid down during growth spurts (Currey, 1984; 2002). Lamellar bone is highly organized and characterized by collagen fibers and mineral crystals that are organized in layers, however, it is slow forming. Lamellar bone that is

formed as primary bone is known as circumferential lamellar bone. Here lamellae are formed parallel to the bone surface. Circumferential lamellar bone may be variably vascularized, often containing numerous primary vascular canals. In some cases, vessels may be surrounded by several concentric lamellae around them, forming what is known as a primary osteon (Enlow, 1962; 1964; Enlow and Brown, 1957; Martin *et al.*, 1998). Compact coarse cancellous bone is a type of bone tissue with a lamellar organization, in which the spaces have infilled during endosteal growth. It is usually formed at the proximal or distal ends of the diaphysis during metaphyseal modeling (Enlow, 1962; Enlow, *et al.*, 1982). Plexiform bone, a type of fibrolamellar bone, is a rapidly formed type typically associated with large, fast growing mammals. It is formed by the deposition of a network of woven trabeculae on the periosteal surface followed by infilling of lamellar bone, see (Enlow 1962; 1963; Enlow, 1982; Francillon-Viellot *et al.*, 1990; de Ricqlés *et al.*, 1991) for more details on these tissue types (see Figure 2.5).

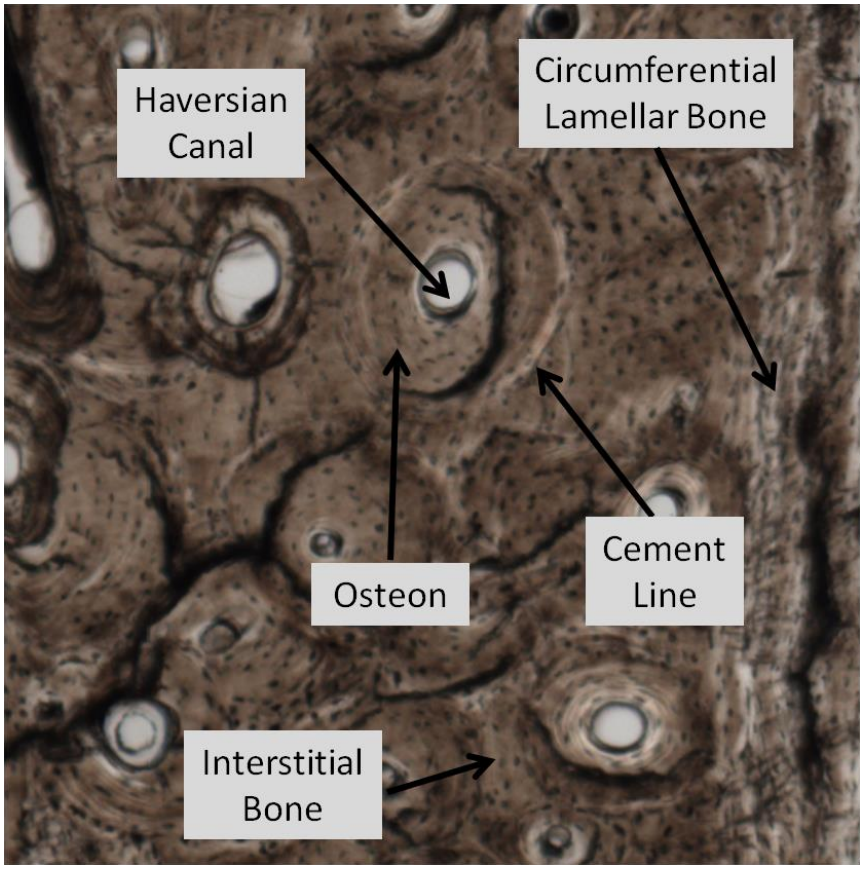

Figure 2.5: Different types of bone tissue identifiable under a microscope. In this piece, circumferential lamellar bone (a type of primary bone) and osteonal bone (a type of secondary bone) are visible. Field width = 5mm

2.2.6: Bone Remodeling (Intracortical Remodeling)

Bone does not become static once the entire skeleton has been laid down. Throughout life, regions within the bones are constantly being resorbed by osteoclasts and reformed by osteoblasts in a process known as secondary remodeling. In cortical bone, the newly deposited bone is called a secondary osteon, or Haversian system. These systems consist of concentric lamellae placed surrounding a Haversian canal. These secondary osteons can be identified by a cement line which delineates them from the

surrounding bone and represents a reversal line formed when there was a switch from bone resorption to bone deposition (see Figure 2.5). Primary osteons (formed around vascular systems in primary bone tissues during modeling) do not have these cement lines so the two can be distinguished from each other. New osteons may be deposited in areas containing previously formed primary bone, or they can replace or partially replace previously formed secondary osteons. The remnant primary tissue and remnants of older osteons that are incompletely replaced, form what is known as interstitial bone. Any tissue that is composed of bone formed by the intracortical remodeling process (in which an area of bone is removed and subsequently replaced in the same location by new Haversian systems) is called secondary bone tissue. Therefore any complete Haversian systems plus the remnants of previously formed Haversian systems are included in an area defined as secondary bone tissue. (Frost, 1986; Enlow, 1962; 1963; 1976; 1982; Enlow and Hans, 1996; Martin *et al.*, 1998).

It has been hypothesized that there are bone cells that can sense mechanical load, likely osteocytes, and are key in stimulating remodeling (Corwin *et al.*, 1991; Lanyon, 1993; Mullander and Huiskes, 1995; 1997). According to Martin (2000), under normal loading, osetocytes keep remodeling at a minimum rate by inhibiting the activation of bone lining calls. However, if the load were to significantly decrease, the signaling to inhibit the activation would decrease, which would lead to an increase in remdodeling. An increase in loading, leading to increased fatigue damage could interrupt the signal and also lead to increases in remodeling. This may explain the increases in remodeling observed for both excessively high and low loadings conditions (Li *et al.*, 1990; Martin, 2000; Schaffler *et al.*, 1990).

2.2.7: Bone Properties Relative to Structure

The tissue organization that comes about from both the modeling and remodeling processes affects the properties of bone at both the local level and whole bone levels. There is ample data demonstrating that primary and secondary bone tissue have different mechanical properties (Martin *et al.*, 1998) such that primary bone is stronger than secondary bone (Reilly and Burnstein, 1975; Carter *et al.*, 1976; Carter and Hayes, 1977). Most of these studies have looked at the comparisons between non-human plexiform bone and Haversian bone. Large areas of primary circumferential lamellar bone are difficult to find in a human sample. Vincentelli and Grigorov (Vincentelli and Grigorov, 1985) looked at human bone, specifically in the tibia, and although they were not able to completely isolate the different tissue types, their results indicated that samples with mostly primary bone had an approximately 22% greater ultimate tensile strength and an approximately 11% higher elastic modulus than samples with mostly secondary bone. In a nanoindentation study of the human femur, Rho *et al.* (2002) found that interstitial tissue was approximately 10% stiffer than secondary osteonal bone. Zysset e*t al.* (1999) found that the average elastic modulus of osteonal bone to be 19.3 ± 5.4 GPa and the average the elastic modulus of interstitial lamellar bone to be 21.2 ± 5.3 GPa, in a nanoindentation study of the diaphysis of the human femur.

Secondary bone is generally more porous compared to primary bone, due to the Haversian canals in the osteons. Additionally, newly formed osteons reduce the degree of mineralization in a piece of tissue. Burr and colleagues (Burr *et al.*, 1988) also suggest that the cement lines around secondary osteons may also affect the viscoelasticity of the bone. These factors combined may contribute to the decreased strength of osteonal bone

relative to primary bone. The osteons, however, may contribute to a reduction in crack propagation (Guo *et al.*, 1998; Akkus *et al.*, 1999; O'Brien *et al.*, 2005). In a finite element study, Najafi *et al.* (2007) found that microcracks would follow the cement lines and not enter the osteons.

2.2.8: Bone Quality

Bone quality is a difficult to define term, as it is a framework that encompasses all of the characteristics of bone that affect fracture risk. There are many variables that can predict fracture risk for a population overall, however, the fracture risk for many individuals cannot be adequately assessed using these variables alone (Donnelly, 2011; Hernandez and Keaveny, 2006; Fyhrie, 2005; Felsenberg and Boonen, 2005). For this reason, the many variables that affect bone quality need to be considered as part of the whole picture. The inorganic (mineral) phase of bone is crucial to the stiffness properties of bone, while the organic (collagen) phase is crucial in the toughness of bone (Carter and Hayes, 1977; Currey, 1984; Jepsen *et al.*, 1997; Landis, 1995; Wang *et al.*, 2003). The tensile strength and viscoelasticity of the collagen matrices are affected by intermolecular cross-linking (Paschalis *et al.*, 2004). Accumulation of microdamage can also have a negative effect on the mechanical properties of bone tissue (Forwood and Parker, 1989; Schaffler *et al.*, 1989; Burr *et al.*, 1997). Within the scope of this project, many of these variables cannot, or will not, be examined, but their influence on bone quality cannot be disregarded.

Several studies have shown that the preferred collagen fiber orientation in bone is an indicator of bone strength (Martin and Ishida, 1989; Boyde and Riggs, 1990; Goldman,

2003b, Martin and Boardman, 1993; Riggs *et al.*, 1993; Mason *et al.*, 1995). Areas with the largest amount of longitudinally oriented fibers are best suited to withstand high tensile strains. Areas of bone with the largest amount of transversely oriented fibers are best suited to withstand high compressive strains (Ascenzi and Bonucci, 1967; 1968; Ascenzi and Benvenuti, 1986). Collagen fibrils are arranged in parallel within an individual lamellae, however, the orientation differs in alternate lamellae. This gives an overall plywood-like structure, and causes a distinctive optical pattern when viewed under polarized light (Ascenzi and Benvenuti, 1986; Giraud-Guille, 1988; Weiner and Traub, 1992; Weiner *et al*., 1997; Ziv et al., 1996).

Beyond tissue type and fiber orientation, bone composition and organization at the tissue level can play a very important role in mechanical strength of the bone at the whole bone level. At the finest level of bone's hierarchical structure, bone has an organic matrix which is deposited as unmineralized osteiod and contains primarily Type I collagen, proteoglycans and water. The collagen provides flexibility as well as tensile strength to the bone. The organization, orientation, and cross-linking of the collagen fibrils have been shown to be related to the mechanical properties of the bone (Knott and Bailey 1998; Zioupos *et al.*, 1999). Over time, bone mineralizes as apatite crystals are deposited on and in the matrix, thus displacing some of the water (Martin *et al.*, 1998; Boskey *et al.*, 1999). The mineral adds compressive strength and rigidity to the bone (Martin *et al.*, 1998), and the degree of mineralization can have a huge impact on the mechanical properties. Heavily mineralized bone has a higher breaking stress compared to less mineralized bone, however, overly mineralized bone can become brittle (Vose, 1959; Currey, 1969; Bonfield and Clark, 1973). Pathak *et al.* (2011; 2012) demonstrated that

increases in mineralization, as measured by Raman spectroscopy, directly correlated to increases in elastic modulus, as measured by nanoindentation. Bone mineralization density, collagen fiber organization and porosity are discussed below, relative to their relationship to bone remodeling and bone strength.

There are two ways to measure mineralization, areal/volumetric mineralization and specific mineralization. Areal and volumetric mineralization, otherwise known as bone mineral density (BMD) is a measure of the amount of mineral per unit area or volume of whole bone and is a function of both mineralization and porosity. Areal BMD is measured with a DEXA (dual energy x-ray absorptiometry) scan while vBMD is measured with techniques such as computed tomography. Both are non-invasive techniques (Delmas and Seeman, 2004; Engelke *et al.*, 2009). Specific mineralization is the amount of mineral within a bone excluding porous spaces. It can be measured a number of ways *(ex vivo)* including ash fraction analysis (Tommasini et al. 2008) quantitative microradiography (Engstrom, 1952; Amprino, 1958; Vincentelli and Evans, 1971; Martin and Armelagos, 1985), or quantitative backscattered electron microscopy (Boyde *et al.*, 2005; Roschger *et al.*, 2008). An understanding of specific mineralization can also come from spectroscopic analysis of the bone using Fourier Transform Infrared Spectrocopy (FTIR) and Raman Spectroscopy because the spectra of the mineral components are distinct (Akkus *et al.*, 2003; Boskey *et al.*, 1992; 1999 Boskey and Mendelsohn, 2005). These techniques can be used to study bone and provide information on the type of mineral phases present and quantitative information on the changes in the mineral and matrix (Boskey and Mendelsohn, 2005). Boskey *et al* . (1992) found that the mineral to matrix ratio was found to be a marker of bone mineralization using infrared

absorption. The amount of mineral, as well as the type of mineral, has a significant effect on the bone strength (Currey, 1988; Martin and Ishida, 1989). As bone ages, the amount of mineral contained in the bone matrix increases and this causes the bone to be more brittle (Currey, 1979; Reid and Boyde, 1987; Boskey *et al.*, 1999; Akkus *et al.*, 2003).

2.2.9: Bone Mechanics

Changes in the form and function of a bone will lead to changes in its shape and internal structure, following what is known as Wolff's Law (Ruff *et al.*, 2006), in order to optimize the shape for loading. At birth, long bones have a cylindrical shape and during growth, they take on a complex shape that is reflective of the loading conditions they undergo during locomotion (Biewener and Bertram, 1993; Enlow 1962; 1964). The tibia (the subject of this thesis), for instance, develops a fairly triangular cross section. The tibia is primarily loaded in bending through the anterior-posterior axis, with the anterior region under tension (Aamodt *et al.*,1997; Gross *et al.*, 1992; Macdonald *et al.*, 2009; Peterman *et al.*, 2001; Rubin, 1984). Peterman *et al.* (2001) found that the local bone strains were linearly related to the ground reaction forces, however, the authors were unable to explain about one quarter of the variation in strain. This was likely due to the complex nature of the mechanics of the tibia. During gait, the geometry and muscle moment arms change. Further, since the largest strains found in their study were not due to ground reactions, but rather muscle actions, the impact of muscle strength and muscle attachments need to be considered.

Bone deposition and remodeling are greatly influenced by strain, from both ground reaction forces as well as muscle attachments. Using finite element analysis

supplemented by computer assisted optimization, Mittlemeier *et al.* (1994) were able to model the effects of locomotion and muscle loading on the shape of the femur. It was found that the adductor muscles had strong influences on the shape of the femur. In the tibia, muscles will also play an important role in the shape, as well as the strain at different locations in the bone, specifically the soleus muscle. The origin of the soleus muscle is along the proximal posterior surface of the tibia, along the soleal line, and this muscle puts some areas of the tibia in tension but not others. This leads to an uneven distribution of new bone growth as well as increased remodeling.

Even after growth is finished (e.g. the growth plates close), bones will continue to model to a small degree throughout life, resulting in changing geometric properties. Subperiosteal expansion with age was first shown in the tibia by Smith and Walker (1964). Ruff and Hayes (1982) presented evidence for a model for generalized subperiosteal expansion with aging, but indicated that the modeling process was affected by site-specific loading conditions, some of which were sex-specific. They found that areas subjected to higher loads *in-vivo* exhibited the greatest increases with age of total subperiosteal area. Changes in daily loading conditions will lead to changes in bone size and shape. In a study of the effects of exercise on the tibia of adolescents, Macdonald *et al.* (2009) investigated 202 male students aged 9-11 years, and assigned randomly to a control group or an intervention group. The students in the intervention group engaged in 60 minutes of physical activity per week, including a bone loading program. The investigators found that the group who underwent an exercise program gained bone along the AP axis. As the AP axis is the axis of greatest bending rigidity, increases here lead to a large increase in overall stiffness.

The primary mode of loading in the diaphysis of long bones is bending (Peterman *et al.*, 2001), and the resistance to bending is characterized by the area moment of inertia (*I*), (see Equation 2.1). *I* is generally calculated relative to the neutral axis and parallel to the bone cross section Macdonald *et al.*, 2009). There are two perpendicular axes which reflect the axes along which the structure can be most or least easily bent. The axis of greatest bending rigidity, I_{max} reflects the axis along which the structure is most resistant to bending and the axis of least bending rigidity, I_{min} along which the structure is least resistant to bending, see Figure 2.6. For a cylinder with a round cross-section $I_{max}=I_{min}=I_o$ (see 2.1).

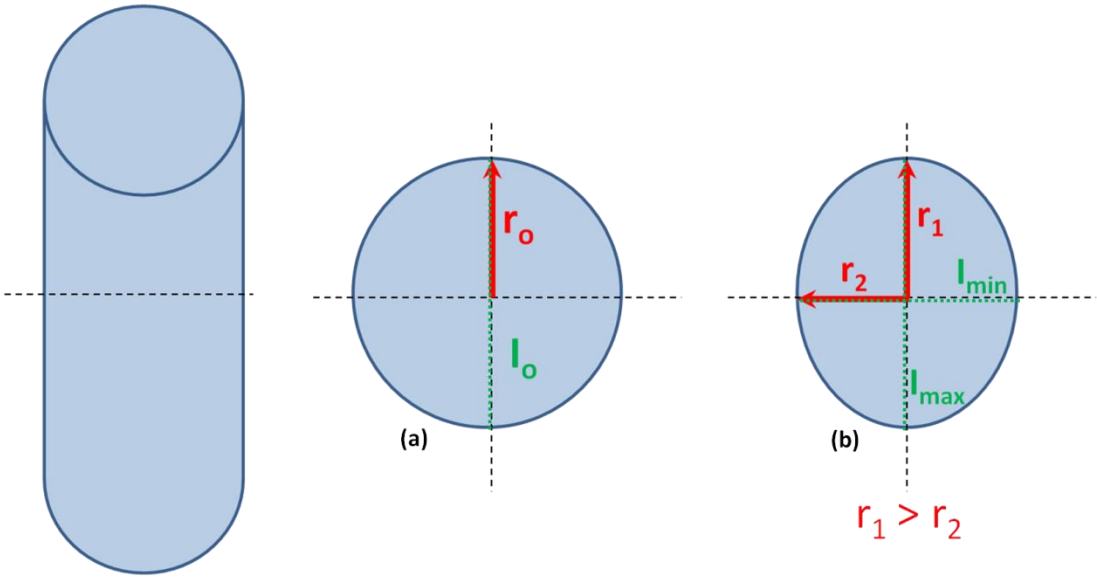

Figure 2.6: Relationship between radius and I of a cylinder with an (a) round cross-section and (b) elliptical cross-section.

$$I_o = \frac{\pi}{4} r^4 \qquad (2.1)$$

Ruff and Hayes (1983a) studied the cross sectional geometries of the tibia and the femur of 119 individuals from the Pecos Pueblo, New Mexico archaeological site. Differences in cross sectional properties were found between the femur and the tibia, and between different sites within each bone. In the tibia, they found the maximum second moment of inertia and the ration between I_{max} and I_{min} was greatest between the midshaft and the proximal end. In the femur, the ratio between Imax and I_{min} was greatest in the proximal end and smallest at the midshaft. These differences corresponded to differences in loading patterns between the two bones.

2.2.10: Geometry - Microstructure Tradeoffs

Skedros (2012) argued that there is a division of labor between modeling and remodeling. Overall stiffness and strength of a bone can be adequately adapted through modeling, however, local changes in toughness and fatigue resistance must be accomplished by remodeling, or else the bone would be too massive and overbuilt. The careful balance between whole bone and local properties requires tradeoffs between the overall geometry and the local microstructure.

The cross sectional geometry of long bones is determined by both the loading conditions of the bone during growth and hereditary factors (Enlow, 1963; Frost, 1973; Susanne *et al.*, 1983; Pandey *et al.*, 2009). Previous studies have shown that there are relationships between the geometric properties of a bone and its tissue level porosity and mineralization. Specifically, the robustness of a long bone, defined here as the cross-sectional area normalized to total length (Jepsen *et al.*, 2011), directly relates to the bone's resistance to bending along the long axis of the bone, with slender bones being

less resistant to bending than robust ones. These relationships may arise from the need for higher elastic modulus to compensate for poor geometry, in terms of bending properties.

Such compensatory relationships have been well-documented using an inbred mouse model (Jepsen *et al.*, 2001; 2003; 2009 Tommasini *et al.*, 2008). In a series of studies, it was demonstrated that while C57BL/6J (B6) and A/J mouse strains had very different overall geometries of their bones, leading to very different polar moments of inertia, they both had similar whole bone stiffnesses and maximum strengths. However, it was found that the tradeoff that allowed these two to have similar properties could be identified in the failure mode. The bones of AJ mice undergo brittle failure while the bones of B6 mice undergo ductile failure (Jepsen *et al.*, 2001; Jepsen *et al.*, 2003). The more brittle post-yield behavior of AJ mice was reflected in a higher ash content (Currey, 1984; Jepsen *et al.*, 2001; 2003), higher mineral to matrix ratio (Courtland *et al.*, 2009; Pathak, 2009), and reduced viscoelastic response (Pathak *et al.*, 2011; 2012).

The relationships between geometry and microstructure have also been studied in humans (Goldman *et al.*, 2005; 2009; Lazenby, 1989; Tommasini *et al.*, 2005; 2007; 2008; Ural and Vashishth, 2006). Tommasini *et al.* (2005; 2007; 2008) studied geometry-property relationships in the human tibia following a similar methodology to that in the Jepsen *et al*. mouse study. Tommasini *et al.* investigated the relationships between measures of cross-sectional geometry, mechanical properties, specifically monotonic failure properties from 4-point bending and damage accumulation, measures of microstructure, specifically porosity and tissue type, and measures of mineralization, specifically ash content. These studies demonstrated that individuals with relatively

slender geometries had different tissue compositions (e.g. higher ash content, increased primary lamellar bone) relative to those with more robust geometries, suggesting that there was a relationship between tissue structure/matrix composition and averaged tissue properties (by ash content) and geometry. Significant positive correlations were observed between measures of bone size and measures of tissue ductility (post-yield strain and total energy) as well as between measures of slenderness and damageability. Significant negative correlations were observed between measures of bone size (moment of inertia and section modulus) and tissue modulus. Significant negative correlations were also observed between measures of cross-sectional geometry and ash content, as well as between geometry and the amount of unremodeled tissue.

2.2.11: Age and Sex Variation

Bone continues to change throughout life, and the accumulation of these changes can cause the bones of an older individual to be different in many ways from those of a younger individual. There is subperiosteal expansion of the long bones with aging, which may counteract the effect of endosteal resorption, which also occurs with aging (Smith and Walker, 1964; Garn *et al.*, 1967; Ruff and Hayes, 1982). Ruff and Hayes (1982) found that both males and females increase their I_{max}, the maximum second moment of inertia, at the midshaft of the femur with age, although females, on average, had an approximately 50% lower I_{max} than males. It was also found that there were only small increases, or even decreases, at the proximal and distal ends of both the femur and tibia, for cross sectional area and second moment of inertia. Ruff and Hayes (1983b) found that overall, both males and females had an increase in subperiosteal area and second moments of area with age. It was also found that while both males and females

experienced endosteal resorption and cortical thinning with age, this effect was more pronounced in females.

Bone also becomes more porous with age, which is largely due to remodeling (Jowsey, 1964; Jowsey, 1966; Martin and Burr, 1982, Cooper *et al.*, 2005; Zebaze *et al.*, 2011; Fiek *et al.*, 1996; Thomas *et al.*, 2005). The local mineralization increases with aging, as the interstitial bone has a low probability of being remodeled (Jowsey, 1964; Jowsey, 1966; Boyce and Bloebaum, 1993; Boyde *et al.*, 1993; Grynpas, 1993; Roschger *et al.*, 1995; Goldman *et al.*, 2005). Schaffler *et al.* (1995) found that with increasing age, there was an increase in microdamage, likely because of the high degree of mineralization for the interstitial bone and the damage was accruing faster than it could be dealt with by remodeling.

Females have a greater incidence of stress fractures than males early in life, and a greater incidence of fragility fractures than males later in life (Jones *et al.*, 1993; Beck *at al.*, 2000). Bone size and shape are known to be important factors for bone strength (Van der Meulen *et al.*, 2001), so sexual dimorphism may be playing a key role (Seeman, 1997). Tommasini *et al.* (2007) found that females have smaller tibia relative to body size than males, but similar tissue level mechanical properties. It was also found that males and females had similar relationships between cross sectional geometry and tissue level mechanical properties.

There are also differences in tissue level organization between males and females. Goldman *et al.* (2005) found that in the midshaft femur, males had a lower proportion of transversely oriented lamellae in newly formed bones than females. The amount of newly

formed bone with transversely oriented fibers decreased with age, for both males and females.

It is important to understand the age and sex related changes in tissue level organization and properties in order to quantify other factors that play a role in bone structure and quality. Bone is a complex and constantly changing biological material system, and there is increasing evidence that there is a level of co-adaption occurring (Jepsen *et al.*, 2001; 2011; Tommasini *et al.*, 2005; 2007; 2008) . There is likely no single variable that controls the co-adaptation, but rather a delicate balance between many different variables. In this work, the roles of geometry, structure, and composition will be investigated.

Chapter 3: Methods

3.1: Introduction

The goal of this research was to investigate the relationships between the overall geometry, the microstructure, and the composition of the human tibia. The results that will be discussed in later chapters indicate that that individuals with slender tibiae (small cross section normalized to total tibia length) were likely to have lower porosity, high ash content, and greater amounts of primary tissue than individuals with more robust tibiae. This research will answer questions raised by previous research and build a framework for a larger and hopefully clinical study. In order to create this framework, it is necessary to link clinically relevant techniques with higher resolution *ex-vivo* techniques. These methods incorporate both two-dimensional and three-dimensional information, allowing a detailed view of the bone. In order to get the information needed for this study, the destructive technique of ashing the bones to determine mineral content was utilized, and by doing micro computed tomography (μCT) imaging on these pieces first, it was possible to determine the thee-dimensional structure, before destroying the samples. The high resolution *ex-vivo* μCT data can be compared directly with the clinically possible peripheral quantitative computed tomography (pQCT) data.

3.2: Sample Population

Cadaveric tibiae from 10 donor individuals (6 male, 4 female, age 37 ± 8 yrs) were obtained from the Musculoskeletal Transplant Foundation (Edison, NJ, USA) and the National Disease Research Interchange (Philadelphia, PA, USA). These represented a subset of the individuals utilized in Tommasini and colleagues (2005, 2007 and 2008)

studies, although the samples used in this work were from the right leg, contralateral to those used in Tommasini's work (and derived from different sites along the shaft).

3.3: Specimen Preparation Methods

3.3.1: Specimen Collection, Initial Sectioning & Storage

Initial sample preparation and storage was performed at Mt. Sinai School of Medicine (MSSM) in New York, NY by the study collaborator Dr. Karl Jepsen and his students. Samples were fresh frozen after collection, wrapped in phosphate buffered saline (PBS) solution. Bones were later thawed for initial sectioning. Two 2.5 mm thick cross sections and one 5mm thick cross section were removed from each tibia at both the 38% and the 66% of total tibia length locations (measured from the distal end of the bone, see Figure 3.1) using a diamond coated band saw (Exakt Technologies, Inc; Oklahoma City, OK USA). While thawed, soft tissue was removed manually to clean the blocks.

The bones were divided into three regional types for classification purposes (see Figure 3.2). There were two longitudinal regions where cross-sections were removed. These are known as *sites*, and consisted of the 38% and 66% regions of the tibia. Each cross-section was divided into 6 radial *wedges*, which divided the cortex radially, into anatomical regions. The cross-sections were divided into *rings*, which separated the periosteal, mid-cortex, and endosteal regions of the bone.

Block A (2.5 mm) and Block B (2.5 mm) (see Figure 3.1) were defatted by first being placed in a 1:1 volume ratio solution of ethanol and diethyl ether for 24 hours followed by a 2:1 volume ratio solution of chloroform and methanol for 48 hours. The

methanol residue was removed by 2 one-hour chloroform baths and the samples were subsequently placed under a 25 mm Hg vacuum overnight to evaporate the chloroform residue. Samples were then placed in a 25 mm Hg vacuum for 4 hours in distilled water in order to rehydrate them, and then stored in PBS solution throughout further processing, remaining frozen at -20 °C before and after each imaging step. Block A (2.5 mm) was imaged using pQCT (XCT 2000; Stratec Medizintechnik, Pforzheim, Germany), and later ashed at 600 °C for 18 h, following the protocols detailed in Tommasini *et al.*, 2008.

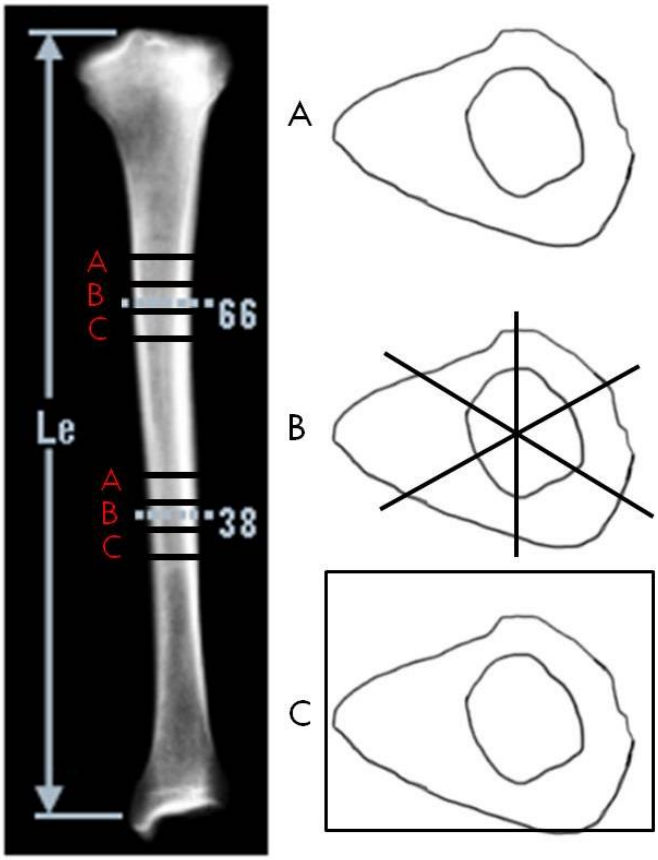

Figure 3.1: Overall schematic of sample locations in the tibia, showing the 3 sample locations at both the 38% and 66% sites. Location A is a 2.5 mm thick cross section used for pqCT and ashing. Location B is a 2.5 mm thick cross section later cut into 6 radial wedges used for µCT and ashing. Location C is a 5 mm thick cross section embedded in PMMA and later made into ~100 µm thick sections histology sections.

Block B (2.5 mm) was further sectioned into 6 radial wedges, as shown in Figures 3.1 and 3.2, and imaged using a Skyscan 1172 µCT scanner (Skyscan, Kontich, Belgium) and then ashed. This initial sectioning was performed at Mt. Sinai School of Medicine (MSSM) in New York, NY by the study collaborator Dr. Karl Jepsen and his students, and samples were then transferred to Drexel University for µCT imaging, then returned to MSSM for ashing.

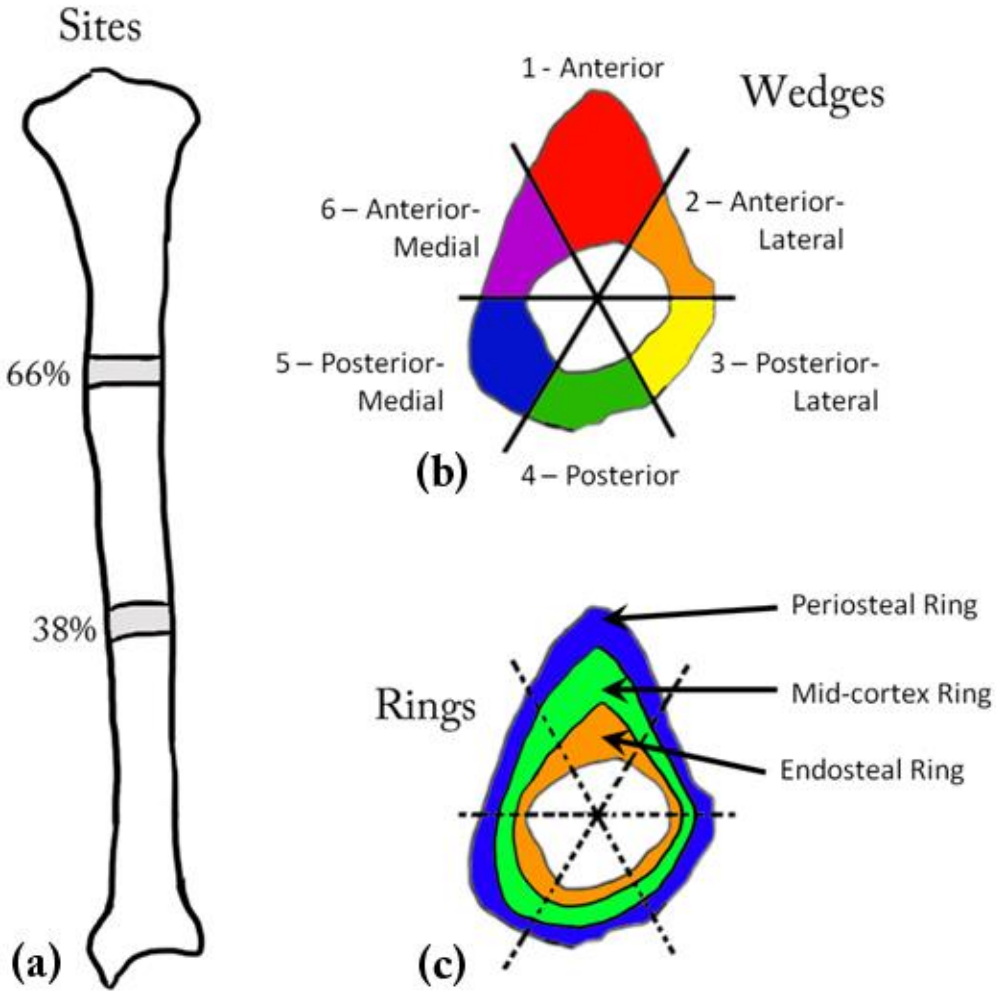

Figure 3.2: The terminology for the locations of the samples. (a) Two cross-sectional sites, (b) six wedges at each site, and (c) three rings at each site.

3.3.2: Preparation of Histological Sections

Block C (5 mm block) was prepared for embedding. The blocks were defatted using the method described above, except the last step was modified so that chloroform residue was removed with an ethanol rinse prior to embedding in poly-methylmethacrylate (PMMA) according to procedures described and modified from Goldman et al. (1999) (see Figure 3.3). Note that in this embedding method, no softener (dibutyl phthalate) was used. This made the resulting PMMA mixture more brittle, but would allow for the utilization of the bone blocks later for Backscattered Electron Microscopy.

Excess PMMA was then trimmed off of one side of each embedded block using a Buehler Isomet 1000 saw (Lake Bluff, IL), and the exposed bone was ground smooth with a series of graded carbide papers, and attached to slides using Technovit 7200 VLC light-cure adhesive (Exact Technologies, Oklahoma City, OK). The mounted block was then cut to approximately 300µm thickness using a Buehler Isomet 1000 saw and ground using a series of graded carbide papers (to 2400 grit) until a thickness of approximately 100 µm was reached (see Goldman *et al.*, 2009 for details). This sample preparation was performed at Drexel University (Philadelphia, PA) by Ashley Campbell.

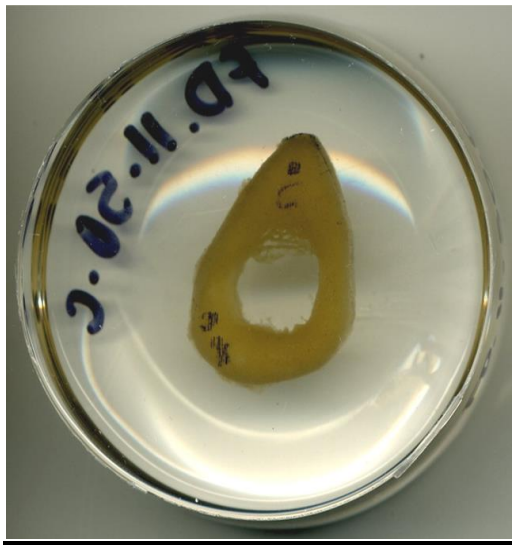

Figure 3.3: Embedded 5 mm cross section before sectioning and preparation for histological imaging.

3.4: Data Acquisition Methods

3.4.1: Peripheral Quantitative Computed Tomography

3.4.1.1: Background of the technique

Peripheral quantitative computed tomography (pQCT) is a form of computed tomography (CT). CT is a three-dimensional radiographic absorptiometric measurement. Imaging is done in two steps, scanning followed by reconstruction. During the scanning phase, x-rays are passed through the sample to a detector on the opposite side, to get a projection x-ray image of the sample. This is done at many different rotation steps to obtain a full set of projections. In the second step, reconstruction, the projections are processed using a computer algorithm in order to obtain a three-dimensional structure of the sample. In order to obtain quantitative density measurements from a CT, standards are used to standardize the gray level values and to help account for soft tissue (Sievänen

et al., 1998). When this is done it is called Quantitative Computed Tomography (QCT). In a living person, QCT can only be performed at peripheral sites, such as the tibia and the radius (Tysarczyk-Niemeyer, 1997), thus it is termed peripheral QCT (pQCT). This is due to constraints on the size that can fit into the machine and because areas that have a large amount of surrounding soft tissue would require too much radiation to go through and could not be safely scanned.

pQCT can be used clinically or on cadaver bones, as was the case for this research, to determine morphological traits, and tissue mineral density (TMD). The resolution of pQCT is high enough to distinguish cortical from cancellous bone areas, which makes it is possible to get cortical TMD measures. The bone mineral density (BMD) measured from regular CT or dual-energy X-ray absorptiometry (DEXA) include the cortical, cancellous, and marrow cavity, and therefore are not a good measurement for a study of the cortical bone. pQCT is a three dimensional technique, while DEXA is only a two dimensional technique.

3.4.1.2: Imaging methods for the current project

Imaging was performed at Mt. Sinai School of Medicine (MSSM) in New York, NY by the study collaborator Dr. Karl Jepsen and his students on a XCT 2000L (Stratec Medizintechnik, Pforzheim, Germany) with a 0.14 voxel size resolution. An adapter was made to hold a clear plastic tubular container with an opening on the anterior surface to accommodate tibiae and enough 1X phosphate buffered solution (PBS) in order to cover the tibia in fluid to simulate soft tissue. Scans were taken at 25%, 38%, 50%, 66% and 75% of total tibia length, taking the distal end plate as the starting reference point, but only the 38% and 66% were used for this study, see Figure 3.1. Data for cross-sectional

area, total bone length, the location of the centroid, and cortical TMD were collected at each of the two sites. The cortical TMD data were included as variables in the statistical analysis along with the other variables mentioned below. The pQCT determined centroid was used to divide the dataset into 6 wedges, with the primary axis defined as the line through the centroid and the anterior tip of the bone.

3.4.1.3: Calculation of robustness

$$\text{Robustness} = \frac{\text{cross sectional area}}{\text{tibia length}} \quad (3.1)$$

Skeletal robusticity, generally speaking, is the strength of a bone as reflected by its geometry (size and shape), and has been calculated many different ways (Jepsen, *et al.* 2003; Tommasini, *et al.* 2005; 2007; 2008; Kimura, 2006; Stock and Shaw, 2007). Originally, the term was used to describe diaphyseal thickness normalized to bone length (Martin and Saller, 1957; Bräuer, 1988). According to Stock and Shaw (2007), interpretations of robusticity are dependent on measures of body size. Bone length correlates well with height, but less so with body weight, which has been found to be a larger contributor to mechanical loading and long bone diaphyseal dimensions (Ruff *et al.*, 1993; Ruff, 2000). According to Ruff (2000), cross-sectional area should be standardized to body weight. For this work, robustness was defined as simply the cross-sectional area normalized by tibia length (see 3.1), without including body weight, as this measure adequately reflected the biological relationships associated with growth both in

width (area) and length (Jepsen, *et al.*, 2011). It was specifically decided to not include body weight in the calculation of robustness, as in order to better allow for the investigation of the local effect that bone size and shape has on the composition and microstructure of bone, rather than the global effect of body weight. The goal is to try to answer a question about the effect of geometry, and by excluding body weight from the calculations, this can be better achieved. The cross-sectional area was determined from the pQCT images for both the 38% and the 66% location. Due to the geometry of the tibia, for any individual, the 66% location was more robust than the 38% location. For some analyses, samples were further categorized as either 'slender' (defined at the 38% location as robustness <1.0 and at the 66% site as robustness <1.5) or 'robust' (at the 38% location as robustness>1.0 and at the 66% site as robustness>1.5). N=5 for all four groups.

3.4.2: Micro Computed Tomography

3.4.2.1: Background of technique

Micro computed tomography (μCT) is a very high resolution computed tomography imaging technique. Due to the high levels of radiation and small sample area, for humans, it is only possible to carry out imaging on cadaver bones. μCT can be performed *in-vivo* in small animals, such as mice, however, the resolution is lower for *in-vivo* imaging than it is for *ex-vivo* imaging. With CT for *in-vivo* studies, the subject stays still, and the X-ray source and detector rotate around the subject. For *ex-vivo* μCT, the X-ray source and detector do not move, and the sample rotates (see Figure 3.4).

In bone research, μCT is largely used for studies on trabecular bone or to simply calculate total cortical area. At moderate resolution, the structure of the trabecular bone

can be determined (Borah *et al.*, 2001; Jinnai *et al.*, 2002), as well as the overall amount and distribution of cortical bone (Particelli, et al., 2011). However, at high resolutions, aspects of the structure of cortical bone can be studied. Cooper *et al.* (2004) compared the results from µCT and microradiographic techniques of cortical porosity in the human femur, for quantifying cortical porosity, mean pore area, and pore density. Their scans utilized a 10 μm^3 voxel for each pixel resolution, and it was found that the bias between the two techniques was small and the repeatability showed no significant difference between the two methods for cortical porosity and mean pore area. There was, however, a significant difference between the two for pore density, which indicated that a resolution of greater than 10 μm^3 was necessary. Cooper *et al.* (2007) determined that a voxel size of 5µm, would not detect the smallest pores, such as osteocyte lacunae, but it was acceptable for detecting much of the cortical porosity (including primary vascular canals, Haversian canals, Volkmann's canals).

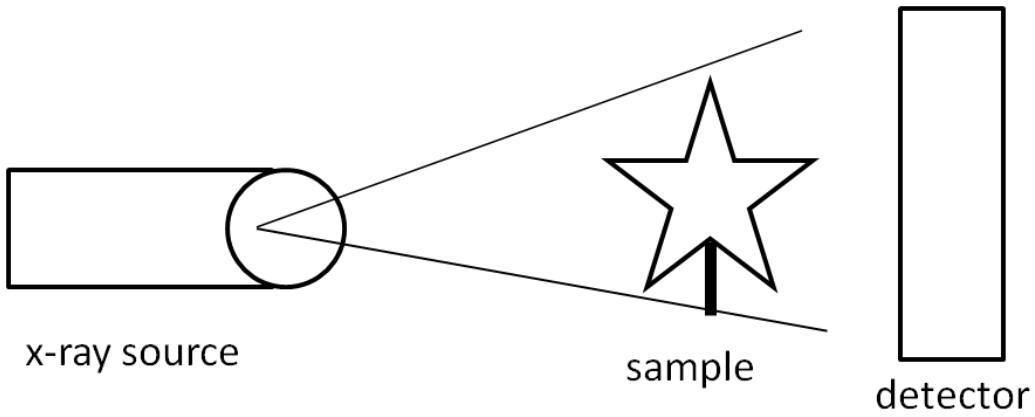

Figure 3.4: Schematic of computed tomography setup. X-rays from the source pass through the sample to the detector to form a projection image.

3.4.2.2: Imaging methods for the current project

The μCT imaging, processing, and analysis was done or overseen at Drexel University by the author using a Skyscan 1172 μCT (Skyscan, Kontich, Belgium). For each individual, two locations in the tibia were imaged using μCT, 38% and 66% of total tibia length. The middle block was used for the μCT imaging, which was 2.5 mm thick and divided into six wedges as describe above in the specimen preparation section (see Figure 3.2). The samples remained frozen until just prior to imaging, and were refrozen directly thereafter.

The scanning protocol was chosen based on a compromise of scan time and scan quality. Samples could not be mounted with a medium to secure them during imaging, as they were to be sent back to MSSM after imaging for ash content experiments. During imaging, the samples needed to stay hydrated, so in order to minimize the risk of them drying out, scan times needed to be reduced as much as possible. Compromises were made on the rotation step size and the number of frames averaged in order to have acceptable scan times.

In order to complete the imaging phase in a timely fashion so that the ash content could be completed, samples were batch scanned, with all six wedges from one site (66% or 38%) of a single individual stacked vertically and scanned together. Each wedge was individually wrapped in Parafilm with some PBS and taped to the sample below it in the stack. The set of samples were places in a plastic vial, which was fixed to the sample holder in the μCT. Due to the inability to affix the samples directly, there were movements in some of the samples, requiring some blocks to be rescanned. Those

samples were rescanned using moist laboratory tissue to wedge the samples in place, rather than Parafilm packages.

There were two other unavoidable sources of noise in the µCT scans. The first was the shape of the samples themselves. µCT works best with cylindrical samples aligned with the axis of rotation of the sample holder; the worst sample shape is a beam, which was the general shape of the bone wedges used in this experiment. This meant that at some rotations, the X-rays only needed to travel a short distance through the sample, and at other rotations the X-rays must travel a far distance through the sample. Lastly, during long scans, fresh samples were prone to movement due to thermal changes in the sample. This, combined with the conditions of the scans, led to some noise that had to be dealt with in post-processing.

The following parameters were used, resulting in scan times of approximately six hours per batch (see Table 3.1).

Table 3.1: Data acquisition parameters for µCT imaging

Parameter	Setting
Camera setting:	near
Filter	Al 1.0mm
Camera pixels	2000 x 1048
Resolution	4.8 µm
Rotation Step	0.50^{o}
Frame averaging	10
Camera offset	yes
Oversized Scan	yes
360^{o} Scan	no

3.4.2.3: µCT reconstruction

The reconstruction of the images was performed by the author at Drexel University using the manufacturers software, NRecon (Skyscan, Kontich, Belgium). The optimal parameters were determined for each sample individually, which led to the gray level values not being usable for quantitative analysis. During reconstruction, beam hardening, post alignment, and ring artifacts were all corrected for. After the data were reconstructed, they had to be digitally realigned in such that each image was a transverse slice through the wedge, in anatomical configuration. This was done in the manufacturer's software, Dataviewer (Skyscan, Kontich, Belgium), which allowed for the

alignment of the set of three-dimensional data in all three planes, and then save the properly aligned dataset, see Figure 3.5.

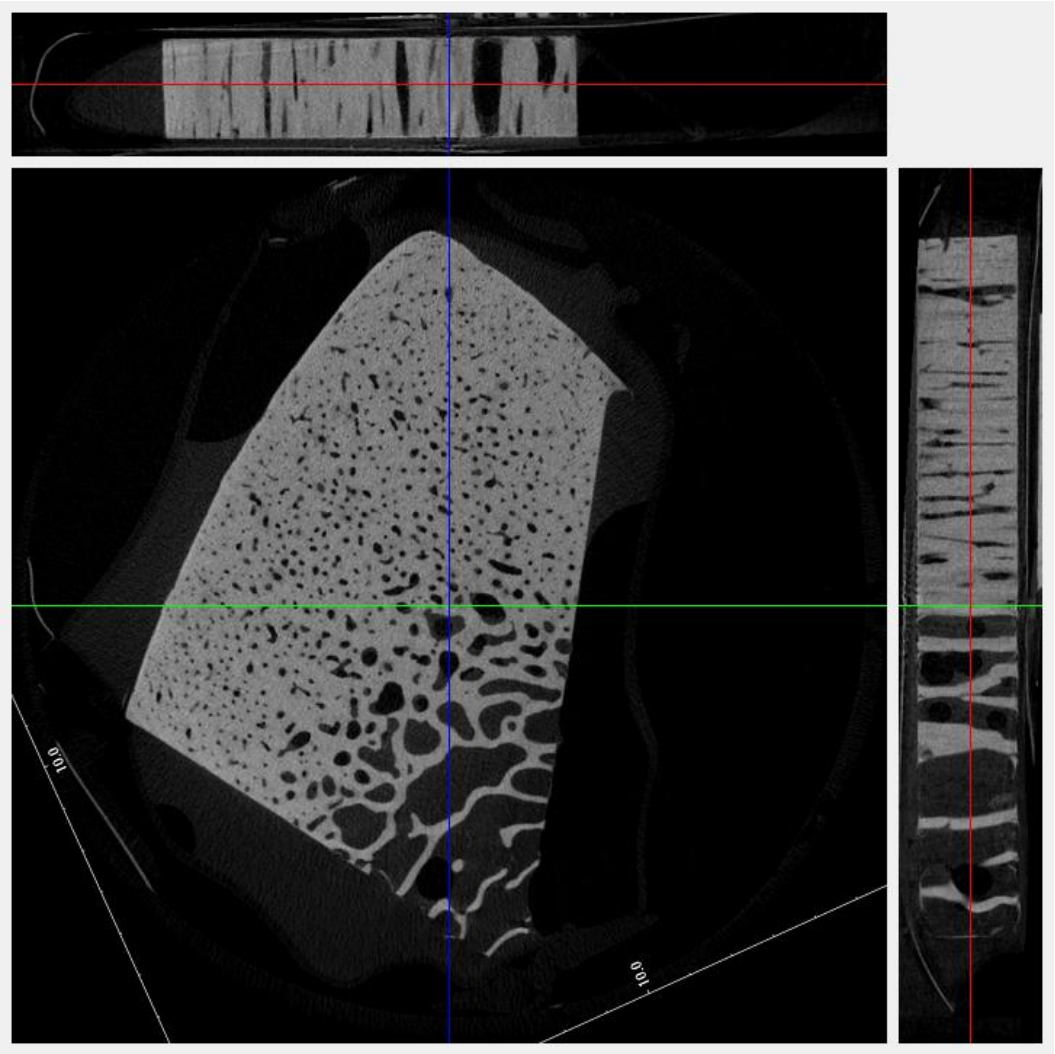

Figure 3.5: Screen capture from DataViewer (Skyscan, Kontich, Belgium) used for aligning the dataset. The three projections allow for proper alignment.

3.4.2.4: µCT region of interest selection and noise reduction

The first step in creating the final image set was the selection of a region of interest (ROI) that included all of the cortical bone but not the cancellous bone or empty space for each wedge. To do this, a coarse ROI was hand drawn around the outside of the bone and precisely at the junction between the cortical bone and cancellous bone. This junction was often very hard to determine, so for this work, it was defined as the point beyond which approximately 50%, by visual determination, was pore (see Figure 3.6). For each sample, the determination of this junction was verified by another researcher in the lab. This ROI was "shrink wrapped", meaning it formed itself to the edge of the bone as part of the processing.

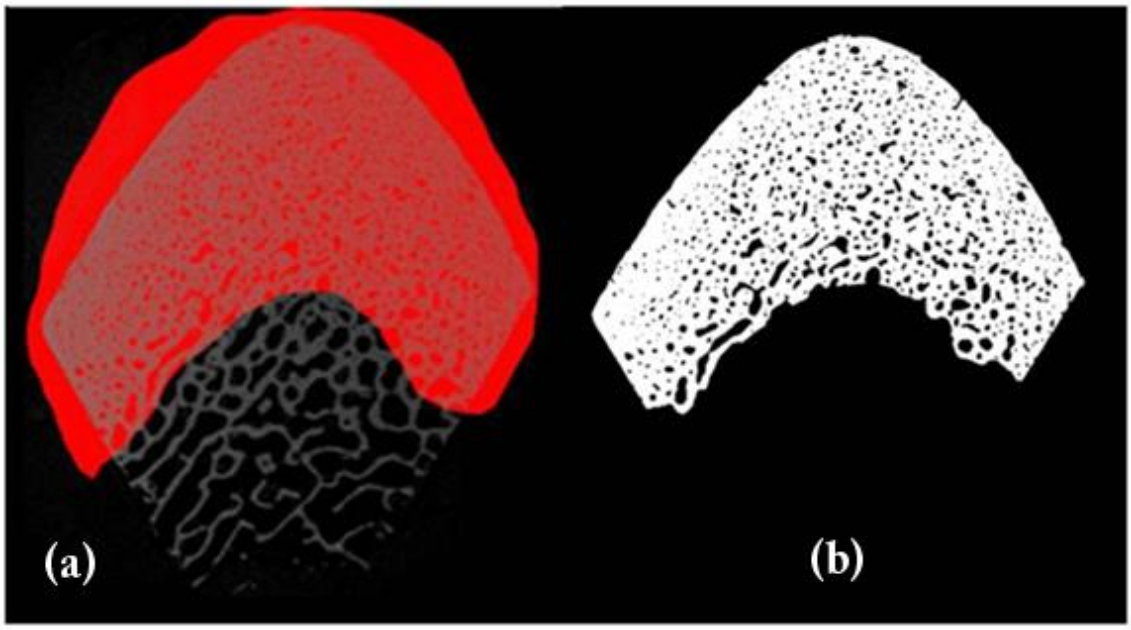

Figure 3.6: Post processing for separating the cortical bone from the cancellous bone. (a) The coarse ROI around the cortical bone in the unprocessed image and (b) the final binary image.

In order to reduce the noise in the images, the first step was to filter the entire image set using a 1 pixel median filter, which was done in Image J (National Institutes of Health, Bethesda, Maryland). The rest of the noise reduction steps were performed as part of a task list in Skyscan analysis software, CTAnalyzer (see Table 3.2).

Table 3.2: Noise reduction steps for μCT images

1.	Thresholding - binarize the image based on a hand selected value.
2.	Sweep - removed all but the largest object, so all unattached bone was removed in 2D.
3.	Despeckle - remove all black speckles less than 5 pixels in area.
4.	Opening - radius 2 pixels - dilate by 4 pixels inside all pores followed by erode by 4 pixels.
5.	Sweep - removed all but the largest object, so all unattached bone was removed in 2D.
6.	ROI Shrink Wrap.
7.	Erosion - erode the ROI by 2 pixels.
8.	2D Analysis - yielded data to be analyzed, including tissue volume and pore volume.

Particularly noisy samples were run through an additional opening and/or closing step in order to remove small areas of porosity that might be due to noise or might

represent small primary vascular canals, so that the final measure would better represent only those pores that are a result of remodeling. A final despeckling step was added to remove all black (pore) regions with an area in two-dimensions of greater than 300 pixels, which was larger than the largest Haversian canals found in the sample using histological approaches. This was done to eliminate large pores, usually towards the endosteal boundary, that might reflect the process of endosteal consolidation and/or trabecularization, rather than the process of intracortical remodeling. Figure 3.7 shows examples of three dimensional rendering of the pore structure obtained from a wedge from a slender and a robust individual.

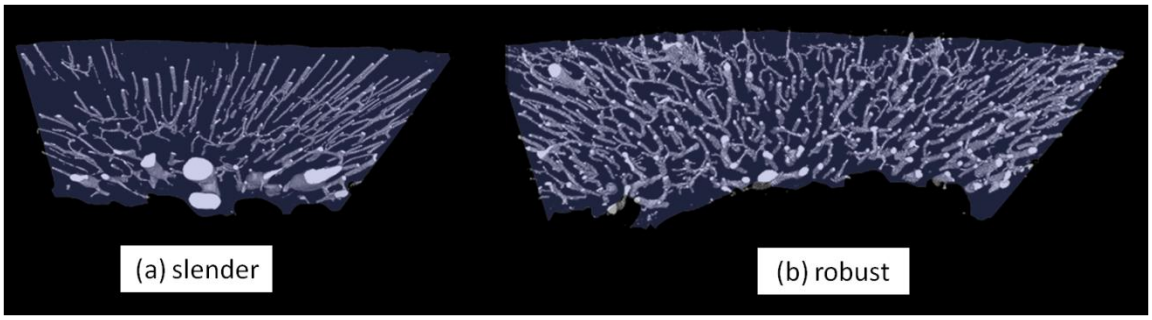

Figure 3.7: Three dimensional pore structure of a wedge from a (a) slender individual and (b) robust individual

3.4.2.5: ROIs within the rings

Three regions of interest (ROIs) were extracted from each wedge, one for each ring, endosteal, periosteal, and mid-cortex, provided that the wedge was wide enough along its center-line to accommodate three 1mm x 1mm x thickness of the sample ROIs (see Figure 3.8). ROI selection was automated by a Matlab® (Mathworks, Natick, MA)

program that chose the periosteal and the endosteal ROIs such that they were as close to the edges of the bones as possible, while staying completely within the bone. The mid-cortex ROI was spaced halfway between the periosteal ROI and the endosteal ROI, when the cortical thickness was great enough to allow all 3 ROIs without any overlap. In the cases of the thickness not being great enough, the midcortex ROI was chosen to be a set distance from the edge of the periosteal ROI and no endosteal ROI was extracted.

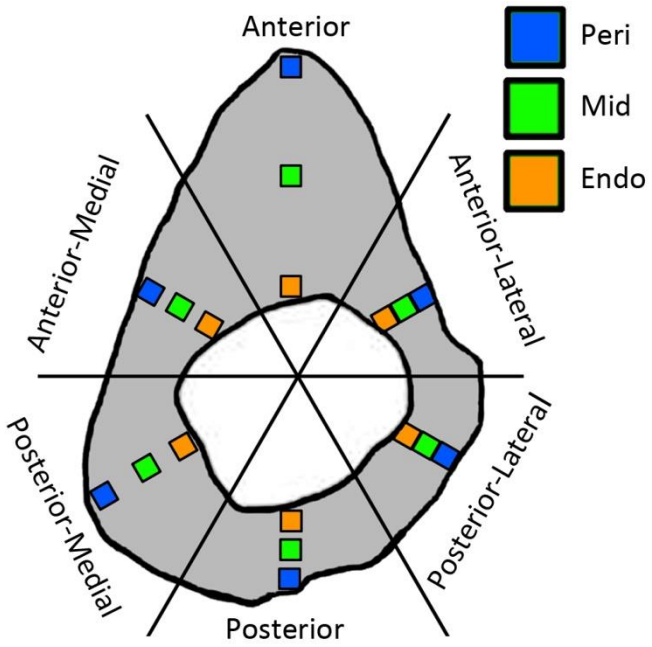

Figure 3.8: Regions of interest for each ring around the cortex: endosteal, mid-cortex, and periosteal.

3.4.3: Ash content

3.4.3.1: Background of technique

Bone is a two-part composite material consisting of an organic phase, collagen, and an inorganic phase, a mineral similar to hydroxyapatite. The mineral content of the bone has a large impact on the mechanical properties of the bone. Bone with a high degree of mineralization has a higher elastic modulus and fracture stress compared to less mineralized bone, however overly mineralized bone can become brittle (Vose, 1959; Currey, 1969; Bonfield and Clark, 1973; Pathak *et al.* 2011; 2012). While elastic modulus was not measured as a part of this project, the relationship between mineralization and elastic modulus is extremely important. Elastic modulus is the slope of the stress-strain curve, and as such, a stiffer material will have a higher elastic modulus. By measuring the ash content, some rough insight into the elastic modulus can be determined.

Ash content is a coarse volumetric measure of the amount of mineral in a bone sample. The technique is destructive since it requires the bone to be completely burned (or ashed) in order for the organic component to be burned away, leaving only the inorganic component. The longer bone stays in the body, the more mineralized it becomes, so older tissue will have a higher ash content (Jee, 2001). Bones with a lower remodeling rate would have a higher ash content for the same reason, as bone is staying longer in the body rather than being replaced. Studies have also found a relationship between ash content and age of the individual, with ash content increasing with age (Arnold *et al.*, 1966; Currey, 1979; Currey *et al.* 1996). There have also been studies linking ash content with mechanical properties such as failure stress, modulus of

elasticity, static strength. work to failure, and impact strength (Vos and Kubala, 1959; Currey, 1969).

3.4.3.2: Other techniques that provide information about mineralization density

Although many techniques are utilized to measure 'mineral density', or 'tissue mineral density', such measures are not synonymous with measures of tissue mineralization density. DEXA (dual energy x-ray absorptiometry) is a coarse clinical technique that measures areal density, taking into account both the mineralization of the bone tissue and the porosity. As a 2-dimensional technique with low resolution, DEXA cannot distinguish between cortical and cancellous bone or even eliminate the porosity of the medullary cavity. Computed tomography can be used to measure volumetric density, both at the clinical scale (pQCT) and non-clinical (μCT) (Delmas and Seeman, 2004; Engelke *et al.*, 2009). At the resolution of both techniqes, some intercortical porosity is still included, so again, these are not truly measures of tissue mineralization. Both techniques, however, can destinguish what is cortex and get volumetric information on that bone specifically. pQCT cannot detect intercortical porosity.

μCT with high resolution applications (e.g. a 5 μm resolution), on the other hand, can detect most intracortical porosity and remove it from analysis, and if used with phantoms, can provide information that is reflective of tissue mineralization. A polychromatic X-ray source, as used in desktop μCT units, requires a typically hydroxyapatite (HA) phantom to be used to determine quantifiable mineralization, due to the beam hardening problem (Burghardt *et al.*, 2008; Nazarian, 2008; Zou *et al.*, 2011) A monochromatic x-ray source, as used in synchotron radiation micro-computed

tomography (SR-μCT), does not have a beam hardening problem, and therefore does not require a phantom (Bonse and Busch, 1996; Nuzzo, 2002; Raum *et al.*, 2006; 2007; Rohrbach *et al.*, 2012). For this study, due to time and expense constraints, there was no attempt to use phantoms and achieve quantifiable mineralization data from the μCT scans.

There are many specific mineralization methods that can be used at a very fine scale, which can provide quantitative information on the amount of mineral present in the tissue, such as quantitative microradiography (Engstrom, 1952; Amprino, 1958; Vincentelli and Evans, 1971; Martin and Armelagos, 1985) or quantitative backscattered electron microscopy (qBSE) (Boyde *et al.*, 2005; Roschger *et al.*, 2008). There are other techniques that can be used to determine the type of mineral phase present and changes in the mineral and matrix, such as Fourier Transform Infrared Spectrocopy (FTIR) and Raman Spectroscopy because the spectra of the mineral components are distinct (Akkus *et al.*, 2003; Boskey *et al.*, 1992; 1999 Boskey and Mendelsohn, 2005). These techniques were not part of the design for this project, however care was taken to prepare the samples in such a way that they could be later performed on the remaining embedded bone blocks and/or histological sections.

3.4.3.3: Methods for the current project

After being imaged by pQCT, the cross section was ashed and following μCT, the wedges were ashed, following the methods of Tomassini *et al*. (2008) as described below. Ashing was performed by Felipe Guillermo at Mount Sinai School of Medicine (New York, NY) and data was given to the author for analysis at Drexel University

(Philadelphia, PA). Samples were defatted, rehydrated, and degassed. The sample volume was determined by Archimedes principle. The submerged mass was determined while the samples were submerged in water. Samples were subsequently reweighed after being put through a centrifuge at 3600 rpm with a 16.5 rotor radius for 20 minutes in airtight containers, to obtain the hydrated weight. Samples were weighed once more after drying at 80°C for 21-24 hours until the weight was constant to determine the dry weight. The samples were then ashed at 600°C for 18 hours and reweighed for the ash weight. The final ash content number used was *ash content = hydrated ash weight/sample volume* and *sample volume = hydrated weight-submerged weight*

3.4.4: Histology

3.4.4.1: Background of technique

High resolution optical microscopy allows for various aspects of tissue level organization of bone to be visually discernible. The preparation techniques used resulted in non-decalcified (mineralized) tissue sections. Hence they were not suitable for any studies looking at cells or other soft tissue components, but could be used for a variety of light microscopy based studies including histomorphometric analysis (Parfitt, 1983; Stout *et al.*, 1999), tissue type analysis (McFarlin, 2006; Goldman et al., 2009), and collagen fiber orientation (Boyde and Riggs; 1990; Riggs *et al*., 1993a; 1993b; Bromage *et al.*, 2003; Slayter and Slayter, 1992; Goldman et al., 2003a). The study focused on tissue type analysis. Further, the sections created could be utilized later for imaging in a variety of other techniques, from qBSE, to Raman Spectroscopy, to confocal microscopy. Although staining of the sections could help increase the contrast and visibility of many features, it was not necessary for the purposes of this study.

3.4.4.2: Methods for the current project

Sections (approximately 100µm in thickness; taken from Block C as described in the Specimen Preparation section above) were temporarily coverslipped with glycerin and imaged in their entirety by transmitted (TL) and circularly polarized light (CPL) using a 5x objective on a Zeiss Axioplan 40 (Wexlar, Germany) light optical microscope with an automated stage and an Optronix (South Burlington,VT) digital CCD camera. Focusing and image stitching were controlled through MBF Bioscience's Stereo Investigator (South Burlington, VT) using the Virtual Slice add-on module. The TL and CPL images were layered in Adobe Photoshop (Adobe, Jose, CA) with the opacity of the CPL layer reduced to allow for a combined image, (Figure 3.9). The combined image, as well as the individual images, were run through a custom Matlab® (Mathworks, Natick, MA) program that saved regions of interest following the schematic shown in Figure 3.8, as well as strips that encompassed all three regions of interest for each wedge. The regions of interest were 1.5 mm x 1.5 mm to allow for a wider field of view, beyond the area that was being traced. These ROIs corresponded approximately to the location of ROIs extracted from the MicroCT datasets, and the terminology used (site, wedge, ring) was consistent between the two methodologies.

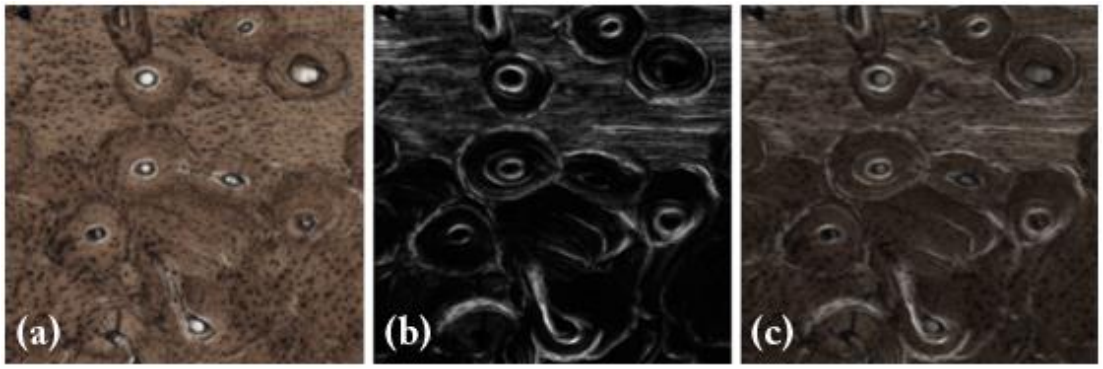

Figure 3.9: Histological thin sections imaged by (a) transmitted light (b) circularly polarized transmitted light, (c) a combination of the transmitted and circularly polarized light images. (Field Width = 1mm)

For the purposes of the present study, only the periosteal and mid-cortex ROIs were included in the analysis. Much of the porosity in the endosteal region is heavily influenced by former trabecular bone that during growth consolidates and becomes cortical bone. This leads to large variations in porosity that may not relate to intracortical remodeling.

Primary bone area, secondary bone area, primary pore area, and secondary pore area were hand traced for each ROI (Figure 3.10) in Adobe Photoshop (Adobe, Jose, CA) using a Wacom (Vancouver, WA) graphics tablet, following the methods of McFarlin (2006). The methodology for extracting regions of interest was developed by the author, with programming assistance from Jerrald Chen (DUCOM Medical Student). The author also developed the methodology for tracing tissue types, and collected data from ROIs derived from two of the six wedges (total of 4 ROIs total from the 66% location). David Lin (DUCOM MS student) repeated the measures from these same ROIs, to determine *inter*-observer error and ensure the methods were repeatable. Data sets were comparable,

therefore Lin continued the tracings for all ROIs (12 total for each location) and data from his tracings were utilized for subsequent analysis.

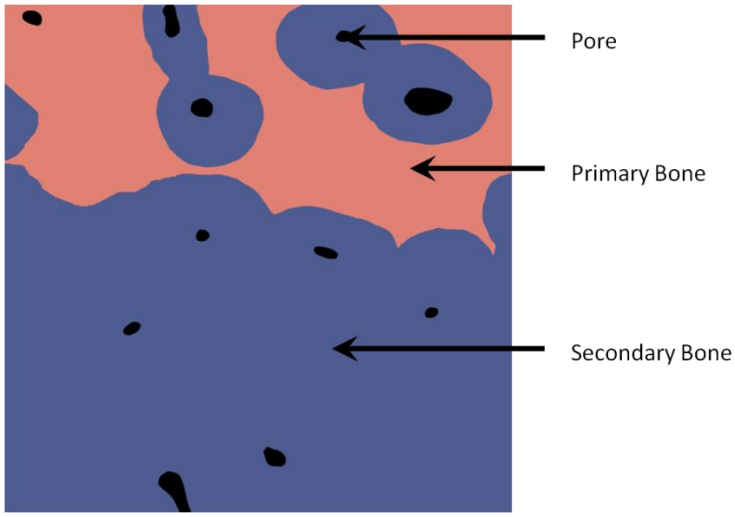

Figure 3.10: The different tissues types after determination and hand tracing. (Field Width = 1mm)

Primary bone was defined as all circumferential lamellar bone and primary osteons. Circumferential lamellar bone can be identified by long regular sheets with low curvature, and if it does have curvature, it generally follows the curvature of the outside cross section. Primary osteons were identified as being surrounded by primary tissue and lacking a cement line. Secondary bone was defined as the remaining area that was not pores, which included secondary osteons, osteon fragments, and secondary interstitial bone. Pores running perpendicular to the surface of the bone were easily traced in their entirety. Only the portion that was in focus in the plane the section was imaged was traced for drifting pores and pores parallel to the surface of the bone. The data for

secondary bone area and secondary pore area were combined to create a secondary tissue area, and from this, a percent secondary tissue was calculated.

The data were analyzed using the statistical software package SPSS (IBM, Armonk, New York) or using Excel® (Microsoft, Redmond, WA). The specific data analysis methods are described in detail within each of the data chapter, as they reflected the specific questions of that chapter. Significance was defined for this work as $p < 0.05$.

Chapter 4: Inter-individual Relationships

4.1: Introduction

Numerous studies have shown that individuals whose bones have more slender geometries are at higher risk for stress fracture in the tibia (Beck *et al.*, 1996; Milgrom *et al.*, 1989). This increase risk may come from tissue composition as well as geometry. It appears that slender individuals compensate for poor geometry by increasing tissue level stiffness (Tommasini *et al.* 2005; 2007; 2008). This results in bone cortices capable of resisting everyday loads, but which may result in decreased tissue ductility and toughness owing to a higher degree of tissue mineralization density (Currey, 2003), which may in turn result in functional inequivalences for slender vs. robust individuals. This tradeoff between increased stiffness and decreased ductility and toughness may be due to the limited range in which bone cells can adjust tissue modulus (Jepsen *et al.*, 2011) and the biological requirements for the bone, such as vascular support.

There are still many questions remaining about the coupled biological responses, or co-adaptations, that may be occurring in the tibia. What mechanism is creating these differences in tissue level stiffness? Is there a different mineralization mechanism in slender bones, or are they laying down bone in the same way, but at a different rate? It is difficult or impossible to study mineralization mechanism differences in a cross-sectional cadaveric human sample, and dynamic studies of remodeling rate cannot be done, however, histological signatures of the remodeling process can be investigated to determine whether remodeling rate may differ between slender and robust individuals.

In order to investigate the possible relationships between robustness and remodeling, the first step was to see if a remodeling signature could be seen on a cross-sectional scale

using porosity and ash content as a reflection of the remodeling process. These were coarse measures that could be quantified readily across an entire section and be used to initially test whether remodeling varied between slender and robust individuals. These measures also have the advantage of being relevant to currently available clinical level imaging techniques (Jepsen *et al.*, 2011). In addition to porosity and ash content , it is important to look at histological measures of secondary bone, as a more direct link to remodeling.

The specific aim of this investigation was to study the relationships between aspects of tissue quality, specifically the amount of porosity, ash content, tissue mineral density, and tissue type, relative to bone robustness at the whole cross-section level, in order to better understand the tissue level adaptations that may occur in the establishment of whole bone function. It is hypothesized that intracortical remodeling was suppressed in slender tibiae, leading to an increase in the average mineralization of the bone tissue. Tissue with a higher degree of mineralization was stiffer, and better able to resist bending, thus the overall bending properties of a slender tibia are brought closer to that of a robust tibia. Conversely, remodeling does not need to be suppressed in robust tibiae, and in fact is needed to maintain adequate porosity so that the bones will not contain too much mass and thus be metabolically expensive to maintain and function in locomotion. To test these hypotheses, intracortical porosity, pQCT derived tissue mineral density and ash content were examined as measures reflective of intracortical remodeling rate. It was expected that slender individuals would demonstrate reduced cortical porosity and increased tissue mineralization (as measured by ash content) reflective of suppressed remodeling. Similarly, increased tissue mineral density, as measured by pQCT, would

also be reflective of this suppressed remodeling, owing to the effects of both decreased porosity and increased tissue mineralization.

4.2: Methods

4.2.1: Sample Population

Cadaveric tibiae from 10 donor individuals (6 male, 4 female, age 37 ± 8 yrs) were obtained from the Musculoskeletal Transplant Foundation (Edison, NJ USA) and the National Disease Research Interchange (Philadelphia, PA, USA). These represented a subset of the individuals utilized by Tommasini and colleagues (2005, 2007 and 2008) studies, although the samples used in this work were from the right leg, contralateral to those used in Tommasini's work (and derived from different sites along shaft).

4.2.2: Sectioning and Imaging

The methods used are described in detail in Chapter 3, but are briefly as follows. Two 2.5 mm thick cross sections and one 5 mm thick cross section were removed from each tibia at both the 38% and 66% of total tibia length locations (measured from the distal end of the bone, see Figure 4.1).

The first of the 2.5 mm sections was imaged using pQCT (XCT 2000; Stratec Medizintechnik, Pforzheim, Germany), to determine the morphometric trait of robustness, defined as cross-sectional area divided by total tibia length (see Figure 4.1), and to determine tissue mineral density (Ct.TMD).

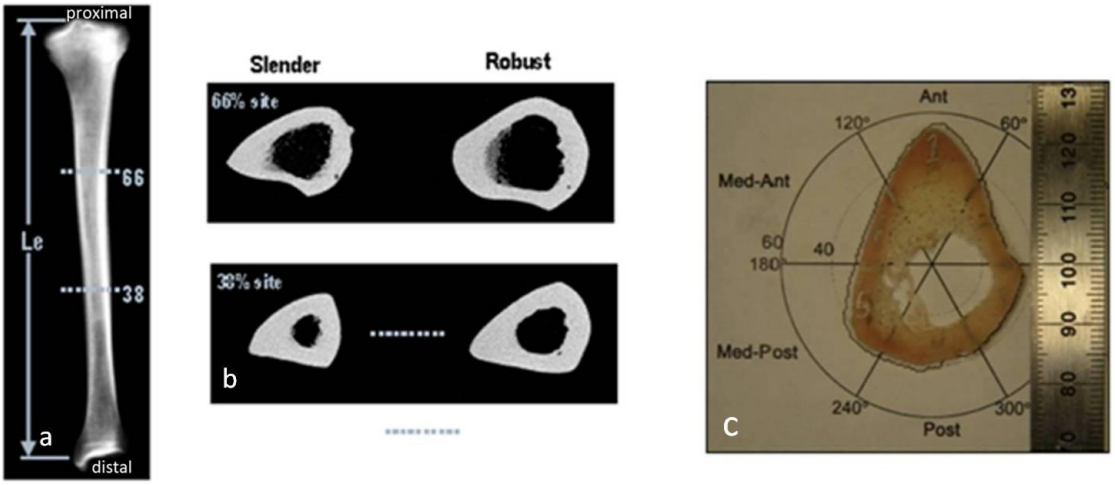

Figure 4.1: (a) Overall shape of the tibia, imaged using pQCT. (b) pQCT images of cross-sections from both the 38% and 66% location of a slender and a robust individual. (c) Photograph of a cross-section with the 6 radial wedges marked.

The second set of cross-sections was further sectioned into 6 radial wedges, as shown in Figure 4.1. The radial wedge samples were imaged using a Skyscan 1172 µCT (Skyscan, Kontich, Belgium) following the procedure detailed in Chapter 3. Images were reconstructed at a 5 µm pixel size, which was sufficient resolution to capture the vascular spaces, but not osteocyte lacunae. A number of noise reduction steps were performed and a region of interest (ROI) was manually selected (see Figure 4.2) from each dataset to exclude cancellous bone (defined visually as regions with greater than ~50% porosity) . For each wedge, total tissue volume (Tt.V) and total canal volume (Tt.Ca.V) were measured. Porosity (Ct.Po, %) was calculated as canal volume normalized by total tissue-volume. These were combined to make a single measure of porosity for the entire cross-section. Additionally, following the procedures outlined in detail in Chapter 3, ROIs were extracted at the endosteal region, the mid-cortex region, and the periosteal region. For this investigation, only the mid-cortex region of interest were evaluated and the porosity

for mid-cortex of all six wedges was combined to give an average cross-sectional porosity for the mid-cortex. The wedges were ashed after μCT imaging, following the procedures outlined in Chapter 3, to obtain compositional data (ash content).

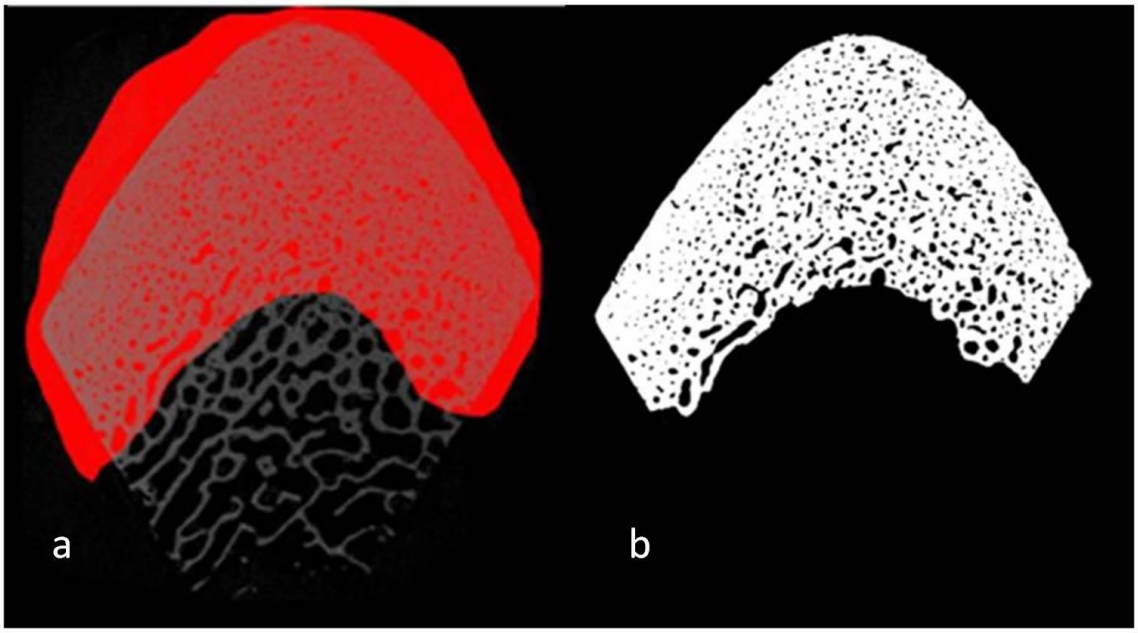

Figure 4.2: (a) Single reconstructed slice from μCT showing the coarse ROI used to remove the trabecular bone before image processing. (b) The same slice after removal of trabecular bone and binarization.

The third cross-section set was fixed, defatted, embedded in PMMA, and cut and thinned to approximately 100μm thick sections fixed to slides. These sections were imaged in their entirety by transmitted and circularly polarized light using a 5x objective, and these two images were combined to make a final image (see Figure 4.3), from which twelve 1mm by 1mm ROIs were extracted as shown in Figure 4.3c. Primary bone area, secondary bone area, primary pore area, and secondary pore area were hand traced for

each ROI (see Figure 4.3e), as described in detail in Chapter 3. The percent secondary porosity (all pores not attributed to primary osteons) and percent secondary tissue were combined to give an overall percent secondary bone value for each ROI. For this work, only the secondary bone data from the 6 mid-cortex regions of interest were analyzed, with data combined to give an average secondary bone for the cross-section at the mid-cortex. Tissue blocks were removed, cleaned, and embedded at Mount Sinai School of Medicine (MSSM) in New York, NY. Sectioning and preparation of the histological thin sections was done at Drexel University.

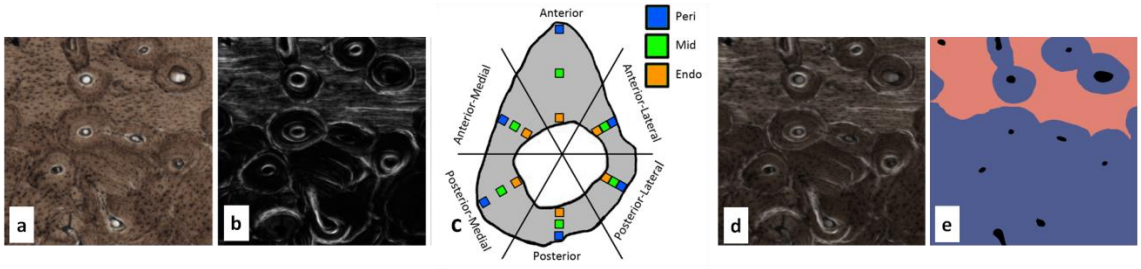

Figure 4.3: (a) ROI from the transmitted light image. (b) ROI from the circularly polarized transmitted light image. (c) A schematic of locations of ROIs. (d) Combined light microscopy image. (e) Hand traced tissue types from the combined light microscopy image.

4.2.3: Statistical Analysis

The linear correlations between variables (robustness, porosity, ash content, TMD, and tissue type) were investigated, as well as the correlations between the 38% and 66% locations of a single variable. The significance these correlations were determined by linear regressions in Microsoft Excel. The correlations were considered significant if $p < 0.05$.

4.3: Results

4.3.1: Validation Study

In this study, the interest lies in investigating the relationship between the robustness of a given bone cross-section and the remodeling process. Therefore, variables that reflect the remodeling process – specifically, porosity, tissue mineralization, and tissue type were chosen, but these variables do not give a direct measure of remodeling. The size range of selected pores were limited to capture those likely to have formed as a result of BMU based remodeling (e.g. Haversian Canals and Volkmann's Canals). To validate that the porosity of the whole cross-section reflected pores that were largely formed through remodeling, porosity of the whole cross-sections was compared to the porosity obtained from 6 smaller mid-cortex ROIs – regions where histological analysis demonstrated that most (~88% on average) of the tissue present was secondarily remodeled. The results demonstrated a significant linear relationship ($p < 0.001$, $R^2 = 0.862$) between the 3D porosity of the entire wedge and the 3D porosity of the mid-cortex only (see Figure 4.4).

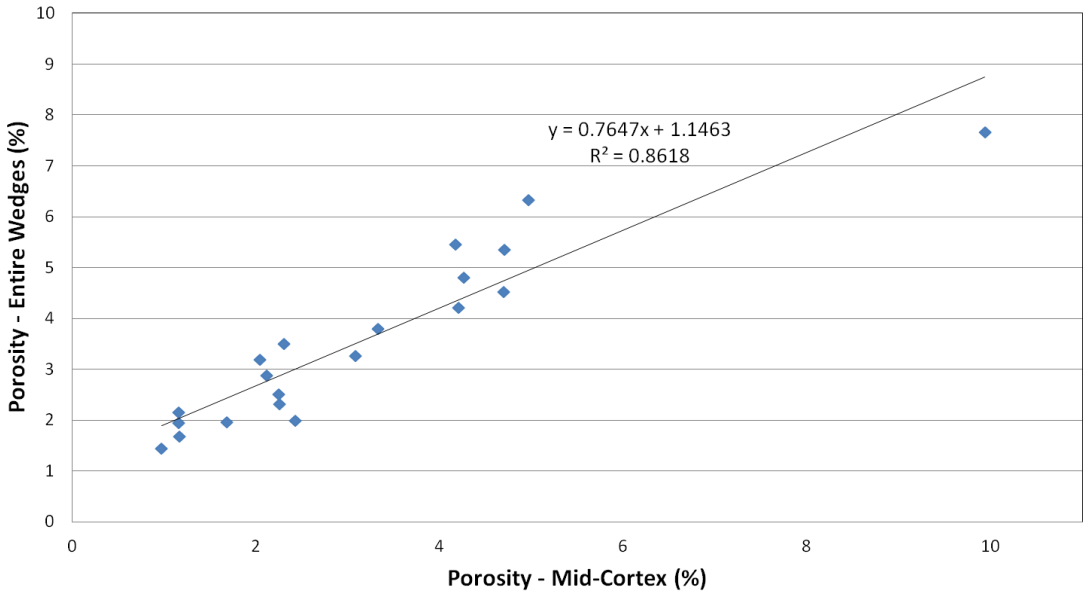

Figure 4.4: Comparison between porosity of the entire wedge and porosity of the mid-cortex only.

4.3.2: Correlations with Robustness

Here, the relationships between each of the variables (using data averaged across the entire cross-section) and robustness were investigated. A significant (p=0.006) positive relationship was found between percent porosity and robustness at the 66% location (R^2=0.638, see Figure 4.5). A significant (p=0.035) negative relationship was found between ash content and robustness at the 66% location as well (R^2=0.445, see Figure 4.6). A significant positive (p=0.003, R^2=0.677) relationship was found between tissue type and robustness at the 66% site (See Figure 4.7). Finally, a significant (p=0.004) negative relationship was found between TMD and robustness at the 66% location (R^2=0.673, see Figure 4.8). No significant relationships were found at the 38% location between robustness and any of the analyzed variables.

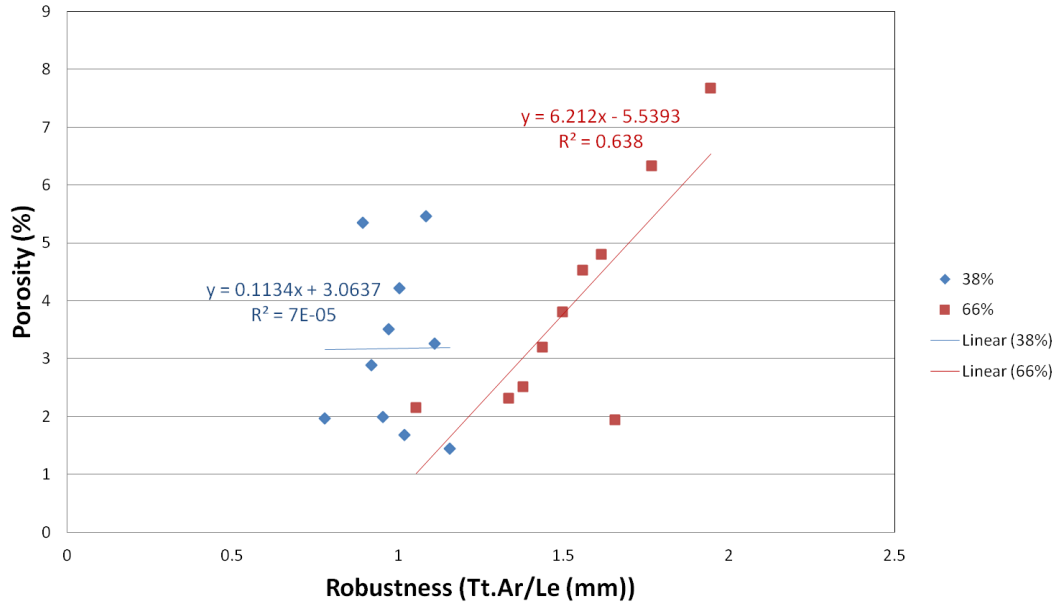

Figure 4.5: Relationship of porosity with robustness.

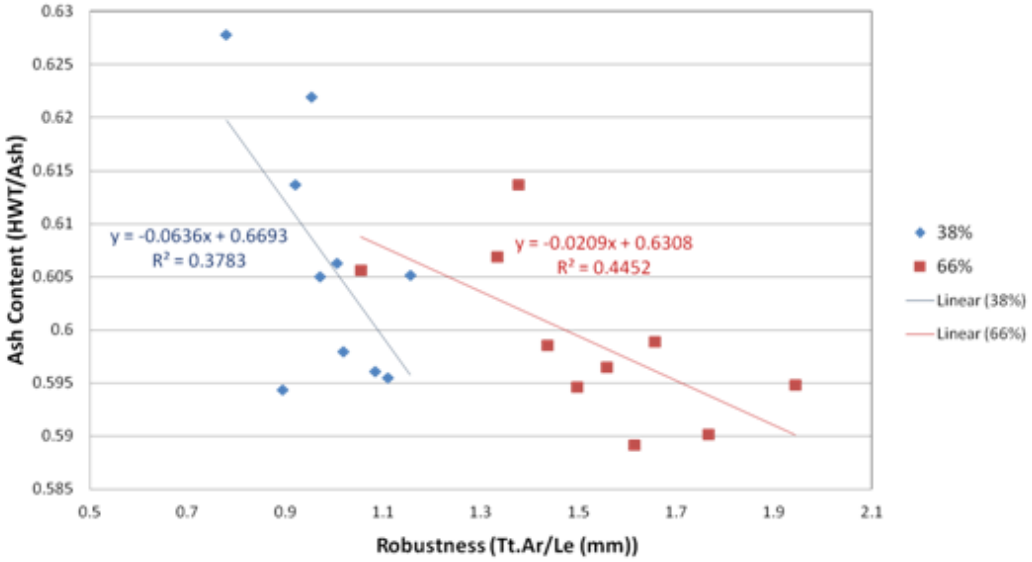

Figure 4.6: Relationship of ash content with robustness.

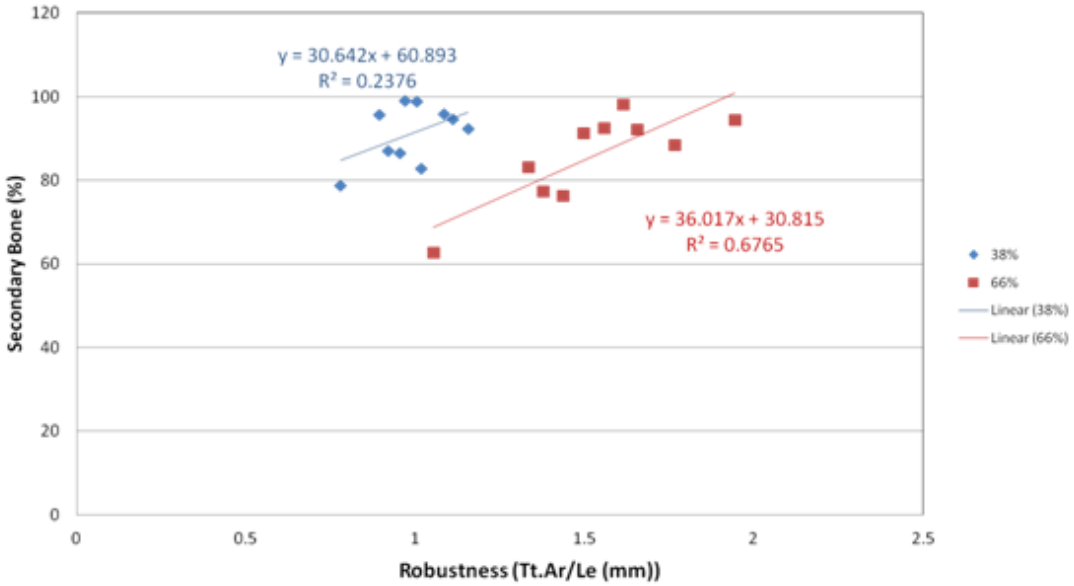

Figure 4.7: Relationship of tissue type with robustness.

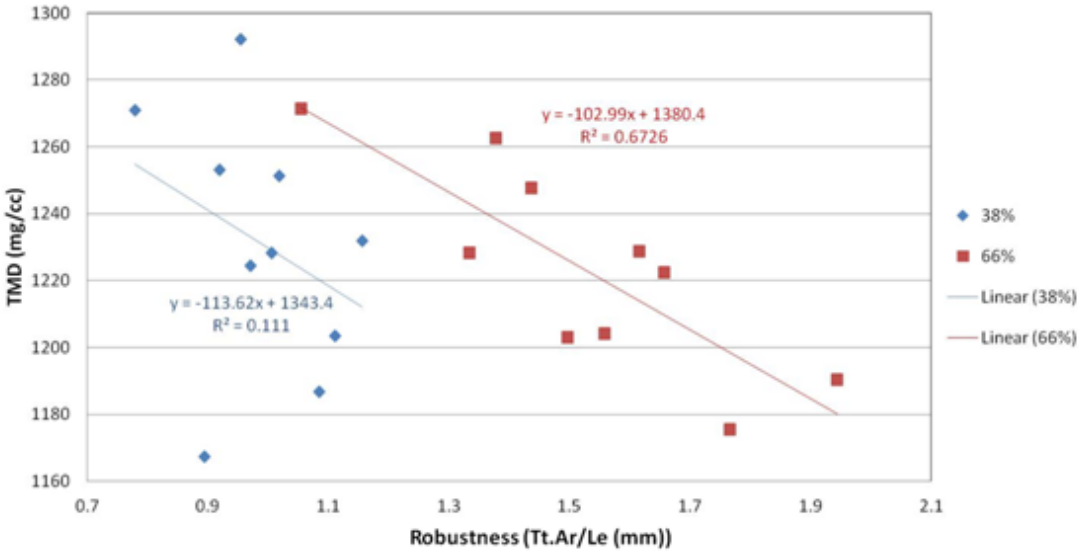

Figure 4.8: Relationship of TMD with robustness.

4.3.3: Relationships between the 38% and 66% sites

To better understand why the correlations between robustness and ash content/ porosity/ tissue type were not significant at the 38% site but were at the 66% site, the relationship between data obtained at 38% and those obtained at 66% were examined.

There were no significant differences ($p < 0.05$) between the proximal (66%) and distal (38%) sites of the tibia for the porosity, ash content, TMD, or amount of secondary tissue in the mid-cortex ring. No significant linear relationship was found between the robustness at the 38% and the 66% location, however, all individuals were more robust at the 66% site than the 38% site (see Figure 4.9). The 66% site was also more variable in robustness relative to the 38% site. Specifically, the coefficient of variation (COV) in robustness at the 66% site was 43% greater than the COV at the 38% site (COV 66%= 16.2% versus COV 38% = 11.3%).

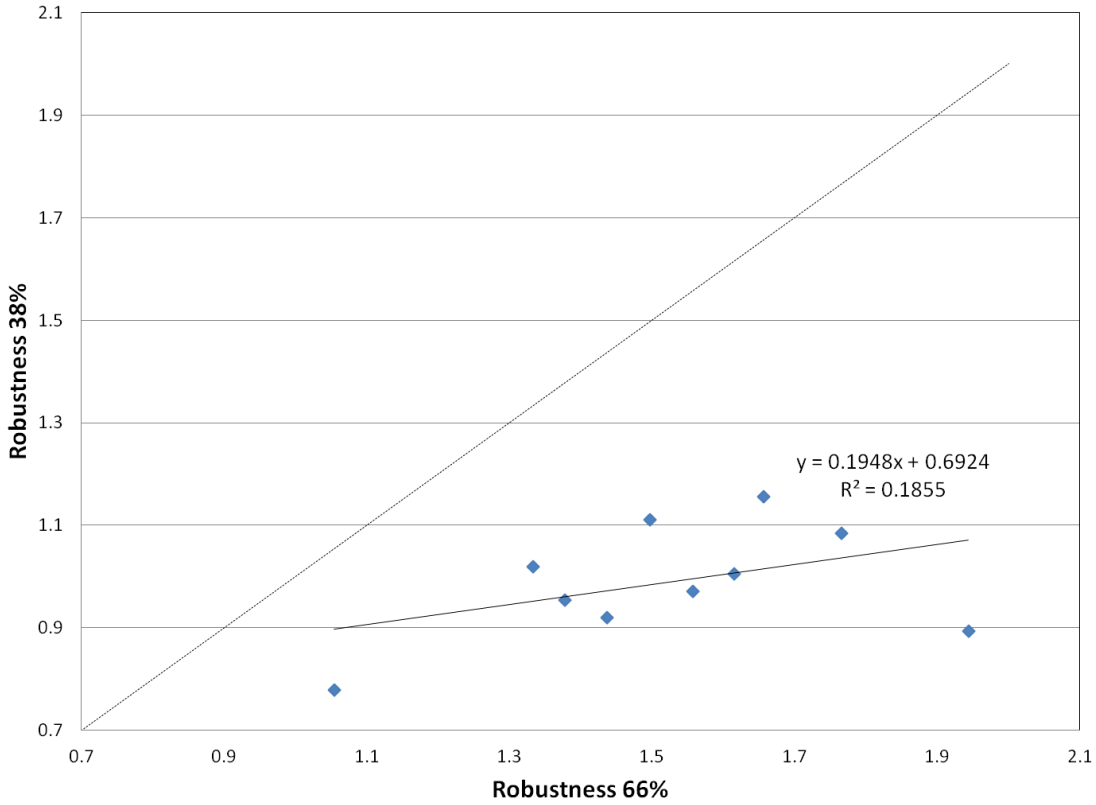

Figure 4.9: Comparison between the robustness of individuals at the 38% and 66% sites shows there is a linear relationship, and for each individual the robustness is lower at the 38% site than it is at the 66% site.

Given these differences in robustness variation between the two sites, it was important to investigate whether the robustness specific differences in porosity and ash content observed at 66% were consistent along the length of the bone . A significant ($p < 0.001$) positive linear relationship between the porosity at the 38% and the 66% location (R^2 and p values) was found. All individuals had greater porosity at the 66% site than the 38% site (see Figure 4.10).

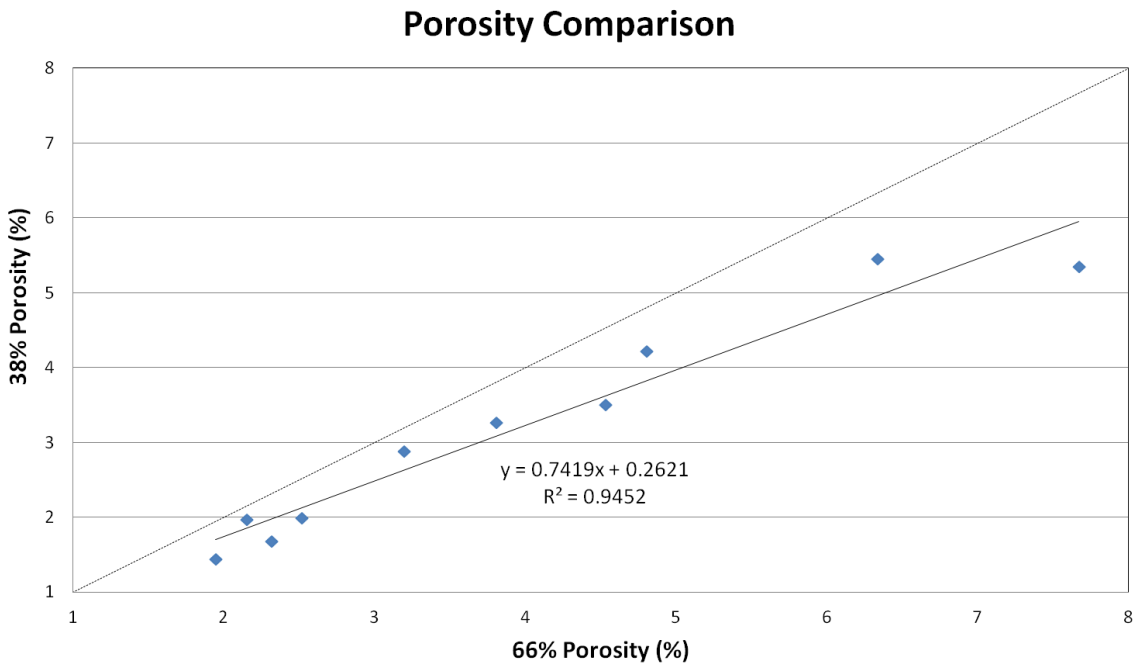

Figure 4.10: Comparison between the porosity of individuals at the 38% and 66% sites shows there is a linear relationship, and for each individual the porosity is lower at the 38% site than it is at the 66% site.

No significant linear relationship was found between ash content at the 38% and the 66% location, however, there was a trend ($p=0.059$). Most, but not all, individuals have lower ash content at the 66% site than the 38% site, see Figure 4.11.

There was also a strong significant ($p<0.001$, $R^2=0.816$) relationship between the amount of secondary bone at the 38% location and the 66% location (see Figure 4.12).

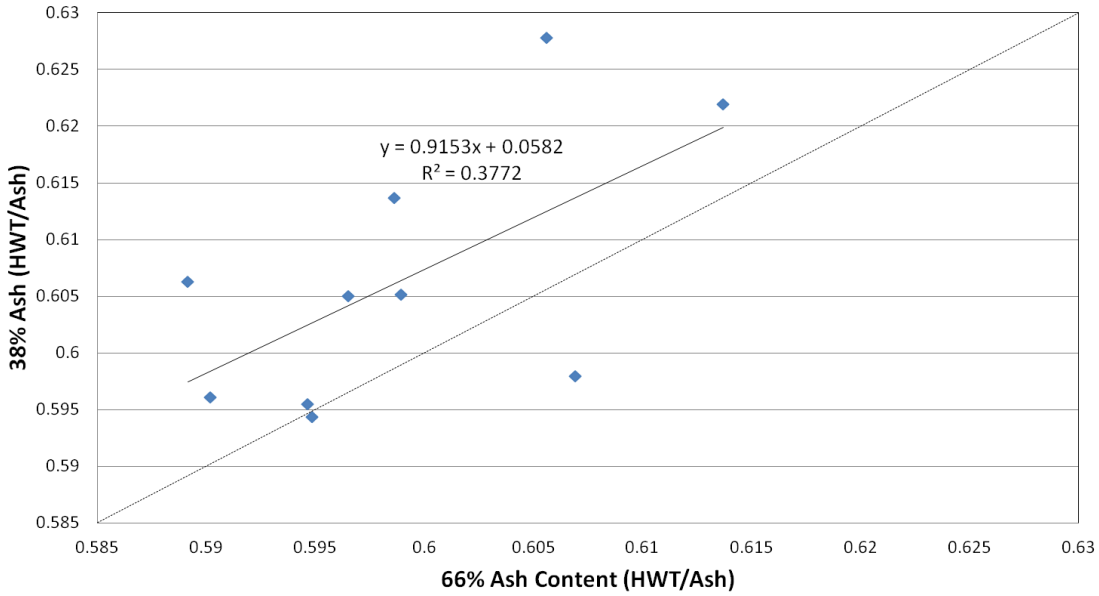

Figure 4.11: Comparison between the ash content of individuals at the 38% and 66% sites shows there is a linear relationship, and for most individuals the ash content is higher at the 38% site than it is at the 66% site.

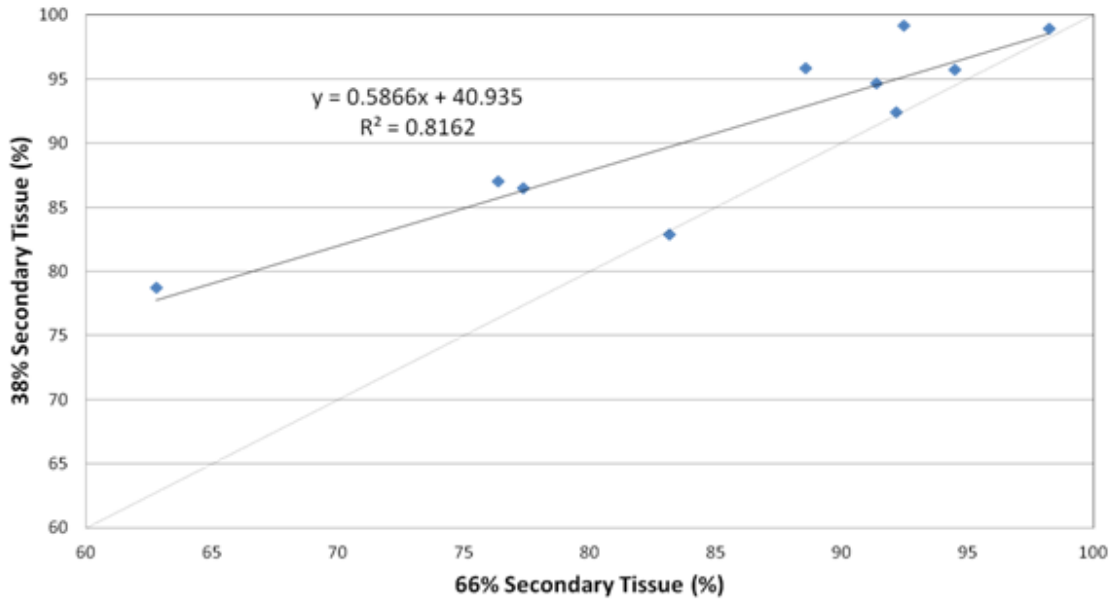

Figure 4.12: Comparison between the amount of secondary bone (mid-cortex ROIs only) of individuals at the 38% and 66% sites shows there is a linear relationship, and for most individuals there is more secondary tissue at the 38% site than there is at the 66% site.

There was a significant ($p < 0.001$) positive linear relationship between the tissue mineral density at the 38% and the 66% location. The TMD between sites was generally about the same with half of the individuals having higher TMD at 66% and half having lower, see Figure 4.13.

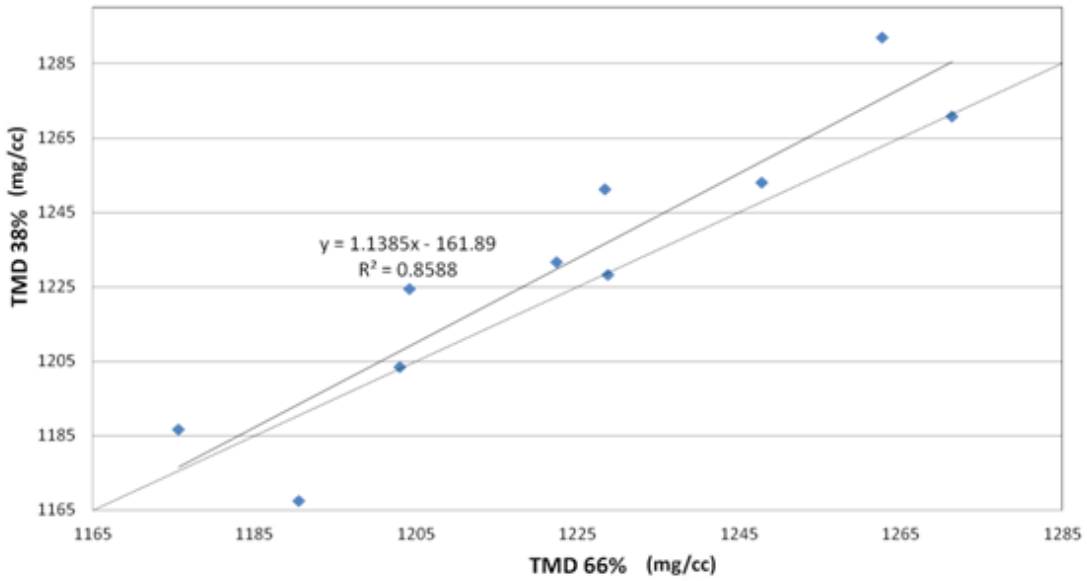

Figure 4.13: Comparison between the TMD of individuals at the 38% and 66% sites shows there is a linear relationship, and for most individuals the TMD is higher at the 38% site than it is at the 66% site.

4.3.4: Correlations between remodeling variables

Since each of the variables (porosity, tissue type and ash content) were reflective of aspects of the remodeling process, it was also important to determine whether the three variables correlated with one another.

A significant negative relationship was found between porosity and cortical tissue mineral density (Ct.TMD) measured by pQCT at the both the 38% ($p=0.005$) and 66%

(p=0.011) anatomical sites (R^2=0.652 and R^2 = 0.579 respectively). The regression shown in Figure 4.14 includes data from both 38% and 66% sites combined (p<0.001, R^2=0.582). Data points from each location are colored separately to illustrate the similarity in results derived from different anatomical sites.

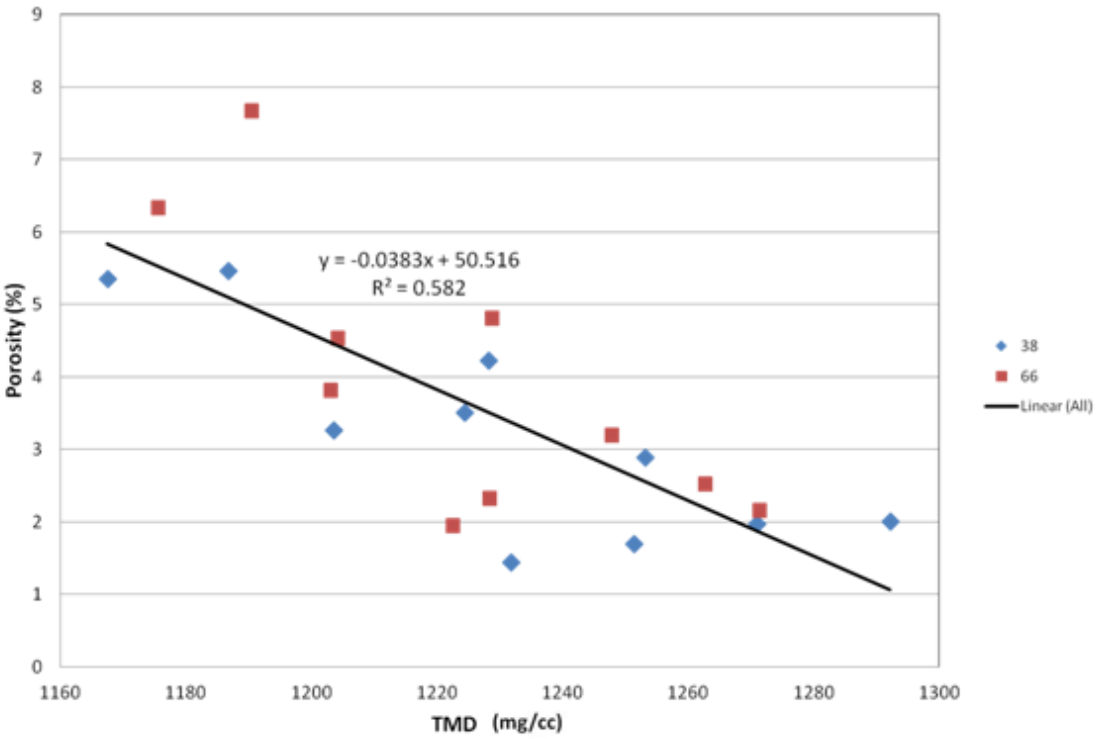

Figure 4.14: Relationship between porosity and TMD is linear through data points from both the 38% and 66% sites.

Ash content was negatively correlated with Ct.TMD, however, this relationship was only significant (p=0.006) at the 66% site (R^2=0.636, see Figure 4.15).

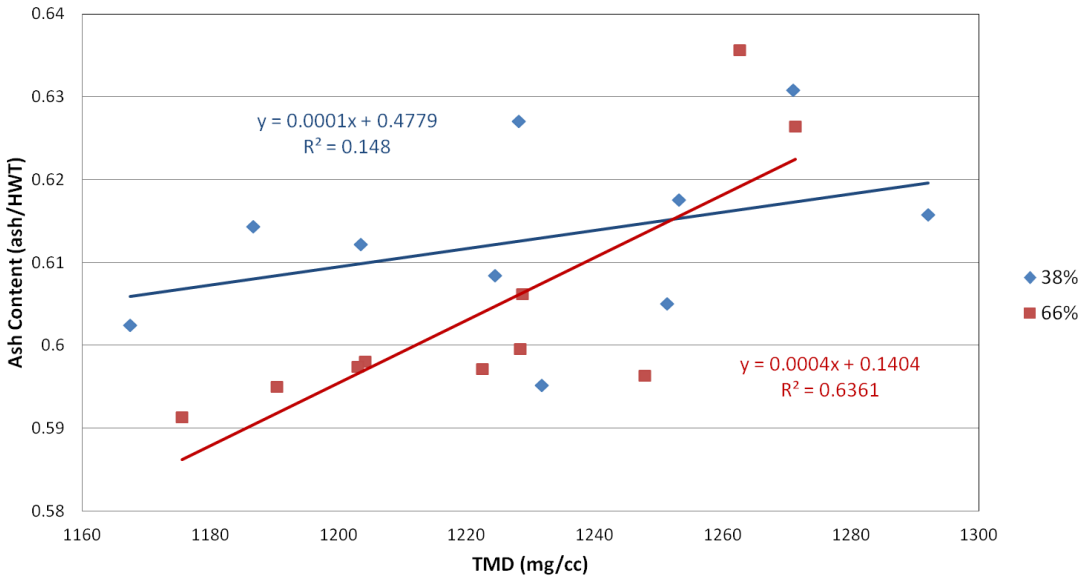

Figure 4.15: Relationship between ash content and TMD is significantly linear only at the 66% site.

The relationship between ash content and porosity was different for slender bones versus robust bones. At the 38% location, there was a negative non-linear relationship between ash content and porosity for slender bones, R^2=0.631 (see Figure 4.16). No relationship was found between ash content and porosity for robust bones. These analyses were performed on the individual wedges combined, rather than a cross-sectional average, in order to be able to better demonstrate the variability present in the cross-sections.

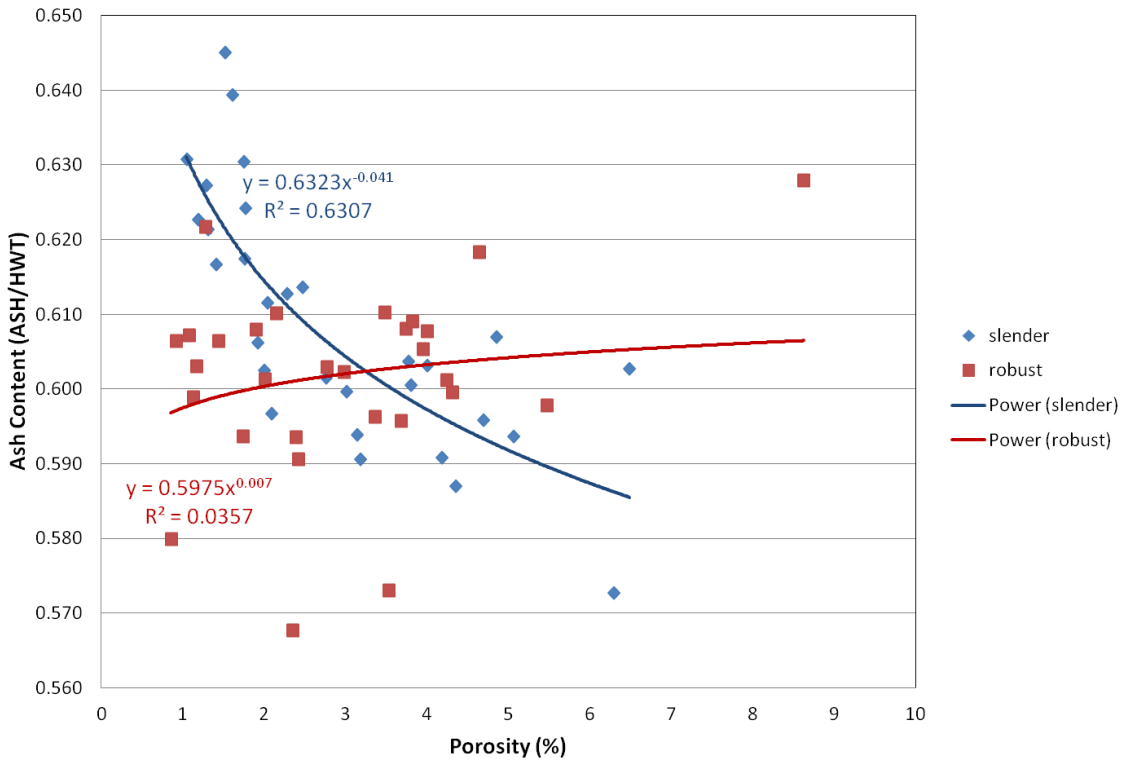

Figure 4.16: Relationship between ash content and porosity at the 38% site.

At the 66% site, ash content and porosity for the slender bones showed a significant negative linear relationship ($p < 0.001$, $R^2 = 0.495$). Again, no significant relationship was apparent for robust bones (see Figure 4.17).

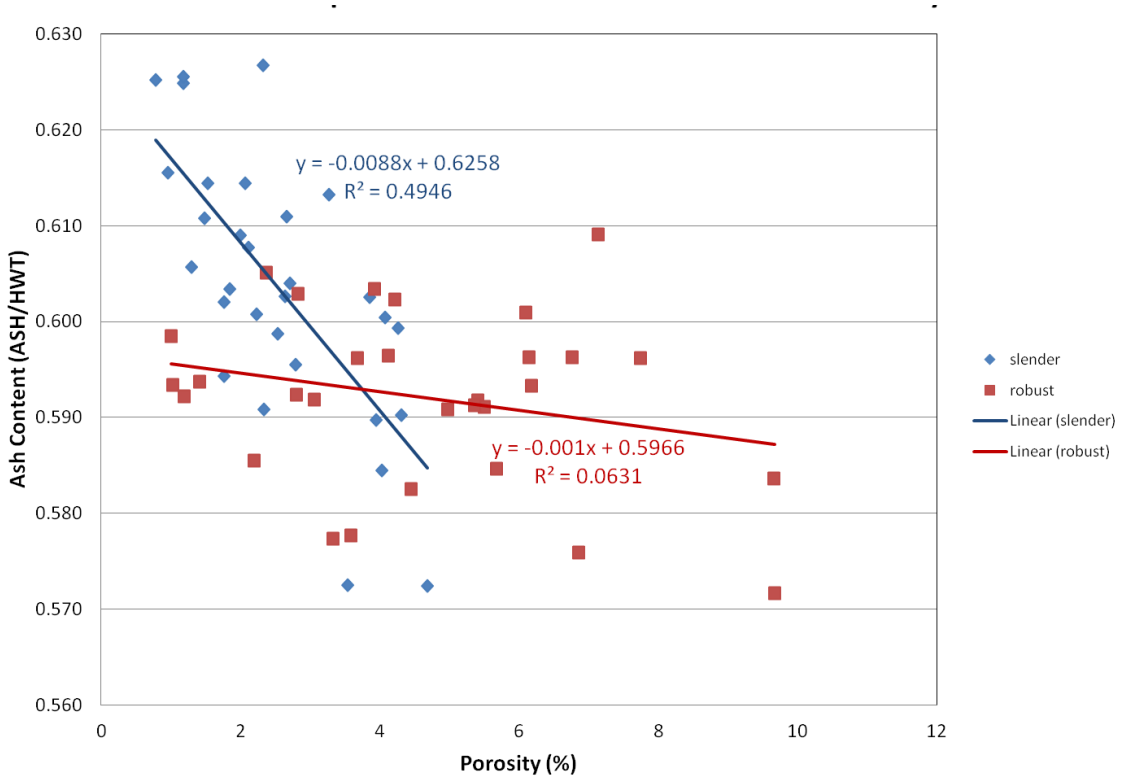

Figure 4.17: Relationship between ash content and porosity at the 66% site.

Tissue type could not be compared with other variables because, by looking at the overall amount of secondary bone in a region (as opposed to using a measure of complete osteons or of whole osteons and fragments [Osteon Population Density]), it is not necessarily possible to differentiate between individuals with a high remodeling rate and those with a low remodeling rate. In areas of the cortex that are highly remodeled, many individuals may have entirely remodeled bone, regardless of how long it took (remodeling rate). This skewed the data, resulting in a very non-normal distribution, and made comparing the amount of secondary tissue to other variables impossible.

4.4: Discussion

4.4.1: Porosity, Ash Content, and Tissue Type as Reflections of Intracortical Remodeling

An underlying assumption of the study was that cortical porosity and ash content were both reflective of the degree of intracortical remodeling. Increased intracortical remodeling would lead to increases in the porosity, as each new remodeling event would lead to the formation of a new Haversian canal. It would also lead to decreased ash content since bone that is newly formed during remodeling has a lower mineralization density relative to the older bone matrix it replaced. Additionally, as bone remodels, more of the cortex will be filled with secondary bone tissue (whole and partial osteons).

In this study, it was found by histological analysis that, on average, 86% of the bone in the mid-cortex ring was osteonal or fragmentary osteonal, produced through the secondary remodeling process. It was also found that the porosity of an entire wedge was strongly correlated to that of a mid-cortex ROI. From this it can be concluded that the three-dimensional porosity measurement reflect the remodeling history of the cross-section.

Previous studies also supported the relationship between increased porosity and increased intracortical remodeling (Cooper *et al.*, 2006; Kennedy *et al.*, 2009; Zebaze *et al.*, 2011; Drapeau and Streeter, 2006; Ural and Vashishth, 2006; Lazenby, 1986; Burr *et al.*, 1990). Burr *et al.*, (1990) found increased porosity in regions of the femoral cortex that also had increased osteon population density. In a study of ovariectomized (OVX) sheep metatarsals, Kennedy *et al.* (2009) demonstrated an increase in bone turnover in the OVX bones, and a concomitant increase in porosity. Cooper *et al.* (2005) and Zebaze *et al.* (2011) studied age related changes in the femoral cortex. It was suggested that with

age, intracortical remodeling would result in increased intracortical porosity, but also in subendocortical trabecularization of the cortical bone with resulting increases in the number and volume of large pores. Similarly, a microCT based 3D porosity study by Cooper *et al.* (2006) showed that age related changes in 3D pore connectivity and size were consistent with remodeling phenomena including the introduction of new Haversian canals interconnected by Volkmann's canals, and coalescence of nearby canals to form enlarged pores, particularly subendosteally. For this study, pore size was not quantified, although pores below 10 μm in diameter were removed using noise reduction techniques and pores larger than 300 μm were excluded, as pores that large were likely not caused by the remodeling process. Further research may focus on subendosteal regions in order to study the process of subendocortical trabecularization further, including its relationship to robustness.

Though ash content is a rather coarse measure of this tissue mineralization, and other techniques are more suitable to study the more subtle changes in mineralization (Bloebaum *et al.*, 1997; Boskey, 2006; Boyde and Jones, 1996; Elliot and Dover, 1984, Roschger *et al.*, 2008;), at the cross-sectional level ash content is an appropriate measure of average mineralization density (Nielsen *et. al.*, 1980) that has been shown to correlate to elastic modulus (Currey, 1988; Martin and Ishida, 1989). At the local level, mineralization has also been shown to correlate to elastic modulus (Pathak *et al.*, 2012; Zysset *et al.*, 1999). Mineralization has been shown to vary with respect to remodeling status (Hernandez, 2008; Meunier and Boivin, 1997), as a high remodeling rate leads to a high amount of bone turnover, and new bone has low mineralization.

The proportion of the cortex that is composed of secondary tissue (osteons and remnants of osteons, plus their central Haversian canals and Volkmann's canals) was reflective of the rate of previous remodeling events as well as the age of the tissue (Keough *et al.*, 2009; Kerley, 1965; Pfeiffer *et al.*, 1995). Bone that has been turning over faster, as well as bone that has been turning over for a longer period of time, would be expected to have a greater proportion of secondary tissue. Older tissue may also be targeted for remodeling, as the tissue may have accumulated microdamage (Bouvier and Hylander, 1981; Martin *et al.*, 1998). Keough *et al.* (2009) found significant positive correlations between age and total osteon count and the average percentage of fragmental bone. Significant negative correlations were found between the percentage of unremodeled tissue and number of non-Haversian canals. In areas that were heavily remodeled, and had been turning over for long periods of time, the amount of remodeled tissue may reach an asymptote, as the entire area was remodeled. At this point, the amount of remodeled tissue would no longer give any information about remodeling rate, and another metric would be more appropriate, such as osteon count, as examined by Keough *et al.* (2009).

4.4.2: Robustness Correlations with Porosity, Tissue Type, and Ash Content

The results demonstrated that at the more proximal (66%) site, robust bones had significantly ($p<0.05$) higher porosity than slender bones, and there was a positive linear relationship between porosity and robustness. At the 38% site, a significant relationship was not observed between porosity and robustness. The analysis also demonstrated a negative relationship between ash content and robustness, but again, this was only significant ($p < 0.05$) at the 66% location. The 'secondary bone (%)' variable provided a

direct measure of the amount of remodeled bone tissue in the mid-cortex. This variable was positively correlated with robustness at 66%, but not at 38%. Given the starting premise, that increased porosity, decreased ash content, and increased secondary bone tissue, were consistent with increased intracortical remodeling, the results were interpreted as suggesting that at the 66% site, robust bones are more heavily remodeled relative to slender bones.

The idea that intracortical remodeling might be modulated by a global variable such as robustness has not been generally considered before. Traditionally, remodeling has been considered as a response to local mechanical strain and microdamage (Drapeau and Streeter, 2006; Martin, 2002; Schaffler *et al.*, 1995). Osteocytes are believed to sense mechanical loads, and activate intracortical remodeling as a response to tensile strain (Corwin *et al.*, 1991; Enlow, 1963; Lanyon, 1993; Mullender and Huiskes, 1995; 1997; Ruff *et al.*, 2006). The results indicated that there was an effect on remodeling from global factors, but it was likely that this effect was not mutually exclusive of the local strain effect. Bone is a complex system and likely has both mechanisms affecting the remodeling rate.

This is not to say that either global factors such as robustness or local factors such as strains are the only factors to affect remodeling. There are also many systematic factors known to affect remodeling, such as nutrition deficiencies, hormonal and metabolic imbalances, lactation and pregnancy (Lanyon, 1993). Further, the amount of remodeled tissue in the cortex also increases with age (Feik *et al.*, 1996; Rauch *et al.*, 2007; Ruff and Hayes, 1988).

4.4.3: Patterns of Variation Between the 38% and 66% Sites

The finding that the remodeling variables correlated with robustness only at the 66% site led to further exploration of the variability between the two sites. It was found that individuals were more robust at the 66% site than the 38% site. This indicated that the tibia had a trumpet-like shape and flares outward proximally. No significant relationship between robustness measures at the two sites were found, so it is known that not all individuals flare the same way or by the same degree. Hrdlicka studied about 2,000 normal adult bones and found that the shape of the tibia varied greatly between them (Hrdlicka, 1898). Howell *et al.* (2010) found that shape of the tibia, specifically the bow angle between the mechanical axis and the anatomical axis, was variable.

Although patterns of robustness differ between the two tibial sites, it was found that porosity and secondary bone are significantly linearly related between the two sites, and ash content shows a tendency towards a negative relationship ($p=0.059$, $R^2=0.377$). This indicated that there was an overall consistency of microstructural variability within individuals, such that an individual with a high degree of porosity and secondary bone at one site would also be highly porous and remodeled at another. Thus, an individual's 66% site was always more porous and remodeled, and usually less mineralized, than its corresponding 38% site. This was consistent with the predictions of the hypothesis, given that the 66% site is more robust.

Despite this consistency between sites, recall that the results only demonstrated a significant relationship between porosity and robustness at the 66%, not at the 38% site. The linear relationship in porosity between sites was interpreted as an indication that they may be influenced by similar global factors, such as robustness. But, given that the 66%

is generally more robust and more variable than the 38% site, the effects of robustness on porosity may only be detectible at the more robust and variable location versus the more slender 38% site. Alternatively, it may be that below a certain robustness, the system is constrained by a minimum required vascular support, which would take precedence over the need to increase the elastic modulus – thus resulting in a lower limit on porosity. On the other hand, very robust individuals, only seen at the 66% location would have stronger pressure to extensively increase porosity in order to decrease mass. Without high levels of robustness at the 38% site, this end of the variability spectrum would not be detectible at the 38% site. Additional samples might help to clarify this relationship at more slender sites.

Although within-individual site-specific differences in remodeling variables were apparent, it should be noted that t-tests comparing porosity, ash content and secondary bone between sites considering the sample in its entirety showed no significant differences between the 66% and 38% sites. In order to interpret this seemingly inconsistent finding, it is necessary to consider other hypotheses concerning tibial geometry. The tibia gets its trumpet-like shape during growth modeling, due to the loading conditions it experiences both from muscle attachments and from weight bearing. This means that the more proximal and distal ends have both different geometries and are subject to different strains. Lieberman and Crompton (1998) hypothesized that in cursorial animals, the distal limb segments are more slender and porous in order to minimize the metabolic burden during locomotion by minimizing the weight. Drapeau and Streeter (2006) tested only the mid-shaft, but looked at both the femur and the tibia of a human sample and did not find support for this hypothesis in humans. Nevertheless it

was hypothesized that the distal third of the tibia may be subject to greater strains than more proximal sites, and therefore be subject to higher remodeling rates, however the authors did not actually study whether such differences in remodeling existed in the tibia. Ural and Vashishth (2006) noticed significant differences in the microstructure/geometry relationships between the proximal and distal segments of the tibia. These differences were attributed to different strains due to muscle attachments. The authors did not report whether the distal diaphysis had indications of a higher remodeling rate (e.g. greater porosity), but based on their hypothesis of greater strain distally, they too would have predicted an increase in remodeling at the distal location. On the other hand, the hypothesis presented in this dissertation is that since the distal tibia is more narrow than the proximal third, the distal tibia should actually demonstrate a decreased remodeling rate relative to the proximal site. Although the study demonstrated no significant differences between the two tibial sites in porosity, secondary bone, ash content, or TMD, most individuals in the study demonstrated relatively lower porosity, increased ash content and increased secondary bone area (See Figures 4.10 – 4.12) distally rather than proximally. By the model presented in this dissertation alone, one would expect there to be less remodeling at the distal tibia, due to its more slender geometry, yet the data indicated that most individuals had more secondary bone distally (an indication of more remodeling), despite lower porosity and increased ash content. These mixed results suggested that both local strain and geometric factors such as robustness may both be impacting bone remodeling in the tibia.

4.4.4: Relationships Between Remodeling Variables

The data showed that higher TMD values relate to both decreased porosity and increased ash content. Interestingly, porosity accounted for a greater proportion of the variation in TMD than ash content, suggesting that pQCT derived TMD values indicates more about the volume of bone tissue rather than the quality of the material. Density measurements are often reported without a good understanding of what the measurements actually mean (Seeman, 1997), despite the fact that it is well established that density includes information about both the amount of material as well as the degree of mineralization of that material (McCalden, *et al*., 1993; Schaffler and Burr, 1988). This study demonstrated the importance of teasing out the contributors to the TMD values reported by pQCT. Once a better understanding of the underlying biology (e.g. remodeling mechanisms) that contributes to the TMD values is obtained, the data acquired from pQCT becomes more valuable, and can be used as a predictor of individual adaptation. In Jepsen *et al.* (2011), for instance, clinical pQCT datasets were used to demonstrate that variations in robustness correlated with predictable functional deficiencies. The authors found that slender tibiae were two to three times less stiff than robust tibiae. It was hypothesized that there was a limit to how much the bone cells could alter the stiffness of slender bones in order to decrease the functional deficiencies, and therefore, functional equivalence could not be reached. The authors did find an increase in tissue modulus, and hypothesized that perhaps, if the bone composition was changed such that functional equivalence was reached between slender and robust bones, then the increase in brittleness that would accompany an increase in mineralization in the slender bones, would cause the slender bones to be too brittle. In order to fully appreciate the

pQCT data, these predictions and hypothesis had to be built on the back of a very strong understanding of underlying biology from *ex-vivo* experimentation such as the focus of this dissertation.

TMD was found to be similar between the 38% and 66% location, and there was a strong linear relationship between the two sites with a slope of 1.1. Since TMD contains information about both mineral content and porosity combined, it is not surprising that it should be consistent between the two sites. It was likely that the tradeoffs between porosity and ash content become normalized at this scale, evening out some of the local variations. This makes TMD ideal for looking at global variation at the clinical level, and make it a very powerful clinical tool, as other measures are site-specific.

The data demonstrated a strong negative correlation between ash content and porosity for more slender bones at both the 38% and 66% locations (R^2=0.631 and R^2=0.495 respectively), but not in more robust bones. Interestingly, the correlation observed at the 38% location was non-linear, with a much lower slope for the most slender individuals. One explanation for this change in slope was that remodeling rate, and resultant porosity, may only be able to decrease to a certain threshold, given that the tissue still needs to maintain vascular support and metabolic requirements. On the other hand, the lack of a significant relationship between ash content and porosity for robust bones may suggest that robust bones were not adjusting their remodeling rate to increase stiffness. A robust bone already has sufficient geometric properties, and increasing stiffness was not a priority. Since robust bones did not need to increase the elastic modulus to reach desired whole bone stiffness properties, it was hypothesized that they would not suppress bone remodeling. Rather, the constraint on robust bones is weight, as

it is metabolically costly to move a robust bone (Lieberman, 2003; Alexander, 1998; Martin, 2003; Currey, 1984; Drapeau and Streeter, 2006; Hildebrand, 1974; Jepsen *et al.*, 2011; Stout *et al.*, 1999). Thus in more robust bones, bone tissue may be removed resulting in more pores – thus reducing bone mass, but bone may not be replaced at an equal rate, thus resulting in a lack of relationship between porosity and tissue mineralization.

Similar relationships were also found between secondary bone and robustness as were found between 3 dimensional porosity and robustness, which also indicates that the differences in porosity relate to remodeling and there was a relationship between overall cross-sectional geometry and remodeling. As with 3D cross-sectional porosity, it was found that there is a strong relationship between the amount of secondary bone at the 38% and 66% locations. However, the amount of secondary bone would max out at 100% (approach an asymptote) and by looking only at amount of primary versus secondary bone, once an area is completely remodeled, it will no longer be possible to determine relationships with remodeling rates. Determining which areas of the cortex are completely remodeled can allow for targeted future investigations towards areas with greater variability.

Porosity, ash content, amount of secondary tissue, and tissue mineral density reflect remodeling. Significant relationships were found between these variables and robustness and by investigating these variables, the relationship between robustness and remodeling can be explored.

4.4.5: Unexplored Sources of Variability

In this study, there was not sufficient information about the life history of the individuals to investigate the effects of systemic variables (e.g. disease and nutritional status). It was found that age explained some of the variation in porosity, however, this effect was dwarfed by the effect of the global variable of robustness, which was significant for porosity, ash content, tissue type and TMD. Given that this sample included only a narrow range of adult ages (23-46 yrs), much of the variability in remodeled bone expected with age would not be apparent in the sample. It is likely that if a sample including a wide range of adult ages were investigates, that age would be a more important contributor to the variation in porosity. Importantly, in the sample used for this research, there was no significant difference between the average ages of the slender and robust individuals. Thus, even if porosity did weakly correlate with age, this relationship would be independent of the relationship between porosity and robustness.

One additional variable that was not considered was sex. The sample included both males and females, but with so few individuals, separating the sample by sex was not possible statistically. It is important to note, however that the female samples were mostly more slender than the robust samples. Tommassini *et al.* (2007; 2008) examined sex differences in this sample (including a larger number of individuals) and concluded that sexual dimorphism did not have an effect on the local mechanical properties, but did affect the overall geometry. The effects of sex versus slenderness will need to be studied further to elucidate the relationship of each to remodeling.

The study was limited in the analysis by the small sample size. With only ten individuals, it is possible that important relationships were lost in the noise of the sample.

The fact that so many strong correlations were found between variables and significant variations, indicated that there were meaningful relationships, and they should be studied further on a larger sample in the future.

4.5: Conclusions

The results indicated that there was a relationship between cross-sectional geometry and local composition and structure. It is believed that these relationships stem from compensatory mechanisms that increase the overall stiffness of slender bones. Previous studies have shown that by geometry alone, a robust bone is stiffer than a less robust one (Ruff, 2000; van der Meulen *et al.*, 2001). A slender bone is at a mechanical disadvantage in bending based on its geometry alone, since bending relates to the forth power of the radius. This disadvantage can be compensated for by increasing the elastic modulus of the bone, and thereby its overall stiffness. One way to increase the elastic modulus of a bone would be to suppress remodeling in order to allow bone to stay in the body for longer and become more mineralized.

To compensate for the geometry of slender bones, it was hypothesized that remodeling was suppressed in these individuals, leading to a lower degree of intracortical porosity and a higher proportion of primary bone tissue with a higher degree of mineralization density (higher ash content). Thus, it was suggested that there are global geometric phenomena, with genetic basis, that influence overall remodeling rates and affect local structure. There is, of course, extensive evidence that remodeling rates are influenced by local strains and microdamage (Burr, 2001; Parfitt, 2001; Martin, 2002). These factors would have an effect on the overall remodeling rate of bone, rather than a site-specific effect, which can come from the response to strain or microdamage. Thus,

there is likely to be regional variation in remodeling rate around the cortex that reflects these local mechanical and systemic metabolic factors, but this variation would be superimposed on the variability in remodeling rate owing to geometry. Further study of the variation in remodeling rate, and resultant tissue level organization and properties is needed in order to tease apart these global vs. local phenomena.

The results suggest that aspects of tissue level organization and composition play a compensatory role in the establishment of adult bone mass during growth and development. These aspects may contribute to differences in bone aging between robust and slender bone phenotypes. It is necessary to move beyond the cross-sectional level in order investigate local loading conditions affect the tissue level organization and composition.

In this study, variability of porosity between different regions of the cortex were investigated. Given that stresses from loading and muscle attachments will not be uniform throughout the entire cortex one would expect that the relative importance of local biomechanical loading vs. robustness would differ depending on location. Similarly, tissue age varies around the cortex due to processes of cortical drift and expansion that occur throughout growth. Because of this, primary bone tissue laid down during earlier growth phases will be much more highly mineralized than secondary tissue. With a young adult sample, such as the one used in this study, many of the individuals are likely to have large amounts of unremodeled tissue, particularly close to the periosteal surface of the bone (and in some regions, but less extensively, close to the endosteal surface), as that would be where it was most recently laid down, and the remodeling process may not have been initiated there yet (Enlow, 1963). Moreover, more areas of interstitial bone

tissue would be expected since fewer new Haversian systems would be forming to replace older pieces of tissue. If remodeling is suppressed, the slender individuals would be expected to have larger areas of unremodeled primary tissue rather than remodeled secondary tissue. Local variability in these measures are investigated in Chapter 5. There the relationships between porosity, ash content, tissue type and robustness at many different locations throughout the cortex will also be investigated in order to gain a better understanding of the regional variability. This may shed some light on the relationships these variables have with bone growth, loading conditions, and remodeling.

Chapter 5: Site-specific Variations of Porosity, Tissue Mineralization, and Tissue Type around the Cortex and Their Relationships to Robustness

5.1: Introduction

In the previous chapter, the relationship between 'robustness' (cross-sectional area/tibia length) and remodeling (using porosity and ash content as reflections of the process) was examined at the level of the entire cross-section. The study demonstrated that slender bones were significantly less porous, had a higher ash content and a higher tissue mineral density (TMD, as measured by pQCT). At the proximal site (66%), a significant positive linear relationship was found between robustness and porosity, with more robust bones having greater porosity, however, this relationship was not observed at the distal site (38%). Similarly, a significant negative relationship was shown between ash content and robustness, again only at the proximal site. However, since it was also shown that the two sites were highly correlated for the variables, it was suggested that there was a degree of systemic variability. Thus the lack of relationship between robustness and the variables may relate to low variability at the distal site combined with small sample size. It was suggested that these results reflected a suppression of remodeling in slender bones in an effort to increase elastic modulus.

In this chapter, the site-specific relationships between porosity, ash content and tissue type around the tibial cortex relative to cross-sectional geometric properties are investigated. The goal is to better understand the tradeoff between bone mass and elastic modulus that may result from modulations in bone remodeling. The variations within each variable between different rings within a radial wedge and between wedges within a ring will also be investigated. It is hypothesized that there are regional variations around

the tibia in the amount of porosity, ash content, and secondary bone tissue. It is expected that quantifiable differences between the rings and wedges will be found that may relate back to both growth modeling and loading conditions.

The first aim was to characterize the site-specific variability in porosity, ash content, and tissue type, and their relationship to overall robustness. In the previous chapter, it was demonstrated that there were correlations within variables between the proximal and distal sites of the tibia at the cross-sectional level. The aim here was to determine if there were site-specific differences in these relationships. Perhaps due to growth modeling and loading conditions, these relationships may be not be uniform throughout the cortex, and in this chapter, it will be determined where in the cortex these relationships are the strongest. Based on previous studies, and current knowledge of loading of the tibial diaphysis, it is expected that the anterior wedge has the highest porosity and secondary tissue and the lowest ash content. The anterior cortex is loaded primarily in tension (Peterman *et al.*, 2001), which has been shown to relate to increased remodeling (Enlow, 1963; Corwin *et al.*, 1991; Lanyon, 1993; Mullender and Huiskes, 1995; Mullender and Huiskes, 1997; Ruff *et al.*, 2006). Based on the findings of a relationship between these variables and robustness at the cross-sectional level, it is expected that it will be possible to demonstrate this relationship in the site-specific study as well. However, the aim is to determine whether this relationship is detectible in all regions of the cortex, or is more pronounced in some areas.

The findings about site-specific variability will then be interpreted in the context of growth and development and local loading effects. Significant differences are expected to

be found between different areas of the cortex that may be attributable to loading conditions of the tibia, and others more likely related to the growth modeling of the tibia.

5.2: Methods

5.2.1: The Sample

As described previously, the sample consisted of 10 cadaveric tibiae (6 male, 4 female, age 37 ± 8 yrs) collected from the Musculoskeletal Transplant Foundation (Edison, NJ USA) and the National Disease Research Interchange (Philadelphia, PA, USA). The individuals had no known illnesses or bone pathologies.

5.2.2: Sectioning and Imaging

Two 2.5 mm thick cross sections and one 5 mm thick cross section were removed from each tibia at both the 38% and 66% of total tibia length locations (measured from the distal end of the bone, see Figure 5.1a). The first of the 2.5 mm sections was imaged using pQCT (XCT 2000; Stratec Medizintechnik, Pforzheim, Germany), to determine the morphometric trait of robustness, defined as cross-sectional area divided by total tibia length (see Figure 5.1b), and to determine tissue mineral density (Ct.TMD). The second set of cross-sections was further sectioned into 6 radial wedges, as shown in Figure 5.1c.

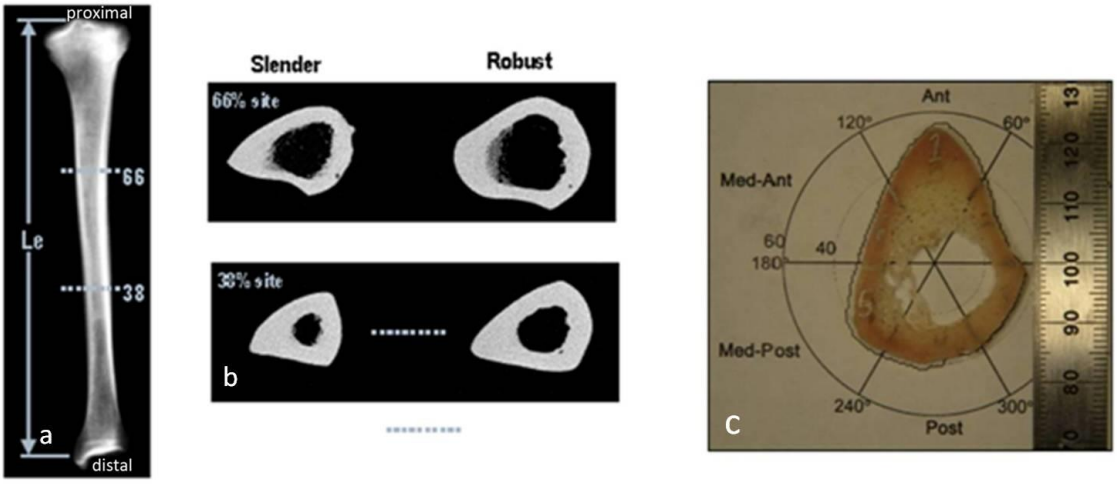

Figure 5.1: (a)The proximal (66%) and distal (38%) sites investigated in this work (b) pQCT images of robust and slender cross section at each site. (c) Photograph of the cross-section before sectioning into radial wedges.

The radial wedge samples were imaged using a Skyscan 1172 µCT (Skyscan, Kontich, Belgium) following the procedure described in Chapter 3. Images were reconstructed at a 5 µm pixel size, which was sufficient resolution to captured the vascular spaces, but not osteocyte lacunae. A number of noise reduction steps were performed and a region of interest (ROI) was manually selected from each dataset to exclude cancellous bone (defined visually as regions with greater than ~50% porosity). For each wedge, total tissue volume (Tt.V), total canal volume (Tt.Ca.V). Porosity (Ct.Po, %) was calculated as canal volume normalized by total tissue-volume (see Figure 5.2). The 3-dimensional porosity was also calculated for regions of interest at the endosteal, mid-cortex, and periosteal rings of the bone to obtain further detail around the cortex. After being imaged by µCT, the wedges were ashed following the methods described in detail in Chapter 3.

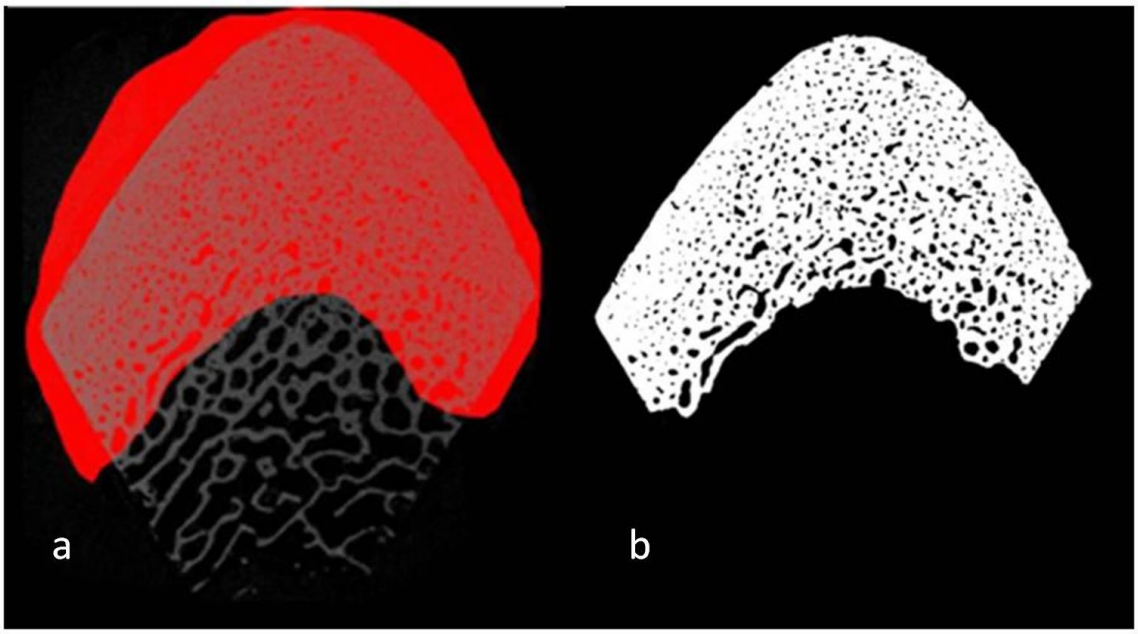

Figure 5.2: (a) coarse ROI and (b) binarized slices µCT image.

The 5mm thick cross section was fixed, defatted, and embedded in PMMA for histological analysis as described in detail in Chapter 3. The amount of secondary bone, defined as the secondary porosity and the secondary tissue, was determined for regions of interest at the mid-cortex and periosteal surface of the bone (see Figure 5.3).

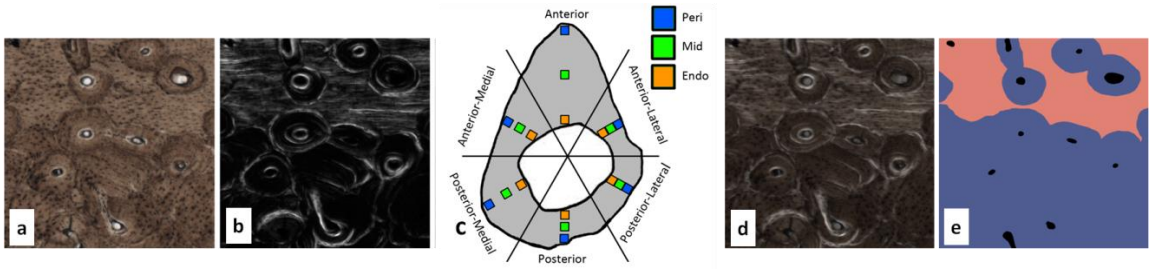

Figure 5.3: LM CPL combined and traced labeled (a) transmitted light microscopy image (b) circularly polarized transmitted light microscopy image c) schematic of locations of ROIs (c) combined image (d) traced tissue types

5.2.3: Statistical Analysis

Analysis of variance (ANOVA) was used to assess the contribution of location (wedge), robustness and age to the variation in porosity and ash content. Least significant difference (LSD) post-hoc tests were used to assess the variability in porosity and ash content between wedges. Linear regressions were performed for the correlations between porosity and ash content for each wedge for the overall sample, and for subsets of slender and robust bones.

5.3: Results

5.3.1: Porosity

MicroCT based porosity data were collected for each wedge of bone tissue around the tibial cortex at the 38% and 66% sites in order to determine whether location in the cortex (wedge) was a significant contributor to variation in porosity, and if so, what the pattern of variability was. The cortex was also further subdivided into three concentric rings in order to further examine differences between the periosteum, mid-cortex, and endosteum. In each wedge, regions of interest were extracted from each ring, giving 3 ROIs for each of the 6 wedges.

5.3.1.1: Multivariate analysis

A multi-factorial ANOVA with wedge and ring as fixed factors and age and robustness as covariates showed that at both the 38% and 66% sites, wedge was a significant contributor to the variation in porosity ($p=0.006$ and $p<0.001$ respectively) as was ring ($p < 0.001$). Age also had a significant effect on porosity distribution ($p<0.002$) at 38% site. At the 66% site, age was only significant when robustness was not

considered in the analysis ($p < 0.001$). Robustness only has a significant effect at the 66% site ($p < 0.001$).

5.3.1.2: Variation in porosity by wedge

Post-hoc tests (in the ANOVA corrected for age and robustness) clarified the pattern of variability in porosity further. For the 38% site, the anterior wedge was significantly ($p < 0.001$) more porous than all other wedges. Additionally the posterior wedge was significantly ($p=0.041$) more porous than the anterior-lateral wedge and the anterior-medial wedge was significantly more porous than the anterior-lateral wedge ($p=0.014$) and the posterior-lateral wedge ($p=0.049$) (see Figure 5.4).

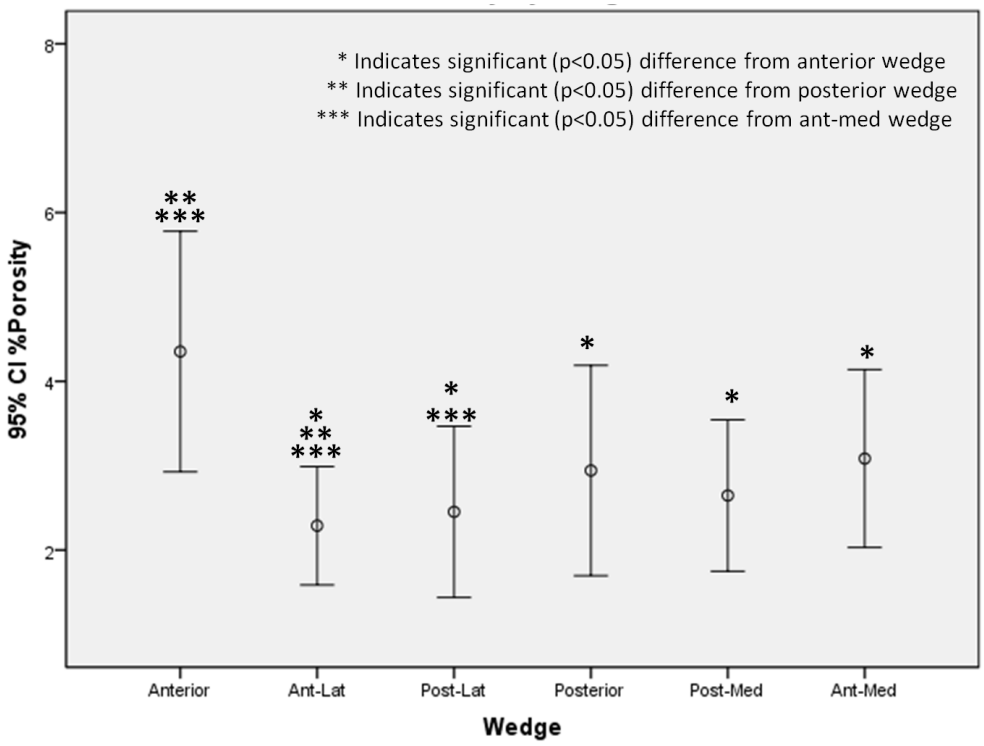

Figure 5.4: Porosity at each wedge around the cortex at the 38% site.

At the 66% site, the anterior wedge was significantly more porous than all other wedges ($p<0.001$). The posterior wedge was significantly more porous than the anterior-lateral wedge ($p < 0.001$), posterior-lateral wedge ($p < 0.001$), and posterior medial wedge ($p = 0.001$). Additionally, the anterior medial wedge had significantly higher porosity than the anterior-lateral wedge ($p=0.001$), the posterior-lateral wedge ($p=0.004$) and the posterior-medial wedge ($p=0.001$) (see Figure 5.5).

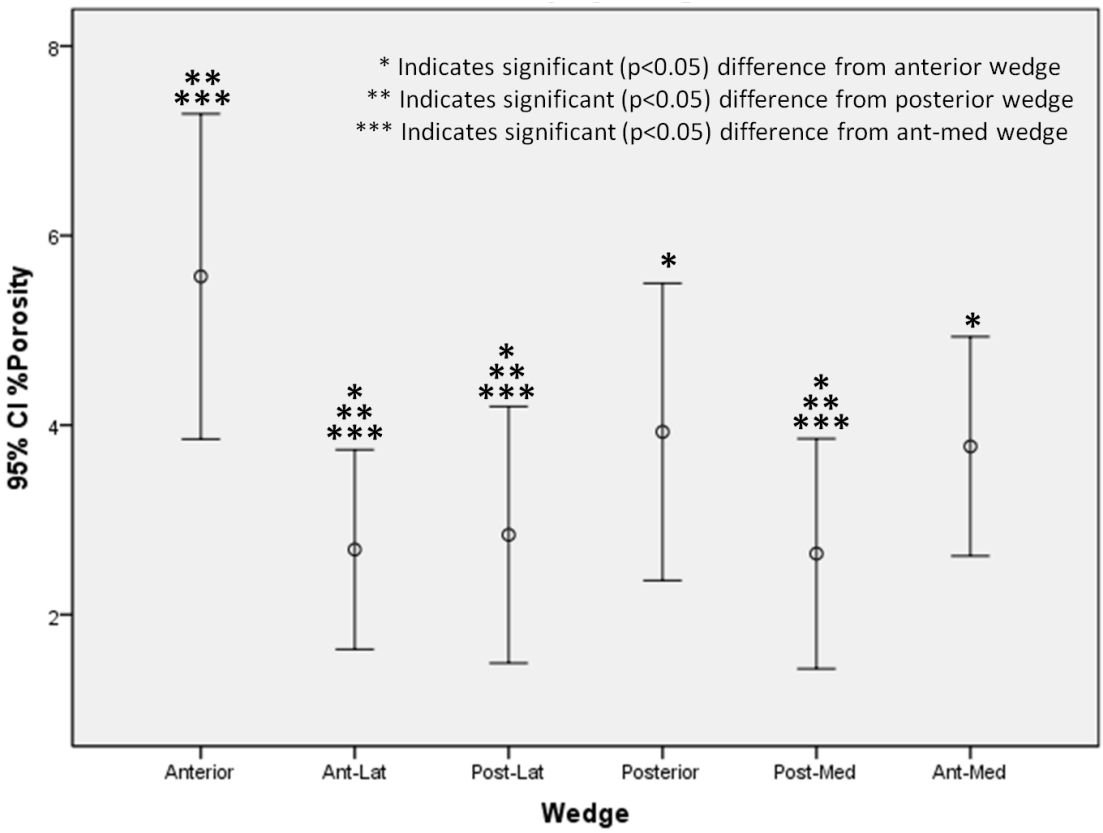

Figure 5.5: Porosity at each wedge around the cortex at the 66% site.

There were no correlations found at the 38% site between porosity and robustness for any wedge (see Figure 5.6). However, strong linear correlations between porosity and robustness were found at each wedge for the 66% site, (see Figure 5.7).

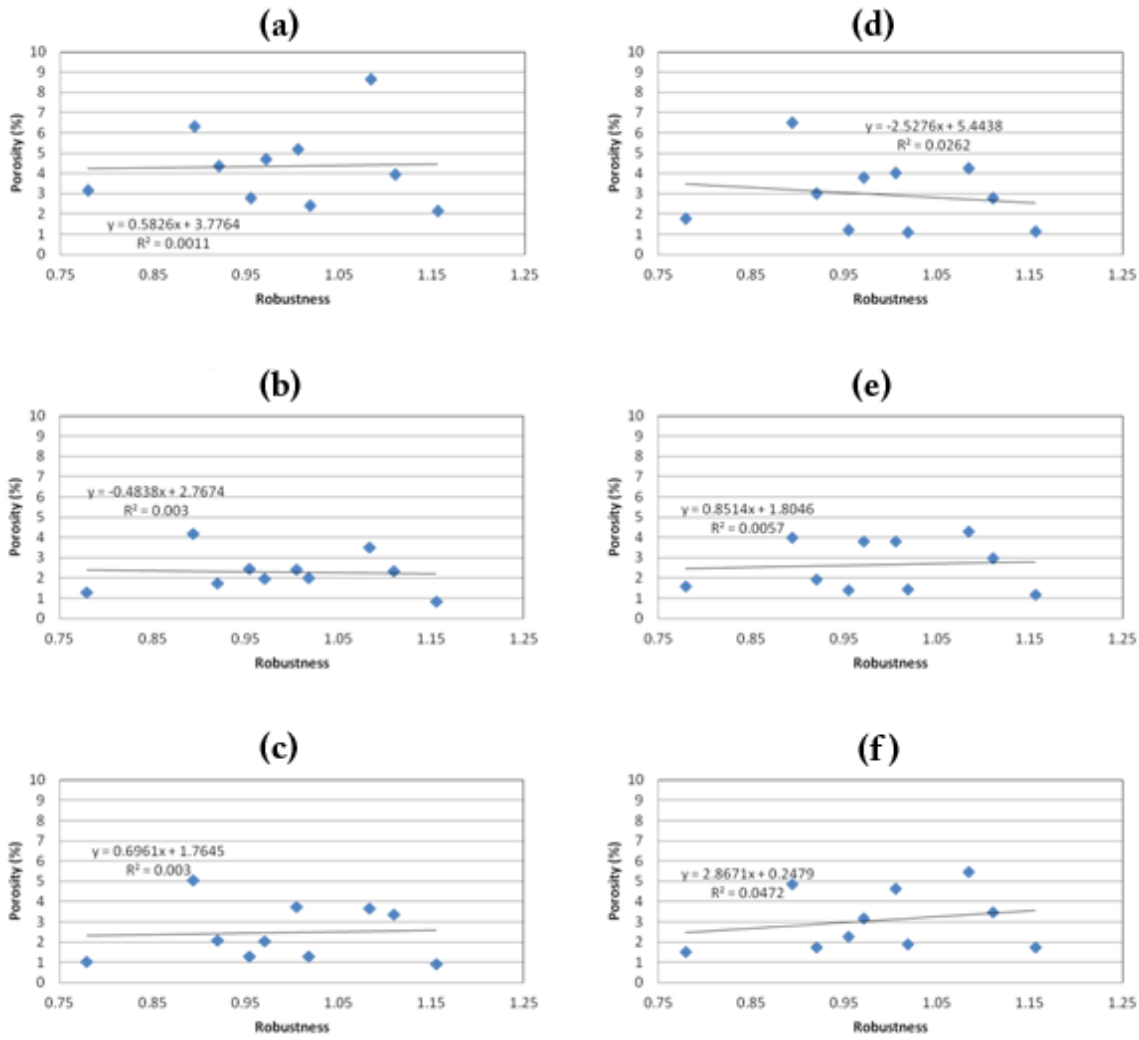

Figure 5.6: Relationships between porosity and robustness at the 38% site at (a) anterior wedge (b) anterior-lateral wedge (c) posterior-lateral wedge (d) posterior wedge (e) posterior-medial wedge (f) anterior-medial wedge.

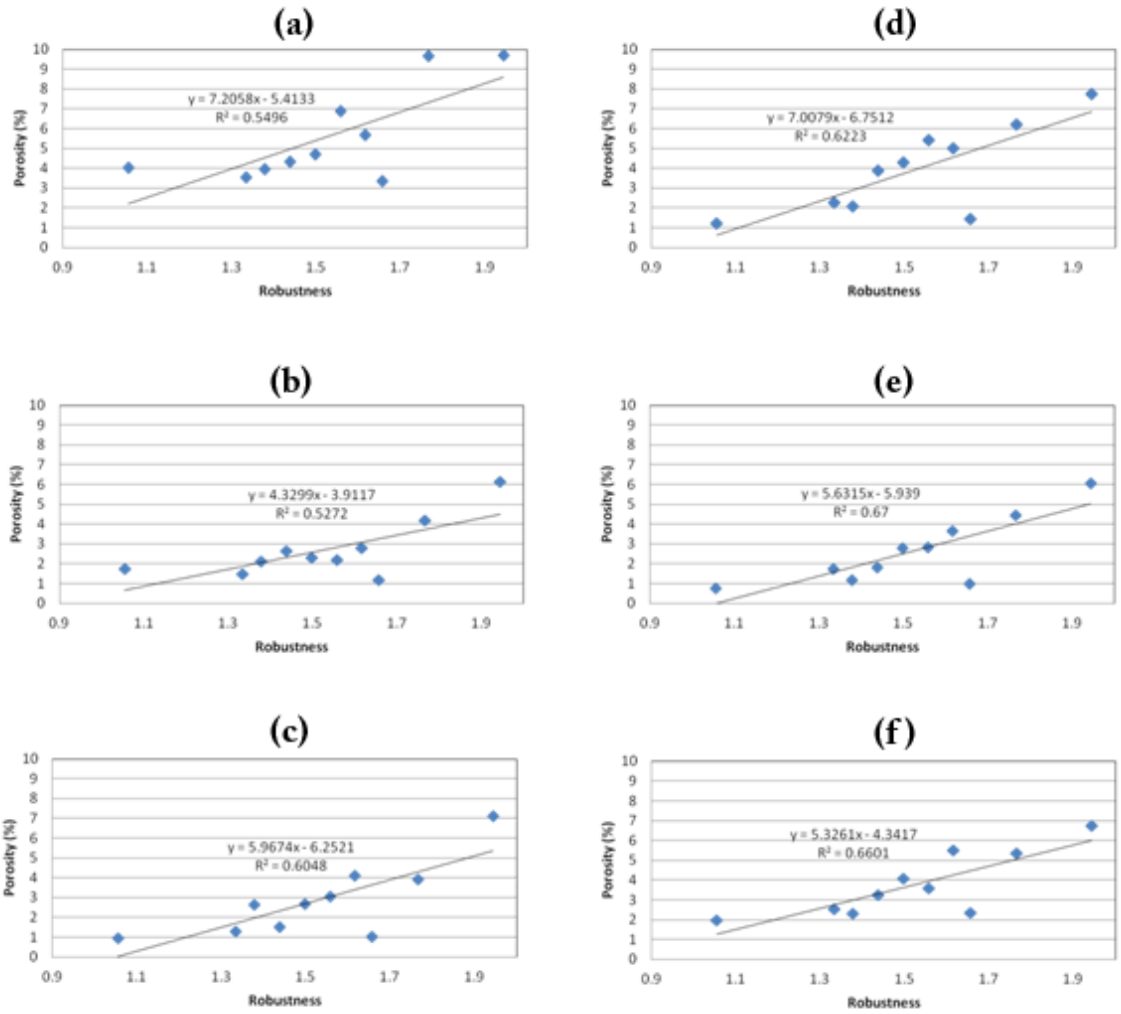

Figure 5.7: Relationships between porosity and robustness at the 66% site at the (a) anterior wedge (b) anterior-lateral wedge (c) posterior-lateral wedge (d) posterior wedge (e) posterior-medial wedge (f) anterior-medial wedge.

5.3.1.3: Variation in porosity between rings

Considering all wedges combined, it was found that there were significant differences in 3-dimensional porosity were found at both the 38% and 66% sites between the endosteal rings and both the mid-cortex and periosteal rings. At both sites, the

endosteal ring had significantly higher ($p<0.001$) porosity. The periosteal ring had, on average, lower porosity at both sites, but this was not significant ($p=0.646$ at 38% and $p=0.238$ at 66%) (see Figure 5.8).

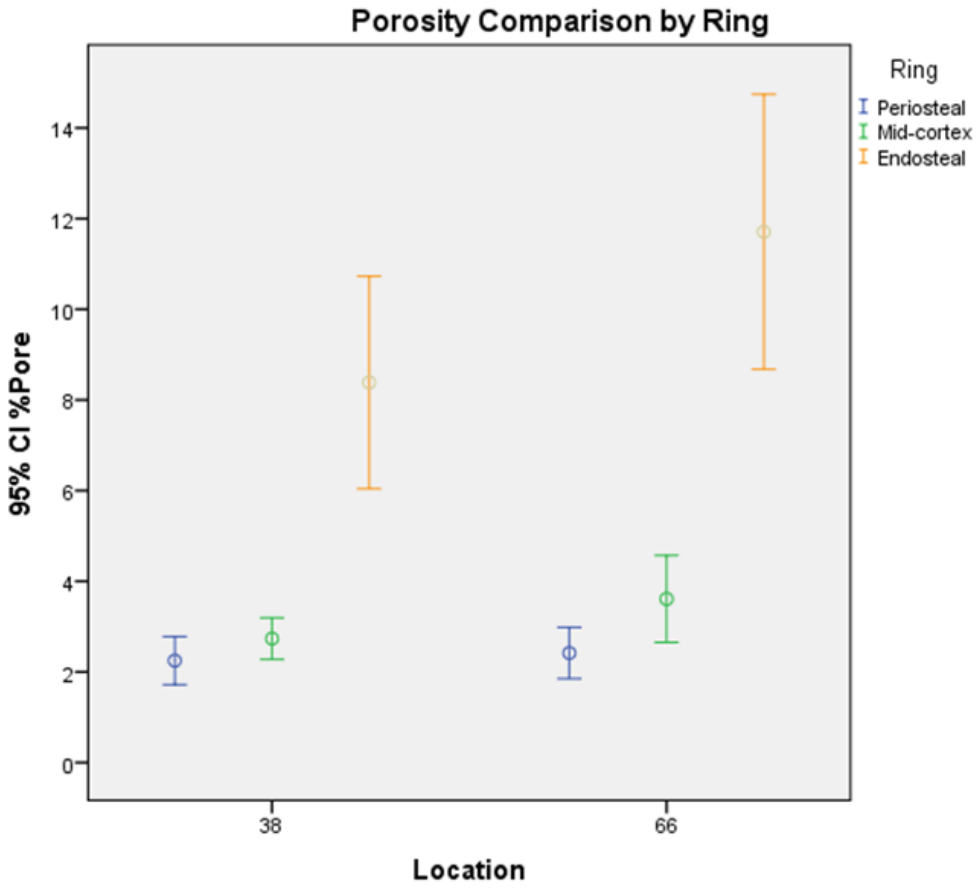

Figure 5.8: Porosity comparison by ring for each location.

Considering ring variability by individual wedge at the 38% site, the endosteal ring had significantly ($p < 0.005$) higher porosity than both the mid-cortex and periosteal rings for the anterior, posterior-medial, and anterior-medial wedges. The endosteal ring also

had significantly (p = 0.036) higher porosity than the periosteal ring in the posterior wedge. There were no significant (p < 0.05) differences between the mid-cortex ring and the periosteal ring at any wedge (see Figure 5.9).

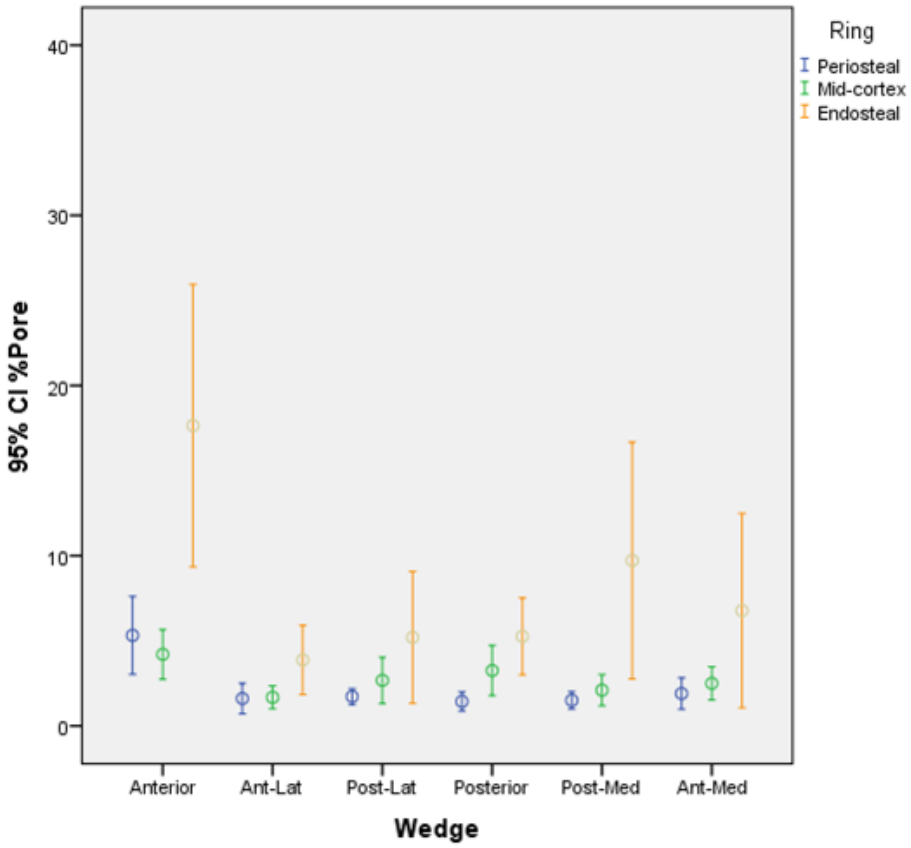

Figure 5.9: Porosity between rings for each wedge at the 38% site.

At the 66% site, the endosteal ring had significantly higher porosity than both the mid-cortex and periosteal rings for the anterior (p < 0.001), posterior-lateral (p < 0.05) , posterior (p < 0.001) , and anterior-medial (p < 0.001) wedges. The mid-cortex ring had

significantly ($p < 0.05$) higher porosity than the periosteal ring only at the posterior wedge (see Figure 5.10).

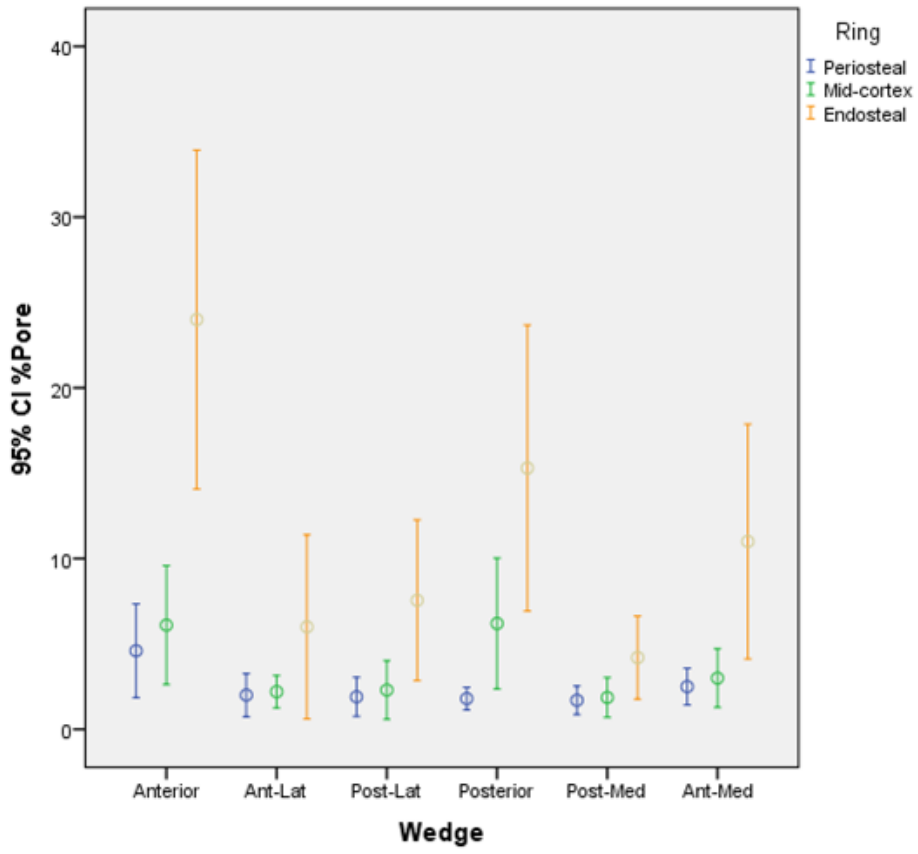

Figure 5.10: Porosity between rings for each wedge at the 66% site.

5.3.1.4: Variation in porosity within rings by wedge

Considering just the mid-cortical ring of the 38% site, the anterior wedge had significantly higher porosity than the anterior-lateral and posterior-medial wedges. There were no other significant differences (see Figure 5.11 and Table 5.1).

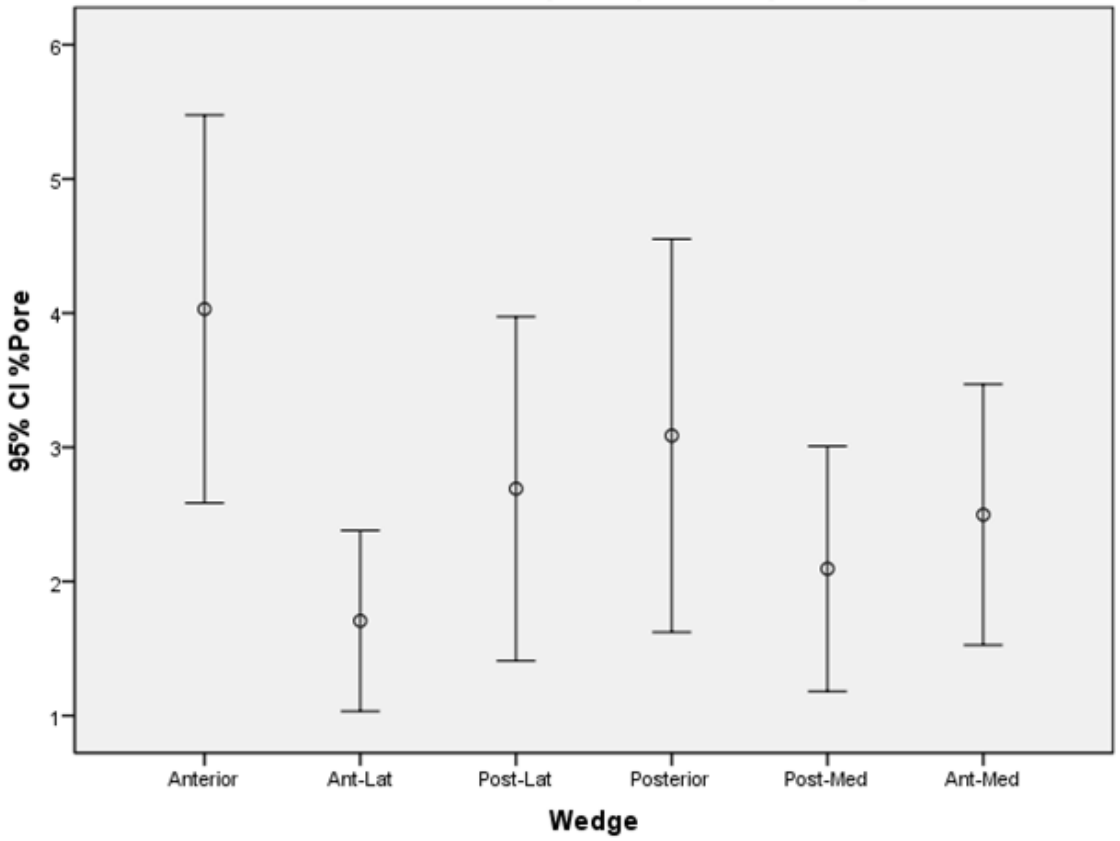

Figure 5.11: Porosity in the mid-cortex ring for each wedge at the 38% site.

Table 5.1: ANOVA table for 38% mid-cortex porosity by wedge

38% Mid-Cortex Region Porosity Differences

	Anterior	Ant-Lat	Post-Lat	Posterior	Post-Med	Ant-Med
Anterior	x	0.006	0.107	0.255	0.021	0.066
Ant-Lat	0.006	x	0.235	0.097	0.639	0.339
Post-Lat	0.107	0.235	x	0.632	0.471	0.815
Posterior	0.255	0.097	0.632	x	0.231	0.476
Post-Med	0.021	0.639	0.471	0.231	x	0.626
Ant-Med	0.066	0.339	0.815	0.476	0.626	x

At the mid-cortex of the 66% site, the anterior wedge had significantly higher porosity than all other wedges, apart from the posterior wedge. The posterior wedge had significantly higher porosity than all wedges apart from the anterior wedge (see Figure 5.12 and Table 5.2).

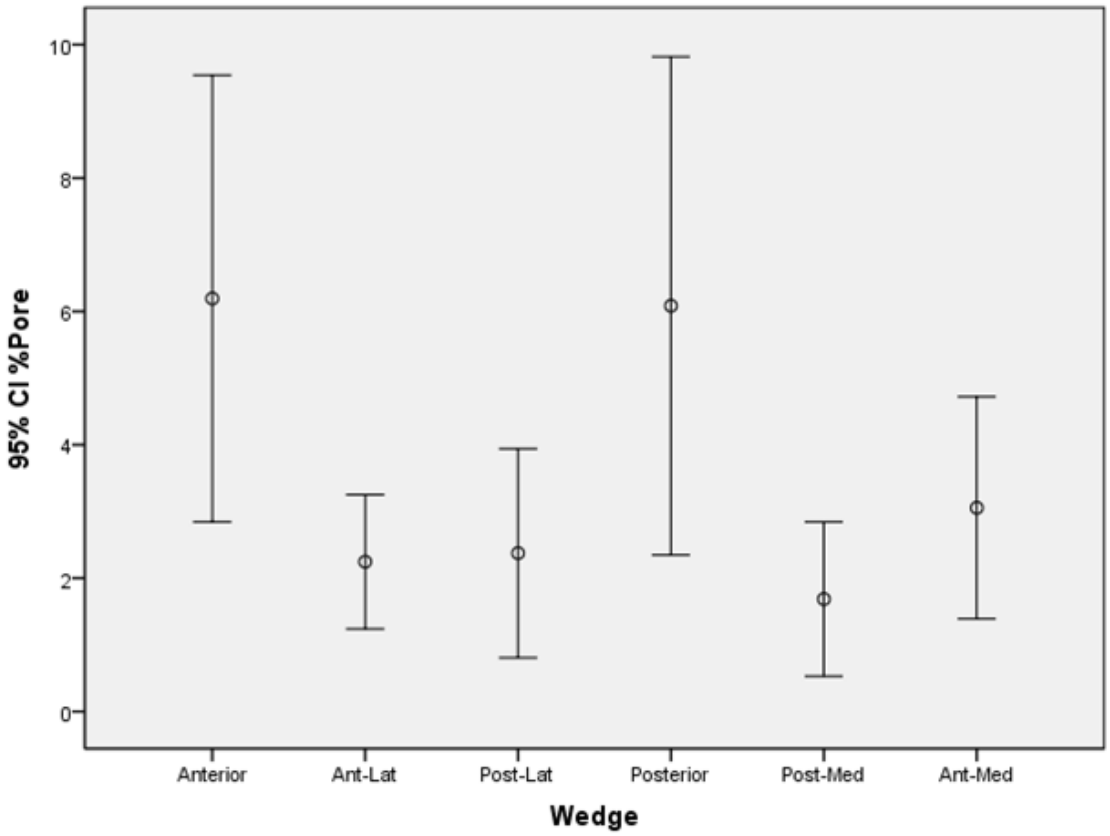

Figure 5.12: Porosity in the mid-cortex ring for each wedge at the 66% site.

Table 5.2: ANOVA table for 66% mid-cortex porosity by wedge

	Anterior	Ant-Lat	Post-Lat	Posterior	Post-Med	Ant-Med
Anterior	x	0.000	0.000	0.894	0.000	0.000
Ant-Lat	0.000	x	0.876	0.000	0.499	0.329
Post-Lat	0.000	0.876	x	0.000	0.406	0.411
Posterior	0.894	0.000	0.000	x	0.000	0.000
Post-Med	0.000	0.499	0.406	0.000	x	0.100
Ant-Med	0.000	0.329	0.411	0.000	0.100	x

Considering only the periosteal ring, the anterior wedge has significantly higher porosity than all other ROIs. This was significant at both the 38% site and the 66% site (see Figures 5.13 and 5.14 and Tables 5.3 and 5.4).

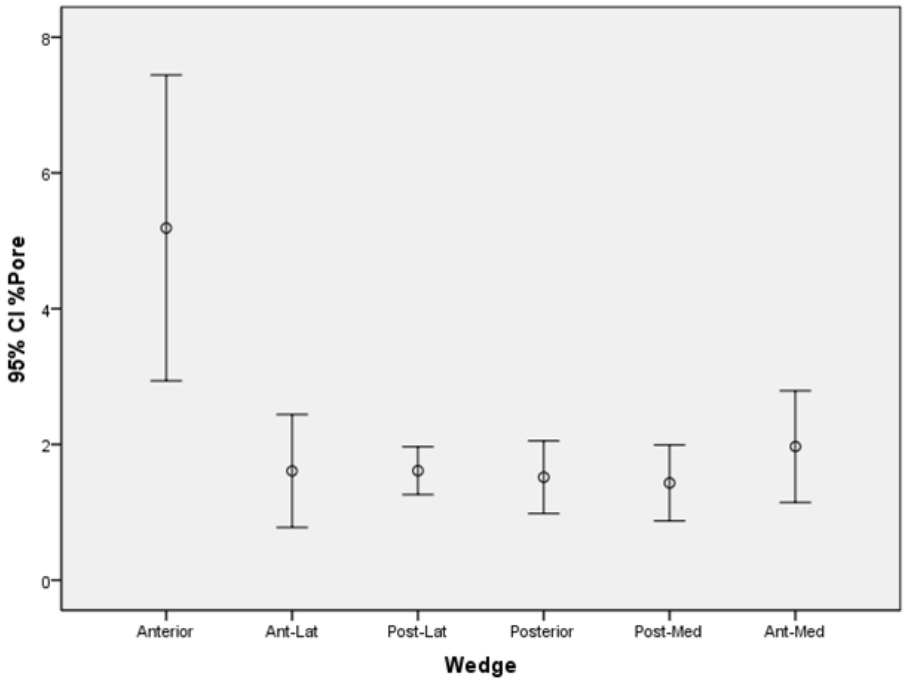

Figure 5.13: Porosity in the periosteal ring for each wedge at the 38% site.

Table 5.3: ANOVA table for 38% periosteal porosity by wedge

	Anterior	Ant-Lat	Post-Lat	Posterior	Post-Med	Ant-Med
Anterior	x	0.000	0.000	0.000	0.000	0.000
Ant-Lat	0.000	x	0.995	0.892	0.794	0.595
Post-Lat	0.000	0.995	x	0.887	0.789	0.599
Posterior	0.000	0.892	0.887	x	0.900	0.505
Post-Med	0.000	0.794	0.789	0.900	x	0.428
Ant-Med	0.000	0.595	0.599	0.505	0.428	x

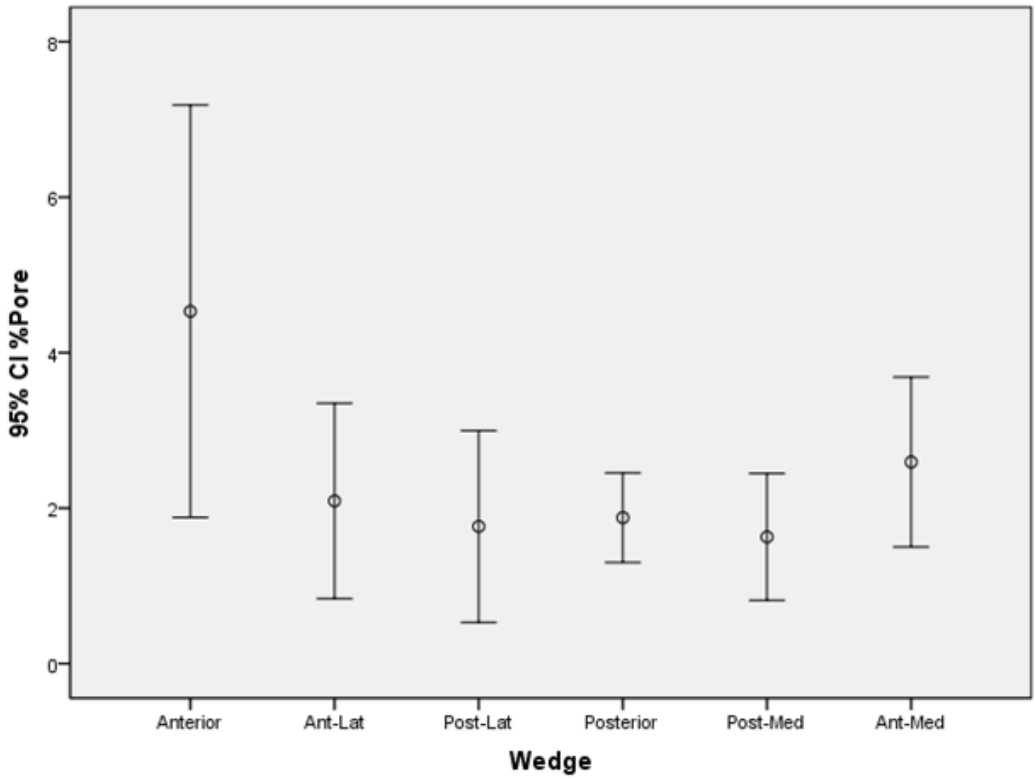

Figure 5.14: Porosity in the periosteal ring for each wedge at the 66% site.

Table 5.4: ANOVA table for 66% periosteal porosity by wedge

	Anterior	Ant-Lat	Post-Lat	Posterior	Post-Med	Ant-Med
Anterior	x	0.000	0.000	0.000	0.000	0.005
Ant-Lat	0.000	x	0.628	0.750	0.494	0.460
Post-Lat	0.000	0.628	x	0.867	0.842	0.222
Posterior	0.000	0.750	0.867	x	0.715	0.291
Post-Med	0.000	0.494	0.842	0.715	x	0.156
Ant-Med	0.005	0.460	0.222	0.291	0.156	x

5.3.1.5: Relationship Between Porosity and Robustness by Wedge and Ring

At the 38% site in the endosteal ring, there were no significant ($p < 0.05$) relationships between porosity and robustness for any wedge around the cortex (see Figure 5.15). At the 66% site in the endosteal ring, there was a significant positive linear relationship between porosity and robustness for the posterior wedge ($p = 0.012$) and the posterior-medial wedge ($p = 0.004$) (see Figure 5.16). No other wedges had significant linear relationships between porosity and robustness for the endosteal ring.

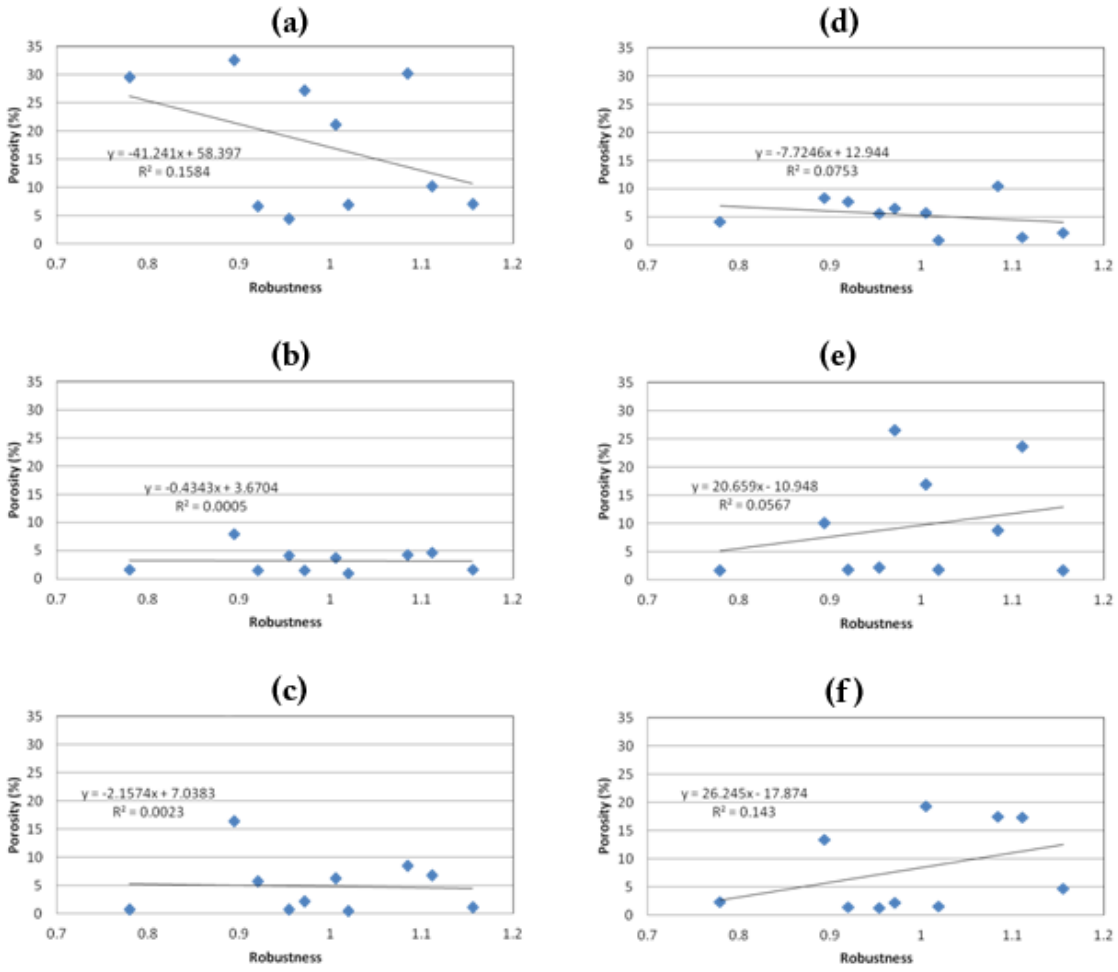

Figure 5.15: Relationships between porosity and robustness in the endosteal ring at the 38% site at the (a) anterior wedge (b) anterior-lateral wedge (c) posterior-lateral wedge (d) posterior wedge (e) posterior-medial wedge (f) anterior-medial wedge.

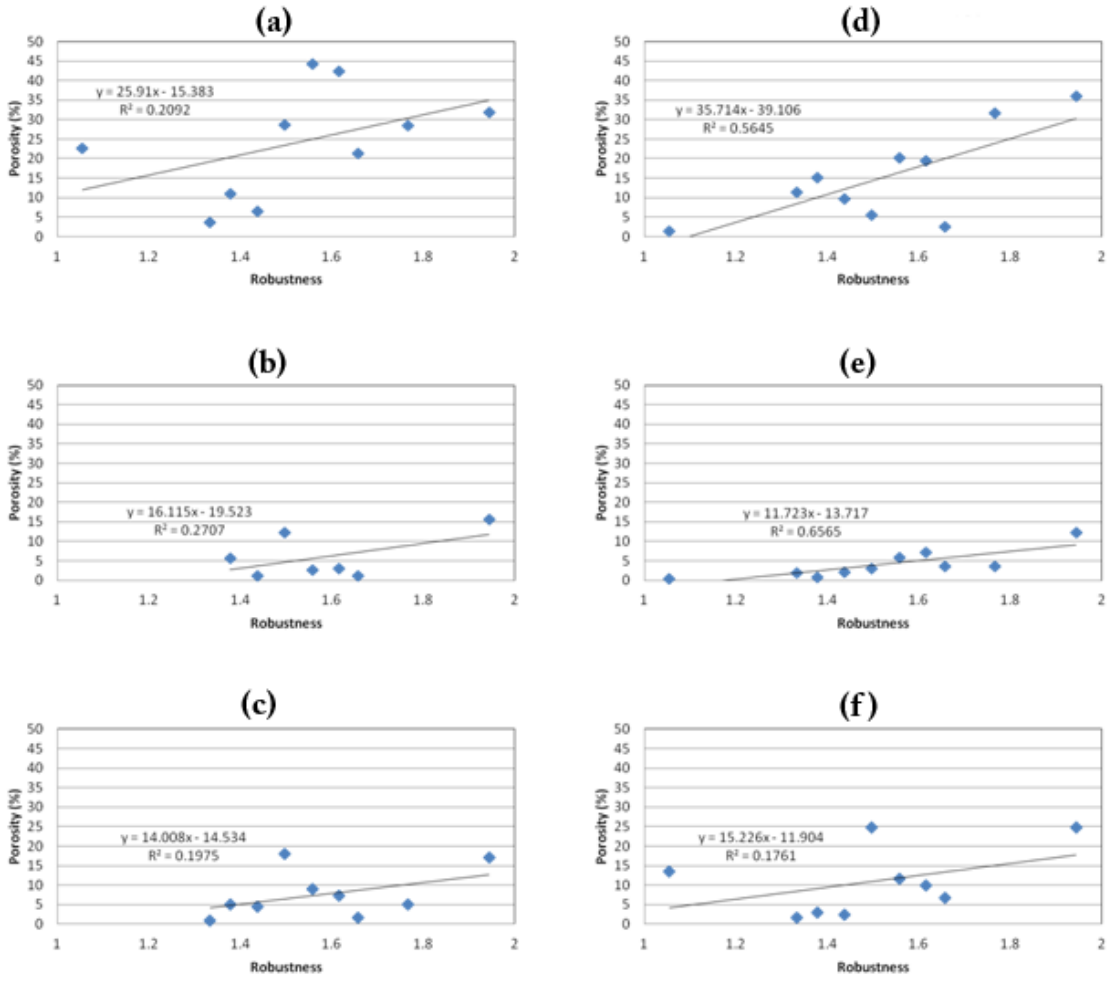

Figure 5.16: Relationships between porosity and robustness in the endosteal ring at the 66% site at the (a) anterior wedge (b) anterior-lateral wedge (c) posterior-lateral wedge (d) posterior wedge (e) posterior-medial wedge (f) anterior-medial wedge.

At the 38% site in the mid-cortex ring, there were no significant relationships between porosity and robustness for any wedge around the cortex (see Figure 5.17). However, at the 66% site, there were significant ($p < 0.05$) positive linear relationships between porosity and robustness every wedge around the cortex (see Figure 5.18).

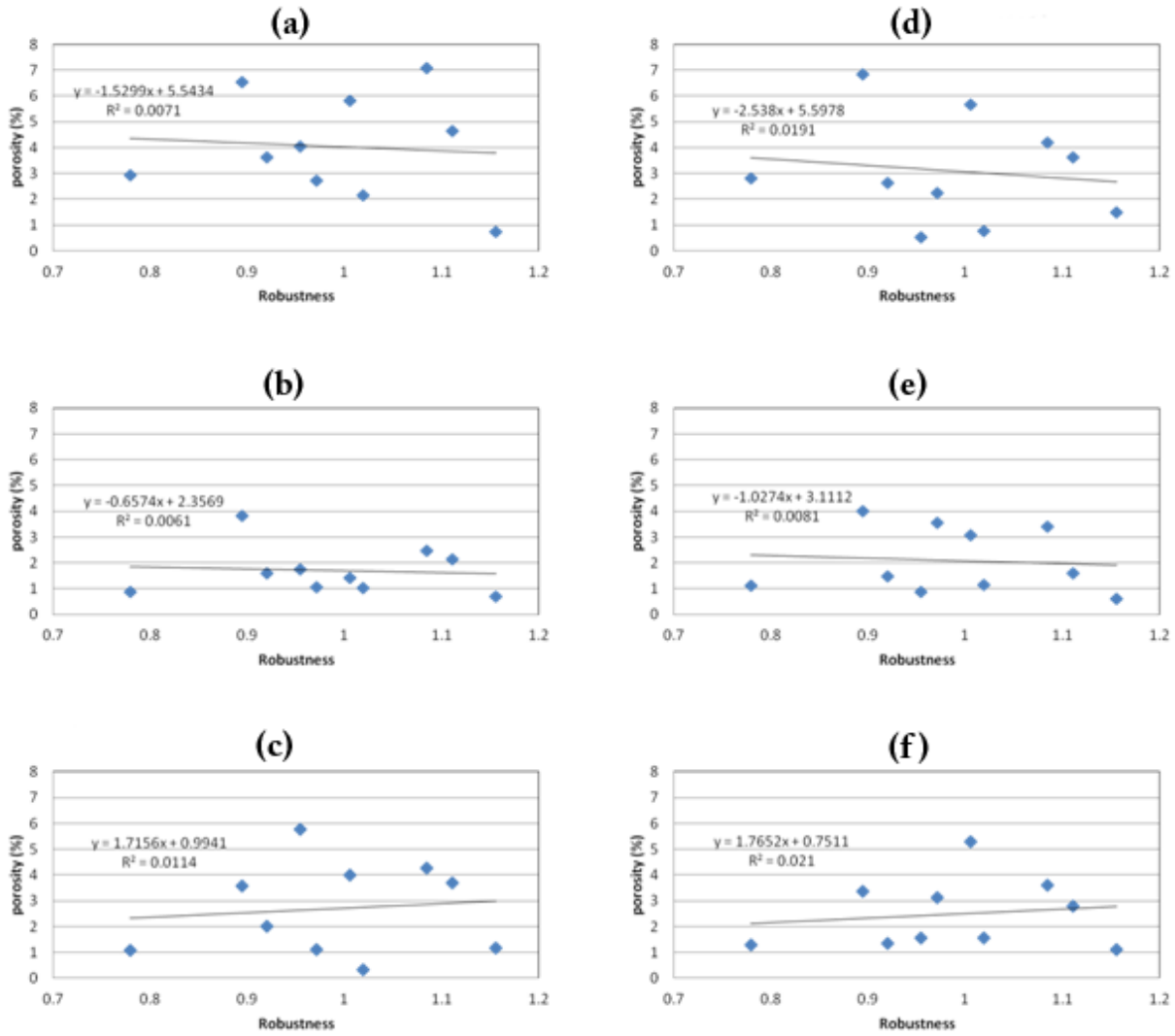

Figure 5.17: Relationships between porosity and robustness in the mid-cortex ring at the 38% site at the (a) anterior wedge (b) anterior-lateral wedge (c) posterior-lateral wedge (d) posterior wedge (e) posterior-medial wedge (f) anterior-medial wedge.

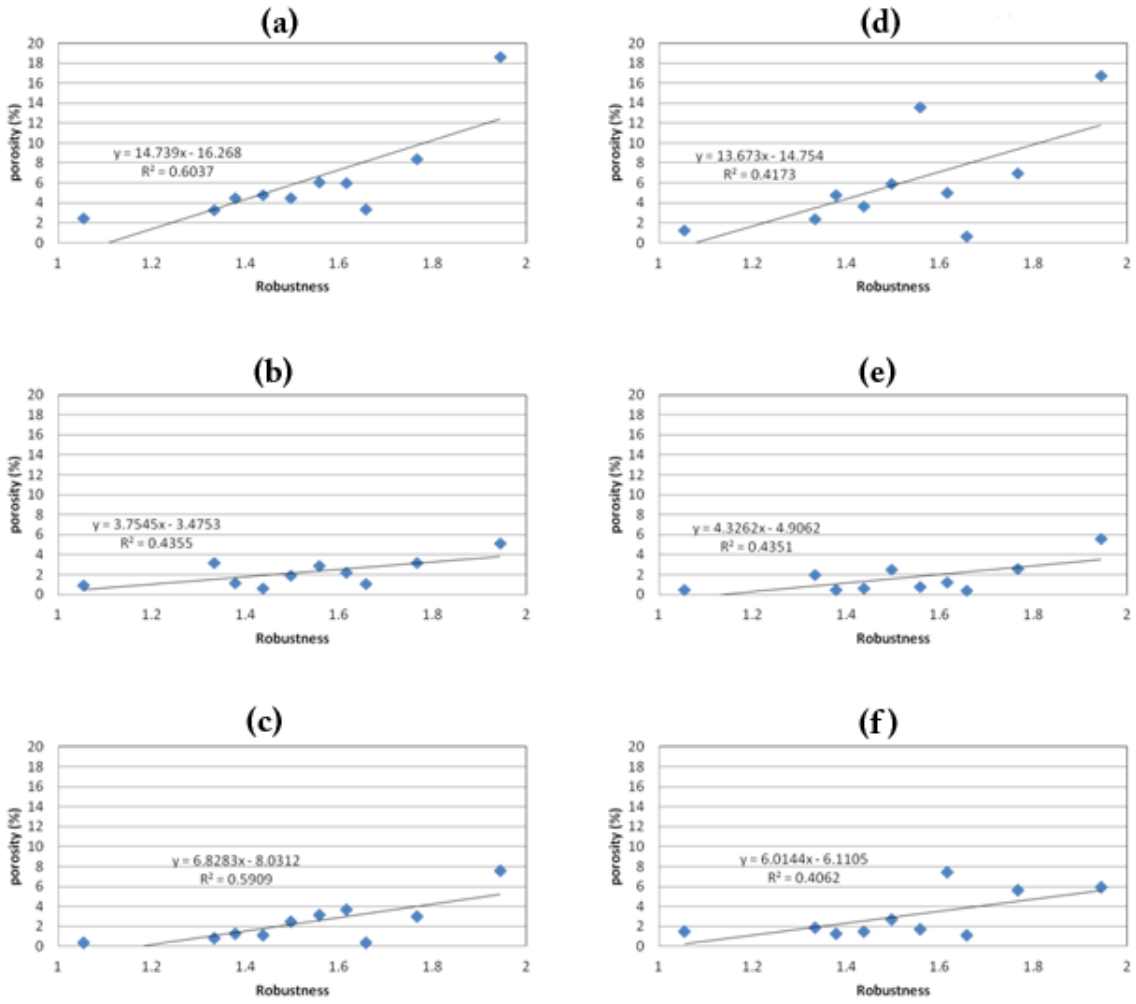

Figure 5.18: Relationships between porosity and robustness in the mid-cortex ring at the 66% site at the (a) anterior wedge (b) anterior-lateral wedge (c) posterior-lateral wedge (d) posterior wedge (e) posterior-medial wedge (f) anterior-medial wedge.

At the 38% site in the periosteal ring, there were no significant relationships between porosity and robustness for any wedge around the cortex (see Figure 5.19). However, at the 66% site, there were significant positive linear relationships between porosity and robustness at the anterior ($p = 0.017$) and the posterior wedges ($p = 0.004$).

There was a strong trend at the posterior-medial wedge, however, it was not significant ($p = 0.056$) (see Figure 5.20).

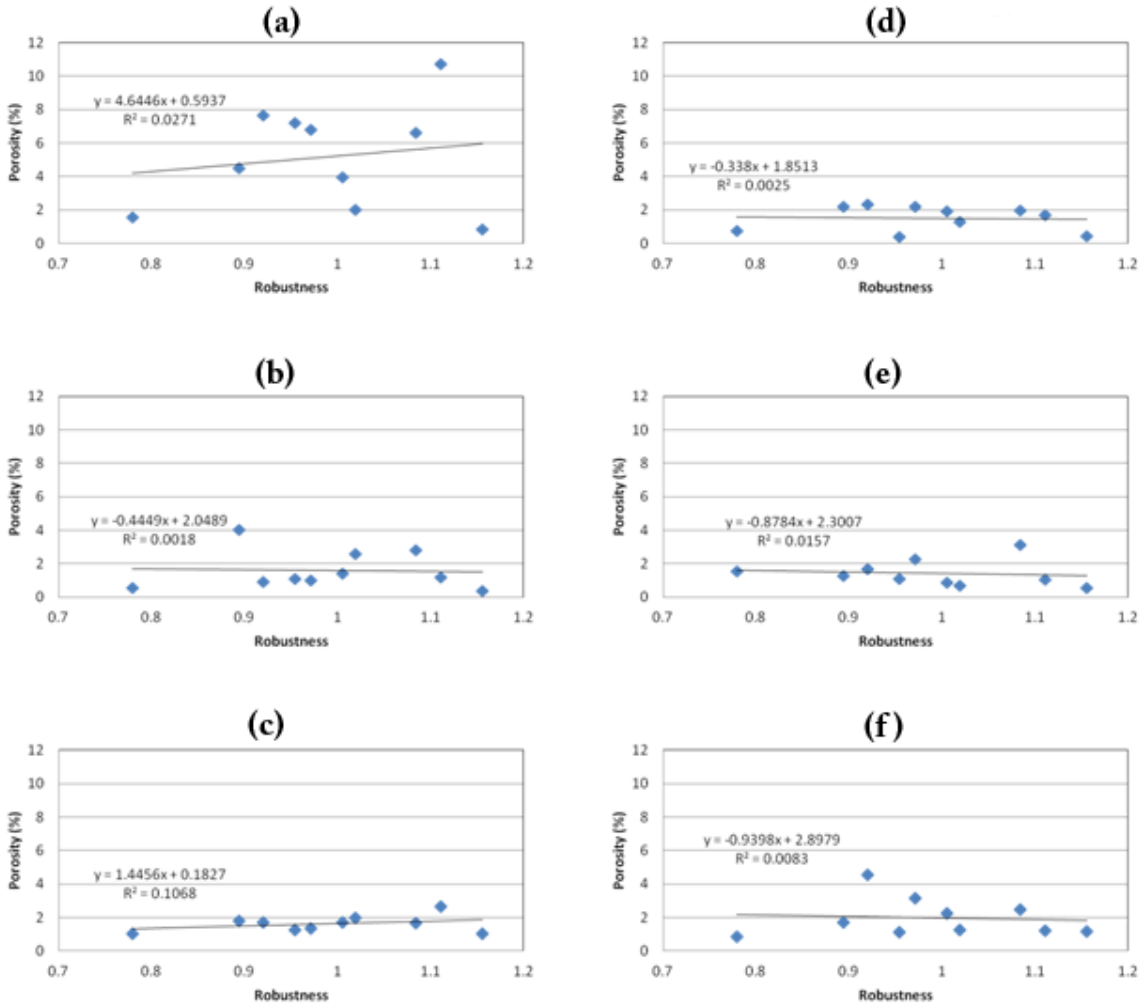

Figure 5.19: Relationships between porosity and robustness in the periosteal ring at the 38% site at the (a) anterior wedge (b) anterior-lateral wedge (c) posterior-lateral wedge (d) posterior wedge (e) posterior-medial wedge (f) anterior-medial wedge.

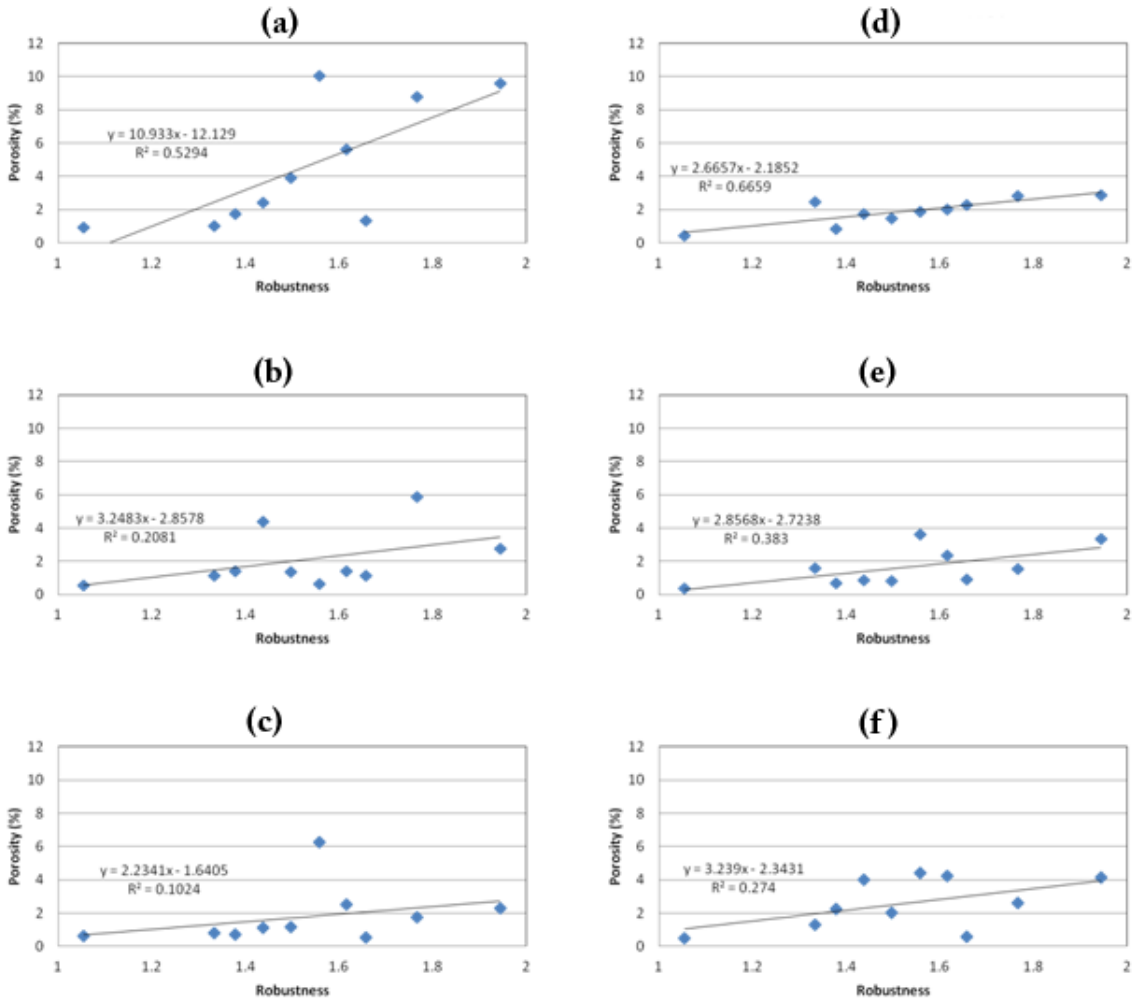

Figure 5.20: Relationships between porosity and robustness in the periosteal ring at the 66% site at the (a) anterior wedge (b) anterior-lateral wedge (c) posterior-lateral wedge (d) posterior wedge (e) posterior-medial wedge (f) anterior-medial wedge.

5.3.2: Ash Content

Each of the wedges analyzed above for porosity was then ashed in order to measure the average tissue mineralization density for the whole wedge. As with the porosity variable, the goal was to determine whether location around the cortex (wedge) was a

significant contributor to variations in ash content, and if so, what the pattern of variability was. An additional goal was to assess the effects of age and robustness on ash content. Methodologically, it was not possible to separately analyze ash content by ring, because ashing is a destructive process. Once the wedges were ashed, there was no more material available for regional compositional analysis.

5.3.2.1: Multivariate analysis

A multifactorial ANOVA with wedge, age, and robustness as covariates demonstrated that wedge was a significant contributor to the variation in ash content ($p = 0.001$) at 38% $p < 0.001$ at 66%). At the 38% site, robustness was a significant covariate ($p < 0.001$). Age was marginally significant, but only when analyzed together with robustness ($p=0.041$). At the 66% site, only robustness was a significant covariate ($p < 0.001$).

5.3.2.2: Variation in Ash Content by Wedge

Post-hoc tests (in the ANOVA corrected for age and robustness) showed that for both the 38% and the 66% site, the ash content of the anterior wedge was significantly ($p < 0.001$) lower than all other wedges. There were no significant relationships between any of the other wedges (see Figure 5.21 and 5.22).

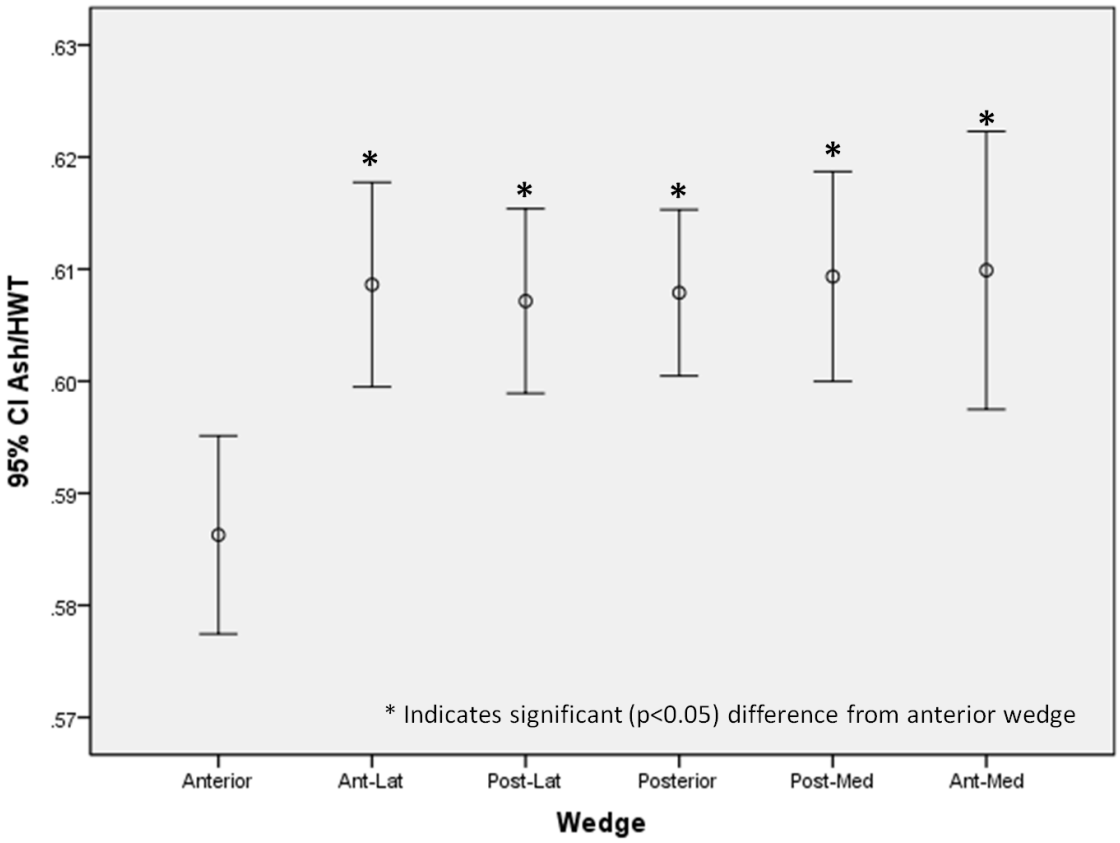

Figure 5.21: Variation of ash content at the 38% site around the cortex.

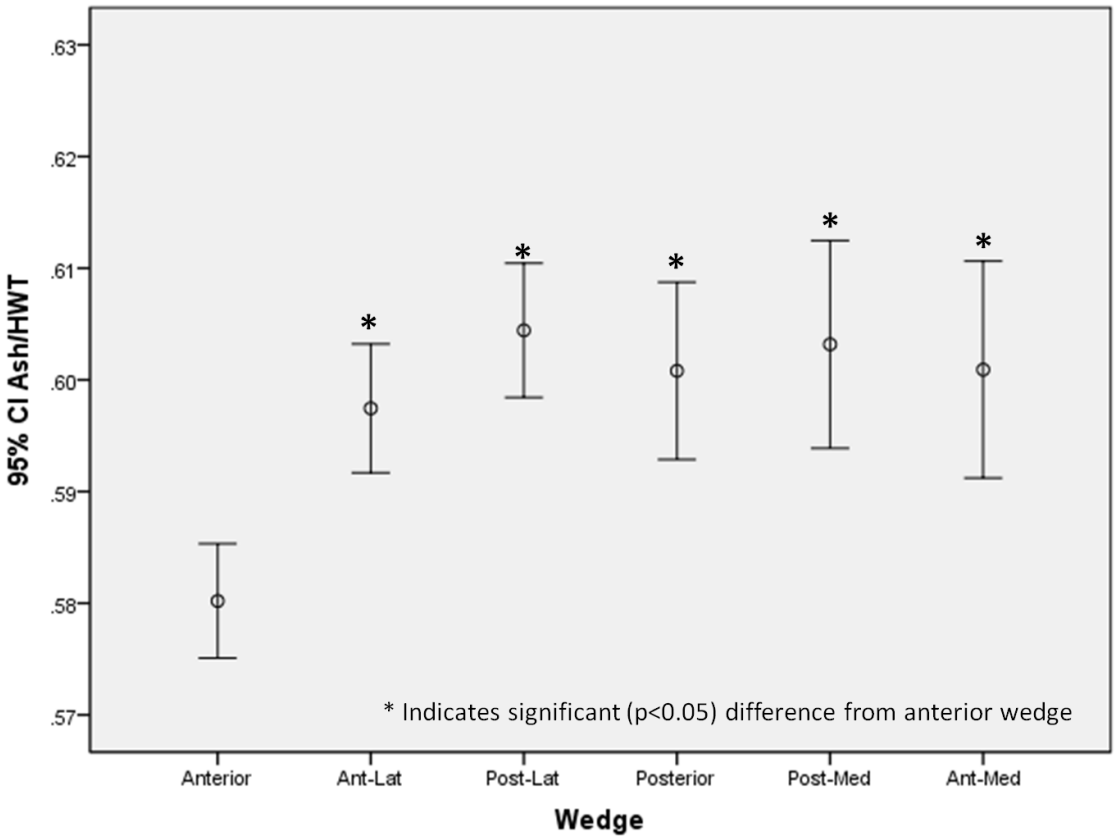

Figure 5.22: Variation of ash content at the 66% site around the cortex.

At the 38% site, there was a trend at the posterior wedge for a relationship between ash content and robustness, but it was not significant (p=0.058). The same was found at the anterior-medial wedge (p = 0.055). The relationship between ash and robustness was significant at the posterior medial wedge (p = 0.027) (see Figure 5.23).

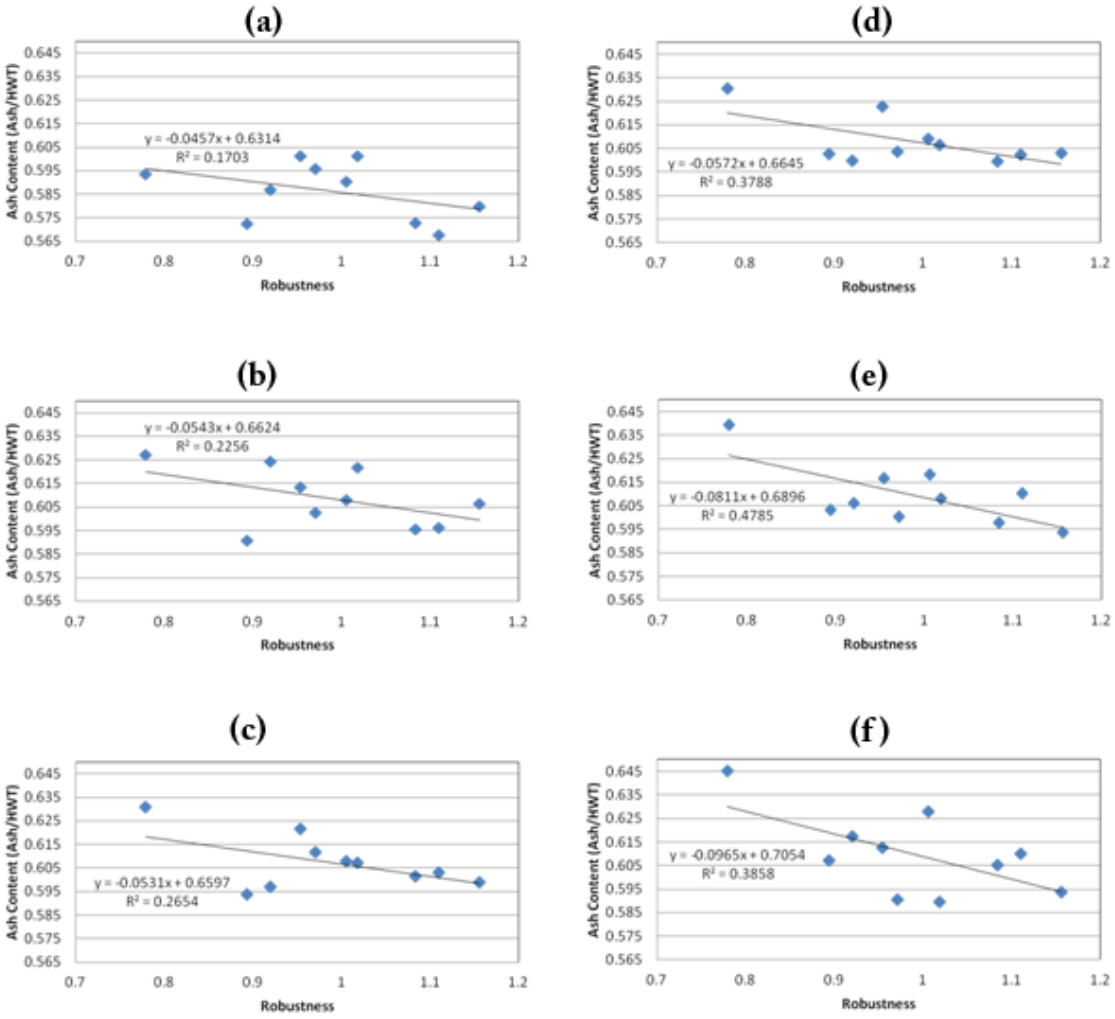

Figure 5.23: Relationship between ash content and robustness at the 38% at the (a) anterior wedge (b) anterior-lateral wedge (c) posterior-lateral wedge (d) posterior wedge (e) posterior-medial wedge (f) anterior-medial wedge.

At the 66% site, there was a strong linear correlation between ash content and robustness at the posterior wedge ($p = 0.006$). There was also a significant relationship at the posterior-medial wedge ($p = 0.023$) (see Figure 5.24).

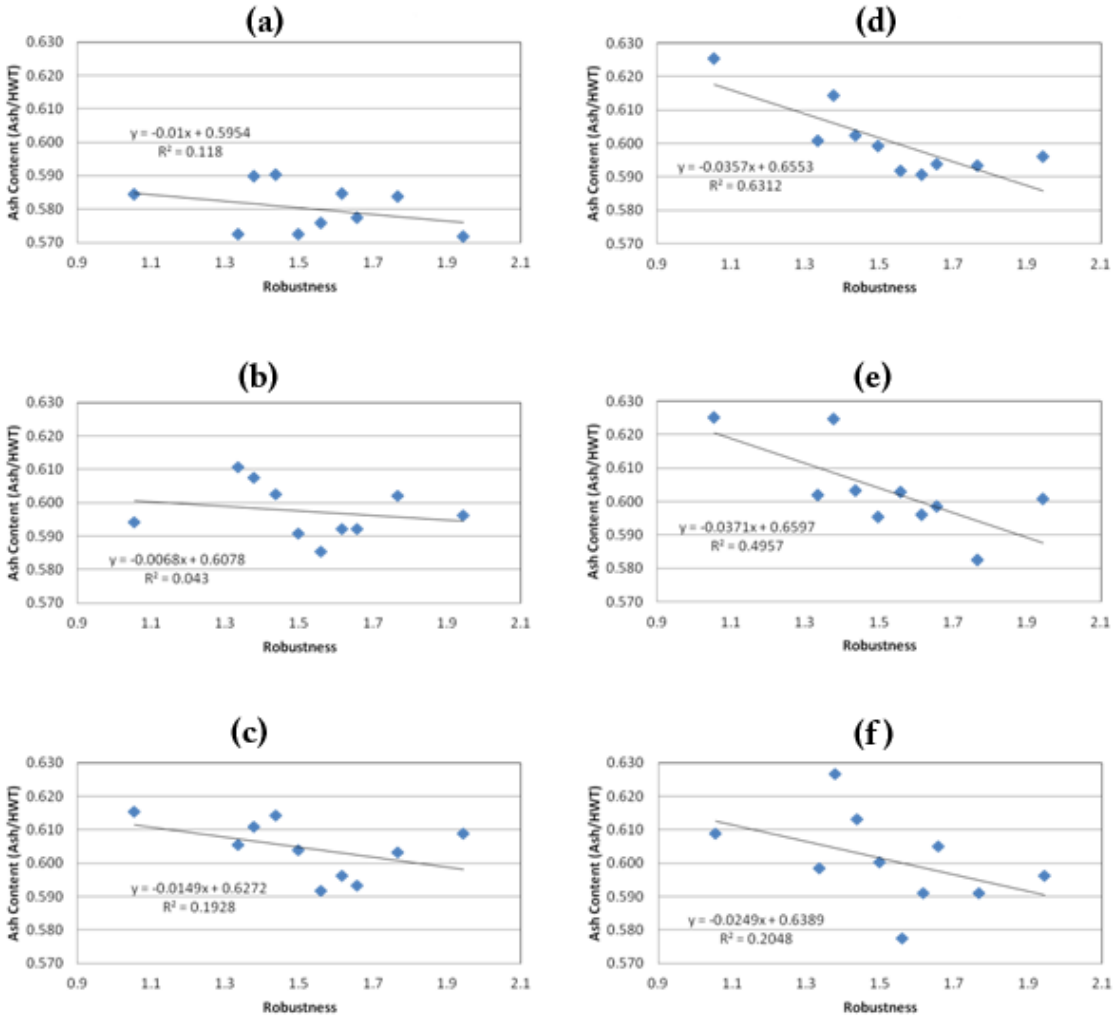

Figure 5.24: Relationship between ash content and robustness at the 66% at the (a) anterior wedge (b) anterior-lateral wedge (c) posterior-lateral wedge (d) posterior wedge (e) posterior-medial wedge (f) anterior-medial wedge.

5.3.3: Tissue Type

For this analysis, the amount of secondary bone (defined as secondary tissue plus secondary porosity) was determined for 1mm x 1mm regions of interest within the

periosteal and mid-cortex rings for each wedge. The goal was to quantify the variation of secondary bone varies around the cortex and between rings.

5.3.3.1: Multivariate analysis

A multifactorial ANOVA with wedge, age, and robustness as covariates demonstrated that wedge was a significant contributor in the amount of secondary bone at both the 38% and 66% sites ($p < 0.001$). Robustness was only a significant contributor when analyzed without considering age at both the 38% and 66% sites ($p = 0.036$ and $p = 0.027$, respectively). Age was significant at both the 38% and 66% sites ($p = 0.002$ and $p = 0.009$, respectively).

5.3.3.2: Variation in tissue type between rings

At both the 38% and 66% sites, the mid-cortex ring had significantly ($p < 0.001$ and $p = 0.003$, respectively) more secondary tissue than the periosteal ring (see Figures 5.25)

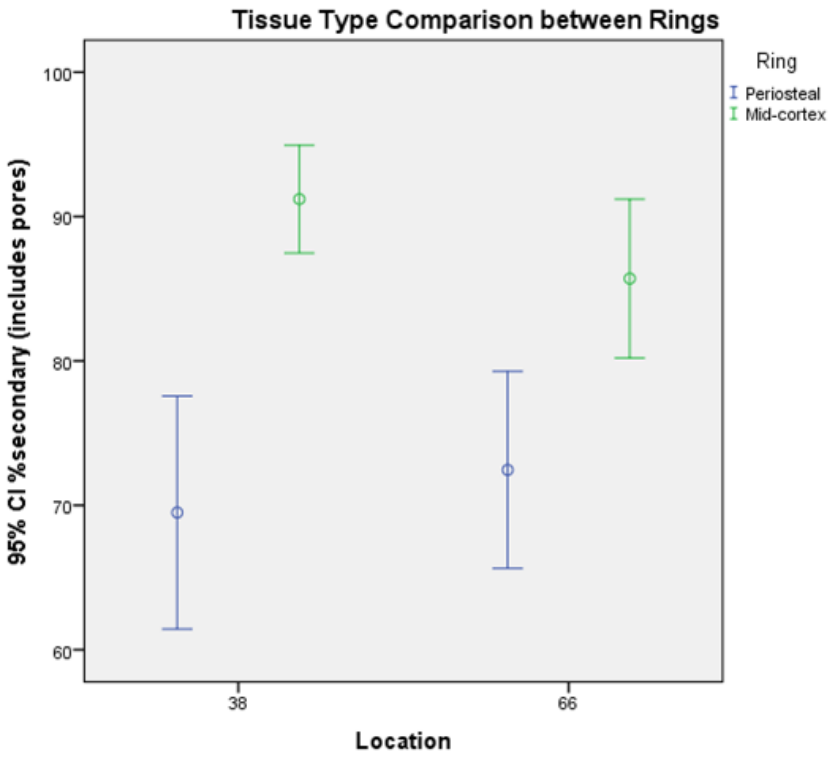

Figure 5.25: Comparison of amount of secondary tissue between mid-cortex and periosteum at each site.

At the 38% site, the mid-cortex ring had significantly greater amounts of secondary tissue than the periosteal ring in the anterior-lateral wedge ($p < 0.001$), the posterior wedge ($p = 0.003$), the posterior-medial wedge ($p < 0.001$), and the anterior-medial wedge ($p < 0.001$) (see Figure 5.26).

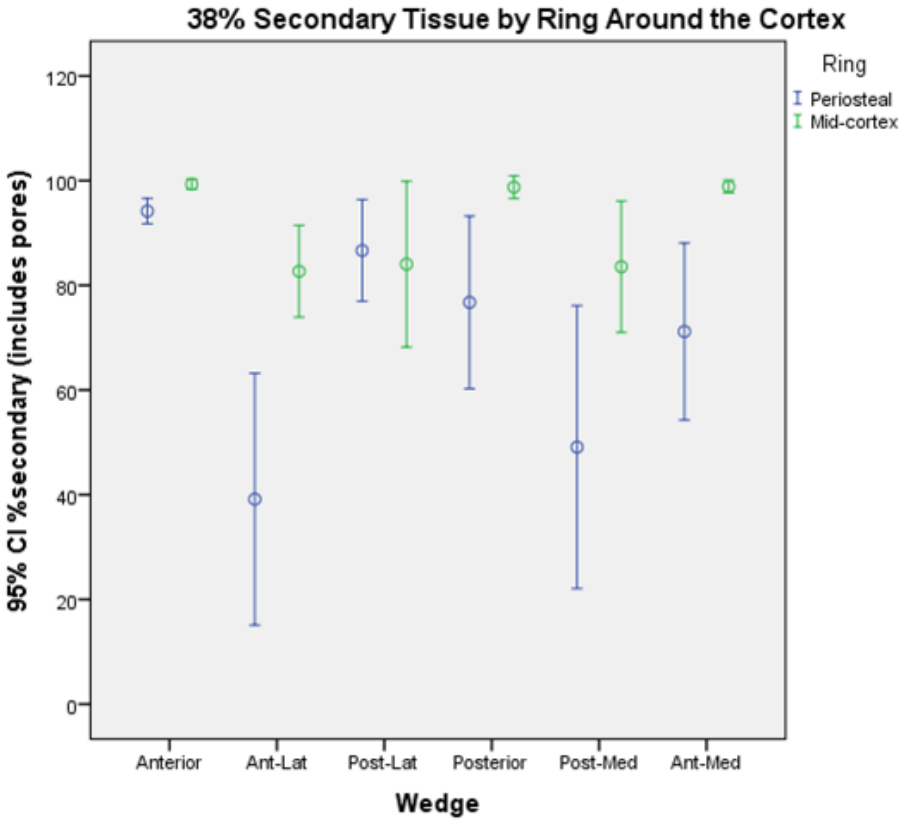

Figure 5.26: Amount of secondary tissue at each wedge by ring at the 38% site.

At the 66% site, the mid-cortex ring had significantly ($p < 0.001$) greater amounts of secondary tissue than the periosteal ring at the anterior-lateral and anterior-medial wedges (see Figure 5.27).

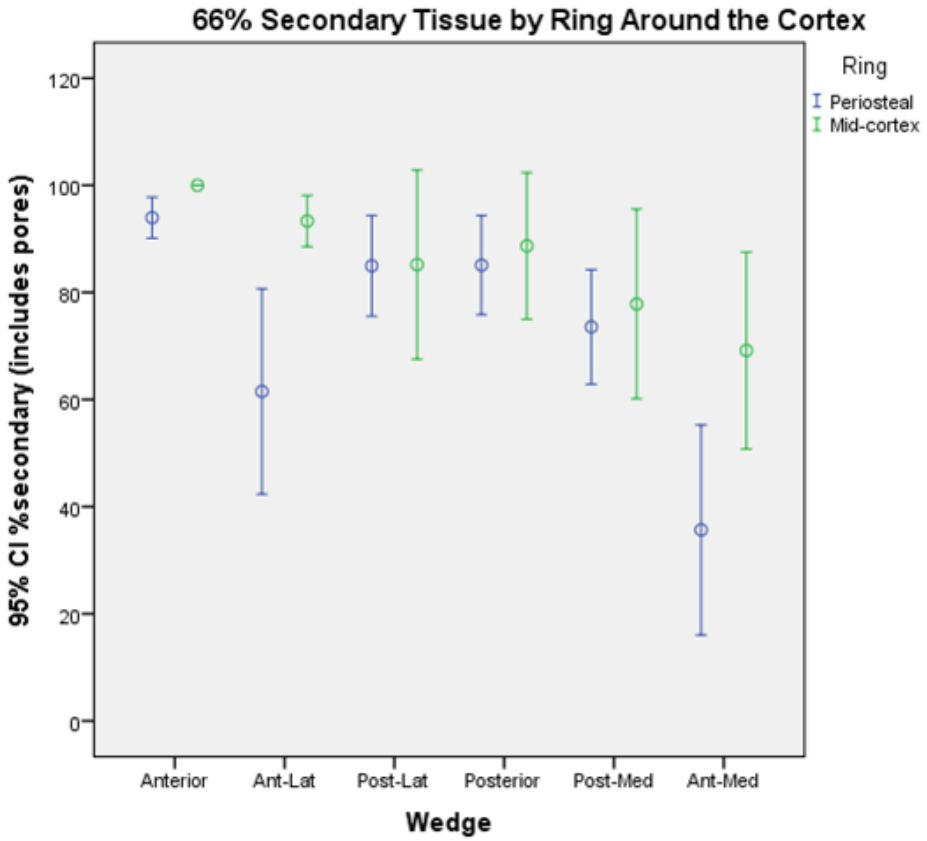

Figure 5.27: Amount of secondary tissue at each wedge by ring at the 66% site.

5.3.3.3: Variations in tissue type within rings by wedge

At both the 38% and 66% sites within the mid-cortex and periosteal rings, there were many significant differences between the amount of secondary tissue around the cortex. Within the mid-cortex ring, for the 38% site, the anterior, posterior, and anterior-medial wedges had greater amounts of secondary tissue than the anterior-lateral, posterior-lateral, and posterior-medial rings (see Figures 5.28 and 5.29 and Tables 5.5 and 5.6). Within the mid-cortex ring, for the 66% site, the anterior wedge has greater

amounts of secondary tissue than the poster-medial and the anterior-medial wedges. The anterior-medial wedge has significantly smaller amounts of secondary tissue than the anterior, anterior-lateral, and posterior wedges.

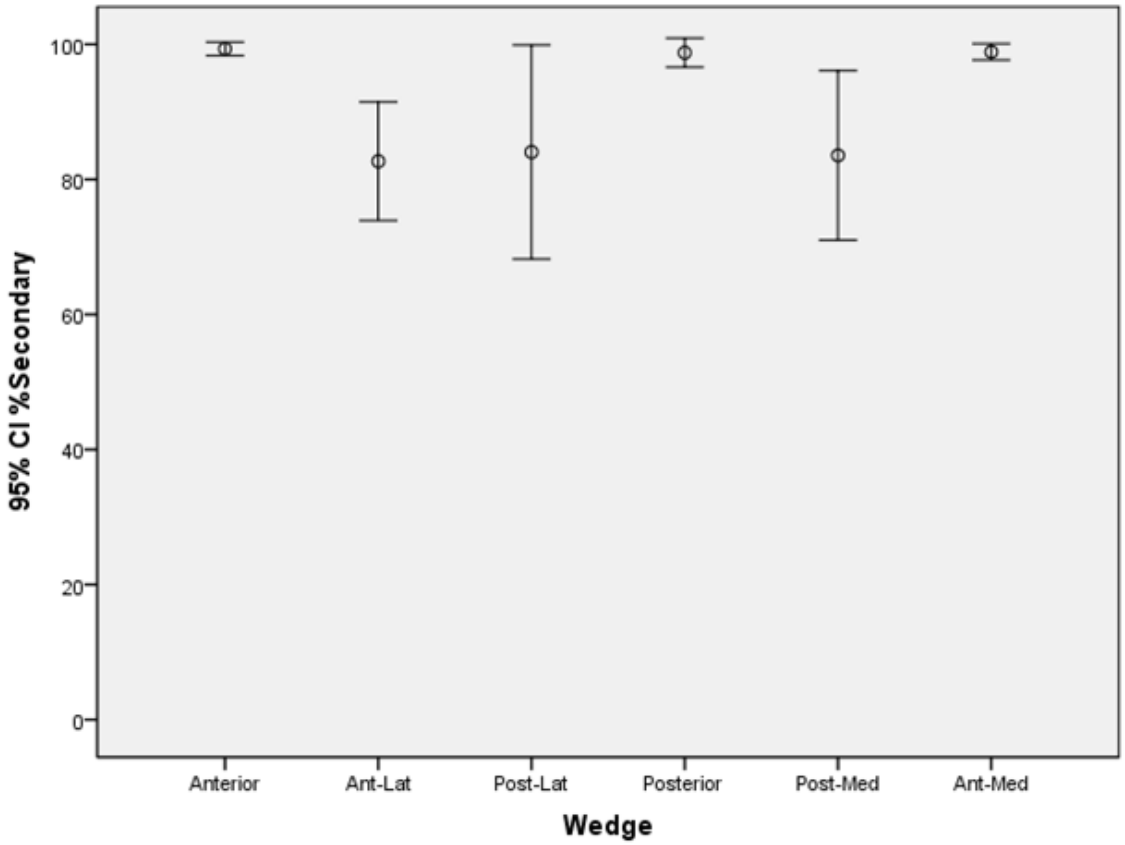

Figure 5.28: Amount of secondary tissue at each wedge in the mid-cortex ring at the 38% site.

Table 5.5: ANOVA table for 38% mid-cortex amount of secondary bone by wedge.

38% Mid	Anterior	Ant-Lat	Post-Lat	Posterior	Post-Med	Ant-Med
Anterior	x	0.002	0.005	0.914	0.004	0.931
Ant-Lat	0.002	x	0.793	0.003	0.866	0.003
Post-Lat	0.005	0.793	x	0.007	0.925	0.006
Posterior	0.914	0.003	0.007	x	0.005	0.983
Post-Med	0.004	0.866	0.925	0.005	x	0.005
Ant-Med	0.931	0.003	0.006	0.983	0.005	x

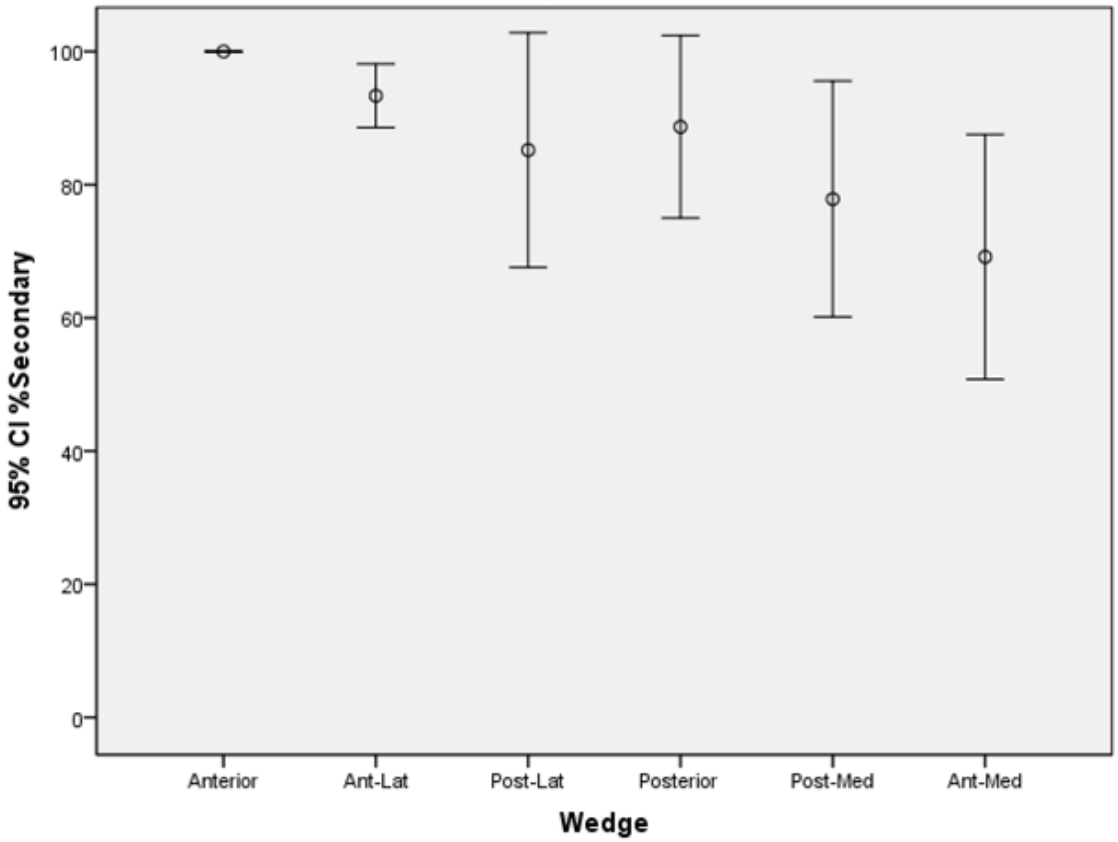

Figure 5.29: Amount of secondary tissue at each wedge in the mid-cortex ring at the 66% site.

Table 5.6: ANOVA table for 66% mid-cortex amount of secondary bone by wedge.

66% Mid	Anterior	Ant-Lat	Post-Lat	Posterior	Post-Med	Ant-Med
Anterior	x	0.409	0.070	0.163	0.008	0.000
Ant-Lat	0.409	x	0.313	0.562	0.058	0.004
Post-Lat	0.070	0.313	x	0.665	0.362	0.050
Posterior	0.163	0.562	0.665	x	0.181	0.018
Post-Med	0.008	0.058	0.362	0.181	x	0.282
Ant-Med	0.000	0.004	0.050	0.018	0.282	x

Within the periosteal ring, for both the 38% and 66% sites, the anterior wedge had the greatest amount of secondary tissue. At the 38% site, the anterior-lateral wedge had the least amount of secondary tissue followed closely by the posterior-medial wedge. At the 66% site, the anterior-medial wedge has the least amount of secondary tissue, followed by the anterior-lateral wedge (see Figures 5.30 and 5.31 and Tables 5.7 and 5.8).

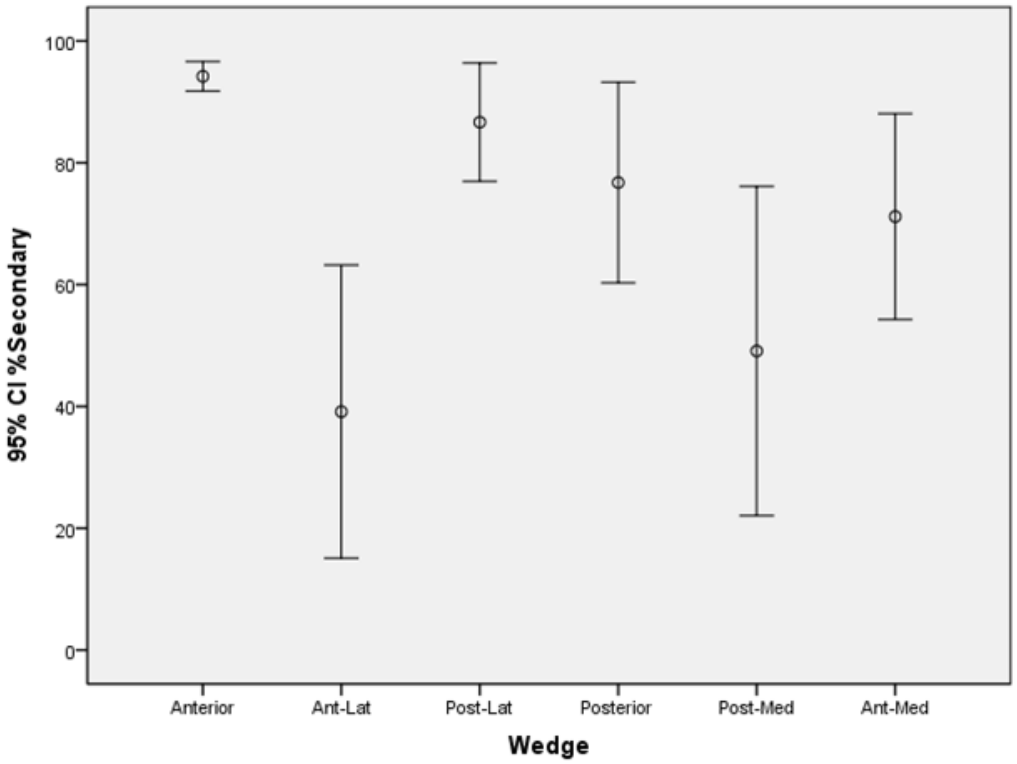

Figure 5.30: Amount of secondary tissue at each wedge in the periosteal ring at the 38% site.

Table 5.7: ANOVA table for 38% periosteal amount of secondary bone by wedge

38% Peri	Anterior	Ant-Lat	Post-Lat	Posterior	Post-Med	Ant-Med
Anterior	**x**	0.000	0.320	0.025	0.000	0.004
Ant-Lat	0.000	**x**	0.000	0.000	0.191	0.000
Post-Lat	0.320	0.000	**x**	0.193	0.000	0.044
Posterior	0.025	0.000	0.193	**x**	0.001	0.460
Post-Med	0.000	0.191	0.000	0.001	**x**	0.005
Ant-Med	0.004	0.000	0.044	0.460	0.005	**x**

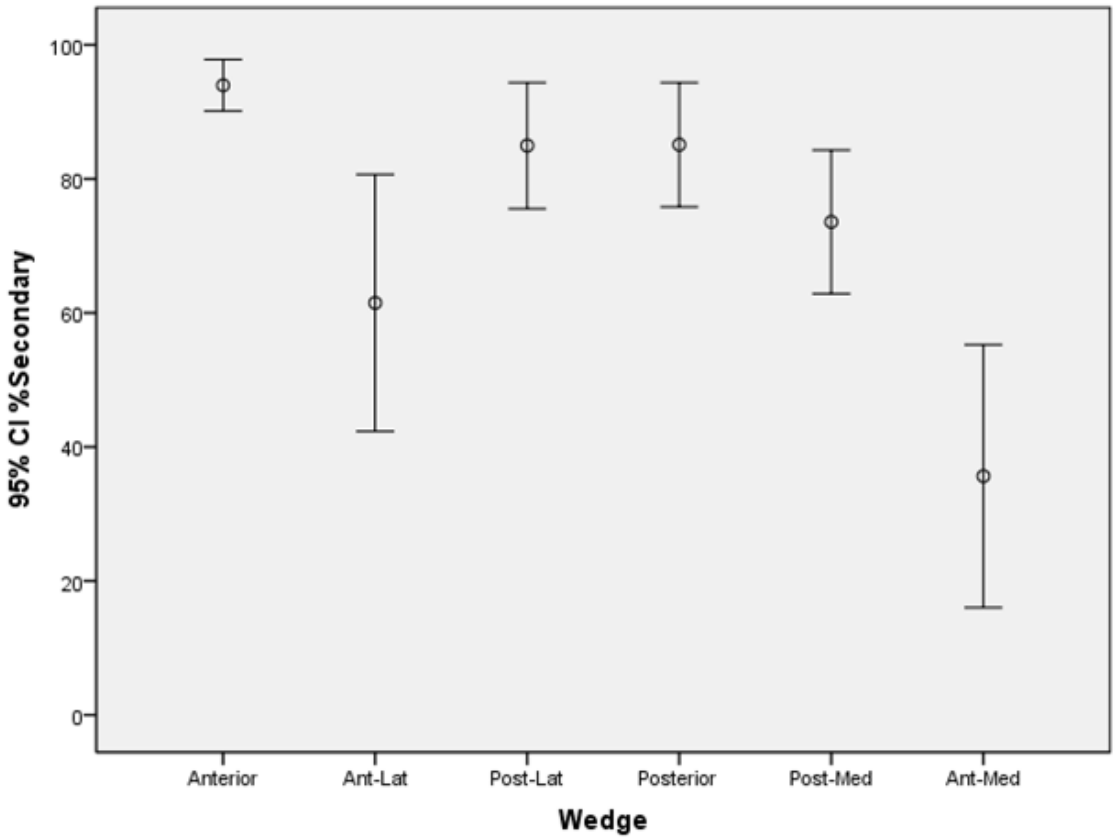

Figure 5.31: Amount of secondary tissue at each wedge in the periosteal ring at the 66% site.

Table 5.8: ANOVA table for 66% periosteal amount of secondary bone by wedge

66% Peri	Anterior	Ant-Lat	Post-Lat	Posterior	Post-Med	Ant-Med
Anterior	x	0.000	0.202	0.209	0.005	0.000
Ant-Lat	0.000	x	0.002	0.001	0.089	0.001
Post-Lat	0.202	0.002	x	0.984	0.108	0.000
Posterior	0.209	0.001	0.984	x	0.104	0.000
Post-Med	0.005	0.089	0.108	0.104	x	0.000
Ant-Med	0.000	0.001	0.000	0.000	0.000	x

5.3.4: Correlations Between the Two Sites, 38% and 66%

As was found for the entire cross-section (Chapter 4), there was a strong relationship between the amount of porosity at the 38% site and the 66% site when analyzed by wedge. As shown in Figure 5.32, porosity was correlated between sites for each wedge around the cortex.

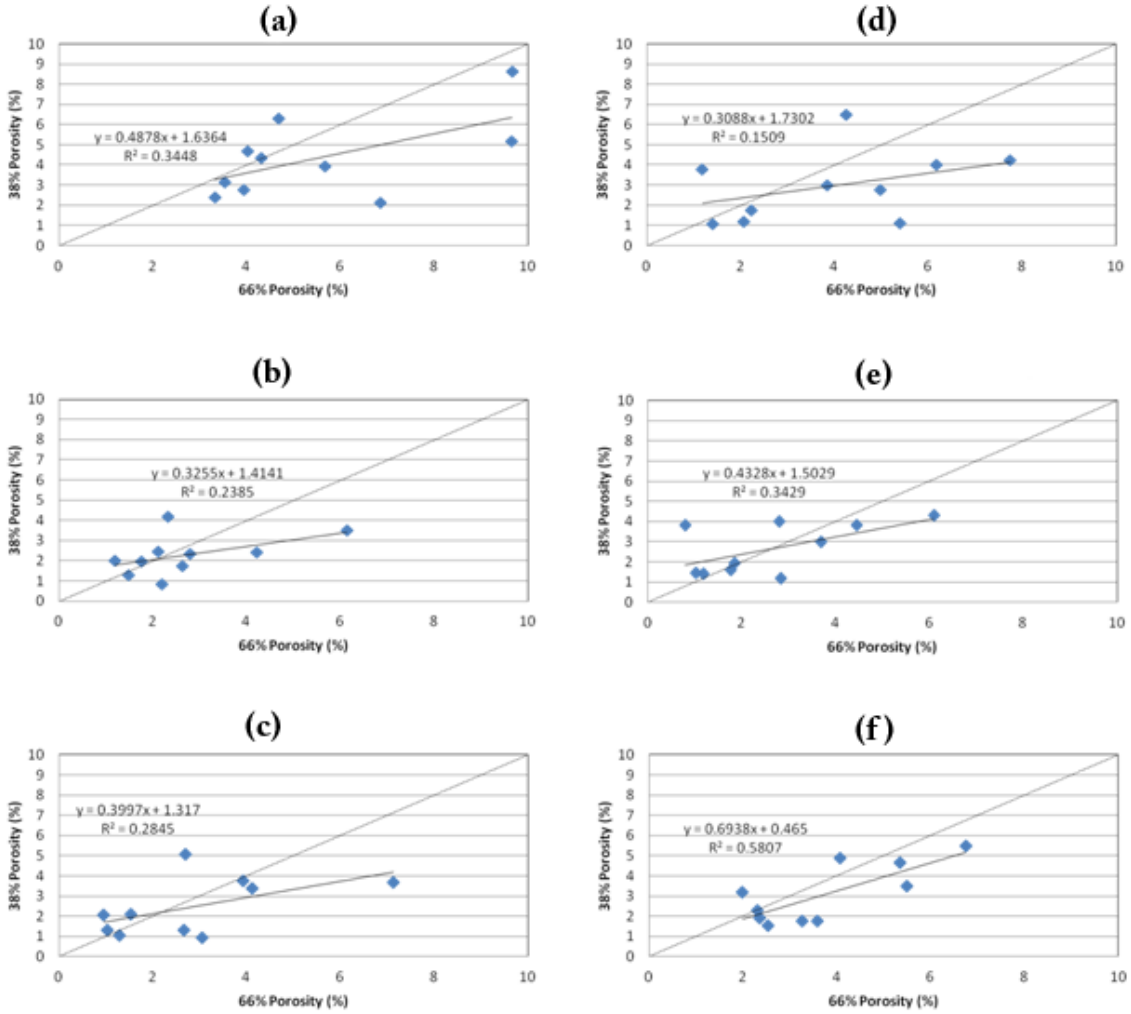

Figure 5.32: Comparison between the porosity of the 38% and the 66% sites at the (a) anterior wedge (b) anterior-lateral wedge (c) posterior-lateral wedge (d) posterior wedge (e) posterior-medial wedge (f) anterior-medial wedge.

Within the endosteal ring, the amount of porosity between the 38% and 66% sites was significantly correlated for all wedges apart from the posterior and posterior-medial wedges. Within the mid-cortex ring, the amount of porosity between the 38% and 66% sites was significantly correlated for all wedges. Within the periosteal ring, only the amount of porosity between the 38% and 66% sites for the anterior-medial wedge was significantly correlated (see Figure 5.33, 5.34, and 5.35).

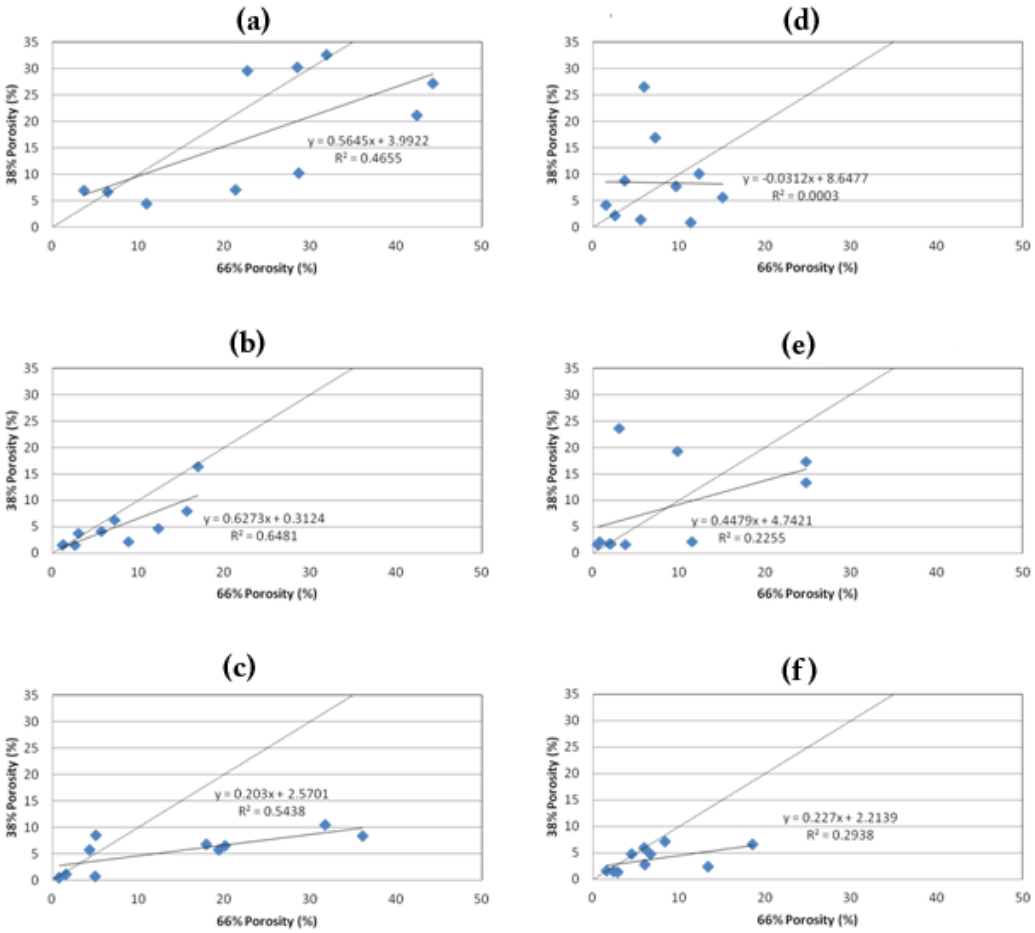

Figure 5.33: Comparison between the µCT derived porosity of the endosteal ring of the 38% and the 66% sites at the (a) anterior wedge (b) anterior-lateral wedge (c) posterior-lateral wedge (d) posterior wedge (e) posterior-medial wedge (f) anterior-medial wedge.

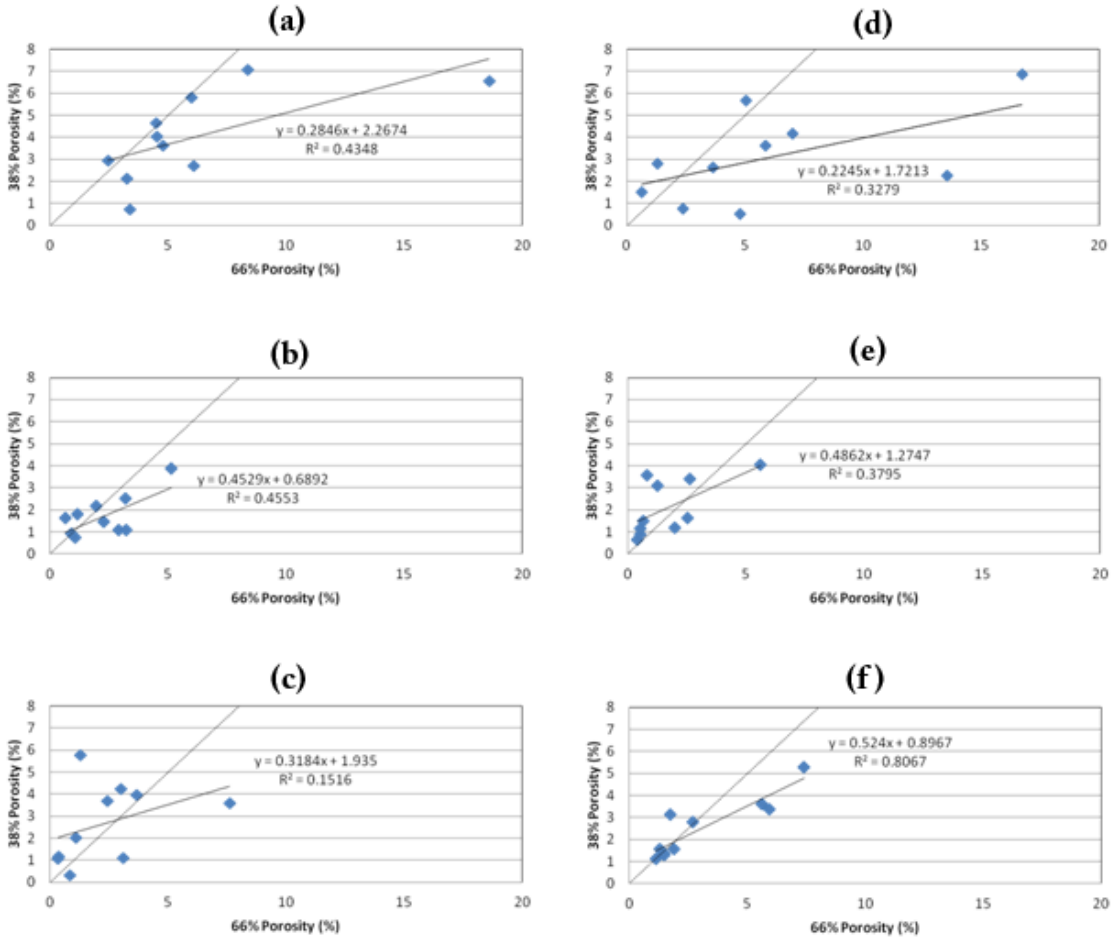

Figure 5.34: Comparison between the µCT derived porosity of the mid-cortex ring of the 38% and the 66% sites at the (a) anterior wedge (b) anterior-lateral wedge (c) posterior-lateral wedge (d) posterior wedge (e) posterior-medial wedge (f) anterior-medial wedge.

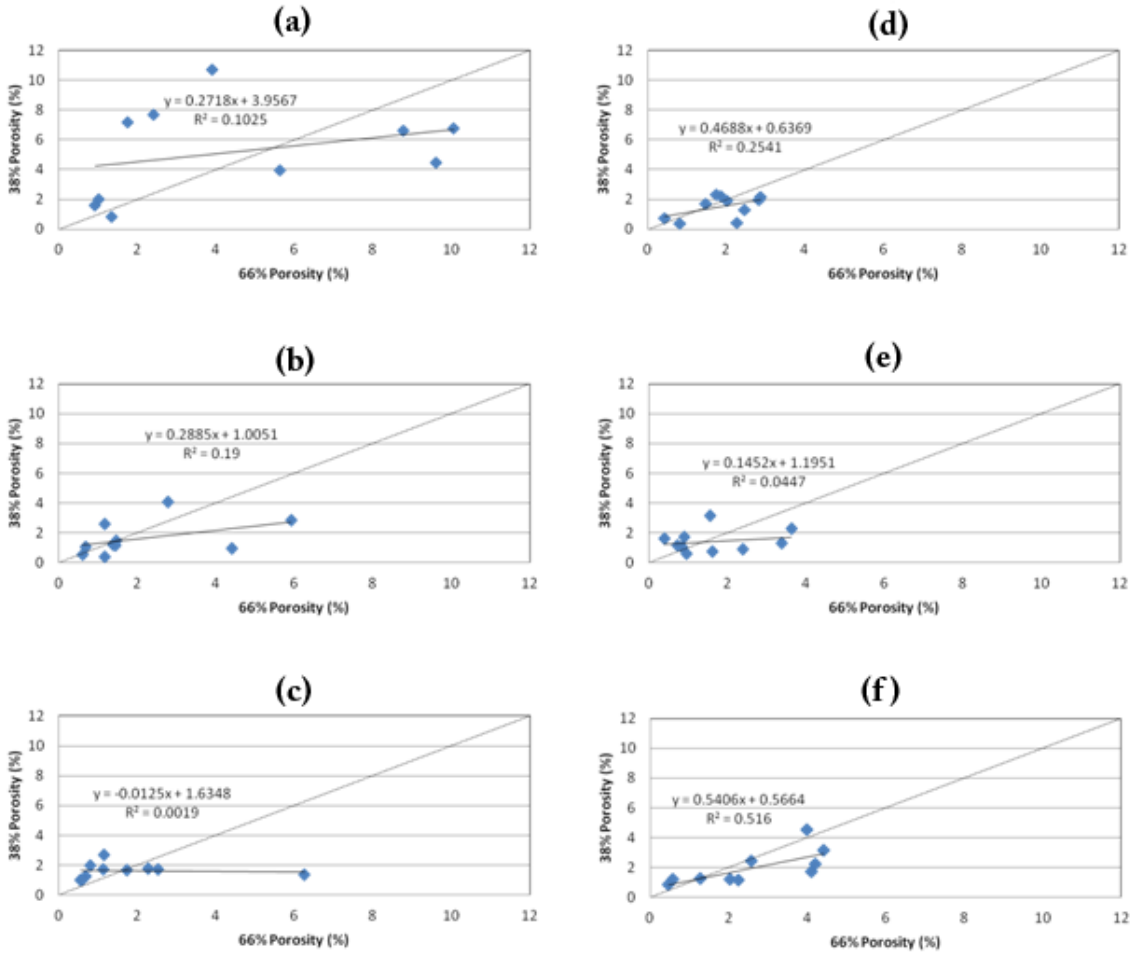

Figure 5.35: Comparison between the μCT derived porosity of the periosteal ring of the 38% and the 66% sites at the (a) anterior wedge (b) anterior-lateral wedge (c) posterior-lateral wedge (d) posterior wedge (e) posterior-medial wedge (f) anterior-medial wedge.

As was found for the entire cross-section (Chapter 4), there was a strong relationship between the ash content at the 38% and the 66% sites. However, this relationship was only significant in some wedges, specifically, the posterior wedge ($p = 0.001$) and the posterior-medial wedge ($p = 0.022$) (see Figure 5.36).

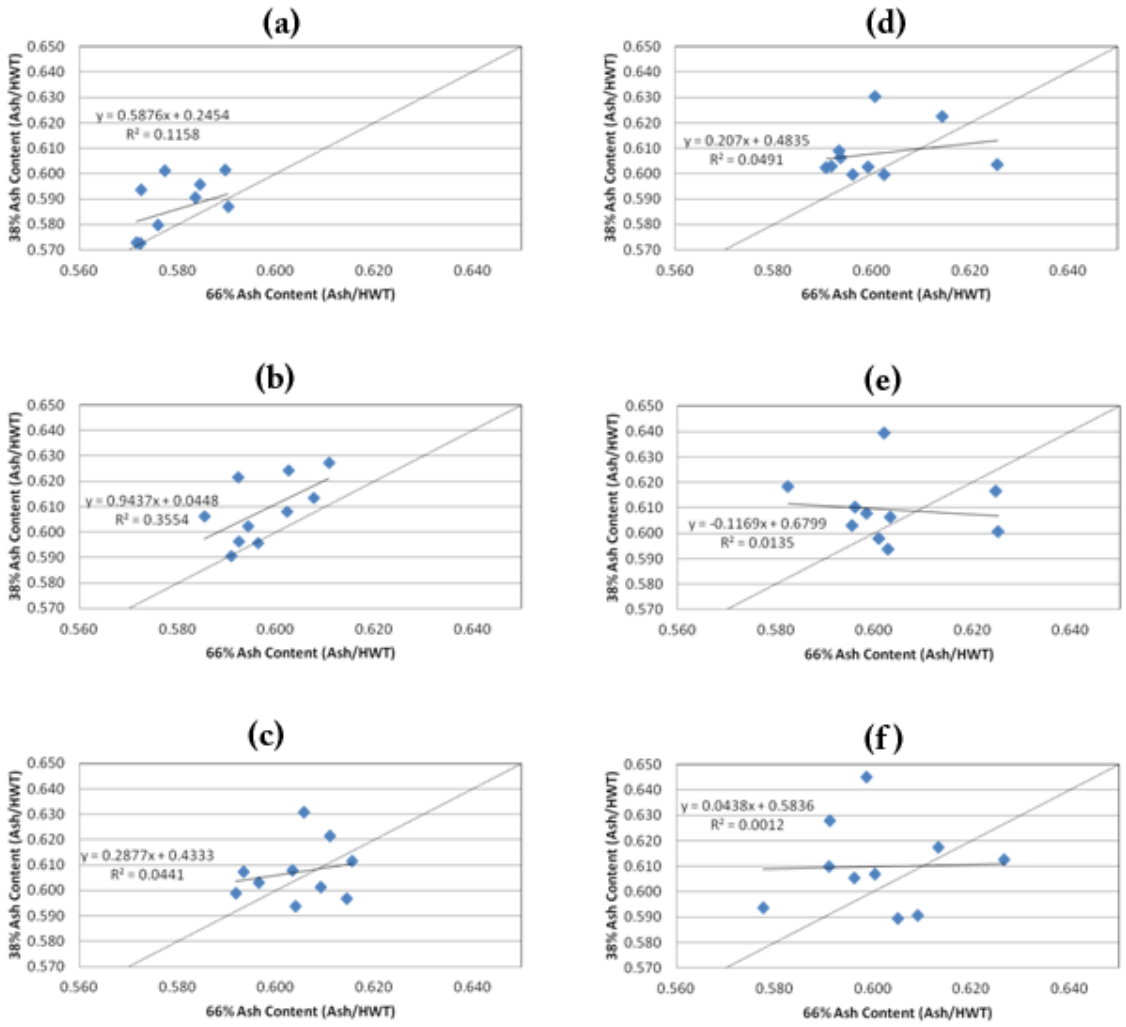

Figure 5.36: Comparison between the ash content of the 38% and the 66% sites at the (a) anterior wedge (b) anterior-lateral wedge (c) posterior-lateral wedge (d) posterior wedge (e) posterior-medial wedge (f) anterior-medial wedge.

5.3.5: Co-variation Between Variables

For each of the six wedges, the relationship between ash content and porosity was analyzed. First, all individuals were considered as a single group, and then the sample was separated into slender and robust individuals.

At the 38% site, the slope for the combined slender and robust individuals was significant ($p = 0.037$) at the anterior-lateral wedge, suggesting increased tissue mineralization with decreasing porosity. When only slender individuals were considered, only the anterior wedge showed a significant ($p < 0.05$) relationship, although the anterior-lateral was nearly significant ($p = 0.059$). There was a large increase in the R^2 value of correlation for all wedges, for slender individuals over all individuals. When only robust individuals were considered, there were no significant correlations and for most wedges, there was a large decrease in the R^2 value of correlation (see Figure 5.37).

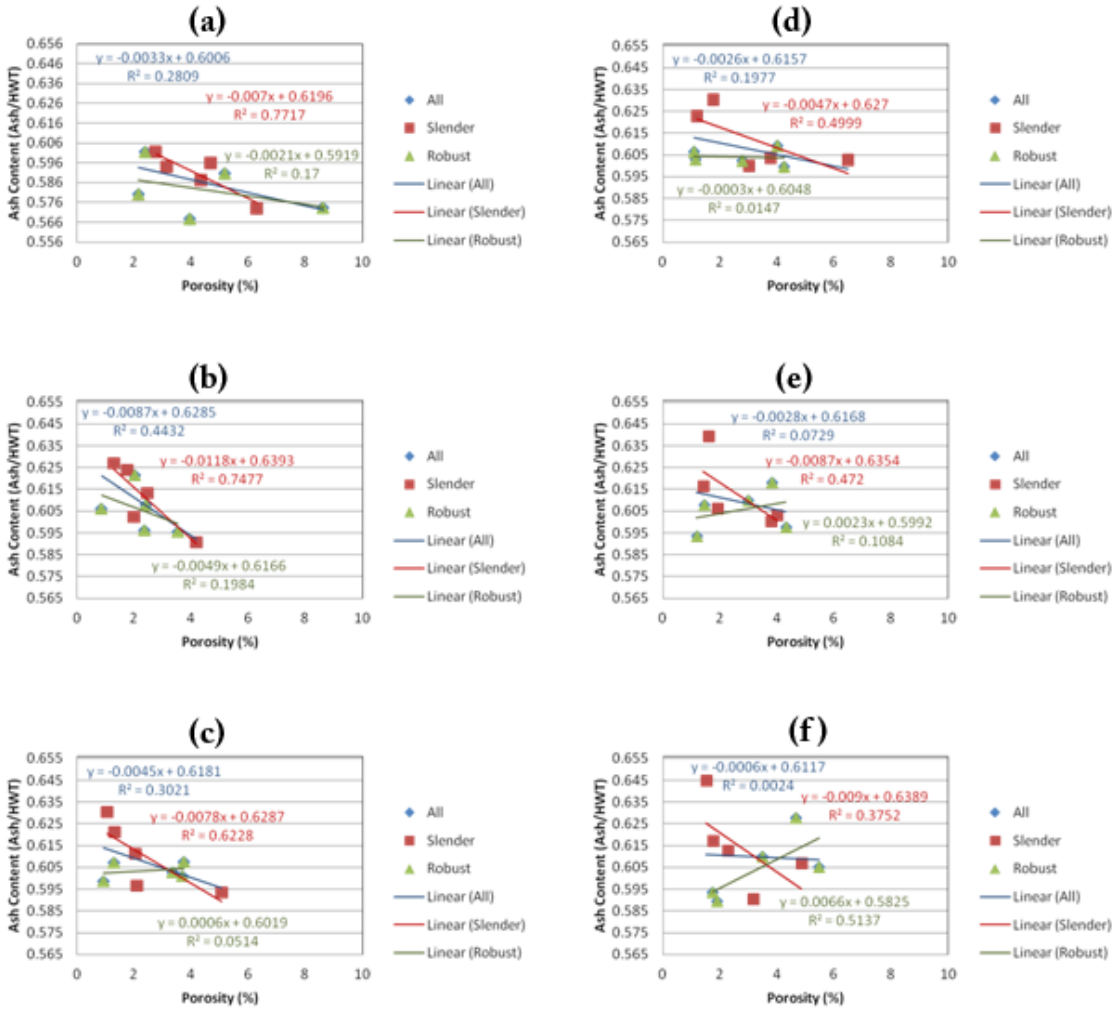

Figure 5.37: Relationships for all individuals, slender individuals, and robust individuals, between ash content and porosity at the 38% location at the (a) anterior wedge (b) anterior-lateral wedge (c) posterior-lateral wedge (d) posterior wedge (e) posterior-medial wedge (f) anterior-medial wedge.

For the 66% site, no significant correlation was observed when slender and robust data were combined, however, the relationship between ash content and porosity in the posterior wedge was nearly significant ($p = 0.060$). For the slender individuals, there was a significant ($p = 0.026$) relationship between variables found in the posterior-medial

wedge. For some of the wedges (anterior-lateral, posterior-lateral, posterior, and posterior-medial), the R^2 values increased when only slender individuals were included, rather than when all individuals were considered. At the anterior, posterior, posterior-medial and anterior-medial wedges, the linear relationship considering only the robust individuals showed lower R^2 value of correlation than was evaluated with all individuals included (see Figure 5.38).

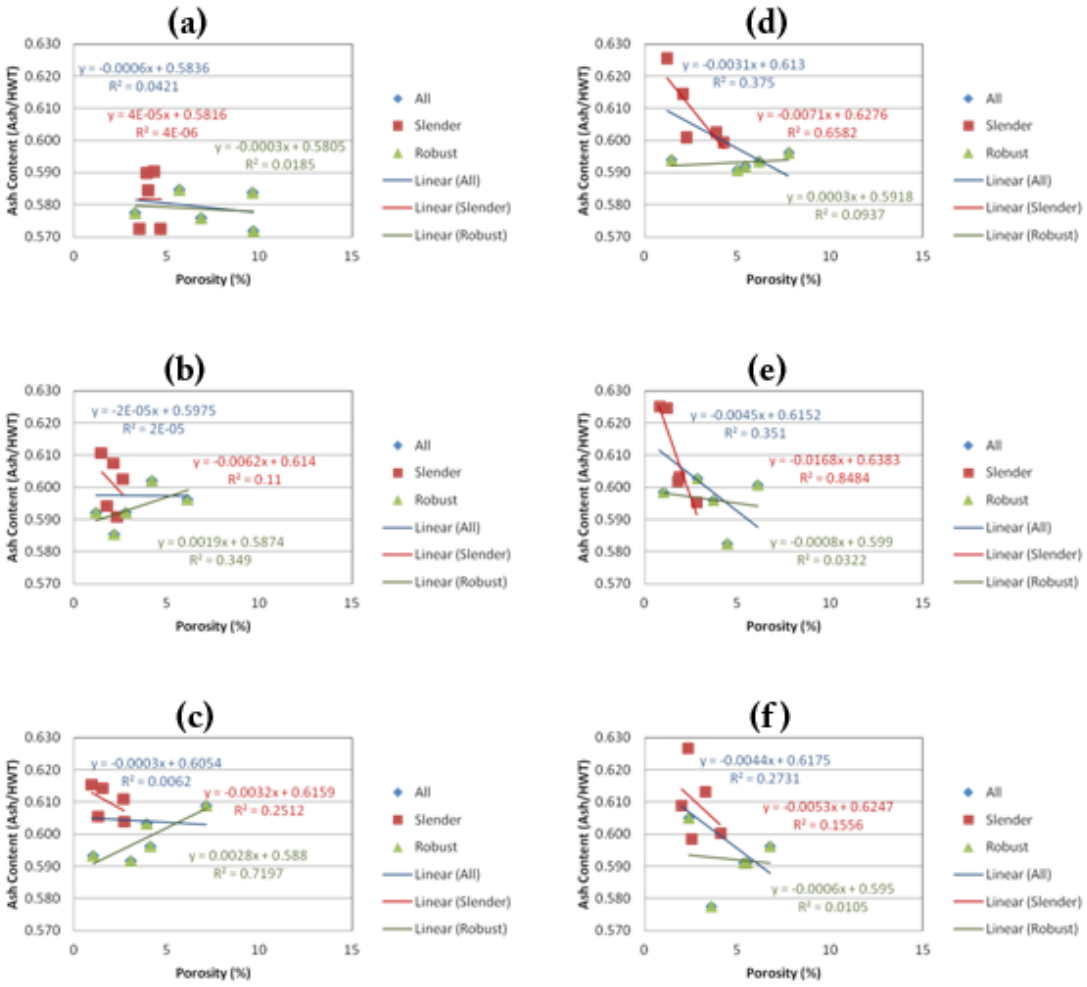

Figure 5.38: Relationships for all individuals, slender individuals, and robust individuals, between ash content and porosity at the 66% location at the (a) anterior

wedge (b) anterior-lateral wedge (c) posterior-lateral wedge (d) posterior wedge (e) posterior-medial wedge (f) anterior-medial wedge.

5.3.6: Comparison Between µCT Porosity and LM Secondary Tissue

The µCT derived 3-dimensional porosity data and the LM derived 2D porosity data were linearly related, although the slope was closer to 1 for the 66% than the 38% site (see Figure 5.39). The µCT derived porosity data generally followed the same trends as the LM derived porosity, but not the trends for the amount of secondary tissue (see Figures 5.40 and 5.41). At the both 38% and 66% sites in the mid-cortex and the periosteal rings, the anterior wedge had the highest porosity and secondary tissue. The most notable and consistent difference between the porosity and the secondary tissue trends occurred at the anterior-medial wedge for both 66% sites in the mid-cortex ring and the periosteal ring. In these cases, there was a large decrease in LM derived secondary tissue compared to other wedges without a corresponding drop in comparative µCT and LM derived porosity.

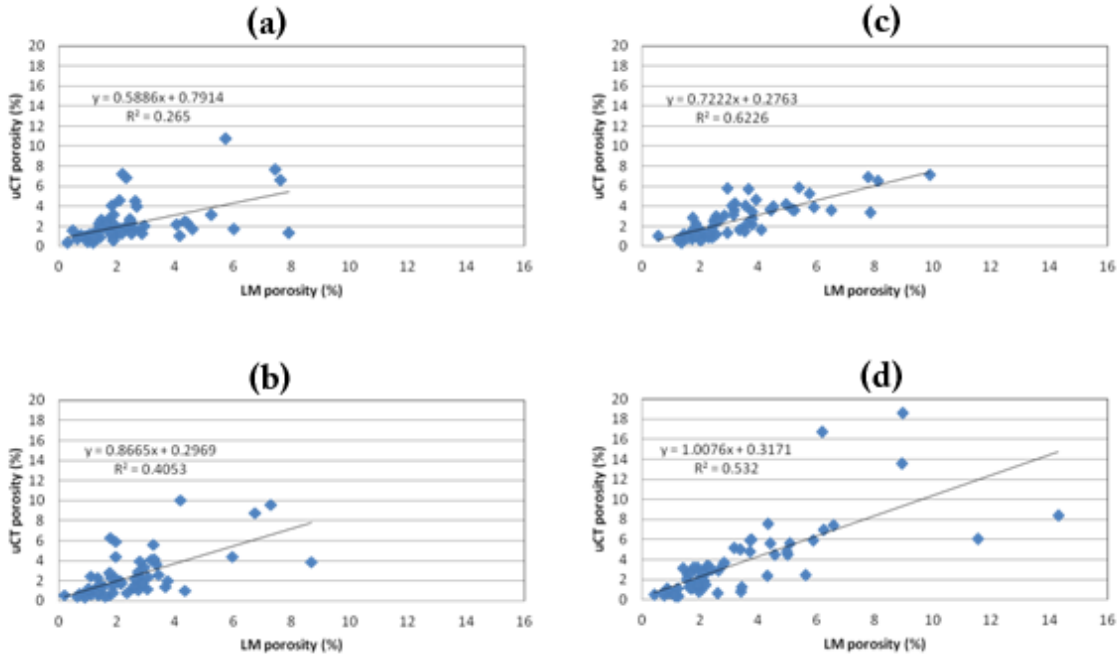

Figure 5.39: Linear comparison of µCT derived porosity and LM derived porosity from the (a) periosteal ring at the 38% site (b) periosteal ring at the 66% site (c) mid-cortex ring at the 38% site (d) mid-cortex ring at the 66% site

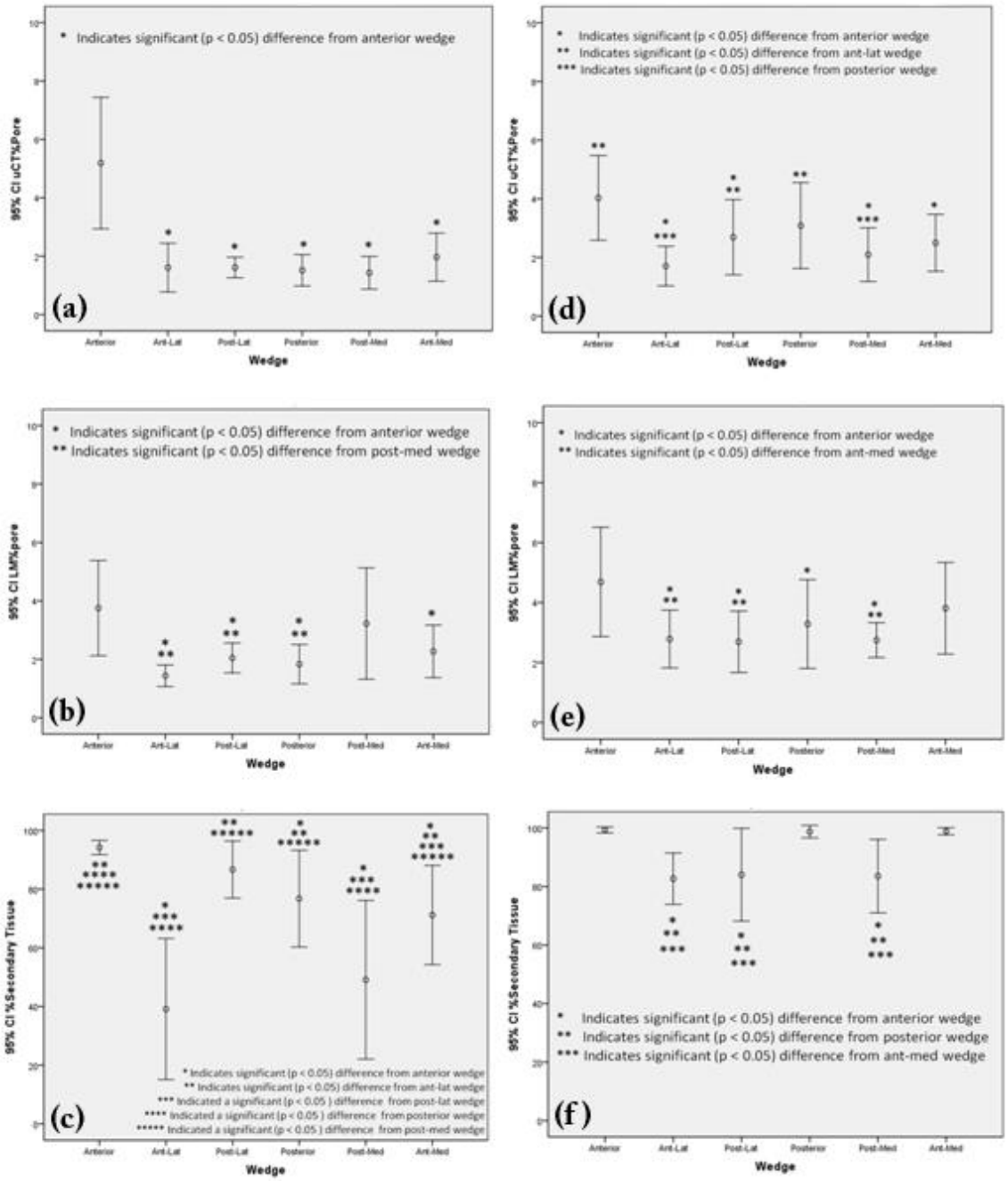

Figure 5.40: Comparison at each wedge around the cortex between LM derived and µCT derived data at the 38% site. (a) µCT derived porosity - periosteal ring (b) LM derived porosity - periosteal ring (c) LM derived amount of secondary tissue - periosteal ring (d) µCT derived porosity - mid-cortex ring (e) LM derived porosity - mid-cortex ring (f) LM derived amount of secondary tissue - mid-cortex ring.

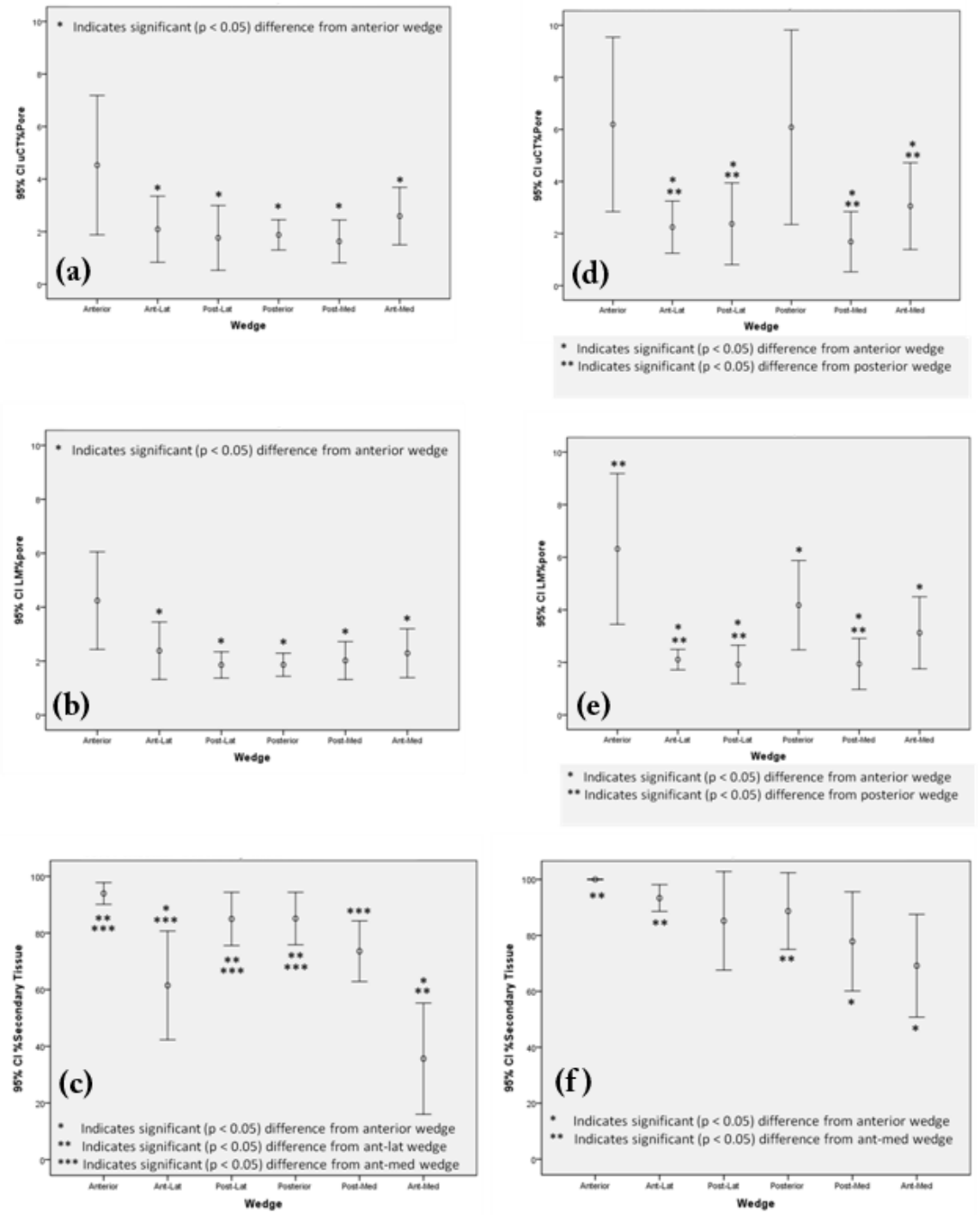

Figure 5.41: Comparison at each wedge around the cortex between LM derived and µCT derived data at the 66% site. (a) µCT derived porosity - periosteal ring (b) LM derived porosity - periosteal ring (c) LM derived amount of secondary tissue - periosteal ring (d) µCT derived porosity - mid-cortex ring (e) LM derived porosity - mid-cortex ring (f) LM derived amount of secondary tissue - mid-cortex ring.

5.4: Discussion

5.4.1: Variation in Porosity, Ash Content, and Tissue Mineralization as a Reflection of Robustness and Age

The multifactorial ANOVA demonstrated that wedge was a significant contributor to variation in porosity and ash content at both the 38% and 66% sites, and ring was a significant contributor to porosity. Robustness was also a significant contributor to variation in porosity, but only at the 66% site, and a significant contributor to variation in ash content at both the 38% and 66% sites. Interestingly, once robustness was taken into account, the contribution of age to variation in porosity and ash content was minimal. These results supported the previous findings of correlations between porosity and robustness, as well as ash-content and robustness as presented in Chapter 4. Those findings showed that correlations were significant only at the 66% site. In this study, robustness, but not age, was found to be a significant contributor to ash content at 38% site as well.

The relatively weak contributions of age to porosity variation was not unexpected given that this sample was from a relatively narrow and young adult age range (20-40). Many studies have shown that porosity significantly increases with age (Parfitt, 1984; Recker *et al.*, 1992; Feik *et al.*, 2000; Parfitt, 2004; Thomas *et al.*, 2005), but these studies incorporated the full range of adult variation. Given that peak bone mass is not reached until the 3rd decade of life (Recker *et al.*, 1992) increases in porosity owing to aging would not be expected to be significant until beyond the age range incorporated into this sample. Nonetheless, previous studies of intracortical porosity even in this young

adult age range did show significant variations, with increased porosity in the 5th decade relative to the 4th (Thomas *et al.*, 2005).

At the 66% site, age did not have a significant effect on ash content variation around the cortex, but robustness did. At the 66% site, age only had a significant effect when considered with robustness, which was significant when considered on its own and with age. These results suggested that age had a small influence on robustness, such that older individuals in the sample tended to be slightly more robust, which was likely due to endosteal resorption and periosteal deposition that is part of aging (Lazenby, 1986; Ruff and Hayes, 1988, Ruff and Hayes, 1983b; Smith and Walker, 1964). Once the effect of aging on robustness was taken into account, age had little influence on the ash content distribution overall, whereas robustness was a significant contributor to the variation.

Due to the small sample size, a decision was made not to include sex in the analysis. Sex has been shown to be a contributor to robustness (Tommasini *et al.*, 2007), but with only 4 females and 6 males in the study, the effects from sex could not be determined. In future work, the effect of sex should be investigated.

5.4.2: Regional Variability

5.4.2.1: Regional variability in porosity

Using ANOVA with LSD post-hoc tests, the regional variation in porosity and ash content were explored by examining the differences between each of the six radial wedges. The anterior wedge consistently had the highest porosity at both the 38% and 66% sites. At the 66% site, the anterior-lateral and the posterior-medial wedges consistently had low porosity compared to the other wedges. The porosity results are

generally summarized in Tables 5.9 and 5.10. Wedges with high porosity are marked with 'H', those with low porosity are marked with 'L' and those that are neither high nor low, compared to the other wedges are marked '-'.

Table 5.9: Wedges with high and low porosity at the 38% site.

	Anterior	Ant-Lat	Post-Lat	Posterior	Post-Med	Ant-Med
Overall Wedge Porosity	H	L	L	H	-	H
Mid-cortex Porosity	H	L	-	-	L	-
Periosteal Porosity	H	L	L	L	L	L

Table 5.10: Wedges with high and low porosity at the 66% site.

	Anterior	Ant-Lat	Post-Lat	Posterior	Post-Med	Ant-Med
Overall Wedge Porosity	H	L	L	H	L	H
Mid-cortex Porosity	H	L	L	H	L	L
Periosteal Porosity	H	L	L	L	L	L

An understanding of the local strains experienced at the tibial shaft can help with interpretation of these results. The predominant mode of tibial loading during walking has been shown to be bending (Peterman *et al.*, 2001), with the highest compressive strains located posteriorly and the highest tensile strains located anteriorly. The axis of greatest bending rigidity (I_{max}) is generally located along the anterior-posterior axis in the tibia (Macdonald *et al.*, 2009), reflecting the adaptation of bone to the high bending forces in this plane. Bone remodeling is believed to respond to tensile stress, both from bodyweight loads through the bone in response to locomotion and loads from muscles (Enlow ,1963; Corwin *et al.*, 1991; Lanyon, 1993; Mullender and Huiskes, 1995; Mullender and Huiskes, 1997; Ruff *et al.*, 2006). Because of the high degree of bending

along this axis, with the anterior being in tension (Peterman *et al.*, 2001), it was expected that the highest remodeling rates would be located anteriorly, and thus high levels of porosity, which is supported by the results.

Based on the bending loads predicted in the tibial shaft, one would have expected a much lower degree of porosity posteriorly relative to anteriorly, as the anterior cortex was loaded in tension and the posterior in compression. Although the loading patterns are different from humans, Cynomolgus monkeys also have tensile anterior cortices and compressive posterior cortices. According to a study by Nonaka *et al.* (2006), in the distal tibia of the Cynomolgus monkey, the posterior cortex had a much lower amount of porosity than the anterior cortex. The results indicated that the posterior wedge tended to be the second most porous region of the tibia at both the 66% and 38% sites. At the 66% site, the posterior wedge was significantly higher in porosity than postero-medial and antero-lateral wedges, suggesting more remodeling at this cortex than might be expected for one loaded in compression. An explanation may relate to the origin of the soleus muscle, which is along the proximal posterior surface of the tibia, along the soleal line. The muscle attachment would be expected to impart a tensile stress on the bone, thus an increase in remodeling would be expected in that area over what might be otherwise expected.

5.4.2.2: Regional variability in ash content

It was found that the anterior wedge had significantly lower ash content than all other wedges, however, there were no significant differences between any of the other wedges.

Ash content is a coarse measurement of mineralization and a destructive technique, and as such, it is does not lend itself to regional analysis. Furthermore, it is not a very sensitive technique and may not be possible to discern small, but significant differences in tissue mineralization that may exist between other areas of the cortex that might have been detectable by other techniques, such as microradiography (Engstrom 1952; Amprino 1958; Vincentelli and Evans 1971; Martin 1985), quantitative backscattered electron imaging (qBSE) (Boyde and Jones, 1983; Grynpas, 1993, Goldman *et al.* 2005; Roschger *et al.*, 1995; Bloebaum *et al.* 1997), or FTIR and Raman Spectroscopy (Boskey and Mendelsohn 2005; Boskey *et al.*, 1992; Miller *et al.*, 2007). All of these are more suitable for examining compositional differences around the cortex. Micro-computed tomography techniques, if properly normalized with a hydroxyapatite phantom, can also be used to determine local mineralization.

Although no studies comparing regional variation in ash content in human cortical bone were found, a number of studies have employed clinical methods, such as pQCT to study variations in tissue quality (vBMD) around the cortex. As reported in Chapter 4, mineral density measures obtained by pQCT (Ct.TMD) correlated strongly with the μCT derived porosity data, and to a lesser extent with ash content. Thus one can look at regional differences in vBMD reported in these studies and relate them to the regional differences found in porosity. For instance, Rantalainen *et al.* (2011) studied the apparent mineral density (vBMD) around the tibial cortex (anterior, lateral, posterior, medial) in young adult women who were involved in one of five types of athletic activities. The activities were grouped as high impact, odd impact, high magnitude, low

impact repetitive, high impact repetitive and referents. It was found that the vBMD was lower for the athletes in the high impact or odd impact groups for all sectors than the referents. For the endurance runners, who were in the repetitive low impact group, vBMD was lower than referents only at the anterior sector. Rantalainen and colleagues speculated that athletes involved in weight-bearing impact sports may have higher remodeling rates, leading to lower vBMD owing to the production of new low mineralization density Haversian systems and a reduction in the amount of highly mineralized primary bone interstitial tissue. Given the finding that vBMD relates to both porosity and ash content, these results are consistent with those presented in this dissertation. Cooper *et al.* (2008) investigated the variation of cortical volumetric density (CoD) within the adolescent human tibia. It was also found that there were significant differences around the cortex, specifically that cortical density (CoD) was highest at the posterior- medial and posterior-lateral sections of the tibia and lowest at the anterior sections. The largest differences were found between the anterior-medial cortex and the posterior-medial cortex. The CoD measurements were reflective of both ash content and porosity, and the low value at the anterior cortex was consistent with the findings. Cooper and colleagues also found that the variation was greater within an individual than between the two sexes. This indicates that there is a large degree of adaptation to loading which is reflected in microstructural and compositional variations which are detectable by pQCT.

There have been few studies that have been able to investigate site-specific volumetric tissue mineralization in bone. Rohrbach and colleagues (2012) investigated

the mineralization in the human femur in the anterior, medial, posterior, and lateral regions of the cortex using synchrotron based μCT (SR-μCT), a method which, due to its monochromatic beam and high resolution, can reliably be used to quantify tissue mineralization. It was found that tissue mineralization was lower in the posterior region than the medial and lateral. Intracortical remodeling was not investigated in that study, however, the investigators did find the highest porosity to be in the posterior region. This may indicate that the mineralization differences are due, at least in part, to intracortical remodeling. Goldman *et al.* (2005) investigated the mineralization around the femoral cortex using quantitative backscattered electron microscopy (qBSE). The lowest mineralization was found in the posterior cortex, followed by the anterior-lateral cortex. The posterior-medial cortex was found to have the highest mineralization. This pattern of mineralization may be related to the loading conditions of the femur. The posterior-medial cortex is loaded under compression and the anterior-lateral cortex is loaded under tension. There are also muscle attachments that exert a tensile force in the posterior direction. Future research on the tibia should include a less coarse measurement of mineralization, such as that derived from Raman spectroscopy or qBSE, in order to determine whether there are regional patterns in the mineralization distribution that cannot be detected by pQCT or ash content techniques.

5.4.2.3: Regional variability in tissue type

During the developmental growth of the skeleton, patterns in bone growth greatly affect the structure, composition, and organization of adult bone. Specific growth patterns can have long reaching ramifications on the organization of adult bone. During this process, bone is not laid down evenly along the periosteal and endosteal surfaces of the

bone. Instead, bone is deposited in some areas and resorbed in others. This process is called “growth remodeling” (Enlow , 1962; Enlow, 1963; Enlow *et al.*, 1982), more commonly referred to as ‘modeling’ (Frost, 1973), and leads to a shift in the position of bone over time, as growth and resorption do not occur uniformly. This shift is known as cortical drift and affects the heterogeneity of the bone tissue organization across the cortex (Enlow, 1963). Earlier in the chapter, variability in porosity was discussed relative to variability in intracortical remodeling. Because of the modeling process, one would also expect to find differences in the amount of primary and secondary bone not only around the cortex (wedge), but also between the mid-cortex and periosteal regions (rings). It was predicted that the periosteal ring would have the greatest amount of primary bone (and conversely the least secondary [remodeled] bone) in some regions around the cortex, specifically in the direction of cortical drift, but not in others. The data supported this expectation. In general, the periosteal ring did have greater amount of primary tissue, but it is only significant in certain areas specifically the anterior-lateral, posterior, posterior-medial and anterior-medial wegdes at the 38% site and the anterior-lateral and anterior-medial wedges at the 66% site. This is likely a consequence of modeling history, as well as local strains. The anterior wedge has consistanly relatively high amounts of secondary tissue at both the 38% and 66% sites for both the periosteal and mid-cortex rings. Tables 5.11 and 5.12 summarize the relative amounts of secondary tissue with high amounts labeled 'H', low amounts labeled 'L', and neither high nor low labeled '-'.

Table 5.11: Wedges with high and low amounts of secondary tissue at the 38% site.

	Anterior	Ant-Lat	Post-Lat	Posterior	Post-Med	Ant-Med
Mid-cortex Secondary	H	L	L	L	L	H
Periosteal Secondary	H	L	H	H	L	-

Table 5.12: Wedges with high and low amounts of secondary tissue at the 66% site.

	Anterior	Ant-Lat	Post-Lat	Posterior	Post-Med	Ant-Med
Mid-cortex Secondary	H	H	-	H	L	L
Periosteal Secondary	H	L	H	H	-	L

Goldman *et al.* (2009) investigated the direction of drift in the human femur by drawing boundary lines around areas of high percentages of primary tissue on the periosteal and endosteal surfaces. It was found that the direction of drift changed with age, with the toddler and young child sample sets (age 2-8) showing posterior-medial drift and the early adolescent sample set (14-16) showing anterior-lateral drift. The direction of drift during growth and developement in the human tibia has not been well studied. Some recent publications have, however, begun to shed light on the pattern of tibial drift. Gosman *et al.* (2013) investigated drift in both the human femur and tibia at different sites throughout the length using high resolution X-ray computed tomography (HrCT) at five different age steps from 0 to 18 years . At the 65% and 35% sites it was found that the direction of drift for the tibia was posterior-medial. The investigators also found that the drift pattern occurred at a younger age for the tibia than for the femur, with the greatest changes in cross-sectional size and shape of the tibia occuring between the first two groups (0-1.9 years and 2-4.9 years) and again between the fourth and fifth

groups (9-13.9 years and 14-17.9 years). The second stage of rapid change may relate to prepubertal changes in periosteal expansion and endosteal reshaping due to hormonal and body mass changes. A qualitative exampination of the tibial cross-sections from the fourth and fifth age groups showed a large decrease in porosity for the fifth age group. Cambra-Moo and colleagues (2012) studied a very small sample of archaeological tibiae (1 infant, 1 juvenile, and 2 adults) and detailed some qualitative results. In the infant, the anterior and posterior cortices were found to be heavily remodeled. Evidence of remodeling (secondary osteons) was also found in the mid-cortex and endosteal regions of the lateral cortex. In the medial cortex, resorption spaces were found in the endosteal region and fibrolamellar bone in the periosteal region. The juvenile individual demonstrated large amounts of fibrolamellar bone in the periosteal region of the medial and lateral cortices. The adult individuals still contained some fibrolamellar bone, but the cortex was largely colonized by Haversian systems. There were also fewer resorption spaces in the adult individuals, with most of them being located in the endosteal region of the medial and posterior-medial cortices. These findings are consistent with a medial drift direction beginning in infancy and extending through the growth period.

Growth remodeling can leave complex patterns in the structure of the bone long after the the adult skeleton has been achieved. The findings presented in this dissertation also support a medial drift, with low amounts of secondary tissue (and consequently high amounts of primary bone tissue) in the the posterior-medial wedge at both the 38% site and the anterior-medial wedge at the 66% site. The results of regional porosity and tissue

type are summarized in Tables 5.13 and 5.14, as these variables together around the cortex and between wedges can shed light on bone growth and loading.

The posterior-medial cortex is the most common location of tibial stress fractures in military recruits (Giladi *et al.*, 1985; Milgrom *et al.*, 1985, Crossley *et al.*, 1999). The results show that the posterior-medial cortex has low porosity and high amounts of secondary tissue, indicating that the remodeling rate is low in this area. The results also indicate that this is the direction of drift, and therefore, the tissue in this area may be older than tissue in other areas of the cortex, as it was laid down during growth. These factors may be responsible for the higher incidences of stress fractures in this region of the cortex.

Table 5.13: Summary of regional porosity and tissue types results at the 38% site.

	Anterior	Ant-Lat	Post-Lat	Posterior	Post-Med	Ant-Med
Overall Wedge Porosity	H	L	L	H	-	H
Mid-cortex Porosity	H	L	-	-	L	-
Periosteal Porosity	H	L	L	L	L	L
Mid-cortex Secondary	H	L	L	L	L	H
Periosteal Secondary	H	L	H	H	L	-

Table 5.14: Summary of regional porosity and tissue types results at the 66% site.

	Anterior	Ant-Lat	Post-Lat	Posterior	Post-Med	Ant-Med
Overall Wedge Porosity	H	L	L	H	L	H
Mid-cortex Porosity	H	L	L	H	L	L
Periosteal Porosity	H	L	L	L	L	L
Mid-cortex Secondary	H	H	-	H	L	L
Periosteal Secondary	H	L	H	H	-	L

The relatively low amount of secondary bone in the lateral cortex observed in the sample (anterior-lateral for both the 38% and 66% sites), as well as by Cambra-Moo *et al.*(2012), may be related to overall subperiosteal expansion during growth, rather than drift. A larger study that investigates the age related changes in drift is necessary to determine if there is a more complicated drift patterns in the tibia, than the simple medial drift reported by Cambra-Moo *et al.*(2012), which might explain the low amounts of secondary tissue found in the periosteal ring of the anterior-lateral wedge. Because the tibia rapidly reaches its adult shape, which is established by age 18 (Gosman *et al.*, 2013), many of the effects of growth and development may be hard to tease out in this young adult sample. As the age range of individuals in study for this dissertation is 23 - 46 years (mean age 37 years), the primary bone laid down during growth may have been largely remodeled for many individuals.

In order to get a better understanding of the effect of growth, it is important to characterize the endosteal bone tissue, which was not done in this study. Areas of endosteal resorption can be good indicators of drift direction when coupled with areas of periosteal deposition, unfortunately, differentiating between resorption spaces and large pores caused by trabecular consolidation can be very difficult, and it was not possible to differentiate the tissue types in the endosteal ring for the current study. Future work includes revisiting the samples, perhaps with the addition of other imaging or staining techniques, in order to more accurately measure the amount of secondary tissue in the endosteal ring.

5.4.3: Relationships with Robustness

5.4.3.1: Porosity and robustness

At the 66% site, in the entire wedge, strong correlations were found between porosity and robustness for all wedges. The investigation of the porosity by ring demonstrated strong correlations between porosity and robustness at the 66% site in the endosteal ring for the posterior and medial wedges, but not in any other ring or wedge.

Previous studies have found relationships between bone geometry / biomechanical axes and regional variations in porosity. Feik *et al.* (2000) investigated the cross-sectional geometry differences of the midshaft femur for different age groups and Thomas *et al.* (2005) investigated the regional differences in porosity of the same sample. Differences in porosity were found around the cortex, as well as differences in porosity for different age groups at each location. Feik *et al.* (2000) found that resorption was greatest in the anterior cortex and apposition was least in the posterior cortex. For all age groups, Thomas *et al.*(2005) found that the posterior cortex had the highest porosity, and the posterior cortex was particularly high for the young individuals. In the Thomas study, samples were grouped based on the ratio between the medullary area (MA) and the total subperiosteal area (TSPA). When grouped by sex, it was found that ~43% of the total female sample had a relatively high ratio. It was also found that in the young, there was the least porosity and the least variation around the cortex. In the middle group by age, there was higher overall porosity and clear differences around the cortex. Although some variability in porosity could be explained by age, the authors were better able to interpret variation in porosity around the cortex in relation to their geometric variable, rather than when grouped by age. This variability was especially true amongst female individuals.

This would suggest that individuals with varied geometry may age differently from one another, as one would predict within the slender verse robust framework. Further, the authors also hypothesized that the difference in porosity with age may have been due to decreases in muscle strength and pull with age and changes in gait and posture. Further studies of bone aging with respect to robustness should consider these factors as well.

5.4.3.2: Ash content and robustness

At both the 38% site and the 66% site, there was a significant relationship between ash content and robustness at the anterior-medial wedge. At the 66% this relationship was also significant for the posterior-medial wedge, and this relationship nears significance for the 38% site. The small number of significant relationships between ash content and robustness compared with the large number between porosity and robustness, may reflect the complexity of the system, however, ash content was a relatively insensitive technique and it may not be adequate to detect the small differences. Again, as discussed earlier, more sensitive techniques for analyzing subtle differences in local tissue mineralization (e.g. qBSE or Raman Spectroscopy) may provide more insight into the regional variability in the relationship between ash content and robustness.

5.4.4: Relationships Between the 38% and 66% Sites

In the analysis of the entire cross-section (Chapter 4), it was found that there was a strong relationship between porosity and robustness, but only at the 66% site. In the current analysis, strong relationships were confirmed to exist at all wedges around the cortex for the 66% site, and none of the wedges at the 38% site. However, a strong relationship between the amount of porosity at the two sites, 38% and 66%, was

identified in all wedges. This further supported a global relationship between porosity and robustness that is key at both proximal and distal sites, but also around the cortex. Again, this relationship may not be apparent at the 38% site because of the relatively small amount of variation in robustness at that site (see Chapter 4).

The amount of porosity in the 38% and 66% sites were highly correlated at every wedge as well as within the different rings. This indicates that there was a systemic relationship, even though it was not possible to determine the relationship directly when examining the porosity / robustness relationships, which were only significant at the 66% site. This held true for the amount of porosity between the two sites in the mid-cortex ring, and generally for the endosteal ring, which was significantly correlated between the two sites for all regions apart from posterior-medial. In the periosteal ring, the amount of porosity was only correlated between the two sites at the anterior-medial region. Due to subperiosteal expansion during growth, the microstructure in the periosteal ring showed the greatest effect from modeling rather than remodeling between the three rings. With the small sample size, it cannot be determine why only significant correlations were found at the anterior-medial region. It may be that there was no correlation between the two sites at many regions around the cortex in the periosteal ring because the modeling process was markedly different at 38% versus 66%, which was to be expected given that modeling gives the bone its final shape, and the shape of the tibia was very different at the two different locations. There may also be a relationship that cannot be quantified due to sampling error.

At the posterior and posterior-medial wedges, there were significant correlations between the ash content at the 38% and 66% site, but not at other wedges. This could indicate that in some areas of the cortex the global variable robustness was playing a key role in regulating ash content, however, in other areas this effect was being overshadowed by some other cause. The fact that the 38% sites and 66% sites were not correlated in every wedge may indicate that the two sites had different mineralization rates in some areas of the cortex that may not be fully understood using the ash content technique. Again, examining finer details of tissue composition with qBSE or spectroscopic techniques should help shed more light on these variations.

5.4.5: Co-variation Between Variables

5.4.5.1: Co-variation between ash content and porosity

Even though ash content was lowest and porosity was highest in the anterior wedge, when the two variables were plotted against each other, the regression analysis showed no linear relationship between the two variables at the anterior wedge for either the 38% or 66% sites. No relationship was observed in any other wedge, except for anterior-laterally at 38%. When the data were divided into slender and robust groups, however, an interesting separation was observed between the two groups. In almost all wedges, a negative correlation could be seen in the slender individuals, whereas no correlation was apparent in the robust individuals. These data suggested that there was a different relationship between ash content and porosity for slender individuals than robust individuals. This may indicate that in some areas around the cortex, slender individuals can afford to have highly mineralized bones with low porosity, to increase stiffness, however, some areas are under other constraints. One hypothesis to explain this lack of a

relationship between ash content and porosity for the robust individuals at many wedges is that if a bone is robust enough, then perhaps it does not need to increase its stiffness, and therefore does not need to have the same relationship between ash content and porosity that a slender bone would need. The small sample size makes this analysis statistically weak, especially given that the sample size for the slender and robust groups individually was only 5 individuals each. These data suggested that there was some relationship between ash content and porosity, however, to get a better understanding, this analysis would need to be repeated using a larger sample size.

5.4.5.2: Co-variation of µCT and LM derived porosity and amount of secondary tissue

As has been mentioned previously, both porosity and amount of secondary bone are indicators of remodeling rate. In this study, porosity was determined both in three-dimensions by µCT and in two dimensions by light microscopy. The goal was to investigate the relationship between these two measures of porosity. At the 38% region, for both the midcortex and periosteal rings, the slope of the µCT derived porosity versus the LM derived porosity was less than 1, which indicated that the µCT was underestimating the porosity compared to the results from the LM for the 66%, which had a slope much closer to 1. This may have been due to sampling error, as the µCT data was taken from a site adjacent to where the LM data was taken, so there may have been slight differences in porosity between them. Given the lower porosity at the 38% site, a small difference in the number of pores could lead to a large difference in the % porosity. The trends between the amount of porosity around the cortex were similar for both the 38% and 66% sites for the endosteal and periosteal rings for both techniques.

Another goal was to look at the relationships between the µCT derived porosity and the LM derived amount of secondary tissue. The amount of porosity as measured by µCT did generally reflect the amount of secondary tissue overall, but the trends did not match at every location around the cortex. At the 66% site, the anterior-medial wedge had an increase in porosity compared to the posterior-medial wedge, however, there was a decrease in amount of secondary bone. This led to questions about the porosity size distribution that were not addressed in this work, but should be considered in the future. Areas with large Haversian canals but small osteons would have low porosity and large amounts of secondary tissue, and may explain the differences.

µCT is a three-dimensional technique, and as such, captures the transverse pores that could not be identified by LM. It was also not possible to differentiate between primary and secondary pores in µCT, which may lead to some areas having a greater porosity than could be attributed to secondary remodeling. Overall, µCT derived porosity did reflect the amount of LM derived secondary tissue, but the direct measure of secondary tissue showed finer details and differences that could not be captured by µCT porosity alone.

5.4.6: Reflections of the Bone Remodeling Process

In Chapter 4, it was validated that observed differences in porosity, ash content, and TMD related to remodeling rate. Thus the results were interpreted concerning regional variation in porosity and ash content as reflections of the remodeling process. The amount of secondary tissue is, in some ways, a more direct measure of remodeling, however, measures of tissue type give different information than simply measures of

porosity. It is important to investigate how tissue type varies around the cortex. It must be noted that while porosity can continue to increase with time, once an entire region has been remodeled, there is no longer any way to tease out information about remodeling rate from measures of amount of secondary tissues. Several different samples may all contain 100% remodeled tissue, but have very different remodeling rates. As described previously, the remodeling process occurs throughout life, and as one ages, more primary bone is likely to be remodeled and become secondary bone (Frost, 1963). Because of this, entire areas may be comprised of secondary bone, which does not give a clear picture of remodeling rate. One person may have a fast remodeling rate, and in that case would remodel all of the primary tissue rapidly, and then continue to remodel the secondary tissue, increasing the porosity. Another person may have a slower remodeling rate, and take much longer to replace all of the primary tissue, but once that is done, by looking at amount of secondary tissue alone, there is no way to distinguish between the remodeling rates of the two individuals. Kerely (1965) found that there were four histological factors that could be reliably measured and were related to age. These factors were the number of osteons, the number of osteon fragments, the percentage of circumferential lamellar bone, and the number of non-Haversian canals. By measuring these variables individually, Kerely was able to avoid combining age effects with remodeling rate effects.

While this study for this dissertation simply looked at the total amount of secondary tissue, there are many studies that have utilized other histological variables that relate to remodeling such as whole osteon area, average osteon size, and osteon population density (OPD), which is the number of complete osteons per mm^2 (Drapeau and Streeter, 2006;

Frost 1987a; Frost 1987b; Havill, 2003; Keough *et al.*, 2009; Skedros *et al.*, 2003; Stout and Lueck, 1995; Villa and Lynnerup, 2010). These other methods may be a better metric of remodeling rate, over total secondary tissue. By the nature of the remodeling process, older osteons are remodeled over, leaving a new osteon and osteon fragments. A faster remodeling rate will likely leave more complete osteons than a slower remodeling rate, and this will likely lead to a larger area of completed osteons. However, a faster remodeling rate will lead to smaller osteons, so the size of the osteons is another important indicator of remodeling rate. Osteon population density is another histological indicator of remodeling rate, as a larger number of osteons in a given area indicates a higher remodeling rate. Because only complete osteons were considered with these variables, tissue age plays a smaller role, and the problem of regions being entirely remodeled unrelated to the remodeling rate, was no longer an issue.

5.4.7: Limitations and Future Work

In order to shed light on many of the questions raised by this work, there are a number of other techniques that should be employed to provide more sensitive measures of tissue composition than was possible here – either utilizing spectroscopic methods, such as FTIR and RAMAN or methods such as microradiography and qBSE. This will give a better understanding of local mineralization. In order to gain a better understanding of the histology, in the future, additional data on osteon size, OPD, and whole osteon area could be collected to provide for static histomorphometric assessments of remodeling rate. Finally, extending this analysis to a larger sample of tibiae, and even to other skeletal elements, will provide more information on the extent and potential causes of the

variability seen here. Age is likely a large contributor to regional variability, and the small sample used in this pilot study did not allow for those effects to be fully studied.

5.5: Conclusions

Bone is a complex and anisotropic material. The large bending moments associated with weight bearing and locomotion have an effect on regional remodeling. This effect can also be seen due to strains from muscle on the bone. The muscle attachment sites and areas of strain due to weight bearing loading likely cause increases in porosity, but there seems to be an important geometric factor as well. An increase in strain should result in an increase in remodeling, but the research for this dissertation showed that slender geometry would lead to a decrease in remodeling. These factors both exist in tandem, leading to the overall co-adaptation of the bone. The tibia is complex in its overall geometry and local structure, and should not be assumed to be homogenous. The complexities in the tibia exist not only around the cortex, but also between the concentric ring regions of the bone, and can be largely reflective of growth patterns.

This research, although a pilot study, can help narrow down which areas of the cortex should be further investigated. Areas of the cortex that are extremely remodeled and show little variation between individuals may not help answer questions about the inter-individual variations as well as areas that are less highly remodeled and show clear differences between individuals. Beyond the scope of simply increasing the number of samples, this research has the potential to give meaningful information about fundamental differences between the bones of slender individuals and robust individuals and whether or not they age differently. Currently, bone geometry is not taken into

account when determining the best course of action to combat osteoporosis in an individual. This research and the research that follows it may indicate that different treatments are required depending on overall bone geometry.

Chapter 6: Concluding Statement

The findings throughout this project indicated that the global trait robustness can have local effects on remodeling rate. This can have a significant impact on how bone is researched in the future. The remodeling process is generally thought to be controlled by local strain, with increased strain leading to increased remodeling (Corwin *et al.*, 1991; Lanyon, 1993; Mullander and Huiskes, 1995; 1997). The results of this study indicated that there may be global factors, such as robustness, that also have a controlling effect on remodeling rate. This changes the way one must consider remodeling in the future, and more research needs to be done to determine how extensive the global effects are and how they interplay with the local effects.

This research has begun to shed some light on fundamental differences both between individuals with different bone morphometries and between different areas around the cortex and throughout the length of the tibia within an individual. This research clearly showed that bone cannot be considered to be homogenous, nor can it be assumed that different individuals will have the same bone properties. However, strong correlations were found between individuals, with respect to robustness. This means that in the future, it may be possible to determine the properties of a person's bones based solely on their geometry. Future research based on the work presented here, may be able to diagnose those at high risk for fracture from a simple pQCT scan to determine bone robustness. It may be possible to determine that individuals with slender bones should refrain from certain activities or wear special orthotics, in order to minimize the risk of fracture.

Future research may also determine if slender and robust individuals age differently, which can have an impact on treatment plans for preventing and treating fragility fractures. Currently, those with or at high risk for osteoporosis are prescribed a bisphosphonate treatment, which stops osteoclastic activity (Qaseem *et al.*, 2008). If a person has slender bones, and therefore has had suppressed remodeling throughout life, further suppressing remodeling may not be the best treatment. While this research was not able to answer all of the questions, it did open the door for research that can potentially have a huge clinical impact.

The work presented in this dissertation was a pilot study, and needs to be expanded upon in the future. In this study, it was not possible to tease out any of the relationships that relate to sexual dimorphism, nor was it possible to investigate the full range of age effects. Many of the questions that could not be answered could be investigated with better techniques for local mineralization, including backscatter SEM and Raman spectroscopy mapping. It was also not possible to include any data on mechanical properties, which will hopefully be pursued by later investigators.

List of References

Aamodt, A., Lund-Larsen, J., Eine, J., Andersen, E., Benum, P., and Husby, O. S. (1997). In vivo measurements show tensile axial strain in the proximal lateral aspect of the human femur. J. Orthop. Res. 15, 927-931.

Akkus, N., Suzuki, K., Kawahara, M., and Nishimura, H. (1999). Influence of Performing on the Final Thickness Distribution of the Superplastically Deformed Domes. Mat. Sci. Forum Vol. 304-306, pp. 759-764.

Akkus, O., Polyakova-Akkus, A., Adar, F., and Schaffler, M. B. (2003). Aging of microstructural compartments in human compact bone. JBMR, 18(6), 1012-1019.

Alexander, R. M. (1998). Muscle geometry. J. Physiol., 512(2), 315.

Amprino, R. (1958). Investigations on some physical properties of bone tissue. Acta Anat 34(3), 161–186.

Arnold, J.S.; Bartley, M.H., Tont, S.A., Jenkins, D.P. (1966). Skeletal changes in aging and disease. *Clin Orthop Relat Res*. 49, 17-38.

Ascenzi, A. and Benvenuti, A. (1986). Orientation of collagen fibers at the boundary between two successive osteonic lamellae and its mechanical interpretation. *J. Biomech. 19*, 455–463.

Ascenzi, A. and Bonucci, E. (1968). The compressive properties of single osteons. *Anatom. Rec. 161*, 377-392.

Ascenzi, A. and Bonucci, E. (1967). The tensile properties of single osteons. *Anatom. Rec. 158*, 375–386.

Baron R (1999) Anatomy and ultrastructure of bone. In M.J. Favus (ed.): ***Primer on the Metabolic Bone Diseases and Disorders of Mineral Metabolism.*** Philadelphia: Lippincott Williams & Wilkins, pp. 3-10.

Beck, T. J., Ruff, C. B., Shaffer, R. A., Betsinger, K., Trone, D. W., and Brodine, S. K. (2000). Stress fracture in military recruits: gender differences in muscle and bone susceptibility factors. *Bone 27*(3), 437-444.

Beck, T. J., Ruff, C. B., Mourtada, F. a, Shaffer, R. a, Maxwell-Williams, K., Kao, G. L., Sartoris, D. J., et al. (1996). Dual-energy X-ray absorptiometry derived structural geometry for stress fracture prediction in male U.S. Marine Corps recruits. *JBMR*, 11(5), 645–53.

Belkin SC. Stress fractures in athletes. *Orthop Clin North Am* 1980;11:735–42

Biewener, A. A. and Bertram, J. E. A. (1993). Mechanical loading and bone growth in vivo. In B. K. Hall (ed.) ***Bone Growth B***, vol. 7, pp. 1-36. Nova Scotia, Canada: CRC.

Bonfield, W., and Clark, E. A. (1973). Elastic deformation of compact bone. *J. Mater. Sci. 8*, 1590–1594.

Bonse U, Busch F (1996). X-ray computed microtomography (microCT) using synchrotron radiation (SR). *Prog Biophys Mol Biol* 65:133-169.

Borah, B., Gross, G. J., Dufresne, T. E., Smith, T. S., Cockman, M. D., Chmielewski, P. a, Lundy, M. W., et al. (2001). Three-dimensional microimaging (MRmicroI and microCT), finite element modeling, and rapid prototyping provide unique insights into bone architecture in osteoporosis. *The Anatomical record*, *265*(2), 101–10.

Boskey, A. L., and Mendelsohn, R. (2005). Infrared spectroscopic characterization of mineralized tissues. *Vibrational Spectroscopy*, *38*(1-2), 107–114.

Boskey, A. L., Wright, T. M., and Blank, R. D. (1999). Collagen and bone strength. *JBMR*, *14*(3), 330–335.

Boskey, A. L., Camacho, N.P., Mendelsohn, R., Doty, S.B., Binderman, I. (1992). FT-IR microscopic mappings of early mineralization in chick limb bud mesenchymal cell cultures, Calcif. Tissue Int. 51 (6) 443–448.

Bouvier, M., and Hylander, W.L. (1981) Effect of bone strain on cortical bone structure in macaques (*Macaca mulatta*). *Journal of Morphology* 167*:*1-12.

Boyce, T. M., and Bloebaum, R. D. (1993). Cortical aging differences and fracture implications for the human femoral neck. *Bone 14*, 769–778

Boyde, A. (1972). Elemental particles in bone and dentine. *Calcif Tissue Res*, *10*(3), 256.

Boyde, A., Lovicar, L., and Zamecnik, J. (2005). Combining confocal and BSE SEM imaging for bone block surfaces. *Eur. Cell Mater., 9,* 33-38.

Boyde, A., Elliott, J.C., Jones, S.J. (1993) Stereology and histogram analysis of backscattered electron images: Age changes in bone. *Bone*, 14:205-210

Boyde, A. and Riggs, C. M. (1990). The quantitative study of the orientation of collagen in compact bone slices. *Bone 11*, 35–39.

Boyde, A., Jones, S.J. (1983) Backscatered electron imaging of skeletal tissues. *Metab. Bone Dis. Re. Res*. 5:145-150

Boyle, W.J., Simonet, W.S., and Lacey D.L. (2003) Osteoclast differentiation and activation. *Nature*. 423*:*337-42.

Bräuer, G. 1988. Osteometrie. In: Knussman R, editor. Anthropologie. Stuttgart: Gustav Fischer Verlag. p 160–231.

Bromage, T.G., Goldman, H.M., McFarlin, S.C., Warshaw, J., Boyde, A., and Riggs, C.M. (2003) Circularly polarized light standards for investigations of collagen fiber orientation in bone. *The Anatomical Record, Part B: The New Anatomist* 274B*:*157-168.

Burger, E. H., and Klein-Nulend, J. (1999) Mechanotransduction in bone - role of the lacunocanalicular network. *FASEB*. 13 Suppl*:*S101-12.

Burghardt, A. J., Kazakia, G. J., Ramachandran, S., Link, T. M., and Majumdar, S. (2010). Age- and gender-related differences in the geometric properties and biomechanical significance of intracortical porosity in the distal radius and tibia. *JBMR*, *25*(5), 983–993.

Burghardt, A. J., Kazakia G. J., Laib, A., Majumdar, S. (2008). Quantitative assessment of bone tissue mineralization with polychromatic micro-computed tomography. Calcif Tissue Int. 83(2): 129-138.

Burr DB (2001) Targeted and non-targeted remodeling. *Bone* 30: 582-584.

Burr, D.B., Forwood, M.R., Fyhrie, D.P., Martin, R.B., Schaffler, M.B., Turner, C.H. (1997). Bone microdamage and skeletal fragility in osteoporotic and stress fractures. *J Bone Miner Res* 12:6 – 15.

Burr, D. B., Milgrom, C., Higgins, W. L., Robin, G., and Radin, E. L. (1990). Experimental Stress Fractures of the Tibia. *J. Bone Joint Surg Br*, *72-B*, 370–375.

Burr, D. B., Schaffler, M. B., and Frederickson, R. G. (1988). Composition of the cement line and its possible mechanical role as a local interface in human compact bone. *J. Biomech. 21*, 939–945.

Cambra-Moo, O., Nacarino Meneses, C., Rodríguez Barbero, M. Á., García Gil, O., Rascón Pérez, J., Rello-Varona, S., Campo Martín, M., González Martín, A. (2012). Mapping human long bone compartmentalisation during ontogeny: a new methodological approach. J Struct Biol, 178(3), 338-49.

Carter, D. R. and Hayes, W. C. (1977). Compact bone fatigue damage. *Clin. Orthop. Rel. Res. 127*, 265–274.

Carter, D. R., Hayes, W. C., and Schurman, D. J. (1976). Fatigue life of compact bone – II. Effects of microstructure and density. *J. Biomech. 9*, 211-218.

Castanet, J., Francillon-Vieillot, H., Meunier, F.J., and De Ricqlès, A. (1993) Bone and individual aging. In B.K. Hall (ed.): **Bone.** Boca Raton: CRC Press, pp. 245-284.

Chatzipapas, C. N., Drosos, G. I., Kazakos, K. I., Tripsianis, G., Iatrou, C., Verettas, D.-A. J. (2008). Stress fractures in military men and bone quality related factors. *Int J Sports Med*. 29(11). 922–926.

Cooper, D. M., Ahamed, Y., MacDonald, H. M., McKay, H. A. (2008) Characterising cortical density in the mid tibia: intra-individual variation in adolescent girls and boys. Br J Sports Med 42, 690-695.

Cooper, David M. L., Thomas, C. D. L., Clement, J. G., Turinsky, A. L., Sensen, C. W., and Hallgrímsson, B. (2007). Age-dependent change in the 3D structure of cortical porosity at the human femoral midshaft. *Bone*, *40*(4), 957-65.

Cooper, D. M. L., Thomas, C. D. L., Clement, J. G., and Hallgrímsson, B. (2006). Three-dimensional microcomputed tomography imaging of basic multicellular unit-related resorption spaces in human cortical bone. *Anat. Rec. A*, *288*(7), 806-16.

Cooper, D.M.L., Thomas, C.D.L., Clement, J.G., Hallgrimsson, B. (2005). The role of age and body size in predicting the 3d structure of cortical porosity at the human anterior femoral mid-shaft. *J Bone Miner Res* 20:SU016.

Cooper, D. M. L., Matyas, J. R., Katzenberg, M. a, and Hallgrimsson, B. (2004). Comparison of microcomputed tomographic and microradiographic measurements of cortical bone porosity. *Calcified tissue international*, *74*(5), 437-47.

Courtland, H.-W., Spevak, M., Boskey, A. L., and Jepsen, K. J. (2009). Genetic variation in mouse femoral tissue-level mineral content underlies differences in whole bone mechanical properties. *Cells, tissues, organs*, *189*(1-4), 237-240.

Cowin S. C. (2002) Mechanosensation and fluid transport in living bone. *J Musculoskelet Neuronal Interact.* 2:256-60.

Cowin, S. C., Moss-Salentijn, L., and Moss, M. L. (1991). Candidates for the mechanosensory system in bone. *J. Biomech. Eng. 113*, 191-197.

Crossley, K., Bennell, K. L., Wrigley, T., Oakes, B. W. (1999). Ground reaction forces, bone characteristics, and tibial stress fracture in male runners. *Med Sci Sports Exerc.* 31(8), 1088-1093.

Currey, J. D. (2003). How well are bones designed to resist fracture? *JBMR*, *18*(4), 591-8.

Currey, J. D. (2002). *Bones*. Princeton, NJ: Princeton University.

Currey, J. D. (1988). The effect of porosity and mineral content on the Young's modulus of elasticity of compact bone. *J. Biomech. 21*(2), 131-139.

Currey, J. D. (1984). What should bones be designed to do? *Calcif. Tissue Int., 36,* S7-S10.

Currey, J. D. (1979). Changes in the impact energy absorption of bone with age. *J. Biomech., 12*(6), 459-469.

Currey, J. D. (1969). The mechanical consequences of variation in the mineral content of bone. *J. Biomech. 2*(1), 1-11.

Currey, J. D., Brear, K., Zioupos, P (1996). The effect of aging and the changes in mineral content in degrading the toughness of human femora. *J Biomech.* 29(2), 257-260.

De Ricqlés, A., F. J. Meunier, et al. (1991). Comparative microstructure of bone. *Bone*. B. K. Hall. Boca Raton, CRC Press**:** 1-78.

Delmas, P. D., and Seeman, E. (2004). Changes in bone mineral density explain little of the reduction in vertebral or nonvertebral fracture risk with anti-resorptive therapy. *Bone 34*(4), 599–604.

Diab, T., Condon, K. W., Burr, D. B., and Vashishth, D. (2006). Age-related change in the damage morphology of human cortical bone and its role in bone fragility. *Bone*, *38*(3), 427–431.

Donnelly, E. (2011). Methods for assessing bone quality: a review. *Clinical orthopaedics and related research*, 469(8), 2128-38.

Doty, S. B. (1981) Morphological evidence of gap junctions between bone cells. *Calcified Tissue Int*. 33*:*509-12.

Drapeau, M. S. M., and Streeter, M. a. (2006). Modeling and remodeling responses to normal loading in the human lower limb. *Am. J. Phys. Anthropol.*, *129*(3), 403-409.

Engelke, K., Libanatic, C., Liuc, Y., Wang, H., Austin, M., Fuerst, T., Stampa, B., Timm, W., and Genant, H. K. (2009), Quantitative computed tomography (QCT) of the forearm using general purpose spiral whole-body CT scanners: accuracy, precision and comparison with dual-energy X-ray absorptiometry (DXA), *Bone*, *45*(1), 110-118.

Engstrom, A. (1952). X-ray absorption methods in histochemistry. *Lab Invest 1*(2): 278-285.

Enlow, D. H. (1962). A study of the post-natal growth and remodeling of bone. *Am. J. Anat.*, *110*, 79-101.

Enlow, D. H. (1963). *Principles of bone remodeling; an account of post- natal growth and remodeling processes in long bones and the mandible.* Springfield: Thomas.

Enlow, D., Bianco, H., Eklund, S. (1976). The remodeling of the edentulous mandible The Journal of Prosthetic Dentistry, 36 (6) Pages 685-693.

Enlow, D. H. (1982). *Handbook of Facial Growth*. Philadelphia: W.B. Saunders.

Enlow, D. H., and Brown, S.O. (1957) A comparative histological study of fossil and recent bone tissues. *Part II. Texas Journal of Science* 9*:*186-214.

Enlow, D. H., and Hans, M.G. (1996) Essentials of Facial Growth. Philadelphia: W.B. 622 Saunders Company.

Feik, S. A, Thomas, C. D., Bruns, R., and Clement, J. G. (2000). Regional variations in cortical modeling in the femoral mid-shaft: sex and age differences. *Am. J. Phys. Anthropol.*, *112*(2), 191-205.

Feik, S. A, Thomas, C. D., and Clement, J. G. (1996). Age trends in remodeling of the femoral midshaft differ between the sexes. *J. Orthop. Res.*, *14*(4), 590-597.

Felsenberg, D., Boonen, S. (2005). The bone quality framework: determinants of bone strength and their interrelationships, and implications for osteoporosis management. *Clin. Therapy*, 27(1), 1-11.

Forwood, M. R., Parket, A.W. (1989). Microdamage in response to repetitive torsional loading in the rat tibia. *Calcif. Tissue Int*. 45:47-53

Francillon-Vieillot, H., de Buffrenil, V., Castanet, J., Geraudie, J., Meunier, F.J., Sire, J.Y., Zylberberg, L., and de Ricqlès, A. (1990) Microstructure and mineralization of vertebrate skeletal tissues. In J.G. Carter (ed.): ***Skeletal Biomineralization: Patterns, Processes and Evolutionary Trends.*** New York: Van Nostrand Reinhold, pp. 471-530.

Francillon-Vieillot, H., V. de Buffrénil, J. Castanet, J. Géraudie, F. Meunier, J. Y. Sire, L. Zylberberg, and A. de Ricqlès (1989), Microstructure and mineralization of vertebrate skeletal tissues, in Skeletal Biomineralization: Patterns, Processes and Evolutionary Trends, Short Course Geol. Ser., vol. 5, edited by J. G. Carter, pp. 175–234, AGU, Washington, D. C.

Frasca, P., Harper, R. A., and Katz, J. L. (1977). Collagen fiber orientations in human secondary osteons. *Acta Anat*, *98*(1), 1-13.

Frost, H. M. (1987a) Secondary osteon populations: an algorithm for determining mean bone tissue age. *Yrbk. Phys. Anthropol*. 30:221-238

Frost, H. M. (1987b) Secondary osteon population densities: an algorithm for estimating the missing osteons. *Yrbk. Phys. Anthropol*. 30:239-254.

Frost, H. M. (1986) ***Intermediary Organization of the Skeleton***. Boca Raton: CRC Press.

Frost, H. M. (1973). *Orthopaedic Biomechanics*. (C. C. Thomas, Ed.) *Orthopaedic Biomechanics*. Springfield.

Frost, H. M. (1963). ***Bone Remodeling Dynamics***. Springfield: Thomas Books.

Fyhrie, D.P. (2005). Summary - Measuring "Bone Quality". *J Musculoskelet Neuronal Interact.* 5(4), 318-20.

Garn, S. M., Rohmann, C. G., Wagner, B., and Ascoli, W. (1967). Continuing bone growth throughout life: a general phenomenon. *Am. J. Phys. Anthropol.*, *26*(3), 313-317.

Giladi, M., Milgrom, C., Simkin, A., Stein, M., Kashtan, H., Margulies, J., Rand, N., Chisin, R., Steinberg, R., Aharonson, Z., Kedem, R., and Frankel, V.H. (1987). Tibial bone width. A risk factor for stress fractures. *J. Bone Joint Surg.*, *69B*, 326-329.

Giladi, M., Ahronson, Z., Stein, M., Danon, Y. L., Milgrom, C. (1985). Unusual distributions and onset of stress fractures in soldiers. *Clin Orthop.* 192, 142-146.

Gilbert, R. S. and Johnson, H. A. (1966) Stress fractures in military recruits. A review of twelve years experience. *Milit. Med.* 131, 716721.

Giraud-Guille, M.M. (1988) Twisted plywood architecture of collagen fibrils in human compact bone osteons. *Calcified Tissue International* 42, 167-80.

Goldman, H.M. (2001) Histocomposition and geometry at the human mid-shaft femur. Ph.D., City University of New York, New York.

Goldman, H. M., McFarlin, S. C., Cooper, D. M. L., Thomas, C. D. L., and Clement, J. G. (2009). Ontogenetic patterning of cortical bone microstructure and geometry at the human mid-shaft femur. *Anat. Rec.*, 292(1), 48-64.

Goldman, H. M., Thomas, C. D. L., Clement, J. G., and Bromage, T. G. (2005). Relationships among microstructural properties of bone at the human midshaft femur. *J. Anat.*, *206*(2), 127-39.

Goldman. H. M., Bromage, T.G., Boyde, A., Thomas, C. D., Clement, J. G. (2003a). Intrapopulation variability in mineralization density at the human femoral mid-shaft. J Anat 203:243-255.

Goldman. H. M., Bromage, T.G., Boyde, A., Thomas, C. D., Clement, J. G. (2003b). Preferred collagen fiber orientation in the human mid-shaft femur. Anat Rec A Discov Mol Cell Evol Biol 272:434-445.

Goldman, H.M., Kindsvater, J., and Bromage, T.G. (1999) Correlative light and backscattered electron microscopy of bone - Part I: Specimen preparation methods. *Scanning* 21*:*40-43.

Gosman, J. H., Hubbell, Z. R., Shaw, C. N., Ryan, T. M. (2013). Development of cortical bone geometry in the human femoral and tibial diaphysis. Anat Rec. 296: 774-787.

Gross, T. S., McLeod, K. J., and Rubin, C. T. (1992). Characterizing bone strain distributions in vivo using three triple rosette strain gages. *J. Biomech.*, *25*(9), 1081-1087.

Grynpas, M. (1993). Age and disease related changes in the mineral of bone. *Calcif. Tissue Int*., 53:S57-S64

Guo, X. E., Liang, L. C., and Goldstein, S. A. (1998). Micromechanics of osteonal cortical bone fracture. *J. Biomech. Eng*., 120(1), 112-7.

Havill, L. M. (2003). Osteon remodeling dynamics in Macaca mulatta: normal variation with regard to age, sex, and skeletal maturity. Calcified tissue international, 74(1), 95-102.

Hernandez, C.J., Keaveny, T.M., (2006). A Biomechanical Perspective on Bone Quality. *Bone*, 39(6), 1173-81.

Hernandez, C. J. (2008). How can bone turnover modify bone strength independent of bone mass? Bone, 42, 1014-1020.

Hildebrand, M. (1974). *Analysis of Vertebrate Structure*. New York: John Wiley and Sons.

Howell, S. M., Kuznik, K., Hull, M. L., Siston, R. A. (2010). Longitudinal Shapes of the Tibia and Femur are Unrelated and Variable. *Clin Orthop Relat Res* 468(4): 1142-1148.

Hrdlicka, A (1989). Study of the Normal Tibia. *Am. Anthropol* 11(10), 307-312.

Jee, W. (2001). *Integrated Bone Tissue Physiology: Anatomy and Physiology*. In S. C. Corwin (Ed.), ***Bone Mechanics Handbook*** (2nd ed., pp. 1–68). Informa Healthcare.

Jee, W. (1988). *The Skeletal Tissues.* In L. Weiss (Ed.), ***Cell and Tissue Biology: A Textbook of Histology*** (6th ed., pp. 207–249). Urban and Schwarzenberg.

Jepsen, K. J., Centi, A., Duarte, G. F., Galloway, K., Goldman, H., Hampson, N., Lappe, J. M., Cullen, D. M., Greeves, J., Izard, R., Nindl, B. C., Kraemer, W. J., Negus, C. H., and Evans, R. K. (2011). Biological constraints that limit compensation of a common skeletal trait variant lead to inequivalence of tibial function among healthy young adults. *JBMR*, *26*(12), 2872–2885.

Jepsen, K. J., Hu, B., Tommasini, S. M., Courtland, H.-W., Price, C., Cordova, M., and Nadeau, J. H. (2009). Phenotypic integration of skeletal traits during growth buffers genetic variants affecting the slenderness of femora in inbred mouse strains. *Mamm. Genome*, *20*, 21–33.

Jepsen, K. J., Hu, B., Tommasini, S. M., Courtland, H.-W., Price, C., Terranova, C. J., and Nadeau, J. H. (2007). Genetic randomization reveals functional relationships among morphologic and tissue-quality traits that contribute to bone strength and fragility. *Mammalian genome*, *18*(6-7), 492-507.

Jepsen, K. J., Akkus, O. J., Majeska, R. J., and Nadeau, J. H. (2003). Hierarchical relationship between bone traits and mechanical properties in inbred mice. *Mamm. Genome*, *14*(2), 97-104.

Jepsen, K. J., Pennington, D. E., Lee, Y. L., Warman, M., and Nadeau, J. (2001). Bone brittleness varies with genetic background in A/J and C57BL/6J inbred mice. *JBMR 16*(10), 1854-62.

Jepsen, K. J., Pennington, D. E., Lee, Y. L., Warman, M., and Nadeau, J. (2001). Bone brittleness varies with genetic background in A/J and C57BL/6J inbred mice. *JBMR*, *16*(10), 1854-62

Jinnai, H., Watashiba, H., Kajihara, T., Nishikawa, Y., Takahashi, M., and Ito, M. (2002). Surface curvatures of trabecular bone microarchitecture. *Bone*, *30*(1), 191-4.

Jones, B., Bovee, M., Harrism J., Cowin, D. (1993). Intrinsic risk factors for exercise related injuries among male and female army trainees. *Am. J. Sports Med. 21*, 705-710.

Jowsey, J. (1966) Studies of Haversian systems in man and some animals. *Journal of Anatomy* 100:857-864.

Jowsey, J. (1964) Variations in bone mineralization with age and disease. In HM Frost (ed.): *Bone Biodynamics*. Boston:Little, Brown and Co., pp. 461-479.

Kay, M.I., and Young, R.A. (1964) Crystal Structure of Hydroxyapatite. *Nature* 204: 1050-1052

Kennedy, O. D., Brennan, O., Rackard, S. M., Staines, A., O'Brian, F. J., Taylor, D., Lee, C. (2009) Effects of Ovariectomy on Bone Turnover, Porosity, and Biomechanical Properties in Ovine Compact Bone 12 Months Postsurgery. *J. Orthop. Res.* 27(3): 303-309.

Keough, N., L'Abbé E. N., Steyn, M. (2009). *The evaluation of age-related histomorphometric variables in a cadaver sample of lower socioeconomic status: implications for estimating age at death.* Forensic Sci Int. 191, 1-3.

Kerley, E. R. (1965) The microscopic determination of age in human bone. *Am. J. Phys. Anthropol*. 23:149-63

Kimura, T. (2006). Robustness of the whole Jomon femur shaft assessed by cross-sectional geometry. *Anthropological Science*, 114(1), 13-22.

Knott, L. and Bailey, A. J. (1998). Collagen cross-links in mineralizing tissues: a review of their chemistry, function, and clinical relevance. *Bone* 22(3), 181-187.

Landis, W. J. (1995). The strength of a calcified tissue depends in part on the molecular structure and organization of its constituent mineral crystals in their organic matrix. *Bone*, 16:533-44

Lanyon, L. E. (1993). *Biomechanical properties of bone and response of bone to mechanical stimuli: Functional strain as a controlling influence on bone modeling and remodeling behavior.* In BK Hall (ed.): ***Bone*.** Boca Raton: CRC Press.

Lazenby, R. (1992) A geometric and microradiographic study of the functional adaptation in the human skeleton. Ph.D. Dissertation, McMaster University.

Lazenby, R. (1986). Porosity-geometry interaction in the conservation of bone strength. *J. Biomechanics*, *19*(3), 257-258.

Lian, J. B., and Stein, G. S. (1999) The cells of bone. In M. J. Seibel, S. P. Robins and J.P. Bilezikian (eds.): ***Dynamics of Bone and Cartilage Metabolism.*** New York: Academic Press, pp. 165-186.

Li, X.J., Jee, W.S., Chow, S.Y. and Woodbury, D.M. (1990). Adaption of cancellous bone to ading and immobilization in the rat: a single photon absorptiometry and histomorphometry study. *Anat. Rec.* 227:12-24.

Lieberman, D. E. (2003). Optimization of bone growth and remodeling in response to loading in tapered mammalian limbs. *J. Exp. Biol.*, *206*(18), 3125-3138.

Lieberman D. E. and Crompton A.W. (1998). Responses of bone to stress: constraints on symmorphosis. In: Webel ER, Taylor CR, Bolis L, editors. Principles of animal design: the optimiza- tion and symmorphosis debate. Cambridge: Cambridge University Press. p 78–86.

Macdonald, H. M., Cooper, D. M. L., and McKay, H. a. (2009). Anterior-posterior bending strength at the tibial shaft increases with physical activity in boys: evidence for non-uniform geometric adaptation. *Osteoporos. Int.*, *20*, 61-70.

Majeska, R.J. (2001) Cell biology of bone. In S.C. Cowin (ed.): ***Bone Mechanics Handbook*.** Boca Raton: CRC Press, pp. 2, 1-24.

Marotti, G. (1993). A new theory of bone lamellation. *Calcif Tissue Int*, *53 Suppl*(1), S47-55.

Marshall, D., Johnell, O., and Wedel, H. (1996). Meta-analysis of how well measures of bone mineral density predict occurrence of osteoporotic fractures. *BMJ*, *312*(7041), 1254-1259.

Martin, R. B. (2003). Fatigue damage, remodeling, and the minimization of skeletal weight. *J. Theor. Biol.*, *220*(2), 271-276.

Martin, R. B. (2002). Is all cortical bone remodeling initiated by microdamage? *Bone*, *30*(1), 8-13.

Martin, R. B. (2000). Toward a unifying theory of bone remodeling. *Bone* 26*:*1-6.

Martin R, Saller K. 1957. Lehrbuch der Antropologie. Stuttgart: Gustav Fischer Verlag.

Martin, D. L., and Armelagos, G. J. (1985). Skeletal remodeling and mineralization as indicators of health: An example from prehistoric Sudanese Nubia. *J. Hum. Evol. 14*, 527-537.

Martin, R. B., Burr, D. B., and Sharkey, N. A. (1998). *Skeletal Tissue Mechanics*. New York, Springer.

Martin, R. B., and Boardman, D. L. (1993). The effects of collagen fiber orientation, porosity, density, and mineralization on bovine cortical bone bending properties. *J. Biomech.*, *26*(9), 1047-1054.

Martin, R. B., and Ishida, J. (1989). The relative effects of collagen fiber orientation, porosity, density, and mineralization on bone strength. *J. Biomech.*, *22*(5), 419-426.

Martin, R.B., and Burr, D.B. (1982) A hypothetical mechanism for the stimulation of osteonal remodelling by fatigue damage. *Journal of Biomechanics* 15*:*137-9.

Mason, M. W., Skedros, J. G., and Bloebaum, R. D. (1995). Evidence of strain-mode-related cortical adaptation in the diaphysis of the horse radius. *Bone 17*, 229-237.

Mccalden, R. W., Mcgeough, J. A., Barker, M. B., and Court-brown, C. M. (1993). Age-Related Changes in the Tensile Properties of Cortical Bone. The Relative Importance of Changes in Porosity, Mineralization, and Microstructure. *J. Bone Joint Surg. [Am], 75-A*(8), 1193-1205.

McFarlin SC. Anthropology. New York: City University of New York; 2006. Ontogenetic variation in long bone microstructure in catarrhines and its significance for life history research.

Meunier, P. J., and Boivin, G. (1997). Bone mineral density reflects bone mass but also the degree of mineralization of bone: therapeutic implications. *Bone, 21*(5), 373-377.

Milgrom, C., Giladi, M., Simkin, A., Rand, N., Kedem, R., Kashtan, H., Stein, M., and Gomori, M. (1989). The area moment of inertia of the tibia: a risk factor for stress fractures. *J. Biomechanics*, *22*(11/12), 1243-1248.

Milgrom, C.,Giladi, M.,Stein, M.,Kashtan, H.,Margulies,J.,Chisin, R.,Steinberg,R.,Aharonson,Z.,(1985). Stress fractures in military recruits. A prospective study showing an unusually high incidence. *J. Bone Joint Surg.* 67B,732–735.

Mittlmeir, T., Mattheck, C. and Dietrich, F. (1994). Effects of mechanical loading on the profile of human femoral diaphyseal geometry. *Med. Eng. Phys.* 16:75-81.

Mullender, M. G., and Huiskes, R. (1997) Osteocytes and bone lining cells: which are the best candidates for mechano-sensors in cancellous bone?. *Bone 20*, 527-532.

Mullender, M. G., and Huiskes, R. (1995). Proposal for the regulatory mechanism of Wolff's law. *J. Orthop. Res. 13*, 503-512.

Najafi, A. R., Arshi, A. R., Eslami, M. R., Fariborz, S., and Moeinzadeh, M. H. (2007). Micromechanics fracture in osteonal cortical bone: a study of the interactions between microcrack propagation, microstructure and the material properties. *J Biomech*, 40(12), 2788-95.

Nazarian, A., Snyder, B. D., Zurakowski, D., Muller, R. (2008). Quantitative micro-computed tomography: a non-invasive method to assess equivalent bone mineral density. Bone 43:302-311.

Nielsen, H. E., Mosekilde, L., Mosekilde, Li., Melsen, B., Christensen, P., Olsen, K. J. and Melsen, F. (1980) Relations of bone mineral content, ash-weight and bone mass: Implications for corrections of bone mineral content for bone size. Clin. Orthop. 153, 241-247.

Nijweide, P. J., Burger, E. H., Nulend, J. K., and Van der Plas, A. (1996) The osteocytes. In J. P. Bilezikian, L.G. Raisz and G.A. Rodan (eds.): ***Principles of Bone Biology.*** SanDiego: Academic Press, pp. 115-126.

Norman, T. L., Little, T. M., and Yeni, Y. N. (2008). Age-related changes in porosity and mineralization and in-service damage accumulation. *J. Biomech., 41*(13), 2868-2873.

Nuzzo, S., Peyrin, F., Cloetens, P., Baruchel, J. and Boivin, G. (2002) Quantification of the degree of mineralization of bone in three dimensions using synchrotron radiation microtomography Med. Phys. 29 2672-81

O'Brien, F. J., Taylor, D., Lee, T. C. (2005) The effect of bone microstructure on the initiation and growth of microcracks. *J Orthop Res* 23, 475-480.

Pandey, N., Bhola, S., Goldstone, A., Chen, F., Chrzanowski, J., Terranova, C. J., Ghillani, R., et al. (2009). Interindividual Variation in Functionally Adapted Trait Sets Is Established During Postnatal Growth and Predictable Based on Bone Robustness. *JBMR, 24*(12).

Parfitt, A. M. (2004). What is the normal rate of bone remodeling? Bone, 35(1), 1-3.

Parfitt, A. M. (2001) Skeletal heterogeneity and the purposes of bone remodeling: implications for the understanding of osteoporosis. In R Marcus, D Feldman and J Kelsey (eds.): *Osteoporosis*. San Diego: Academic Press, pp. 433-447.

Parfitt, A. (1984) The cellular basis of bone remodeling: the quantum concept reexamined in light of recent advances in the cell biology of bone. *Calcif. Tissue Int*. 36:S37-S45

Parfitt, A. (1983) The physiological and clinical significance of bone histomorphometric data. In: Recker RR (ed). *Bone histomorphometry techniques and interpretations.* CRC Press, Boca Raton, pp 143-224.

Particelli, F., Mecozzi, L., Beraudi, a, Montesi, M., Baruffaldi, F., and Viceconti, M. (2012). A comparison between micro-CT and histology for the evaluation of cortical bone: effect of polymethylmethacrylate embedding on structural parameters. *Journal of microscopy*, *245*(3), 302-10.

Paschalis, E. P., Shane, E., Lyritis, G., Skarantavos, G., Mendelsohn, R., Boskey, A.L. (2004). Bone fragility and collagen cross-links. *JBMR*, 19(12).

Pathak, S. (2009). *Development and validation of a novel data analysis procedure for spherical nanoindentation*. Drexel University.

Pathak, S., Vachhani, S. J., Jepsen, K. J., Goldman, H. M., and Kalidindi, S. R. (2012). Assessment of lamellar level properties in mouse bone utilizing a novel spherical nanoindentation data analysis method. *J Mech Behav Biomed*, 13, 102-17.

Pathak, S., Swadener, J. G., Kalidindi, S. R., Courtland, H.-W., Jepsen, K. J., and Goldman, H. M. (2011). Measuring the dynamic mechanical response of hydrated mouse bone by nanoindentation. *J Mech Behav Biomed Mater*, *4*(1), 34-43.

Peterman, M. M., Hamel, A. J., Cavanagh, P. R., Piazza, S. J., and Sharkey, N. A. (2001). In vitro modeling of human tibial strains during exercise in micro-gravity. *J. Biomech.*, *34*(5), 693–698.

Pfeiffer, S., Lazenby, R., and Chiang, J (1995). Brief Communication: Cortical remodeling data are affected by sampling location. *Am. J. Phys Anthropol*. 96, 89-92.

Qaseem, A., Snow, V., Shekelle, P., Hopkins, R., Forciea, M. A., and Owens, D. K. (2008). Pharmacologic treatment of low bone density or osteoporosis to prevent fractures: a clinical practice guideline from the American College of Physicians. *Ann. Intern. Med.,* 149(6), 404-15.

Rantalainen, T., Nikander, R., Daly, R. M., Heinonen, a, and Sievänen, H. (2011). Exercise loading and cortical bone distribution at the tibial shaft. Bone, 48(4), 786-91.

Rauch, F., Travers, R., and Glorieux, F. H. (2007). Intracortical remodeling during human bone development-a histomorphometric study. *Bone*, *40*(2), 274-280.

Raum, K., Hofmann, T., Leguerney, I., Saied, A., Peyrin, F., Vico, L., Laugier, P. (2007). Variations of microstructure, mineral density and tissue elasticity in B6/C3H mice. Bone. 41(6): 1017-1024.

Raum, K., Leguerney, I., Chandelier, F., Talmant, M., Saïed, A., Peyrin, F., Laugier, P. (2006). Site-matched assessment of structural and tissue properties of cortical bone using scanning acoustic microscopy and synchrotron radiation μCT. Phys Med Biol. 51:733-46.

Recker, R. R., Davies, K.M., Hinders, S.M., Heaney, R.P., Stegman, M.R. and Kimmel, D.B. (1992). "Bone gain in young adult women", JAMA. 268(17):2403-2408

Reid, S. A., and Boyde, A. (1987). Changes in the mineral density distribution in human bone with age: image analysis using backscattered electrons in the SEM. *JBMR 2*, 13-22.

Reilly, D. T. and Burstein, A. H. (1975). The elastic and ultimate properties of compact bone tissue. *J. Biomech*. 8, 393-405.

Rho, J. Y., Zioupos, P., Currey, J. D., and Pharr, G. M. (2002). Microstructural elasticity and regional heterogeneity in human femoral bone of various ages examined by nano-indentation. *J. Biomech.*, 35(2), 189–98.

Riggs, B. L., Melton III, L. J., Robb, R. A., Camp, J. J., Atkinson, E. J., Peterson, J. M., Rouleau, P. A., McCollough, C. H., Bouxsein, M. L. and Khosla, S. (2004). Population-based study of age and sex differences in bone volumetric density, size, geometry, and structure at different skeletal sites. *JBMR*, *19*(12), 1945–1954.

Riggs, C. M., Vaughn, L. C., Evans, G. P., and Boyde, A. (1993a). Mechanical implications of collagen fibre orientation in cortical bone of the equine radius. *Anat. and Embryol. 187*, 239–248.

Riggs C. M., Lanyon L. E., and Boyde A. (1993b) Functional associations between collagen fibre orientation and locomotor strain direction in cortical bone of the equine radius. Anatomy and Embryology 187, 231-238.

Rohrbach, D., Lakshmanan, S., Peyrin, F., Langer, M., Gerisch, A., Grimal, Q., Laugier, P., Raum, K. (2012). Spatial distribution of tissue level properties in a human femoral cortical bone. Journal of biomechanics, 45(13), 2264–70.

Roschger, P., Paschalis, E. P., Fratzl, P., and Klaushofer, K. (2008). Bone mineralization density distribution in health and disease. *Bone*, 42(3), 456–66.

Roschger, P., Plenk Jr., H., Klaushofer, K., Eschberger, J. (1995) A new scanning elecron microscopy approach to the quantification of bone mineral distribution: backscattered electron image grey-levels correlated to calcium K alpha-line intensities. *Scanning Microsc*. 9:75-86; discussion 86-8.

Rubin, C. T. (1984). Skeletal strain and the functional significance of bone architecture. *Calcif. Tissue Int.*, *36 Suppl 1*, S11–S18.

Ruff, C. B. (2000). Body size, body shape, and long bone strength in modern humans. *J. Hum. Evol.*, *38*(2), 269–290

Ruff, C. B., Trinkaus, E.,Walker, A., Larsen, C.S., 1993. Postcranial robusticity in Homo. I. Temporal trends and mechanical interpretation. *Am. J. Phys. Anthropol*. 91, 21e53.

Ruff, C. B., and Hayes, W. C. (1988). Sex differences in age-related remodeling of the femur and tibia. *J. Orthop. Res.*, *6*(6), 886–896.

Ruff, C. B. and Hayes, W. C. (1983a). Cross sectional geometry of Pecos Pueblo Femora and Tibiae - A biomechanical investigation: I Method and general patterns of variation. *Am. J. Phys. Anthropol.* 60:359-381.

Ruff, C. B. and Hayes, W. C. (1983b). Cross sectional geometry of Pecos Pueblo Femora and Tibiae - A biomechanical investigation: II Sex, age and side differences. *Am. J. Phys. Anthropol.* 60:383-400.

Ruff, C. B., and Hayes, W. C. (1982). Subperiosteal expansion and cortical remodeling of the human femur and tibia with aging. *Science*, *217*(4563), 945–948.

Ruff, C., Holt, B., and Trinkaus, E. (2006). Perspectives Who ' s Afraid of the Big Bad Wolff ?: "' Wolff ' s Law "' and Bone Functional Adaptation. *Bone*, *498*, 484–498.

Schaffer, R. A., Rauh, M. J., Brodine, S. K., Trone, D. W., Macera, C. A. (2006). Predictors of Stress Fracture. Susceptibility in Young Female Recruits. *Am. J. Sports Med.* 34 (1), 108-115.

Schaffler, M. B., Choi, K., and Milgrom, C. (1995). Aging and matrix microdamage accumulation in human compact bone. *Bone*, 17(6), 521–525.

Schaffler M. B., Radin EL, and Burr DB (1989) Mechanical and morphological effects ofstrain rate on fatigue of compact bone. Bone 10*:*207-14.

Schaffler, M. B., and Burr, D. B. (1988). Stiffness of compact bone: effects of porosity and density. *J. Biomech.*, *21*(1), 13–16.

Sievänen, H., Koskue, V., Rauhio, A., Kannus, P., Heinonen, A., Vuori, I. (1998). Peripheral quantitative computed tomography in human long bones: evaluation of in vitro and in vivo precision. *J Bone Miner Res* 13:871–882

Seeman, E. (1997). From density to structure: growing up and growing old on the surfaces of bone. *JBMR*, *12*(4), 509–521.

Skedros, J. G. (2012). Interpreting Load History in Limb-Bone Diaphyses: Important considerations and their biomechanical foundations. In C. Crowder and S. Stout (Eds.), ***Bone Histology: An Anthropological Perspective*** (pp. 153–220). New York.

Skedros, J.G., Hunt, K.J., Hughes, P.E., and Winet, H. (2003) Ontogenetic and regional morphologic variations in the turkey ulna diaphysis: implications for functionald adaptation of cortical bone. *The Anatomical Record, Part A* 273A*:*609-629.

Slayter, E.M., and Slayter, H.S. (1992) Light and Electron Microscopy. Cambridge: Cambridge University Press.

Smith, R. W., Jr., and Walker, R. R. (1964). Femoral expansion in aging women: implications for osteoporosis and fractures." *Science 145*, 156-157

Stock, J. T., and Shaw, C. N. (2007). Which Measures of Diaphyseal Robusticity Are Robust ? A Comparison of External Methods of Quantifying the Strength of Long Bone Diaphyses to Cross-Sectional Geometric Properties. *Am J Phys Anthro. 423*(July), 412–423.

Stout, S. D., Brunsden, B. S., Hildebolt, C. F., Commean, P. K., Smith, K. E., and Tappen, N. C. (1999). Computer-assisted 3D reconstruction of serial sections of cortical bone to determine the 3D structure of osteons. *Calcif. Tissue Int.*, *65*(4), 280–284.

Stout S.D., Lieck, R. (1995) Bone remodeling rates and skeletal maturation in three archaeological skeletal populations. *Am. J. Phys. Anthropol*. 98:161-171

Susanne, C., Defrise-Gussenhoven, E., Van Wanseele, P., and Tassin, A. (1983). Genetic and environmental factors in head and face measurements of Belgian twins. *Acta Geneticae Medicae Et Gemellologiae*, *32*, 229–238.

Thomas, C. D. L., Feik, S. A., and Clement, J. G. (2005). Regional variation of intracortical porosity in the midshaft of the human femur: age and sex differences. *Journal of Anatomy*, *206*(2), 115–25.

Tommasini, S. M., Nasser, P., Hu, B., and Jepsen, K. J. (2008). Biological co-adaptation of morphological and compsition traits contributes to mechanical functionality and skeletal fragility. *JBMR*, *23*(2), 236–246.

Tommasini, S. M., Nasser, P., and Jepsen, K. J. (2007). Sexual dimorphism affects tibia size and shape but not tissue-level mechanical properties. *Bone*, *40*(2), 498–505.

Tommasini, S. M., Nasser, P., Schaffler, M. B., and Jepsen, K. J. (2005). Relationship between bone morphology and bone quality in male tibias: implications for stress fracture risk. *JBMR*, *20*(8), 1372–80.

Tysarczyk-Niemeyer, G. (1997). New Noninvasive pQCT Devices to Determine Bone Structure. *J Jpn Soc Bone Morphom*. 7, 97-105.

Ural, A., and Vashishth, D. (2006). Interactions between microstructural and geometrical adaptation in human cortical bone. *J. Orthop. Res.*, (July), 1489–1498.

Van der Meulen, M. C., Jepsen, K. J., and Mikić, B. (2001). Understanding bone strength: size isn't everything. *Bone*, *29*(2), 101–104.

Villa, C. and Lynnerup, N. (2010). Technical note: A stereological analysis of the cross-sectional variability of the femoral osteon population. Am. J. Phys. Anthropol. 142(3), 491–6.

Vincentelli, R. and Grigorov, M. (1985). The effect of Haversian remodeling on the tensile properties of human cortical bone. *J. Biomechanics 18*, 201–207.

Vincentelli, R., and Evans, F. G. (1971). Relations among mechanical properties, collagen fibers, and calcification in adult human cortical bone. *J. Biomechanics 4*, 193–201.

Vose, G. P., and Kubala, A. L. (1959) Bone strength–its relationship to X-ray-determined ash content. *Hum. Biol. 31*, 261–270.

Weiner, S., and Wagner, H. D. (1998). The material bone: structure-mechanical function relations. *Annu.Rev. Mater. Sci.*, *28*(1), 271–298.

Weiner, S., Arad, T., Sabanay, I., Traub, W. (1997) Rotated plywood structure of primar lamellar bone in the rat: orientations of the collagen fibril arrays. *Bone* 20:509-514

Weiner S, and Traub W (1992) Bone structure: from ångstroms to microns. *FASEB* 6*:*879-885.

Zioupos, P., Currey, J. D., and Hamer, A. J. (1999). The role of collagen in the declining mechanical properties of aging human cortical bone. *J. Biomed. Mater. Res. 45(2)*, 108–116.

Ziv, V., Sabanay, I., Arad, T., Traub, W., and Weiner, S. (1996) Transitional structures in lamellar bone. *Microsc Res Tech* 33*:*203-13.

Zou, W., Hunter, N., and Swain, M. V. (2011). Application of polychromatic μCT for mineral density determination. Journal of dental research, 90(1), 18–30.

Zysset, P. K., Guo, X. E., Hoffler, C. E.,Moore, K. E., and Goldstein, S. A. (1999). Elastic modulus and hardness of cortical and trabecular bone lamellae measured by nanoindentation in the human femur. *J. Biomech*. 32 1005–12.

Appendix A: Abbreviations

ANOVA	Analysis of variance
BMD	Bone mineral density
BMU	Bone multicellular unit
CPL	Circular polarized light microscopy
DEXA	Dual-energy X-ray absorptiometry
FTIR	Fourier transform infrared spectroscopy
HrCT	High resolution computer tomography
LM	Light microscopy
LSD	Fishers least significant difference test
PBS	Phosphate buffered solution
PMMA	Poly(methyl methacrylate)
pQCT	Peripheral quantitative computed tomography
qBSE	Quantitative backscattered electron microscopy
ROI	Region of interest
TL	Transmitted light microscopy
TMD	Tissue mineral density
μCT	Micro computed tomography
Ant	Anterior
Ant-lat	Anterior-lateral
Post-lat	Posterior-lateral
Post	Posterior
Post-med	Posterior-medial
Ant-med	Anterior-medial

Appendix B: Nomenclature

Cancellous bone	Also known as trabecular or spongy bone, this type of bone is characterized by high porosity.
Co-adaption	The adaption of multiple traits in tanden.
Cortical bone	Also known as compact bone, this type of bone is characterized by low porosity.
Diaphysis	The shaft of a long bone.
Epiphysis	The ends of a long bone.
Histology	The structure or organization of tissue.
Metaphysis	The transitional zone of a long bone where the diaphysis and the epiphysis meet.
Morphology	The structure and form of an organism or its parts, in this case, bones.
Ossification	The process by which cartilage if turned into bone.
Osteon	A basic structure of cortical bone, comprising of circularly arrange lamellae around a central Haversian canal.

Appendix C: Terms of Location in the Skeleton

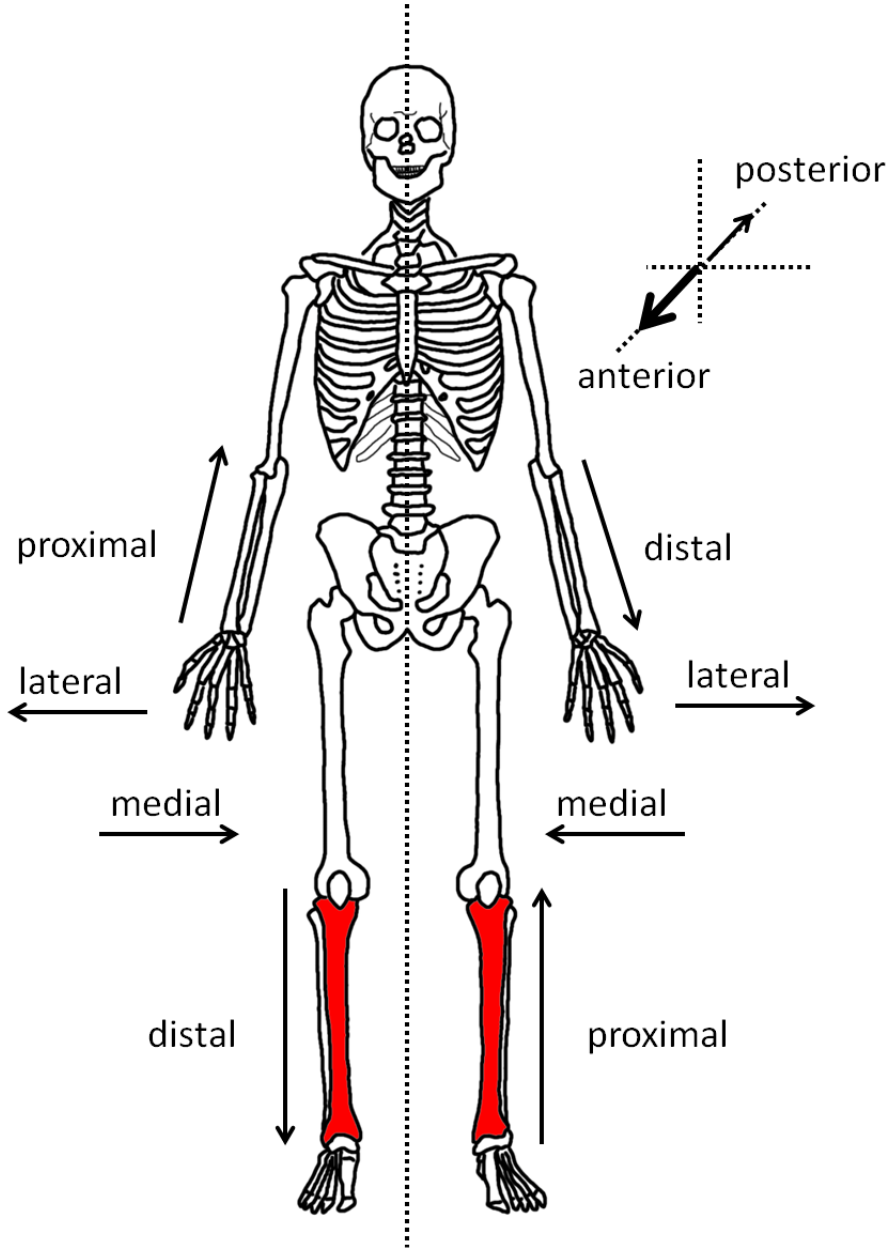

Figure Appendix C: The location of the tibia in the skeleton (red) and the terminology for locations within the skeleton

Appendix D: Tissue Type Images

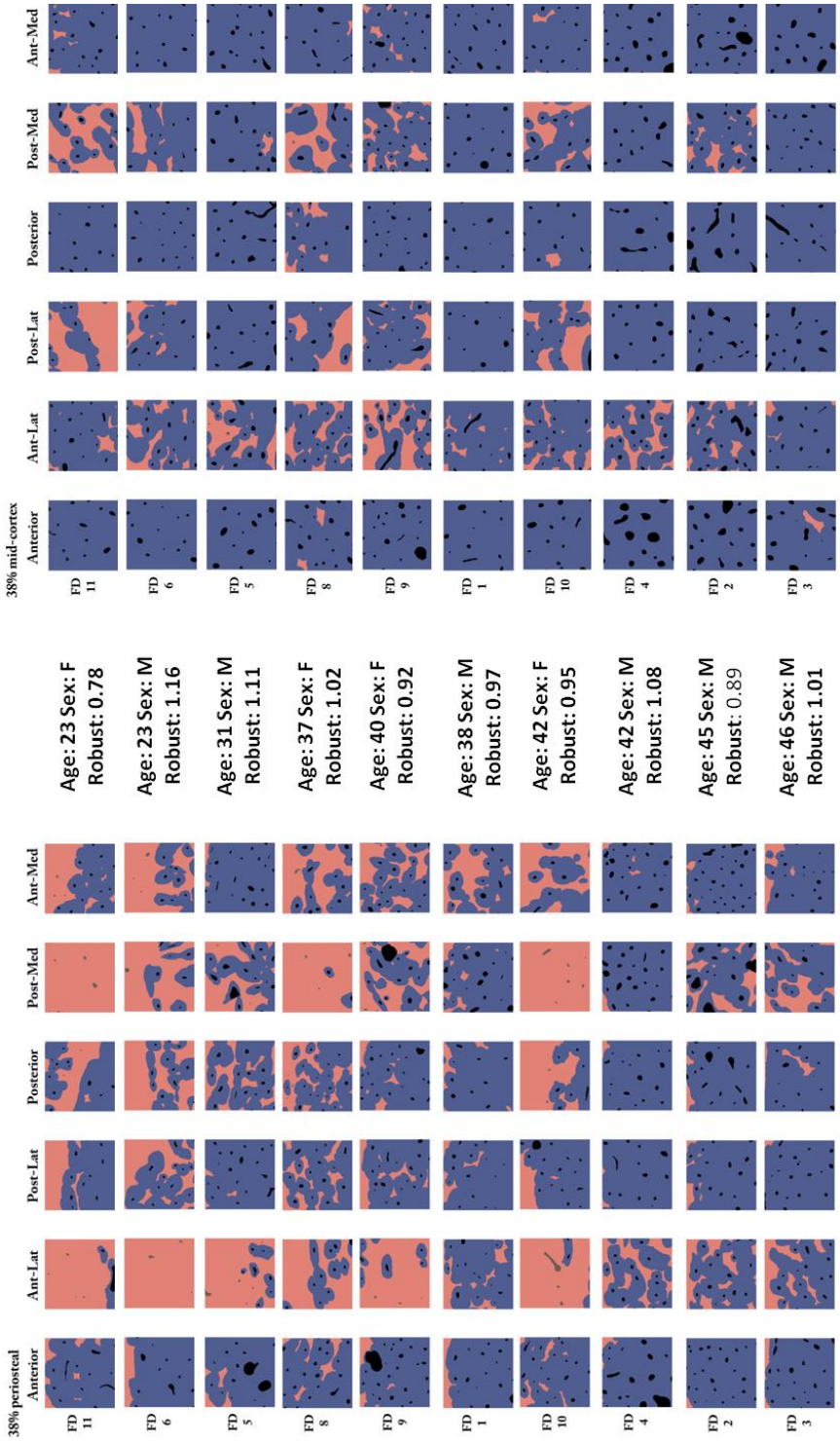

Figure Appendix D.1: Tissue type images from the 38% site arranged age

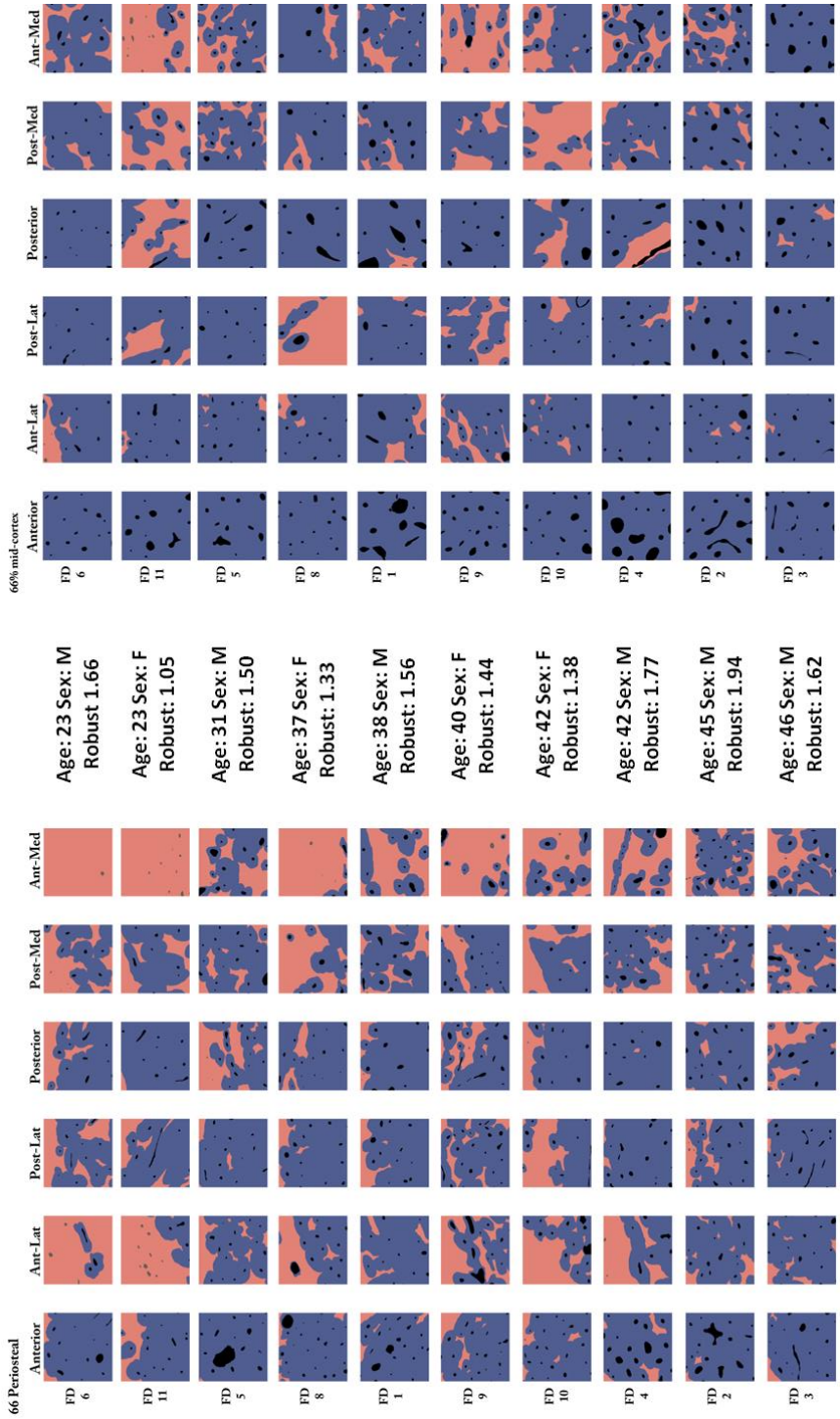

Figure Appendix D.2: Tissue type images from the 66% site arranged age

Vita

Education

Ph.D. Dept. of Materials Science and Engineering, Drexel University (Philadelphia, PA)
M.S. Dept. of Materials Science and Engineering, Drexel University (Philadelphia, PA)
B.S. Department of Physics, West Chester University (West Chester, PA)

Awards and Honors

2011	ASBMR Young Investigator Award
2011	American Association of Anatomists Travel Award
2007	Koerner Family Fellowship
2006	GAANN-DREAM Fellowship
2003, 2005	Dr. Michael F. Martens Award for Achievement in Physics
2004	Physics Honors Society – Sigma Pi Sigma

Papers and Posters

Goldman, H. M., Hampson, N. A., Guth, J. J., Lin, D., Kent, L. and Jepsen, K. J. *Intracortical remodeling parameters are associated with measures of bone robustness.* In preparation.

Jepsen, K. J., Centi, A., Duarte, G. F., Galloway, K., Goldman, H., Hampson, N., Lappe, J. M., Cullen, D. M., Greeves, J., Izard, R.., Nindl, B. C., Kraemer, W. J., Negus, C. H., Evans R. K.. *Biological Constraints That Limit Compensation of a Common Skeletal Trait Variant Lead to Inequivalence of Tibial Function Among Healthy Young Adults.* ***JBMR.*** Volume 26, 2011, Issue 12, page 2872.

Hampson, N. A., Lin, D., Jepsen, K., Goldman, H***. American Society for Bone and Mineral Research (ASBMR) 2012 Annual Meeting.*** *Intra and Inter-individual Variation in Tissue Type as a Reflection of Suppressed Remodeling Rate in Slender Tibiae*

Hampson, N., Gendron, R., Duarte, G., Kalidindi, S. R., Jepsen, K., Goldman, H. ***ASBMR 2011 Annual Meeting.*** *Porosity, Mineralization and Morphology Interactions at the Human Tibial Cortex.*

Hampson, N.A., Duarte, G.F., Gendron, R., Jepsen, K.J. and Goldman, H.M. *ASBMR* ***Special Topics Meeting and 2011 Experimental Biology Annual Meeting.*** *Establishment of Interactions Among Porosity, Mineralization and Morphology at the Human Tibial Cortex.*

Hampson, N., Nizgoda, S., Parker, B., Brody, J., Kalidindi, S, Johanson, N., Goldman, H. ***2008 Sex and Gender Research Forum.*** *Statistical Representation of Femoral Neck Bone Architecture for the Study of Bone Quality****.***